
Electronic Thesis and Dissertation Repository

7-25-2022 10:00 AM

Complex Unicellular Microfossils from the 1.9 Ga Gunflint Chert, Canada

Ana L. González Flores, *The University of Western Ontario*

Supervisor: Jin, Jisuo, *The University of Western Ontario*

Co-Supervisor: Osinski, Gordon, *The University of Western Ontario*

Co-Supervisor: Tsujita, Cameron, *The University of Western Ontario*

A thesis submitted in partial fulfillment of the requirements for the Doctor of Philosophy degree in Geology

© Ana L. González Flores 2022

Follow this and additional works at: <https://ir.lib.uwo.ca/etd>



Part of the [Geology Commons](#), [Other Earth Sciences Commons](#), [Paleobiology Commons](#), and the [Paleontology Commons](#)

Recommended Citation

González Flores, Ana L., "Complex Unicellular Microfossils from the 1.9 Ga Gunflint Chert, Canada" (2022). *Electronic Thesis and Dissertation Repository*. 8796.
<https://ir.lib.uwo.ca/etd/8796>

This Dissertation/Thesis is brought to you for free and open access by Scholarship@Western. It has been accepted for inclusion in Electronic Thesis and Dissertation Repository by an authorized administrator of Scholarship@Western. For more information, please contact wlsadmin@uwo.ca.

Abstract

The presence of eukaryotic life during the early Paleoproterozoic has been a matter of debate because well-preserved fossils older than 1.8 Ga rarely exhibit eukaryotic cellular microstructures. In this study, microfossils from the 1.9 Ga Gunflint Chert were studied using the extended-focal-depth imaging technique, combined with scanning electron microscopy, resulting in recognition of three types of large (10–35 μm diameter) complex unicellular bodies (CUBs) and one type of “multicellular body” (< 50 μm diameter). The CUBs show the following eukaryotic cyst-like structures: (1) radially arranged internal strands similar to those in some acritarchs and dinoflagellates; (2) regularly spaced long tubular processes, stubby pustules, and/or robust podia on the cell surface; (3) reticulate cell-wall sculpturing such as pits, ridges, and scale-like ornaments; and (4) internal bodies that may represent membrane-bounded organelles. These morphological features provide strong evidence for the presence of protists in the late Paleoproterozoic.

Among the three types of CUBs from the Gunflint microbiota, a new species, *Germinosphaera gunflinta* sp. nov., was recognized. This species has the diagnostic characteristics of *Germinosphaera*, such as a subrounded to an ellipsoidal cyst, a robust main podium (up to 15 μm), multiple smaller processes, and scale-like ornaments on the surface. Within a broadly continuous lineage of *Germinosphaera* from the Paleoproterozoic to the early Cambrian, there is a clear increase in cell size from the Paleoproterozoic to the Mesoproterozoic, with the Gunflint species being the smallest and oldest with complex, eukaryote-like, surface ornaments that are well preserved.

Keywords: Cyst-like structures, Gunflint Chert microbiota, Complex unicellular bodies, *Germinosphaera*, *Germinosphaera gunflinta*.

Summary for Lay Audience

The oldest fossilized life forms on Earth, dating to ~3.5 Ga, are represented by bacteria (prokaryotes). These cells, lacking a true nucleus or other organelles, are among the simplest and ubiquitous forms of life on our planet. Prokaryotic organisms dominated the Earth from the Archean to Paleoproterozoic (3.5–1.6 Ga) and spread unopposed across the planet until the appearance of eukaryotes - more complex organisms with cells containing a well-defined nucleus.

Fossil evidence indicates that eukaryotic cells, which make up all complex life, have existed on Earth since at least 1.7 Ga. Considering that complex life is made up of this class of cells – from giant whales to microscopic unicellular algae – the existence, origin, and evolution of eukaryotes are vital to understanding the development of complex life on Earth and other planets that have the necessary conditions to support complex life forms. Due to the relevance of the origin and evolution of these organisms to the understanding of how early life developed on Earth, it is important to establish their morphological characteristics and range of occurrence in the fossil record. This study focuses on chert samples from the Gunflint Formation (1.9 Ga) in Canada. These samples present fossil remains of simple, prokaryotic organisms such as cyanobacteria that are expected for this age. However, co-occurring with these remains are more complex fossil cells with structures that have remained unidentified until now.

Three different unidentified organisms were recognized: 1) star-shaped, 2) irregularly shaped organisms with multiple spikes, and 3) organisms with the main body and one or more podium/podia. Our data suggest eukaryotic affinities for these organisms. Furthermore, through these studies, we recognized a new species, *Germinosphaera gunflinta*, with morphological characteristics typical of eukaryotes.

Co-Authorship Statement

This thesis is divided into four chapters, two of which are written in manuscript format.

Chapter 1 – This chapter serves as an introduction to the thesis and a literature review on topics of great relevance to the studies carried out in this work. Dr. Jin, Dr. Osinski, and Dr. Tsujita assisted with editing this chapter and providing articles from private sources that are not widely available.

Chapter 2 – Submitted to the journal *Astrobiology* in 2021, has been approved by the journal for publication and is in the printing process. All petrographic data collection, image acquisition and processing, and data analysis and writing of this chapter were performed by Ana L. González-Flores, assisted by her co-supervisors Dr. Jin and Dr. Osinski and committee member Dr. Tsujita. They provided critical feedback and made edits to the manuscript.

A version of this chapter has been published:

González-Flores, A.L., Jin, J., Osinski, G.R., and Tsujita, C.J., 2022, Acritarch-like Microorganisms from the 1.9 Ga Gunflint Chert, Canada. *Astrobiology*, v. 22, n. 5, p. 568–578. DOI: 10.1089/ast.2021.0081.

Chapter 3 – Submitted to the *Journal of Paleontology* (June 2, 2022). The collection, data processing, and writing of this chapter were performed by Ana L. González-Flores under the supervision and co-authorship of Dr. Jin, Dr. Osinski, and Dr. Tsujita.

Chapter 4 – Contains the conclusions of the investigation. This chapter was written by Ana L. González-Flores. Co-supervisors Dr. Jin and Dr. Osinski, and Dr. Tsujita reviewed the chapter and provided feedback.

Acknowledgments

First of all, I would like to thank Dr. Jisuo Jin, Dr. Gordon Osinski, and Dr. Cameron Tsujita for their support, patience, teachings, and feedback. I feel extremely lucky to have had the opportunity to work with you, and I want you to know that I will always be grateful for it.

I would also like to acknowledge the support of Marc Beauchamp and Liane Loiselle from the Earth and Planetary Materials Analysis Laboratory (EPMAL); Ivan Barker and Thalia Standish from Surface Science Western; Stephen Wood from the Thin Section Laboratory at the Department of Earth Sciences, UWO; and Tim Goldhawk and Todd Simpson from the Western Nanofabrication Facility (Nanofab), whose help was essential to carry out all the laboratory analyzes carried out in this project.

I benefited greatly from discussions with Colin Sproat and Tianqi Xie, and many graduate student colleagues from the Spacerocks group. I am extremely grateful for the support and great friendship of Michelle Jimenez Sosa, Monica Vazquez, Rebeca Arámbula, and Rosa Arredondo, without whom my time in Canada would have been quite monotonous and dedicated solely to study. They are some of the best people someone could have in their life, and I wish them all success with their postgraduate degrees.

Other fundamental people in my life to whom I also owe my gratitude for being with me every step of this journey are Dichu, Marion, Lou, Montse, Karla and JJ, who will probably never read this work. However, I must mention them anyway since they are like family to me. Despite being apart, they have always given me their unconditional support, even in the most difficult moments of this experience.

To my always hard-working mother, who never gave up or stopped working overtime to allow me to study and have the best opportunities. For all his knowledge and encouragement, to my father for instilling in me a taste for science, culture, and reading. To my brother and Loli, who are of few words but are always there at the end of the day to share a meme or just be by my side to make me laugh and feel better. All of you have always meant the world to me, I love you, and I sincerely hope that I have made you proud.

This project would not have been possible without the funding from the Natural Sciences and Engineering Research Council of Canada (NSERC) Discovery Grant program through grants to Dr. Jisuo Jin and Dr. Gordon R. Osinski. In addition, Michelle Coyne kindly provided us with access to the GSC samples and locality information. And last but not least, I want to thank my thesis examiners. Thank you in advance for your time and constructive feedback on this work. Many thanks!

Land Acknowledgment

I acknowledge that the University of Western Ontario is located on the traditional lands of the Anishinaabek, Haudenosaunee, Lūnaapéewak, and Attawandaron peoples, on land connected with the London and Shadow Township Treaties of 1796 and the Wampum Plate with one Spoon Covenant. This land continues to be home to diverse Indigenous peoples (e.g., First Nations, Métis, and Inuit) whom we acknowledge and appreciate as contemporary stewards of the land.

Table of Contents

Abstract	ii
Co-Authorship Statement	iv
Acknowledgments	v
Table of Contents	vii
List of Tables	x
List of Figures	xi
List of Appendices	xv
List of Abbreviations	xvii
Chapter 1: Introduction	1
1.1 Opening Statement	1
1.2 Paleogeographic Setting	2
<i>1.2.1 Laurentia Craton</i>	3
<i>1.2.2 Superior Province</i>	4
1.3 Paleoproterozoic Climate	5
<i>1.3.1 Great Oxygenation Event (GOE)</i>	5
1.4 General Stratigraphy of the Area of Study	7
<i>1.4.1 Animikie Basin</i>	7
<i>1.4.2 Gunflint Formation</i>	16
1.5 Origins of Eukaryotic Life on Earth	29
1.6 Gunflint Microbiota	31
<i>1.6.2 Microfossil Preservation</i>	35
<i>1.6.3 Biogenicity Debate of Gunflint Microfossils</i>	35
1.7 Astrobiological Significance of the Gunflint Chert Microfossils	36
1.8 Materials and Analytical Methods	37
<i>1.8.1 Gunflint Chert Samples</i>	38
<i>1.8.2 Optical Microscopy</i>	38
<i>1.8.3 Scanning Electron Microscopy (SEM)</i>	39
<i>1.8.4 Electron Microprobe Analysis (EMPA)</i>	41
1.9 Thesis Structure	41
References	43
Chapter 2: Acritarch-like microorganisms from the 1.9 Ga old Gunflint Chert, Canada	72
2.1 Introduction	72

2.2 Materials and Methods	77
2.2.1 <i>Thin sections</i>	77
2.2.2 <i>Optical Microscopy</i>	78
2.2.3 <i>Sample Preparation</i>	81
2.2.4 <i>Imaging Methodology</i>	81
2.2.5 <i>Image Processing</i>	82
2.2.6 <i>Scanning Electron Microscopy</i>	85
2.3 Results	86
2.3.1. <i>CUB Type 1: Spherical cysts with numerous fine processes</i>	87
2.3.2. <i>CUB Type 2: Spherical cells with horny pustules</i>	87
2.3.3. <i>CUB Type 3: Irregular cells with robust podia</i>	89
2.3.4. <i>“Multicellular” bodies (MCBs)</i>	91
2.4 Discussion	92
2.4.1. <i>Eukaryote-like characteristics of the Gunflint CUBs</i>	92
2.5 Conclusions	97
References.....	98
Chapter 3: <i>Germinosphaera gunflinta</i> n. sp. – Protist-like microfossil from the 1.9 Ga Gunflint Chert Formation, northern Ontario, Canada	108
3.1 Introduction	108
3.2 Geological Background	110
3.3 Material and Methods	110
3.4 Systematic Paleontology	113
3.5 Results and Discussion	128
3.5.1 <i>Analysis of cell size over time in Germinosphaera from Paleoproterozoic to Ediacaran</i>	129
3.5.2 <i>Multivariate analysis of morphological characters of Germinosphaera</i>	131
3.5.3 <i>Significance of Germinosphaera gunflinta sp. nov.</i>	135
3.6 Conclusions	137
References.....	137
Chapter 4: Conclusion	148
4.1 Conclusions	148
4.2 Future Work	150
4.2.1 <i>In-depth Taxonomic Study of the Remaining CUB types</i>	150
4.2.2 <i>Gunflint Multicellular Structures</i>	152

4.3 Significance of the Study	152
References.....	153
Appendices	157
A. Optical Microscope CUB types' of measurements and plots for samples GSC24380 (2), GSC24380d and GSC24380e	157
<i>Item 1. Extended focal depth optical imaging process.</i>	157
<i>Item 2. Diameter measurements plots for thin section GSC24380 (2).</i>	159
<i>Item 3. Diameter measurements plots for thin section GSC24380d.</i>	161
<i>Item 4. Diameter measurements plots for thin section GSC24380e.</i>	163
B. Optical Microscope measurements of <i>Germinosphaera</i> specimen.	165
<i>Item 1. Germinosphaera specimen extracted from bibliography and samples GSC24380, GSC24380d and GSC24380e</i>	165
<i>Item 2. Dataset for Figure 3.8, Age vs Size plot</i>	173
<i>Item 3. Dataset for Figure 3.9 Multivariate plot</i>	183
C. Scanning Electron Microscopy (SEM) maps from sample GSC24380d	188
<i>Item 1. GSC24380d element maps</i>	189
D. Electron Microprobe (EMP) WDS maps	195
<i>Item 1. Sample GSC24380d-27 maps</i>	195
<i>Item 2. Sample GSC24380d-31 maps</i>	201
<i>Item 3. Sample GSC24380d-36 maps</i>	207
E. Other analytical methods	210
<i>Item 1. Laser Raman Spectroscopy (LRS)</i>	210
<i>Item 2. Micro-XRF, Micro-CT and Synchrotron analyses</i>	212
References.....	217
Curriculum Vitae	225

List of Tables

Chapter 1:

Table 1.1. Comparison of prokaryotic and eukaryotic organisms (adapted from Levin and King, 2017).

Table 1.2. Taxa reported from the Gunflint Chert and their provisional status by Awramik and Barghoorn, (1977; adapted from Table I)

Table 1.3 Affinities of the Gunflint Chert identified Microfossils, adapted from Awramik and Barghoorn (1977), Table II.

Chapter 3:

Table 3.1. Eigenvalues of variables in the principal component analysis.

List of Figures

Chapter 1:

Figure 1.1. Map of the supercontinent Columbia/Nuna (1590 Mya) depicting its constituent cratons. The stars symbol marks the assumed present-day location of the Gunflint Formation in the Laurentia/North America craton (Adapted from Zhang et al, 2012; Pesonnen et al., 2012; Evans and Mitchell, 2011)

Figure 1.2. a) Sketch map of North America at about 2.0 Ga to show the distribution of Paleoproterozoic basins; b) The occurrence of continental margin iron formation around the Paleoproterozoic supercontinent Columbia. Modified from Cannon et al., (2008) and Pufahl et al. (2014).

Figure 1.3. Geological map of the *Lake Superior district, Canada and U.S.A* showing the Gunflint-Vermillion, Mesabi, Cuyuna, Gogebic, Menominee and Marquette Range banded iron-formations. Gunflint and Rove Formations are depicted on the Thunder Bay region (modified from Mueller, 2019; Ishida et al., 2017; Cannon et al., 2008)

Figure 1.4. Stratigraphy of the major north- and western ranges of the Animikie Basin. Groups are depicted at the left side of each range's stratigraphic column. Adapted from White, 1954; Morey, 1983; McSwiggen et al., 1995; Ojakangas et al., 2001; Schulz and Cannon, 2007; Foley, 2009; and Craddock et al., 2013.

Figure 1.5. Figure 1.5 Stratigraphic sections of the southern ranges of the Animikie Basin. Groups are depicted at the left side of each range's stratigraphic column. Adapted from Adler, 1935;

Cumberlidge and Stone, 1964; Laybourn, 1979; Morey, 1983; Ojakangas et al., 2001; Schulz and Cannon, 2007; Cannon et al., 2008; Craddock et al., 2013; Laird, 2017.

Figure 1.6. Schematic diagram comparing the Gunflint Formation divisions in Gunflint Lake, Minnesota and Thunder Bay, Ontario. Note that, aside from the Kakabeka conglomerate and stromatolitic chert units, the lithologic units within the formation are very different. Modified from Jirsa et al. (2011).

Figure 1.7. Stratigraphy of the Gunflint Formation based on an unweathered drill core 89-MC-1 with interpretation of relative sea-level changes of Pufahl and Fralick (2000) from Gunflint members 1-5. Symbols same as in legend for Fig. 1.4.

Figure 1.8. Photograph of several samples of the Gunflint Chert lent by the Geological Survey of Canada (GSC).

Figure 1.9. a) Lake Superior area map. b) Zoom on Schreiber Channel Provincial Nature Reserve area pinpointing the sample collections (Modified from González-Flores et al., 2022).

Figure 1.10. Image displaying the differences between a eukaryotic cell (left) and a prokaryotic cell (right). Adapted from Science Primer (National Center for Biotechnology Information; 2005).

Figure 1.11. Optical microscopy images from several identified Gunflint Chert microorganisms. Scalebar = 10 μm for all specimen except for (i). Adapted from Awramik and Barghoorn (1977).

Chapter 2:

Figure 2.1. Location map of the Gunflint Chert. A. Map of the northern Lake Superior region showing the Proterozoic Mesabi, Vermillion and Gunflint iron ranges. B. Enlarged view of area

indicated in A at the northern tip of the Gunflint Iron Range, showing the distribution of Proterozoic and Archean rocks.

Figure 2.2. Diameter measurements of CUBs. For every CUB type, two diameters were measured: longitudinal diameter (D1, red) refers to the maximum diameter, and transversal diameter (D2, yellow) at perpendicular angle to D1.

Figure 2.3. Photomicrographs of CUBs. (A, B) CUB Type 1, (C–E) CUB Type 2, (F–I) CUB Type 3, (G–I) three EDF views of the same cell in two hemispheres and “equatorial-centre zone.

Figure 2.4. Extended depth of focus (EDF) optical and SEM images of CUB Type 3.

Figure 2.5. “Multicellular” bodies. (A, C) Broken pieces of rope-like organisms; (D) Cylindrical form with uniserial, longitudinally stacked cells.

Figure 2.6. Histograms of the distribution of longitudinal and transversal diameters of CUB Types 1–3, based on 9,000 EDF images of cells acquired at x160 magnifications from three thin sections (Materials and Methods section for details).

Chapter 3:

Figure 3.1. *Germinosphaera gunflinta* n. sp. Optical images generated from extended depth of focus (EDF) Z-series, sample GSC 24380, Gunflint Formation, Schreiber Beach, northwestern Ontario.

Figure 3.2. Scanning Electron Microscopy (SEM) Backscattered-Electron (BSE) images of *Germinosphaera gunflinta* filtered residual material after light HF (hydrofluoric acid) etching, sample GSC24380d.

Figure 3.3. SEM images of *Germinosphaera gunflinta* after light HF etching, sample GSC24380d. Scalebar depicted individually for each specimen.

Figure 3.4. SEM images of small bulk sample (a, b, d, e) and studs made from its filtered residual material (c, f) after light HF etching, sample GSC24380d.

Figure 3.5. In-situ elemental maps of specimen from Figure 8b, GSC24380d, small bulk sample.

Figure 3.6. Backscattered-Electron (BSE) field-emission electron microprobe (EMPA) images from thin sections GSC24380d and GSC24380e, magnification between 4.00 – 7.00 KX and 15.0 kV EHT.

Figure 3.7. Field-emission electron microprobe (EPM) wavelength dispersive X-ray spectroscopy (WDS) element maps. (a) composition (COMPO) mode image from thin sections GSC24380d; (b) secondary electron image (SEI) image

; (c) WDS Carbon map; (d) WDS Silicon map; (e) WDS Sulphur map; (f) WDS Iron map. Scalebar of 5µm.

Figure 3.8. Average age versus measured cell diameters plot for 146 specimens from collected database on the genus *Germinosphaera*. Average age was calculated from the minimum and maximum age from the respective formation of each specimen when specific age was not provided.

Figure 3.9. Size multivariate plot for 146 specimens from collected database on the genus *Germinosphaera*. Each dot depicts the combined value of 14 different criteria measured for each cell. The dots are colour coded to depict the different species of the genus.

Chapter 4:

Figure 4.1. a) Optical image of CUB Type 1, sample GSC24380#; b) Optical image of *Alicospheridium medusoideum* from Willman and Moczydłowska, (2008); c) Optical image of CUB Type 1, sample GSC24380#; d) Optical image of *Gambierdiscus toxicus* from Knoll, (2015). Scalebar = 10 µm for (a) and (c), 20 µm for (d), and 50 µm for (b).

Figure 4.2. a) Optical image of Multicellular Body of sample GSC24380#, Scalebar = b) Optical images of *Chlorococcum vacuolatum* and c) *Chlorosarcinopsis gelatinosa* from Stanier and Cohen-Bazire, (1977). Scalebar = 10 µm for (b) and 20 µm for (a) and (c).

Figure 4.3. a) Optical image of "bundled filaments" from the GSC24380# sample... Scalebar = 10 µm.

List of Appendices

Appendix A: Optical Microscope CUB types' measurements and plots for samples GSC24380, GSC24380d and GSC24380e.

Item 1: Extended focal depth optical imaging process.

Item 2: Diameter measurements plots for thin section GSC24380 (2).

Item 3: Diameter measurements plots for thin section GSC24380d.

Item 4: Diameter measurements plots for thin section GSC24380e.

Appendix B: Optical Microscope measurements of *Germinosphaera* specimen.

Item 1: *Germinosphaera* specimen extracted from bibliography and samples GSC24380, GSC24380d and GSC24380e.

Item 2: Dataset for Figure 3.9, Age vs Size plot.

Item 3: Dataset for Figure 3.10 Multivariate plot.

Appendix C: Scanning Electron Microscopy (SEM) maps from sample GSC24380d.

Item 1: GSC24380d through 4 maps.

Appendix D: Electron Microprobe (EMP) WDS maps

Item 1: Sample GSC24380d-27 maps.

Item 2: Sample GSC24380d-31 maps.

Item 3: Sample GSC24380d-36 maps.

Appendix E: Other Analytical Methods

Item 1: Laser Raman Spectroscopy (LRS).

Item 2: Micro-XRF, Micro-CT and Synchrotron analyses.

List of Abbreviations

BSE – Backscattered-Electron

CUB – Complex Unicellular Body

EDX – Energy Dispersive X-ray

EMA –Electron Microprobe Analysis

Ga – Billion years

GOE – Great Oxygenation Event

Ma – Million years

MaxD – maximum diameter of cyst

MinD – minimum diameter of cyst

PBD1 – main podium base diameter

PBD2 – secondary podium base diameter #2

PBD3 – secondary podium base diameter #3

PBD4 – secondary podium base diameter #4

PDED1 – main podium distal end diameter

PDED2 – secondary podium distal end diameter #2

PDED3 – secondary podium distal end diameter #3

PDED4 – secondary podium distal end diameter #4

PL1 – main podium length

PL2 – secondary podium length #2

PL3 – secondary podium length #3

PL4 – secondary podium length #4

SEM – Scanning Electron Microscopy

SHRIMP – Sensitive High-Resolution Ion Microprobe

WDS – Wavelength Dispersive X-ray Spectroscopy

Chapter 1: Introduction

1.1 Opening Statement

The validity of fossil evidence of eukaryotic life in rocks older than 1.8 Ga has been a matter of debate in many previous studies due, in part, to the scarcity of micro-and ultracellular structures in unequivocally eukaryotic microfossils of such age. The 1.9 Ga Gunflint Chert of the Paleoproterozoic Gunflint Formation of northern Ontario, Canada, is one example of a unit that has long been suspected but has yet to be proven to contain fossil eukaryotes.

Despite being exceptionally well-preserved, fossils in the Gunflint Chert have undergone cellular degradation and pose challenges to the interpretation of their delicate cellular structures. Among the rich and diverse microbiota preserved in the Gunflint Chert are unidentified organisms due to their complex cell morphology compared to the more morphologically simple prokaryotic species in this unit.

The main objective of this study is to use modern imaging techniques to acquire high-quality images and to describe and interpret the microfossils to better understand their possible biological affinities, especially their possible relationships to known eukaryotic organisms such as acritarchs and other unicellular algae. Similarities in the micro-and ultra-structures of the fossil cells to those of known eukaryotes have been regarded as potential evidence for the presence of protists in the middle to late Paleoproterozoic.

1.2 Paleogeographic Setting

The Paleoproterozoic Era (2.5–1.6 Ga) is the oldest of the three main subdivisions of the Proterozoic Eon (Cohen et al., 2020). It is the most prolonged geologic era in the current chronostratigraphic scheme, and it was during the Paleoproterozoic, that a rigid lithosphere evolved to make modern-style plate tectonics possible (Pannella, 1972; Lahtinen, 2005; Kump and Barley, 2007).

One ancient supercontinent postulated for the Proterozoic Eon is Columbia, also known as Nuna (Figure 1.1). It existed from approximately 1.9–1.5 Ga, one of the oldest supercontinents (Rogers and Santosh, 2002; Evans and Mitchell, 2011; Zhang et al., 2012). It was a proto-craton that consisted of the paleocontinents of Laurentia (mainly North America), Greenland, Baltica, Amazonia, East Antarctica, West Africa, Australia, Siberia, North and South China, India, and Kalahari (Hoffman, 1989; Pesonen et al., 2003; Belica et al., 2014). Strata of the Gunflint Formation were deposited in the Superior Terrane prior to its amalgamation into Laurentia and the Columbia supercontinent.

Columbia is estimated to have been located about 12,900 km from its present-day position and rotated over 90 degrees clockwise from its present-day orientation (Rogers and Santosh, 2002; Pesonen et al., 2003; Bispo-Santos et al., 2008). As a result, most of South America was rotated to form a continental margin. Its western edge aligned with eastern North America, causing the continental margin to extend into southern Scandinavia.

Columbia fragmented at around 1600 Ma in connection with continental dislocation along the western margin of Laurentia (Zhao et al., 2004; Belica et al., 2014). The fragmentation driven by

magmatic activities continued until the end of the disintegration of the supercontinent from approximately 1300 to 1200 Ma (Nordsvan et al., 2017).

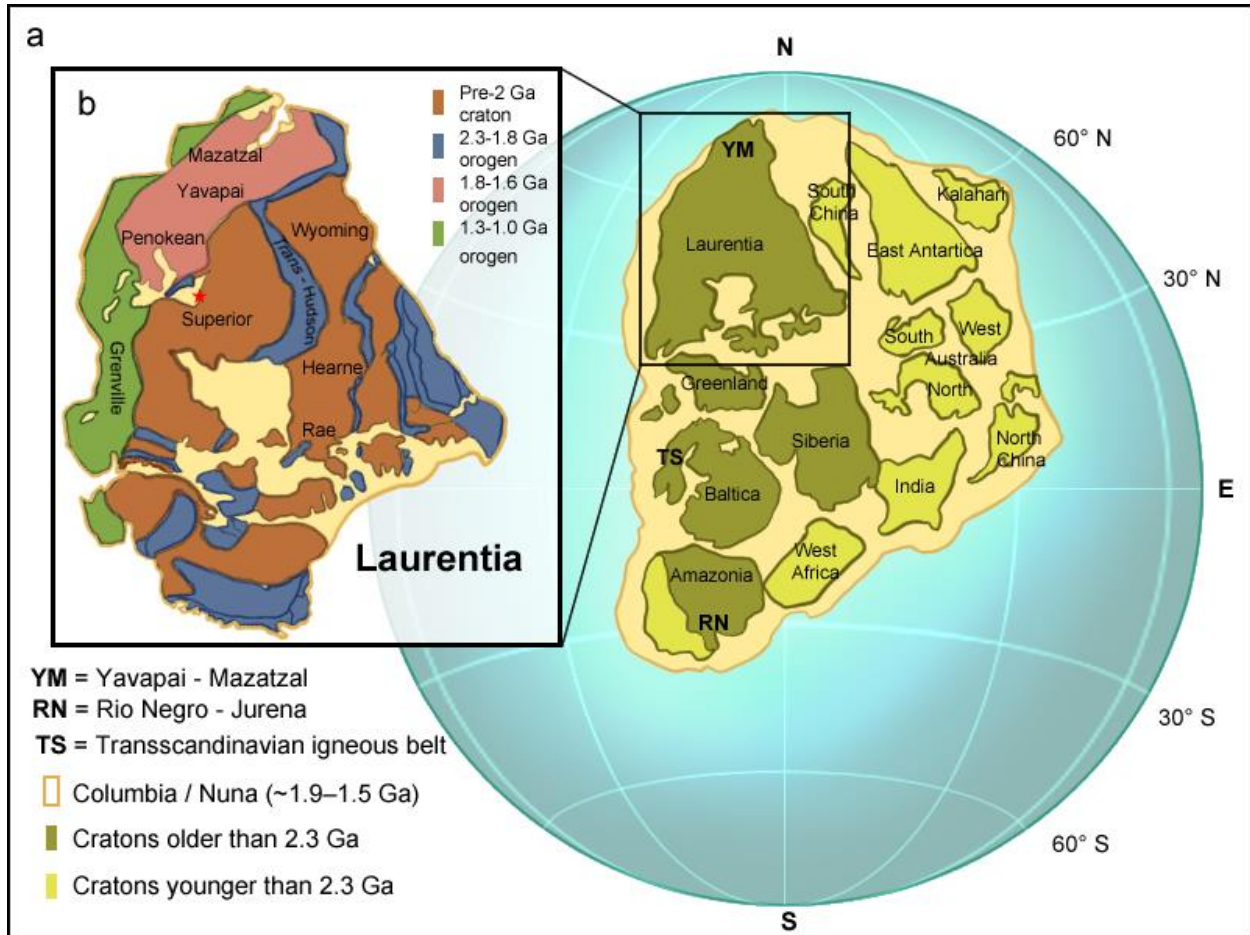


Figure 1.1 a) Map of the supercontinent Columbia/Nuna (~1.9–1.5 Ga) depicting its constituent cratons (Adapted from Zhang et al., 2012; Pesonen et al., 2003; Evans and Mitchell, 2011); b) Zoom-in of Laurentia or North American Craton during the Paleoproterozoic (Adapted from Brennan et al., 2021), the red star indicating the sampling locality on the Superior terrain.

1.2.1 Laurentia Craton

Laurentia, also known as the North American Craton, is a continental craton that formed the ancient geological core of North America (Fig. 1.2). It was initially formed by the amalgamation of seven formerly independent Archean cratons (Superior, Wyoming, Rae, Hearne, Nain, Slave, and Burwell) (Hoffman, 1989; Whitmeyer and Karlstrom, 2007; Torsvik and Cocks, 2017; Levin

and King, 2017; Brennan et al., 2021). During Laurentia's core assemblage, banded iron formations (BIFs) were deposited in areas now located in Michigan, Minnesota, Lake Superior, and Labrador (Levin and King, 2017). The description and significance of BIF are discussed in section 1.4.1.1. By the Paleoproterozoic, Laurentia had become the north-western part of the supercontinent Columbia (Fig. 1.1).

1.2.2 Superior Province

Located at the cratonic center of Laurentia, the Superior province was formed by north-dipping subduction and accretion of alternating belts of metasedimentary and mafic basinal rocks between ~2.75 and 2.65 Ga (Card, 1990; Percival et al., 2006; Percival 2007; Craddock et al., 2013). This region comprises a platform deposited upon a continental margin assemblage and contains localized rifts with thick accumulations of sedimentary and volcanic rocks. Through the Paleoproterozoic, several sea transgressions occurred over the area, and an ocean basin opened south of present-day Lake Superior date (Ojakangas et al., 2001). A northward-migrating foreland basin developed during the deposition of two groups in the Animikie Basin (Fig.1.2b) at the northwestern part of the platform during a fourth marine inundation. This basin as well as the groups it contains are further discussed in section 1.4.1.

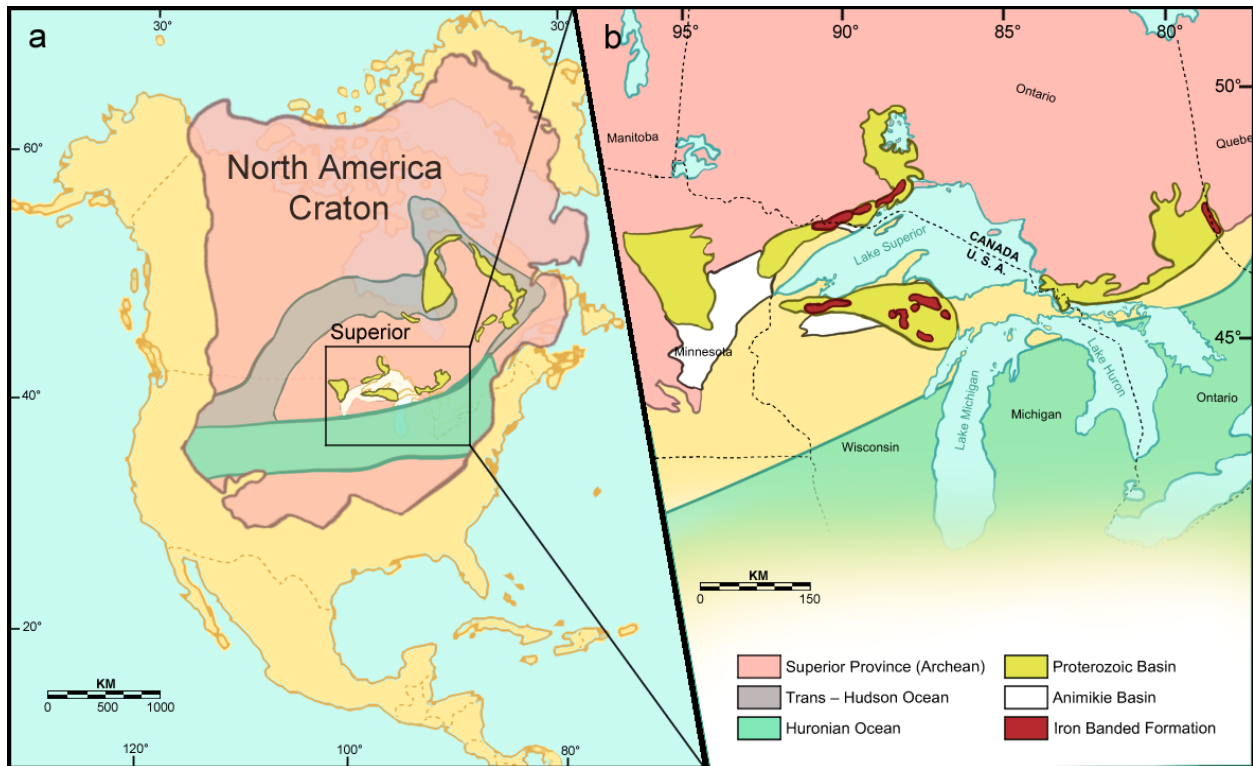


Figure 1.2 a) Sketch map of North America at about 2.0 Ga to show the distribution of Paleoproterozoic basins; b) The occurrence of continental margin iron formation around the Paleoproterozoic supercontinent Columbia. Modified from Cannon et al. (2008) and Pufahl et al. (2014).

1.3 Paleoproterozoic Climate

1.3.1 Great Oxygenation Event (GOE)

The GOE was considered a protracted and critical event that took place approximately 2.4 Ga ago (Lyons et al., 2014; Sosa Torres and Saucedo-Vázquez, 2015; Hodgskiss et al., 2019). During this event, the Earth's atmosphere and the shallow ocean first experienced a sudden rise in the amount of free oxygen (Lyons et al., 2014). One theory states that this increase was likely due to the accumulation of biologically produced molecular oxygen from oxygenic photosynthesis, which changed shallow marine conditions from weakly reducing to oxidizing (Sosa Torres and Saucedo-Vázquez, 2015). Oxygen-producing cyanobacteria are thought to have evolved at least 2.45–2.32 billion years ago (Taylor and Taylor, 1993; Tomitani, 2006). However, as oxygen

remained scarce in the atmosphere until around 2.0 billion years ago (Shaw, 2008) and banded iron formation continued to be deposited until around 1.85 billion years ago (Kasting, 1993), an explanation for the delay of around 400 Ma between the evolution of oxygen-producing photosynthesis and indicators of significant levels of atmospheric oxygen (Shaw, 2008) remains to be found.

The rise in oxygen levels caused the virtual disappearance of the greenhouse gas methane, which oxidized to produce carbon dioxide and water (Kasting and Siefert, 2002; Knauth, 2005; Feulner, 2012; Olson et al., 2016; Krissansen-Totton, 2018). Increased oxygen concentrations also allowed biological diversification of microbial life forms as well as changes in the nature of chemical interactions between rocks and other geological substrates (most notably clay) and the Earth's atmosphere, oceans, and other surface waters (Margulis and Sagan, 1986; Brocks et al., 1999; Trendall and Blockley, 2004; Robert and Chaussidon, 2006). The higher level of free oxygen was also essential for the evolution of more efficient and higher-rate metabolism in eukaryotes.

The GOE also played a crucial role in the deposition of banded iron formations (BIF), which became most widespread during this time. The peak deposition for some BIFs (e.g. those in South Africa and Australia) coincides with the onset of the GOE at ~2.45 Ga (Konhauser et al., 2011; Gumsley et al., 2017; Robbins et al., 2019). Trendall and Blockley (2004) suggested that precipitation and deposition of the iron oxide component of BIF was associated with a significant atmospheric increase in oxygen concentration, from an estimated 0.1% of the atmosphere to 1%, which facilitated the mobility of iron weathered from minerals on land. However, given the low levels of pO_2 present in the Paleoproterozoic atmosphere ($< 10^{-15}$ to < 0.1 of present day atmospheric levels), strongly oxygenated groundwater sources are difficult to envision (Lyons et al., 2014; Robbins et al., 2019).

1.4 General Stratigraphy of the Area of Study

1.4.1 *Animikie Basin*

The Gunflint Formation forms part of the Animikie basin, which is located southwest of Lake Superior's margins in what is modern-day Minnesota and Western Ontario (Fig. 1.3). The Animikie Basin contains Archean basement rocks of two contrasting types, differing in age, rock assemblages, metamorphic grade, and structural style; late Archean greenstone-granite complexes lay at the northern part of the basin, underlining it, and to the South, 3600 m.y. old migmatitic gneiss and amphibolite underlie the basin (Morey, 1983). The Animikie Basin is a 6–12 km thick succession of a basal glaciogenic unit with BIFs and turbidites, and records deposition in a spectrum of environments from marginal-marine to deep marine conditions (Cannon, 1976; Ojakangas et al., 2001; Craddock et al., 2013).

Animikie deposition spanned from ~2.2–1.8 Ga, starting with the passive-margin deposition over the western part of the Huron basin, following 400 Myrs of erosion, and ended by a tectono-thermal event, the Penokean orogeny (Goldich et al., 1961; Morey, 1983; Craddock et al., 2013). The Animikie Basin is transversed by the Great Lakes Tectonic Zone, which is a late Archean crustal boundary of at least 1200 km long (Sims and Day, 1993), and it can be divided into northern and southern segments due to its division by the 1.1 Ma old Midcontinent Rift System (MRS; Ojakangas et al., 2001; Blackburn, 2010).

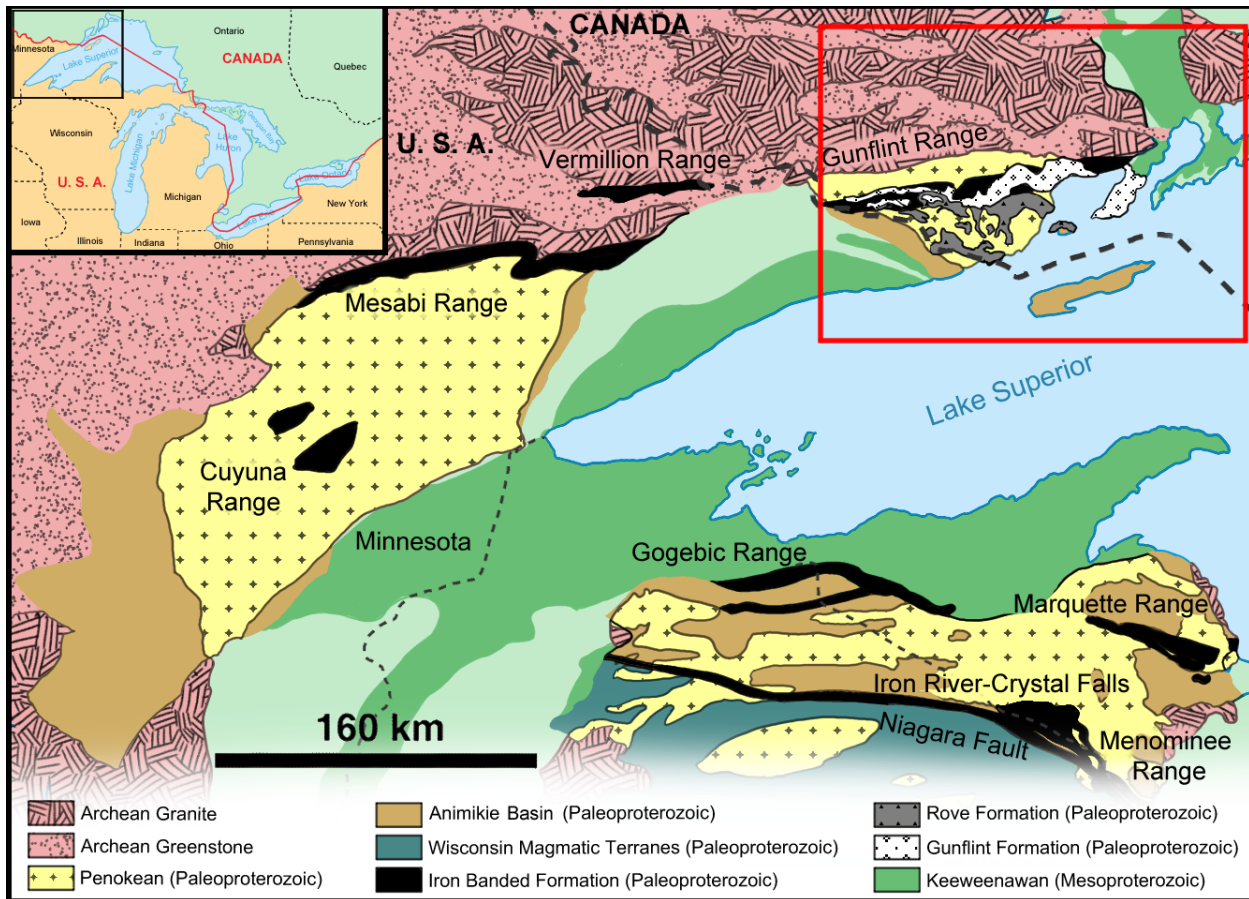


Figure 1.3 Geological map of the Animikie Basin within the Lake Superior district, Canada and the USA. The map shows the Animikie Group, Gunflint and Rove Formations, depicted in the Thunder Bay region marked inside the red rectangle (modified from Cannon et al., 2008; Ishida et al., 2017; Mueller, 2019)

The Proterozoic stratigraphic succession in the Animikie Basin is divided into three predominantly sedimentary packages (Fig. 1.5):

1. The $2,197 \pm 39$ Ma old basal Mille Lacs Group and the $2,207 \pm 5$ Ma old Chocolay Group are on the northwestern and southeastern sides of the basin, respectively (Davis, 1998; Vallini et al., 2006).
2. The ~2500 to 1800 Ma Animikie Group, located on the northwestern margin of the basin, and the lower Menominee and overlying Baraga Group on the southeastern rim of the basin (Green, 1996; Jirsa et al., 2004; Craddock et al., 2013).

- The early Proterozoic, uppermost Paint River Group is located on the southern margin of Lake Superior, part of the continental margin assemblage (north of Niagara Fault), northwestern Michigan (Van Schmus, 1976).

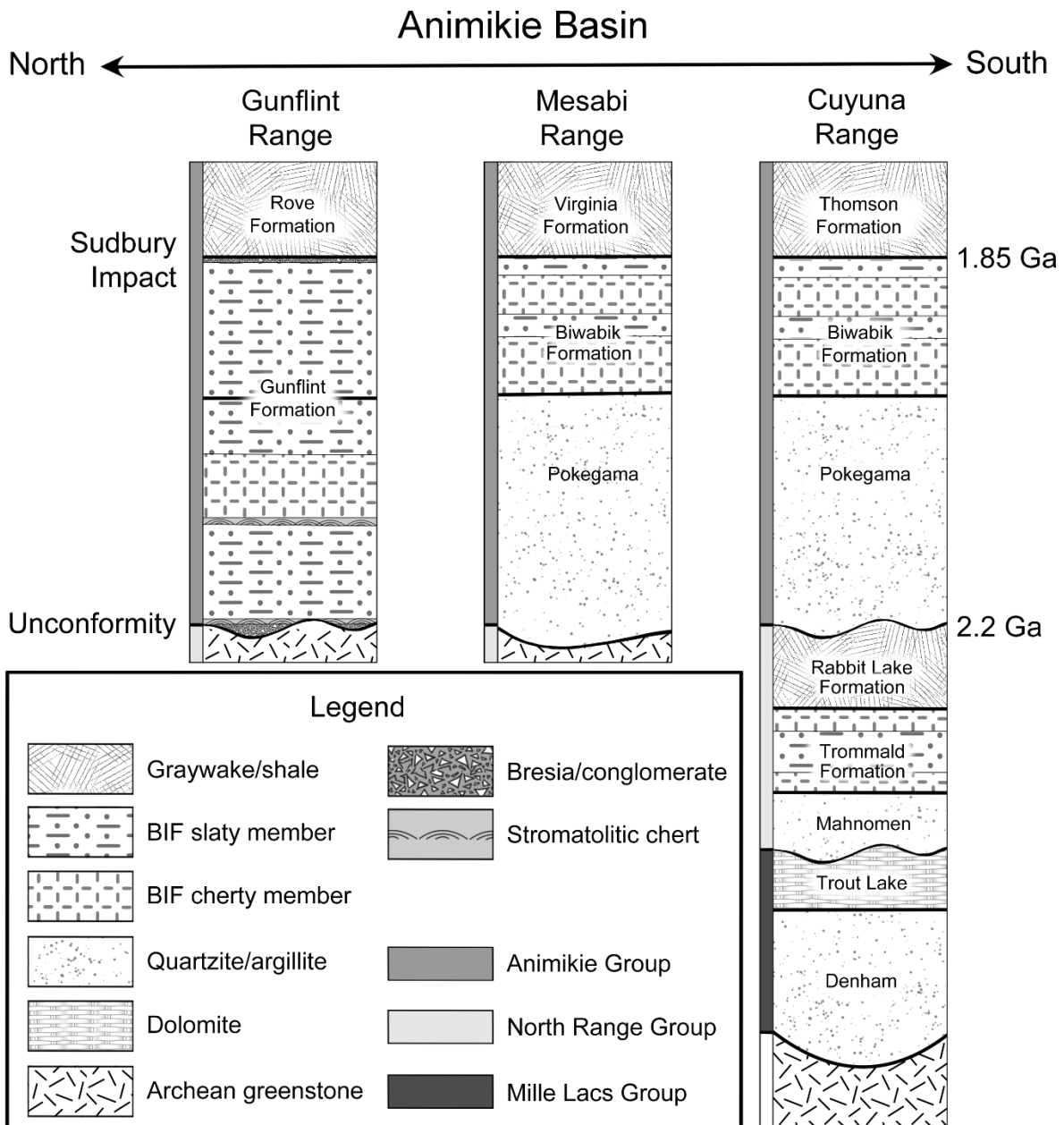


Figure 1.4 Stratigraphy of the major north- and western ranges of the Animikie Basin. Groups are depicted at the left side of each range's stratigraphic column. Adapted from White, 1954; Morey, 1983; McSwiggen et al., 1995; Ojakangas et al., 2001; Schulz and Cannon, 2007; Foley, 2009; and Craddock et al., 2013.

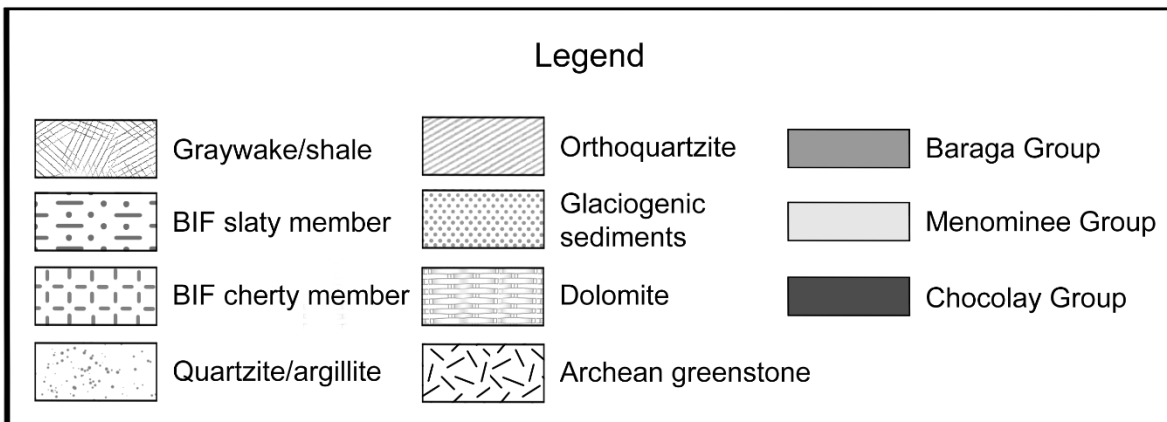
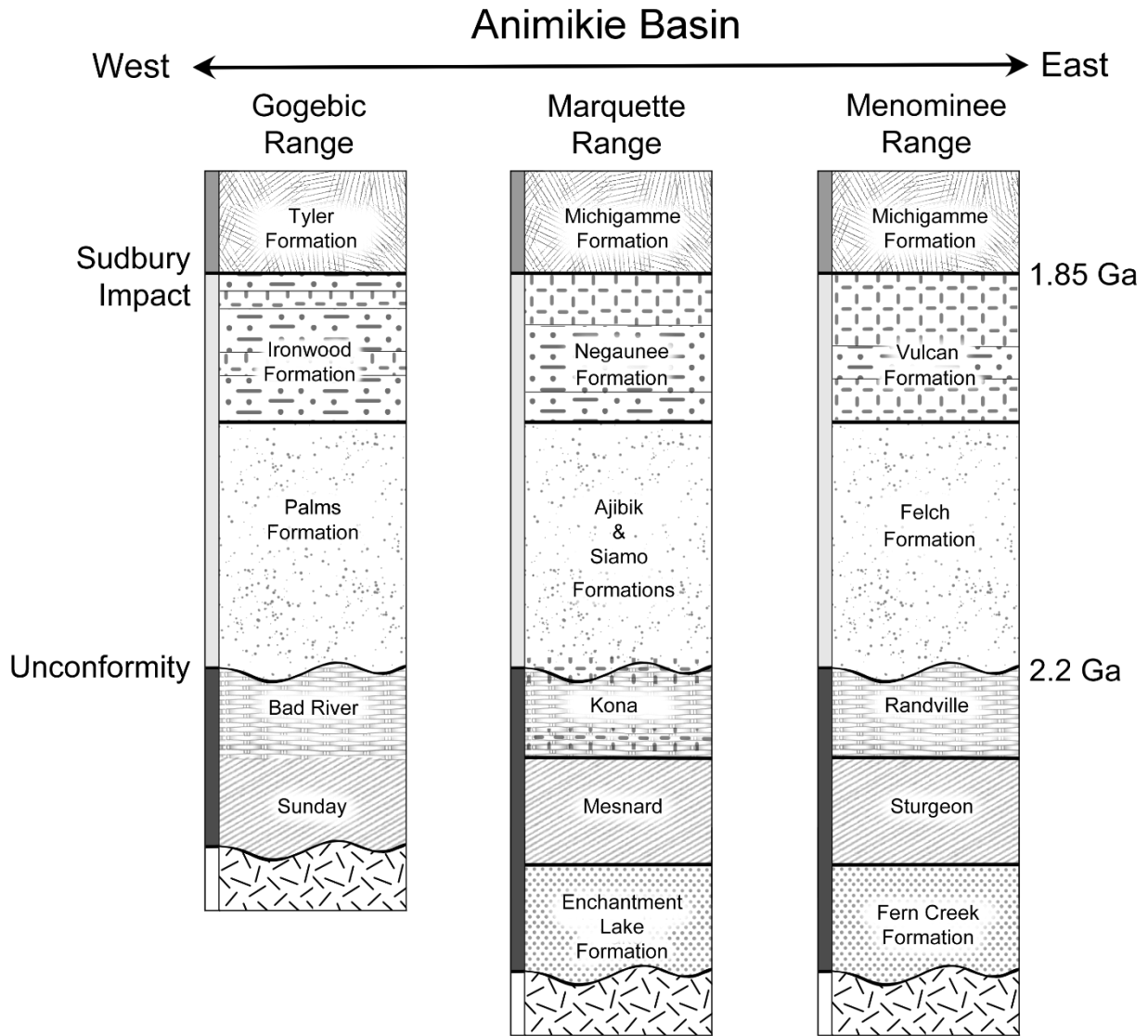


Figure 1.5 Stratigraphic sections of the southern ranges of the Animikie Basin. Groups are depicted at the left side of each range's stratigraphic column. Adapted from Adler, 1935; Cumberlidge and Stone, 1964; Laybourn, 1979; Morey, 1983; Ojakangas et al., 2001; Schulz and Cannon, 2007; Cannon et al., 2008; Craddock et al., 2013; Laird, 2017.

Banded iron formations (BIFs) occur in multiple areas (ranges) around the margins of this basin (Fig. 1.3; Klemic, 1970; Miller and Dransfield, 2011). Geographically, exposures of iron-rich units of this group define narrow belts or "ranges" where iron mine districts were once established (Fig. 1.4):

- i. The Gunflint Range is an inactive iron ore deposit to the northwest of Lake Superior, consisting of, in ascending order, the Gunflint Formation and the Rove Formation.
- ii. The Vermilion Range is an inactive ore deposit to the west of Lake Superior conformed by an iron banded formation and a taconite layer.
- iii. The Mesabi Range, an iron ore deposit to the west of Lake Superior, consisting, in ascending order, of the basal North Range Group, the Pokegama Quartzite layer, succeeded by the Biwabik Iron Formation that, in turn, is overlain by the Virginia Formation.
- iv. The Cuyuna Range is an inactive ore deposit to the south west of Lake Superior, comprising the Mahanomen layer and the overlying Trommald and Rabbit Lake formations.
- v. The Gogebic Range is an inactive ore deposit to the southwest of Lake Superior, composed by the Palms Formation, overlined the Ironwood Formation and the Tyler Formation.
- vi. The Iron River-Crystal Falls Range is an inactive ore deposit to the south of Lake Superior, comprising, in ascending order, the Fern Creek, Saunders, and the Vulcan Iron Formations.

- vii. The Marquette Range is an ore deposit to the south of Lake Superior, composed of, in ascending order, the Fern Creek Tillite, the Surgeon-Mesnard Quartzite, the Ajibik and Siamo Formations, and the Negaunee Iron Formation, overlain by the Michigamme slate.
- viii. The Menominee Range is an inactive ore deposit to the southeast of Lake Superior that consists, in ascending order, of the Fern Creek and Saunders formations, overlain by the Vulcan Iron Formation and Michigamme slate, and the Riverton Iron-Formation and Hiawatha graywacke.

Within the Animikie Basin, the Animikie Group is composed of sedimentary and metasedimentary rocks initially deposited between 2.5 and 1.8 Ga (Jirsa et al., 2004; Mueller, 2019). It includes passive continental margin deposition of basal sandstones, Superior-type BIFs (see more detail in section 1.4.1.1), such as the Gunflint Iron Formation, and upper turbidites (Ojakangas et al., 2001; Craddock et al., 2013).

The Gunflint Formation, also known as the Gunflint Iron Formation, is the basal part of the Gunflint Range, which stretches from northeastern Minnesota, USA, to northwestern Ontario, Canada (Fig. 1.3). Gabbro of the Duluth Complex, which intruded during the formation of the Midcontinent Rift, separates the Mesabi and Gunflint iron ranges (Ojakangas and Matsch, 1982). The iron deposit within this range is a Lake Superior-type BIF of Paleoproterozoic age.

1.4.1.1 Banded Iron Formations (BIFs)

BIFs typically exhibit alternating bands of dark rust-red and light gray rocks. The dark red bands are mainly composed of iron-oxide minerals in the forms of magnetite (Fe_3O_4) and/or

hematite (Fe_2O_3), whereas the lighter bands are chemically precipitated microcrystalline quartz, which occurs as chert in most cases (James, 1954; Trendall, 2002; Katsuta et al., 2012; Condie, 2015; Levin and King, 2017). The thicknesses of the iron and silica bands in BIFs can vary greatly, ranging from millimetres to metres (Trendall, 2002; Katsuta et al., 2012; Condie, 2015).

BIFs are commonly Archean or Paleoproterozoic in age. However, a minor amount of BIFs are Neoproterozoic (Klein, 2005; Ilyin, 2009; Bekker et al., 2010; Abd El-Rahman et al., 2019), usually associated with glacial deposits, often containing glacial dropstones (Klein, 2005). One of the youngest known BIF is an Early Cambrian formation in western China (Li et al., 2018). As BIFs are primarily restricted to early geologic time, it is generally assumed that they may reflect unique conditions of the Precambrian world, such as the relatively low oxygen content in both the atmosphere and the oceans during the early stages of the Great Oxygenation Event around 2.4–2.1 Ga (Cloud, 1973; Holland, 2006; Bau et al., 2022). Episodic occurrences of BIF deposits after 1.8 Ga (Slack and Cannon, 2009) may point to intermittent low levels of free atmospheric oxygen (Lyons and Reinhard, 2009). In contrast, the small peak of BIFs around 750 Ma may have been associated with the hypothetical Snowball Earth (Hoffman et al., 1998).

A BIF classification scheme has yet to be formally established (Trendall and Blockey, 2004). Gross (1980) advocated a twofold BIF classification based on the depositional settings of the basin: Algoma- and Lake Superior-type BIF. Algoma-type BIFs can be found in smaller basins and are associated with volcanic centers, whereas Lake Superior-type BIFs are found within larger basins and are commonly associated with black shales, quartzites, and dolomites formed along a continental margin (Gross, 1980).

Lake Superior-type BIFs primarily formed during the Paleoproterozoic and lacked the europium anomalies of the older Algoma-type BIFs, suggesting a much greater input of iron

weathered from continents (Klein, 2005; Li et al., 2015; Condie, 2015). Lake Superior-type BIFs occur commonly in four lithofacies: sulfide, carbonate, silicate, and oxide (James, 1954). These facies grade into each other in the field reflecting changes in the oxidation state of the water and occur as thin laminae alternating with chert layers (Fallacaro and Calvin, 2002). There are many different hypotheses for the origin of BIFs (Cairns-Smith, 1978; Cloud, 1983; Kappler et al., 2005; Goldblatt et al., 2006; Perkins, 2009; Holm, 2006; Benedetto, 2010; Bau et al., 2022). The most popular theory considers their formation to be primary sedimentary, but others argue for a secondary diagenetic origin (Bau et al., 2022). Being from a primary sedimentary origin, silicate and iron precipitates on the floors of shallow seas that partially flooded cratons would be the main source of BIFs (Benedetto, 2010; Levin and King, 2017). Estimates of BIF deposition rate based on sensitive high-resolution ion microprobe (SHRIMP) have shown the age of associated tuff beds range from 19–270 m/Ma, consistent with annual varves (Trendall and Blockley, 2004). However, Li et al. (2022) noted that restricted rate of upwelling and the low influx of detritus in Archean and Paleoproterozoic oceans would not provide strong support for these depositional models for Superior-type BIFs.

The first photosynthetic bacteria could have played a critical role in forming BIFs. The production of free oxygen would have caused the oxidation of the dissolved iron in seawater (Goldblatt et al., 2006). Oxidized iron is not very soluble in water; this may have resulted in its precipitation and deposition on the seafloor (Hem et al., 1962). The alternation of iron and silica bands can be explained by fluctuations in the population size of cyanobacteria; oxygen accumulation in the water became so abundant that iron could not neutralize all of it, thus reducing the number of cyanobacteria (Benedetto, 2010). The presence of cyanobacteria explains the younger iron formations that were deposited long after the Great Oxidation Event (see Goldblatt

et al., 2006), but this model does not apply to older formations (for example, the 3.8 Ga BIF in the Isua Group of Greenland), due to the low abundance of oxygen in Earth's atmosphere and hydrosphere prior to 2.4 Ga (Perkins, 2009). Another way to explain oxidation would be through the action of anoxygenic phototrophic bacteria (Kappler et al., 2005), a type of bacteria (e.g., purple sulphur bacteria) capable of carrying out non-oxygen-based oxidation of iron.

Iron can be oxidized with little oxygen by photochemical oxidation via exposure to solar ultraviolet radiation (Cairns-Smith, 1978; Kappler et al., 2005). Mesobanding, considered a boundary between bands of minerals, has also been interpreted as a secondary structure, not present in the sediment as initially laid down but produced during compaction of the sediment (Trendall and Blockley, 2004). It is also considered that mesobands could be primary structures resulting from pulses of activity along mid-ocean ridges that change reduced iron availability on time scales of decades (Morris and Horwitz, 1983). Another hypothesis suggests that BIFs are produced by seasonal changes in water temperature (Perkins, 2009).

The source of iron in BIFs has also been a debated topic. Although weathering of iron-bearing rocks on the continents are considered one of the primary sources of iron, a much more considerable amount could be attributed to submarine volcanoes and hydrothermal springs (vents) (Levin and King, 2017). Other possible sources include windblown dust, rivers, and glacial ice from continental margins (Cox et al., 2013).

As for the source of silica, recent studies on the composition of metachert bands from the Neoproterozoic Temagami BIF performed by Bau et al. (2022) show their formation occurred during times when seawater was dominated by low-temperature riverine input from the landmass.

1.4.2 *Gunflint Formation*

The Gunflint Formation (Animikie Group) can be broadly described as a succession largely composed of cherty granular and fine-grained banded/shaley varieties of sedimentary ironstone with lesser amounts of other rock types (Floran and Papike, 1975). Gunflint exposures are located along the north shore of Lake Superior, from northeastern Minnesota to northwestern Ontario (Fig. 1.3). The paleontological importance of the Gunflint Formation lies in the exceptional preservation of microfossils within the stromatolitic "Gunflint Chert" unit in the lower part of the formation (Barghoorn and Tyler, 1965; Cloud, 1965; Hofmann, 1971; Awramik and Barghoorn, 1977; Fralick et al., 2002). However, for context, it is important to describe the stratigraphy and explain the nomenclature of the Gunflint Formation as a whole. Since the earliest studies of the Gunflint Formation were made in its type of area (Gunflint Lake, Minnesota), the formation has been interpreted to have been deposited on the inner, shallow-water part of a marine platform influenced by strong wave and tidal activity (Wacey et al., 2012). It is considered to consist of four main intervals (e.g., Broderick, 1920) according to relative proportions of fine-grained or "slaty" and granular "cherty" sedimentary components. In ascending order, Broderick (1920) called these intervals the lower cherty, lower slaty, upper cherty, and upper slaty members (Fig. 1.6).

In a comprehensive study of the Gunflint Formation in Minnesota and Ontario, Goodwin (1956) noted the bulk of this stratigraphic interval to consist of six main facies: conglomerate, algal chert, taconite, tuffaceous shale, banded chert-carbonate and limestone. The conglomerate facies are restricted to the bottom of the formation, limestone forms the topmost unit, and the remaining four facies occur in two repeating cycles. A condensed description of Goodwin's (1956) main Gunflint facies is as follows:

1. The conglomerate facies appears only at the Gunflint Formation's base, where it unconformably overlies Archean basement rocks. The pebbles are mostly vein quartz and jasper, with the matrix composed of quartz grains and chloritic material depending on the composition of the basement rocks (typically either gneisses or metavolcanic rocks).
2. The "algal" (now more appropriately recognized as "stromatolitic") chert facies was described as being characterized by "reef-like mounds" composed of various thin layers of oolitic/granular chert, magnetite and dolomitic carbonate within and in between these structures.
3. The tuffaceous shale facies consists of black, fissile shale composed of altered volcanic material with thinly laminated bands of grey-black chert.
4. The "taconite" facies is compositionally variable both stratigraphically and geographically but can be generally described as consisting of granular particles of varying proportions of chert, greenalite (a hydrous ferrous silicate), siderite/ankerite (iron carbonate), dolomite and hematite/magnetite (iron oxides) with a chert matrix. Over the past few decades, the term "taconite" has essentially been replaced by the term "chert-carbonate grainstone" (e.g. Jirsa et al., 2011; Fralick et al., 2017). Small (cm-scale) carbonate grains (dolomite/calcite/ankerite) are locally present within this facies. In some places, this granular material contains a significant mudstone content, forming "shaly" units or containing lenses of jasper. In others, the granular material dominates over fine-grained components and forms units exhibiting wavy bedding to cross-bedding.

5. Banded chert-carbonate is described as being composed of gray and brown bands (cm- to dm-scale) of finely laminated chert with thicker bands (dm- to m-scale) of finely spherulitic siderite and cm-scale lenticles of carbonaceous material and fine-grained pyrite.
6. The "limestone" facies consists of limestone or dolostone inter-banded with chert and shale.

Goodwin (1956) described the overall Gunflint succession in Minnesota as beginning with a basal conglomerate unit. Two thicker intervals with a basal conglomerate unit overlain by two thicker intervals: the lower and upper Gunflint members. According to Franklin et al., 1991, the lower Gunflint member consists of, in ascending order: a thin unit of "algal chert" (referred to herein as stromatolitic chert), followed by tuffaceous shale, taconite (chert-carbonate grainstone) and banded chert-carbonate. The latter two facies interfinger and occur in different proportions depending on the area.

The upper Gunflint member follows a similar pattern as the lower member, starting with a thin unit of "algal" chert (upper algal chert) at its base and overlain successively by tuffaceous shale and varying proportions of taconite (chert-carbonate grainstone) and banded chert-carbonate. Overlying the upper Gunflint member and marking the top of the Gunflint succession is Goodwin's (1956) upper limestone member. Further details of the Gunflint succession in the Thunder Bay area were described by Moorhouse (1960) and Goodwin (1960). Moorhouse (1960) modified Goodwin's (1956) lower Gunflint member to extend from the basal conglomerate to a shaley "argillite-tuff" band just above the upper "algal" chert unit and considered the "upper Gunflint" to extend from this level to the base of the Rove Formation (Franklin et al., 1991).

Reflecting significant lateral facies changes between northeastern Minnesota and northwestern Ontario, the four-fold division of the Gunflint Formation established in Minnesota is not easily applied to the Gunflint succession in the latter region (Figure 1.6). However, based on the succession represented in drillcore 89-MC-1 obtained by the Canadian Ministry of Northern Development and Mines, Pufahl and Fralick (2000) recognized five members within the Gunflint Formation based on lithological characteristics. The drillhole location is approximately 50 km southwest of Thunder Bay, Ontario and approximately 250 km southwest of the Schreiber Beach outcrop, further discussed in section 1.4.2.3.

The five members of the Gunflint succession recognized in Pufahl and Fralick (2000) stratigraphic scheme are defined according to facies patterns (Figs. 1.6, 1.7). Member 1 includes the basal "Kakabeka" conglomerate and lower stromatolitic (a.k.a. "algal") chert described by Goodwin (1956). Member 2 consists of flaser, and wavy-bedded chert-carbonate grainstone referred to as "ribbon-carbonates," fining upwards to the middle of the member, then coarsening upward such that chert-carbonate grainstone becomes the dominant lithology at the top of the member. Member 3 is a unit containing stromatolitic chert resembling that observed in member 1. Member 4 comprises chert-carbonate grainstone that grades upward into laminated chemical (hematite and chert-rich) sediment. Finally, member 5 consists primarily of massive and cross-stratified chert-carbonate grainstones that coarsen upward to the member's top.

A more detailed stratigraphic log of the same drill core was presented by Jirsa et al. (2011), who noted the same five units as those cited by Pufahl and Fralick's (2000), plus an additional unit termed the "limestone member" at the top of the formation. Adopting a similar two-fold division as Goodwin (1956) and Moorhouse (1960), Jirsa et al. (2011) also divided the Gunflint succession into upper and lower parts (sequences), with members 1-3 included in the former, and members 4,

5 and the limestone member included in the latter. Another important detail noted by Jirsa et al. (2011) was thin zones of silicification at the tops of members 2 and 5, interpreted as surfaces of subaerial exposure.

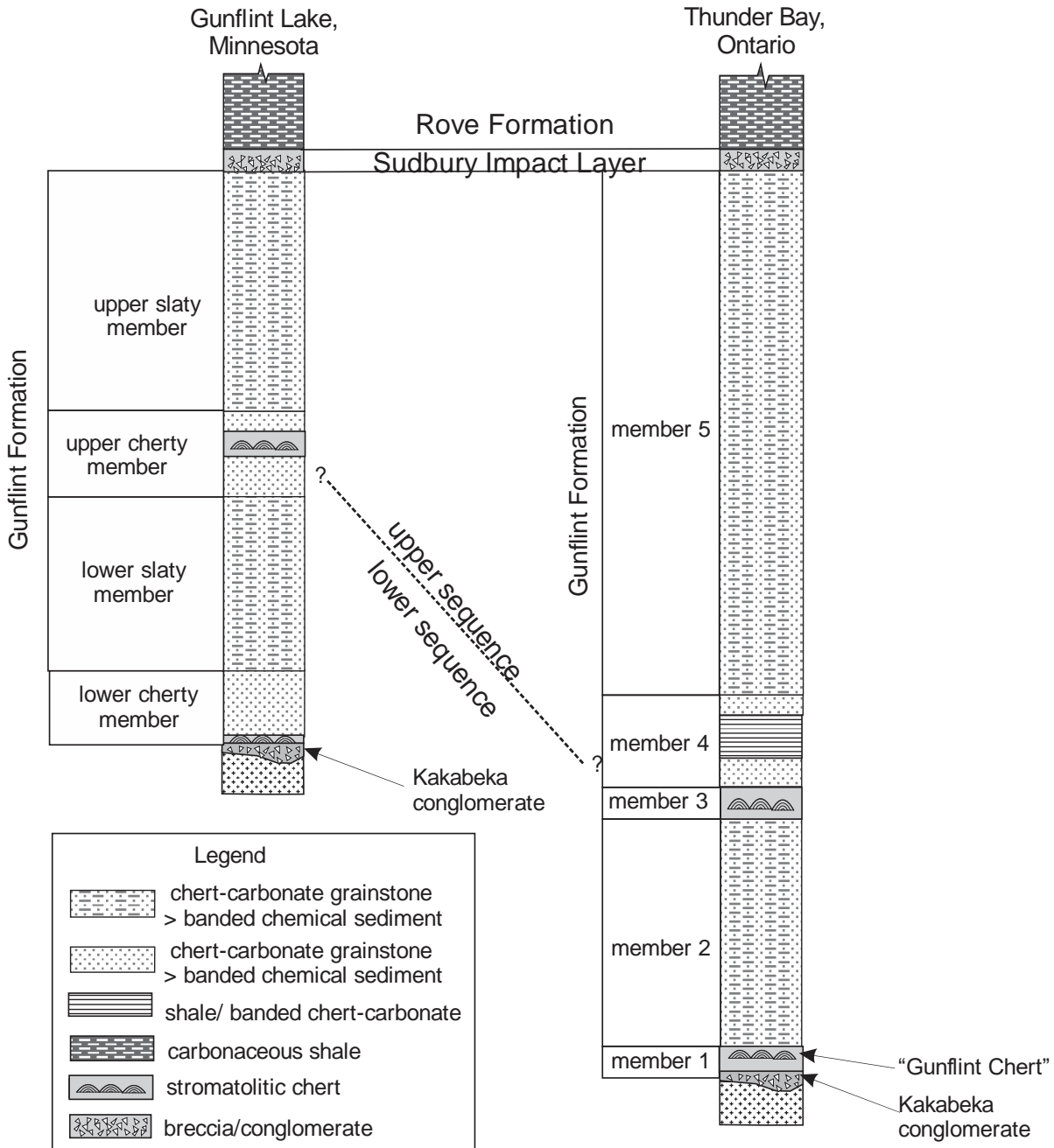


Figure 1.6 a) Schematic diagram comparing the Gunflint Formation divisions in Gunflint Lake, Minnesota and Thunder Bay, Ontario. Note that, aside from the Kakabeka conglomerate and stromatolitic chert units, the lithologic units within the formation are very different. Modified from Jirsa et al. (2011).

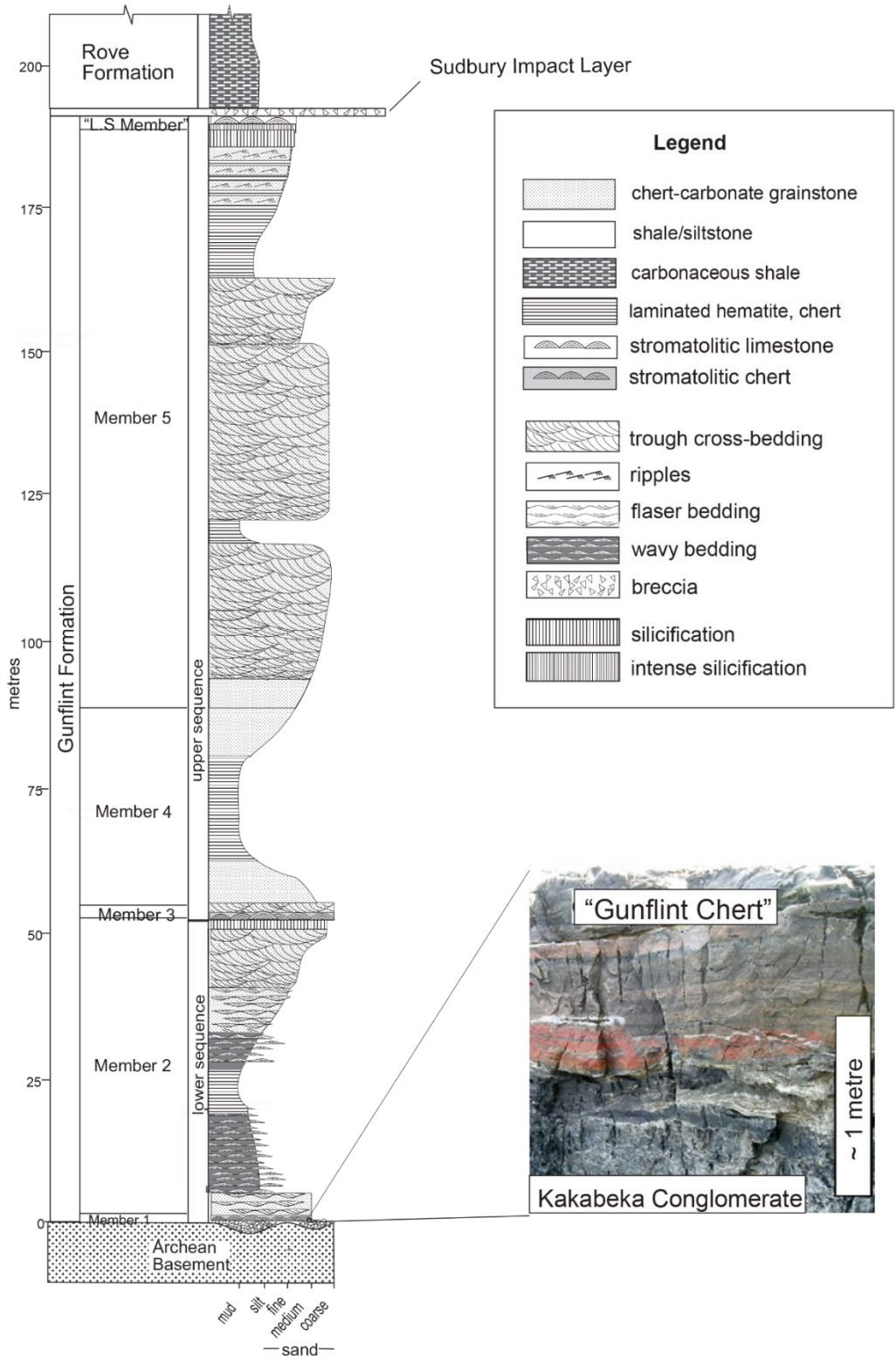


Figure 1.6 b) Stratigraphy of the Gunflint Formation north of Lake Superior based on an unweathered drill core 89-MC-1 taken ~ 50 km southwest of Thunder Bay (see figure 1.5 for the location of the corresponding drill hole). Modified from Fralick et al., 2002; Frei et al., 2009; Jirsa and Fralick, 2010; Jirsa et al., 2011; Frei and Polat, 2013 and Fralick et al., 2017). Close-up photo of Gunflint chert unit at Schreiber Beach outcrop showing stromatolitic structure (courtesy of Dr. Philip Fralick).

Pufahl and Fralick (2000) interpreted the Gunflint succession in the context of relative sea-level changes. The overall Gunflint Formation succession in the Thunder Bay area is interpreted to record at least one, and possibly two, transgressive-regressive cycles (Fig. 1.7). The Kakabeka conglomerate characterizes the base of the first cycle, a supratidal pebbly beach deposit unconformably overlying the Archean basement rocks. With further transgression came the deposition of parallel bedded chert-carbonate grainstone and establishment of stromatolites in the intertidal zone, and the deposition of flaser- and wavy-bedded chert-carbonate grainstones and interbedded shale under shallow subtidal conditions. Peak transgression was presumably reached at the unit of banded chert-carbonate in the middle of member 2, representing the finest-grained lithology in the member.

The lower relative sea level is suggested by an increase in the abundance of chert-carbonate grainstone with cross-bedding. If the silicified horizon at the top of member 2 was produced due to subaerial exposure, as interpreted by Fralick (1988), this feature presumably represents a surface of maximum regression. Member 3 marks the beginning of the next transgressive phase, in which stromatolites are again established in the intertidal zone, followed by the deposition of the chert-carbonate grainstone and banded chert-carbonate of member 4.

Pufahl and Fralick (2000) interpret the deposition of thick units of chert-carbonate grainstone in member 5 to have occurred with transgression to the top of the formation. However, if the silicified beds at the top of member 5 record subaerial exposure like that at the top of member 5 (Jirsa et al., 2011), this could indicate the culmination of a second regression at this level. Moreover, Fralick et al. (2017) recently described a stromatolitic limestone unit (possibly equivalent to Goodwin's (1956) "limestone member" at the top of the formation immediately above the highly silicified beds, suggesting deposition in the intertidal zone.

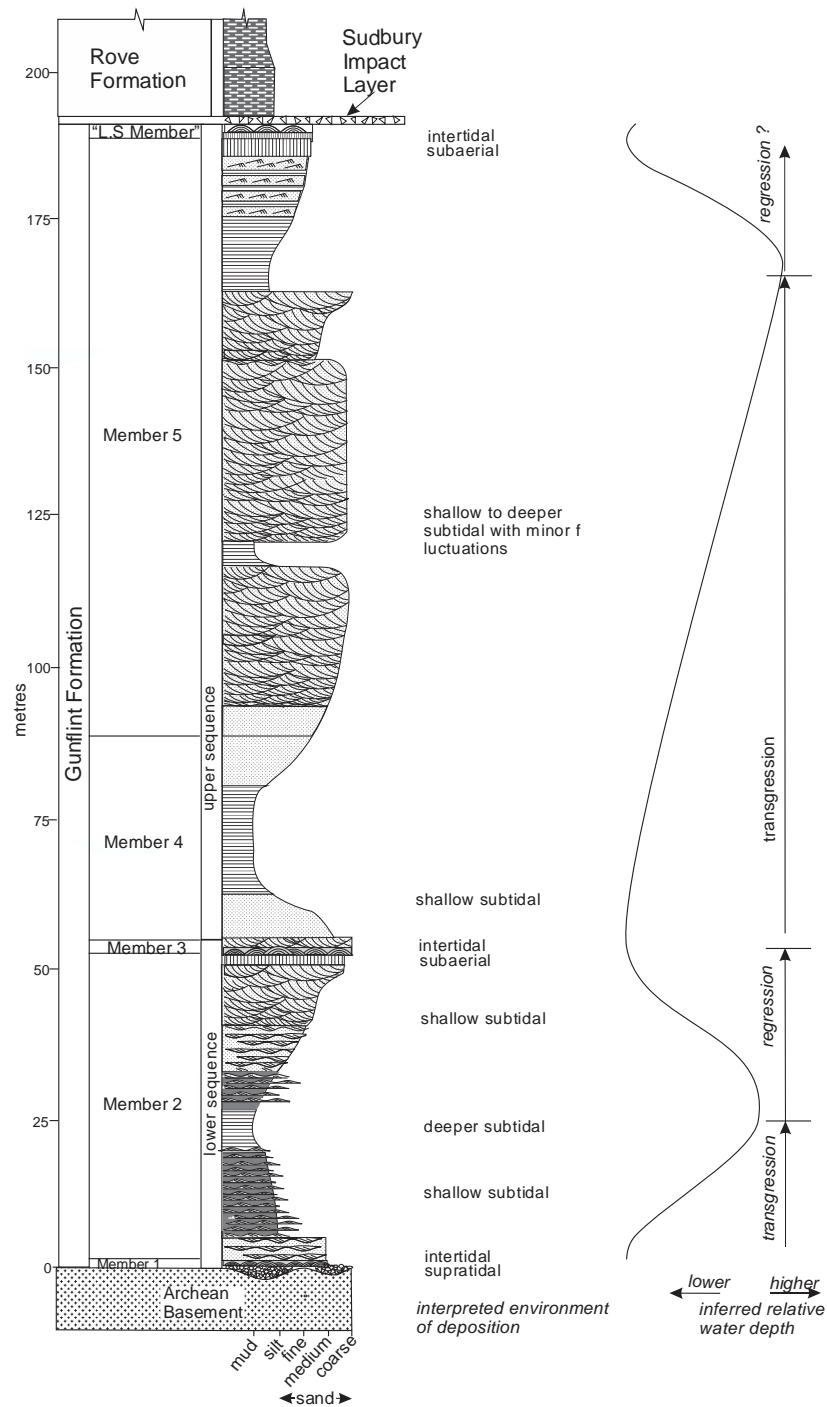


Figure 1.7 Stratigraphy of the Gunflint Formation based on an unweathered drill core 89-MC-1 with the interpretation of relative sea-level changes of Pufahl and Fralick (2000) from Gunflint members 1-5. Regression near the top of the formation added in consideration of silicified regression surface and stromatolitic upper limestone member reported by Fralick et al. (2017) (Modified from Fralick et al., 2002; Frei et al., 2009; Jirsa and Fralick, 2010; Jirsa et al., 2011, Frei and Polat, 2013 and Fralick et al., 2017). Symbols same as in legend for Fig. 1.4a.

The Gunflint Formation is overlain by the Sudbury Impact Layer (Figs. 1.6, 1.7), representing the ejecta blanket of the Sudbury meteorite impact event (Davis, 2008). The age of the Sudbury Impact Layer is approximately 1850 Ma (Craddock et al., 2013). In contrast, the lowermost beds of the Rove Formation have been dated at approximately 1832 Ma, suggesting a hiatus of at least 18 million years, during which the Sudbury impact deposits were exposed to subaerial weathering processes (Davis, 2008; Jirsa and Fralick, 2010). However, 1-6 metres of grainy ankeritic rocks above the Sudbury Impact Layer indicates that minor flooding events were possible during this time.

1.4.2.1 Gunflint Chert

The stromatolitic chert unit of the Gunflint Formation, marking the upper part of member 1 in the lower sequence of the Gunflint Formation, is referred to as the "Gunflint Chert" in this study as well as in those made by P. W. Fralick, M. A. Jirsa and P. K. Pufahl amongst others (Figs. 1.6, 1.7). This microfossil-bearing chert unit has an estimated age of $1878 \text{ Ga} \pm 1.3 \text{ Ma}$, as determined by uranium-lead dating techniques (Fralick et al., 2002; Frei and Polat, 2013) and it directly overlies the Kakabeka conglomerate unit which, in turn, unconformably overlies the Archean basement.

Chert is a fine-grained microcrystalline silica-rich sedimentary rock that can facilitate exceptional preservation of fossils (Knauth, 1979). Depending on its trace element content, it can range in colour from gray to brown, light green or red (Roberts et al., 1990; Mitchell, 1985). For

example, traces of iron commonly impart red and green colours depending on the oxidation state (Thurston, 1972). However, the Gunflint Chert unit is typically black (Fig. 1.8).



Figure 1.8 Photograph of several samples of the Gunflint Chert loaned by the Geological Survey of Canada (GSC). Samples GSC-24547, 24524, 24541, 24540, and 24547, along with their corresponding thin sections, are displayed here.

Chert breaks with a conchoidal fracture when struck with sufficient force to produce Hertzian cone patterns and very sharp edges. This property made chert an excellent material for tool-making in prehistoric times and was often used as a raw material to construct bladed stone tools (Jennings, 2011). Its use was also widespread throughout history in fire-starting tools such as tinderboxes and highly sought after for the manufacture of flintlock firearms, hence the term "gunflint."

The cryptocrystalline nature of chert and its hardness (7 on the Mohs scale) and above-average resistance to weathering, recrystallization and metamorphism make an ideal rock for preserving microfossils. The Gunflint Chert preserves bacteria (including cyanobacteria) and several unidentified organisms that resemble green algae and acritarchs (Schopf, 1999; Awramik and Barghoorn, 1977).

In addition to the 1.9 Ga Gunflint Formation, other relevant examples of chert units worldwide that are known to host Precambrian microfossils include the following:

- i) The Apex Chert of the Pilbara craton (3.5 Ga), Australia, contains eleven taxa of prokaryotes (Wacey et al., 2016).
- ii) The Fig Tree Formation (3.2 Ga) within the Barberton greenstone belt preserves non-colonial unicellular bacteria-like fossils (Barghoorn, 1971; Byerly et al., 1986).
- iii) The Bitter Springs Formation of the Amadeus Basin (850 Ma), Central Australia, contains chert beds with some of the most diverse Proterozoic fossils (Schopf, 1968; Schopf, 1992; Wacey et al., 2019).

1.4.2.2 Origin of the Gunflint Chert

Chert deposits in the Mesozoic and Cenozoic were initially deposited as siliceous ooze in deep-sea environments, composed of diatom and radiolarian tests. There is, however, strong evidence to suggest that Paleoproterozoic cherts, particularly those associated with iron formations, tended to be directly precipitated from seawater (Maliva et al., 2005).

Chert does not commonly form in isolation but tends to form in association with other rocks of a different type. Therefore, four hypotheses have been proposed for the origin of chert deposits:

- i. Biochemical secretion from silica-rich skeletons of diatoms, radiolaria, or siliceous sponges under certain burial conditions (Bates and Jackson, 1984; Maliva and Silver, 1989).
- ii. Diagenetic replacement in which microcrystals grow in irregular masses within soft calcareous sediment to ultimately produce nodules embedded in chalk or another form of limestone (Maliva and Silver, 1988; Hesse, 1989; Boggs, 2006).

- iii. Chemical precipitation characterized by fluctuating pH in waters with high silica content that precipitates sodium silicate minerals (Pufahl and Fralick, 2000; Maliva et al., 2005; Ding et al., 2017; Bau et al., 2022).
- iv. Replacement during formation of calcrete in fossil soils when silica dissolves from overlying volcanic ash beds (Hesse, 1989; Smith and Huckell, 2005).

The way in which chert units form remains a controversial topic, and the Gunflint Chert is no exception. The hypotheses mentioned above may bear various degrees of relevance to the origin of the Gunflint Chert.

In the particular case of the Gunflint Chert, the direct contribution of siliceous skeletons can be discounted because of the absence of siliceous skeletons (such as sponges, diatoms, and radiolarians) during the Paleoproterozoic, whereas biologically mediated SiO₂ precipitations remains a possibility. Diagenetic alteration of primary SiO₂ or other deposits was also a likely mechanism, as significant $\delta^{18}\text{O}$ variations determined from microquartz were thought to have been developed during diagenesis (Marin et al., 2010; Marin-Carbonne et al., 2012; Alleen et al., 2016).

Another suggested formation process for the Gunflint Chert combines the chemical precipitation and replacement methods. For example, the shallow ocean water of the Paleoproterozoic may have had a high content of silica due to acid rain and continuous ash propagation due to volcanic activity (Tosca et al. 2011; Michail, 2022). In addition, episodes of runoff of freshwater into the ocean may have lowered the pH of the ocean water, thereby encouraging the precipitation of the substantial amounts of silicate minerals (Heck et al., 2011).

1.4.2.3 Schreiber Beach Locality

Schreiber Beach, located about 10 km southwest of Schreiber, is within one of the lowest-strain domains in the Schreiber-Hemlo greenstone belt (Fig. 1.9). During the deposition of member 1 of the Gunflint Formation, the Schreiber beach location was likely a shallow marine (possibly intertidal; Pufahl and Fralick, 2000; Brown, 1993) environment, as indicated by the presence of filamentous cyanobacteria, stromatolites, and cross-bedded sandstones. It has also been suggested that the bottom conditions may have been shallow but oxygen-poor if the stromatolite-forming bacteria had iron-oxidizing metabolisms (Planavsky et al., 2009), but that the water surface should have been well-oxygenated (Curran, 2012).

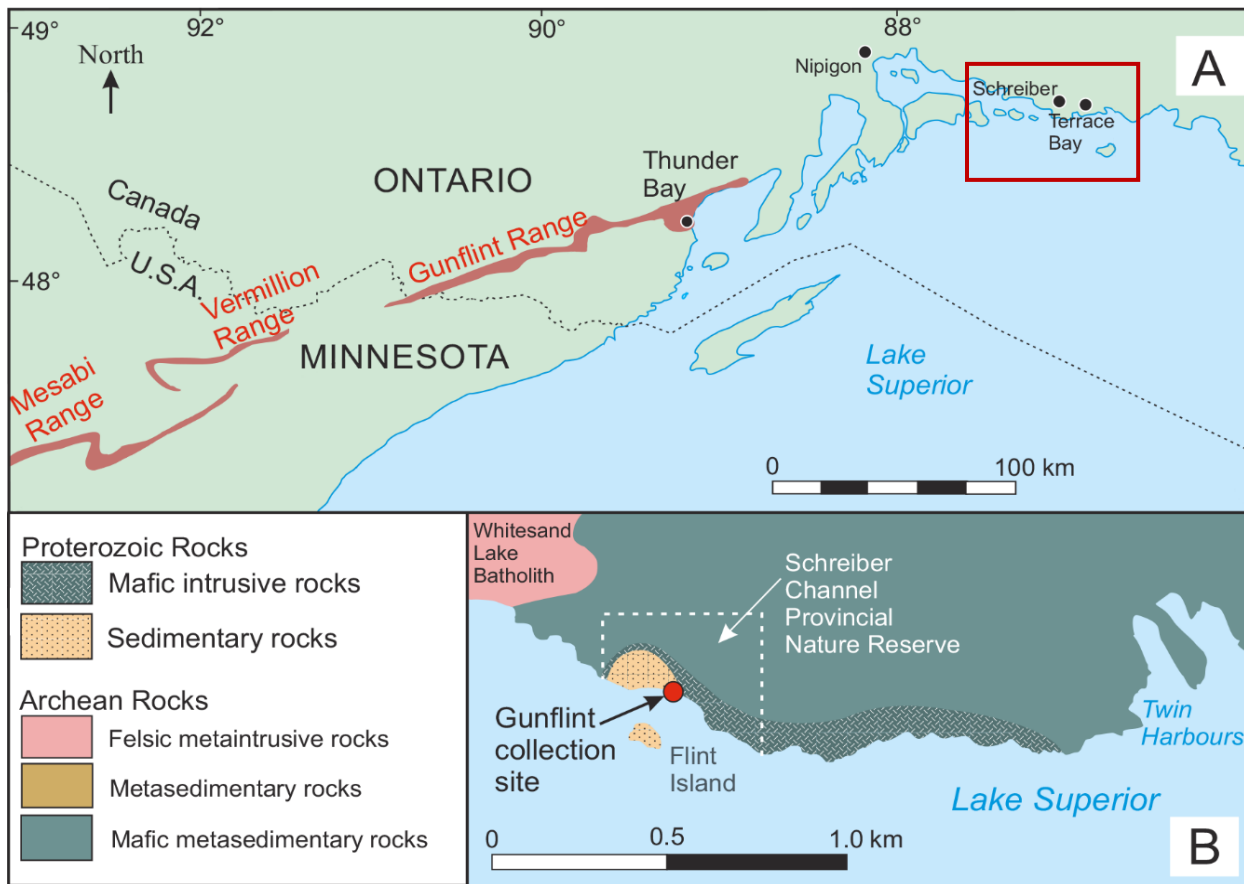


Figure 1.9 a) Lake Superior area map shows the Gunflint, Vermillion and Mesabi ranges and Thunder Bay, Schreiber and Terrace Bay localities. The location of drillhole 89-MC-1 is also indicated. b) Schreiber Channel Provincial Nature Reserve area outlined in rectangle in 1.7a pinpointing the sample collection site of Gunflint Chert samples for this study at Schreiber Beach (Modified from González-Flores et al., 2022).

The Schreiber Beach profile is unconformably underlain by a 0.5–3 m thick Paleoproterozoic basal conglomerate–breccia layer or by the 0.2–1 m thick Gunflint Chert (Fig. 1.6b). The basal conglomerate-breccia unit consists mainly of variably weathered greenstone, gneiss, quartz, and granitic clasts (Frei and Polat, 2013).

1.5 Origins of Eukaryotic Life on Earth

Prokaryotes and eukaryotes are two major divisions of life forms. Prokaryotes are organisms that have genetic material (DNA) that is not packaged into a membrane-bounded nucleus (Fig. 1.10). Instead, they reproduce asexually by cell division. Two of the three life domains, bacteria and archaea, are classified as these types of organisms (Black and Black, 2018). The oldest fossil prokaryotes appeared in the fossil record during the Archean, around 3.5 billion years ago. Because prokaryotes are asexual, simply dividing to reproduce, they are restricted in genetic variability (Table 1.1). For this reason, it might be that the evolution of prokaryotes through more than 2 billion years of Earth's history was slower than the rapid evolution of eukaryotes (Schopf, 1999; Levin and King, 2017).

Eukaryotes include protists, algae, fungi, plants, and animals, characterized by cells with membrane-bounded nuclei and organelles (Fig. 1.10). Eukaryote organelles perform specialized functions, such as photosynthesis by chloroplasts or respiration and metabolism by mitochondria. In addition, eukaryotes reproduce sexually, leading to the rapid increase in genetic variability and hence in the rate of evolution, which may have accelerated the origin and evolution of multicellular animals (Levin and King, 2017).

Putative evidence of eukaryotes extends back to 2.7 billion years ago, as the evidence comes from molecular "fossils" extracted from black shales of Archean age in north-western Australia

(Brocks, 2012), based on preserved organic molecules that only eukaryotes can synthesize (Levin and King, 2017). Such molecular evidence could be coming from contaminants from younger rocks. Knoll (2006) suggests they developed at approximately 1.6–2.1 Ga, and some acritarchs are known from at least 1.65 Ga in age (Table 1.1; Han and Runnegar, 1992; El Albani et al., 2010; Miao et al., 2019; Loron et al., 2021).

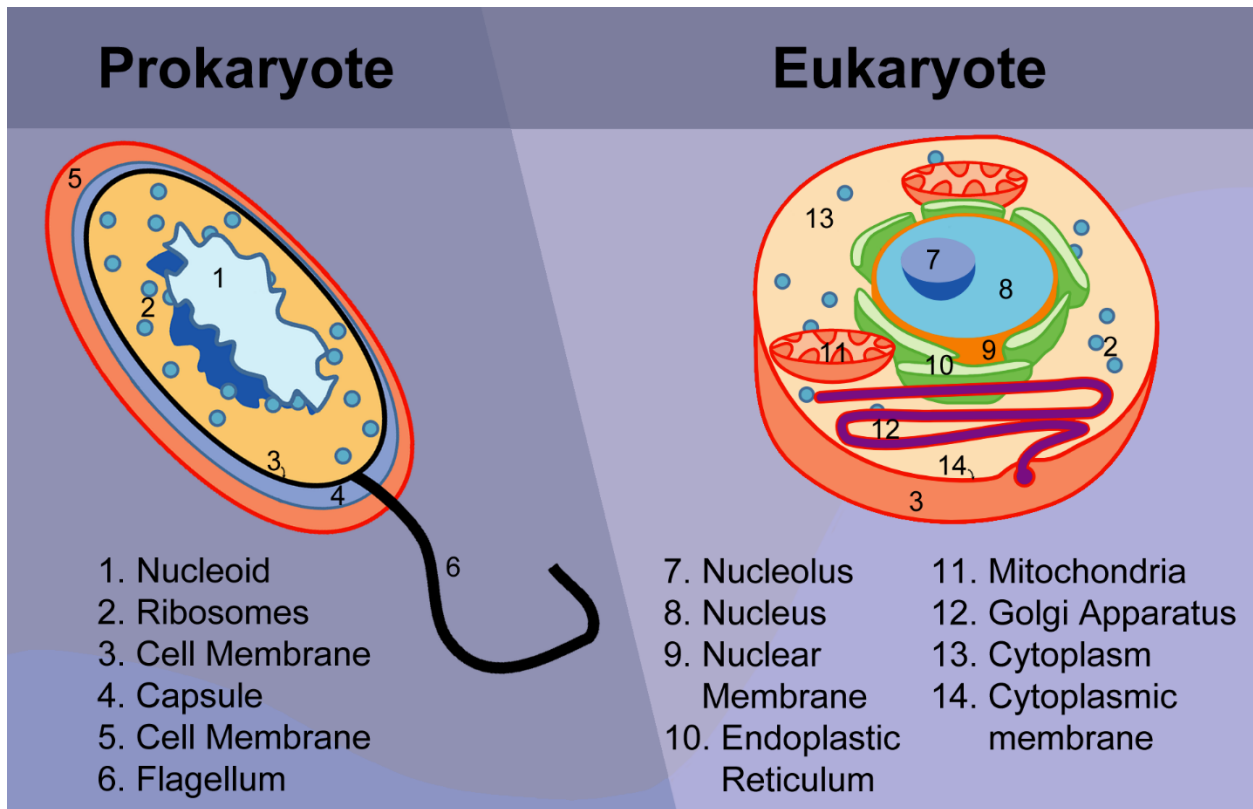


Figure 1.10 Differences between a prokaryote cell (left) and a eukaryote cell (right). Adapted from Science Primer (National Center for Biotechnology Information; 2005).

Table 1.1 Comparison of the main characteristics of prokaryotic and eukaryotic organisms (adapted from Levin and King, 2017).

	Prokaryotes	Eukaryotes
Organisms	Bacteria and Archaea	Protist, Fungi, Plants, and Animals
Cell size	1–10 micrometres	10–100 micrometres
Genetic organization	Loop of DNA in cytoplasm	DNA in chromosomes within membrane-bound nucleus
Organelles	No membrane-bound organelles	Membrane-bound organelles (chloroplasts and mitochondria)

Reproduction	Binary fission, dominantly asexual	Mitosis or meiosis, dominantly sexual
Fossil record first appearance	~3.5 Ga (Schopf, 1987; Gu, 1997; Brasier et al., 2005)	~1.6 Ga from body fossils (Miao et al., 2019) 2.7–2.2 Ga from molecular fossils (Brocks, 2012)

The evolution from prokaryotes to eukaryotes has been explained by the endosymbiosis hypothesis, proposed initially by Margulis (1970; see recent summary by Lane, 2016). In this hypothesis, a host cell would integrate other specialized cells, such as a cyanobacterium or heterotrophic bacterium, which eventually evolved into the chloroplast or mitochondria, respectively, within the host cell (Takemura, 2001; Bell, 2001; Wächtershäuser, 2003; Martin, 2005; Wächtershäuser, 2006).

1.6 Gunflint Microbiota

In terms of diversity, the microbiota of the Gunflint Chert can be considered an essential point of reference for the evolution of early life. Some of the best-preserved organic microfossils from the Precambrian have been found in the Gunflint Chert (Schopf and Kudryavtsev, 2012; Wacey et al., 2012; Brasier et al., 2015; Alleon et al., 2016). Similar types of microbiota have been found in other localities of approximately the same age as the Gunflint Chert; some of the most relevant examples include the following:

1) The 2,209 Ma Duck Creek Dolomite, north-western Australia (Knoll and Barghoorn, 1976; Knoll et al., 1988; Wilson et al., 2010; Barlow and Van Kranendonk, 2018).

2) The 1,946 Ma Frere Formation in the Nabberu Basin, Western Australia (Walter et al., 1976; Tobin, 1990; Grey, 1994).

3) The 2.68 Ga McLeary Formation, Belcher Islands, N.W.T., Canada (Hofmann and Jackson, 1969; Hofmann, 1976; Hodgskiss et al., 2019; Gabriel et al., 2021).

In contrast to other ancient microbiota found in chert units, those in the Gunflint Chert are unusually well preserved and display a variety of complex morphotypes with yet-undetermined taxonomic affinities (Fig. 1.11).

1.6.1 Identified Taxa in Previous Studies

From this vast pool of fossil microbial life forms, 28 species within the Gunflint Chert have been described by Awramik and Barghoorn (1977) and are listed in Table 1.2.

Table 1.2 Taxa reported from the Gunflint Chert and their provisional status by Awramik and Barghoorn (1977).

Taxon
<i>Anabaenidium barghoornii</i> Edhorn, 1973
<i>Animikiea septata</i> Barghoorn and Tyler, 1965
<i>Archaeorestis schreiberensis</i> Barghoorn and Tyler, 1965
<i>Chlamydomonopsis primordialis</i> Edhorn, 1973
<i>Cumulusphaera lamellosa</i> Edhorn, 1973
<i>Entosphaeroides amplius</i> Barghoorn and Tyler, 1965
<i>Eoastrion bifurcatum</i> Barghoorn and Tyler, 1965
<i>Eoastrion simplex</i> Barghoorn and Tyler, 1965
<i>Eomicrhystridium aremoricanum</i> Deflandre, 1968
<i>Eosphaera tyleri</i> Barghoorn and Tyler, 1965
<i>Glenobotrydion aenigmatis</i> Schopf 1968 (see Edhorn 1973)
<i>Gunflintia grandis</i> Barghoorn and Tyler, 1965
<i>Gunflintia minuta</i> Barghoorn and Tyler, 1965
<i>Huroniospora macroreticulata</i> Barghoorn and Tyler, 1965
<i>Huroniospora microreticulata</i> Barghoorn and Tyler, 1965
<i>Huroniospora psilata</i> Barghoorn and Tyler, 1965
<i>Kakabekia umbellata</i> Barghoorn and Tyler, 1965
<i>Palaeoanacystis irregularis</i> Edhorn, 1973
<i>Palaeorivularia ontarica</i> Korde, 1958 (see Oehler, 1976)
<i>Palaeoscytonema moorhousi</i> Edhorn, 1973
<i>Palaeospiralina minuta</i> Edhorn, 1973
<i>Palaeospiralis canadensis</i> Edhorn, 1973
<i>Palaeospirulina arcuata</i> Edhorn, 1973
<i>Primorivularia thunderbayensis</i> Edhorn, 1973
<i>Schizothrix atavia</i> Edhorn, 1973
<i>Sphaerophycus gigas</i> Edhorn, 1973
<i>Veryhachium?</i> sp. Hofmann, 1971
<i>Menneria levis</i> Lopukhin, 1971 (see also Lopukhin, 1975)

In previous studies, sixteen taxa from the Gunflint Chert have been divided into three categories: (1) blue-green algae; (2) budding bacteria; and (3) unassignable affinities, as summarized in Table 1.3.

Table 1.3 Affinities of the Gunflint Chert identified microfossils adapted from Awramik and Barghoorn (1977).

Blue-green Algae	<i>Gunflintia minuta</i>
	<i>Gunflintia grandis</i>
	<i>Animikiea septata</i>
	<i>Huroniospora spp.</i>
	<i>Corymbococcus hodgkissii</i>
	<i>Enterosphaeroides amplus</i>
Budding Bacteria	<i>Eoastrion simplex</i>
	<i>Archaeorestis schreiberensis</i>
	<i>Archaeorestis magna</i>
	<i>Kakabekia umbellata</i>
Unassignable Affinities	<i>Eomicrhystridium aremoricanum</i>
	<i>Eosphaera tyleri</i>
	<i>Xenothrix inconcreta</i>
	<i>Thymos halis</i>
	<i>Exochobrachium triangulum</i>
	<i>Galaxiopsis melanocentra</i>

Awramik and Barghoorn (1977) also determined that there are two distinct assemblage types. One is stromatolitic and dominated by cyanophytes (the *Gunflintia-Huroniospora* assemblage). The other (non-stromatolitic) assemblage type (*Eoastrion* assemblage) may have been planktonic in origin.

Most of the fossilized microorganisms in the Gunflint Chert have relatively small cells (< 4 µm in diameter) with simple walls typical of prokaryotes. Larger-sized structures with more complex morphologies in the category of “unknown affinities” will be the focus of this study.

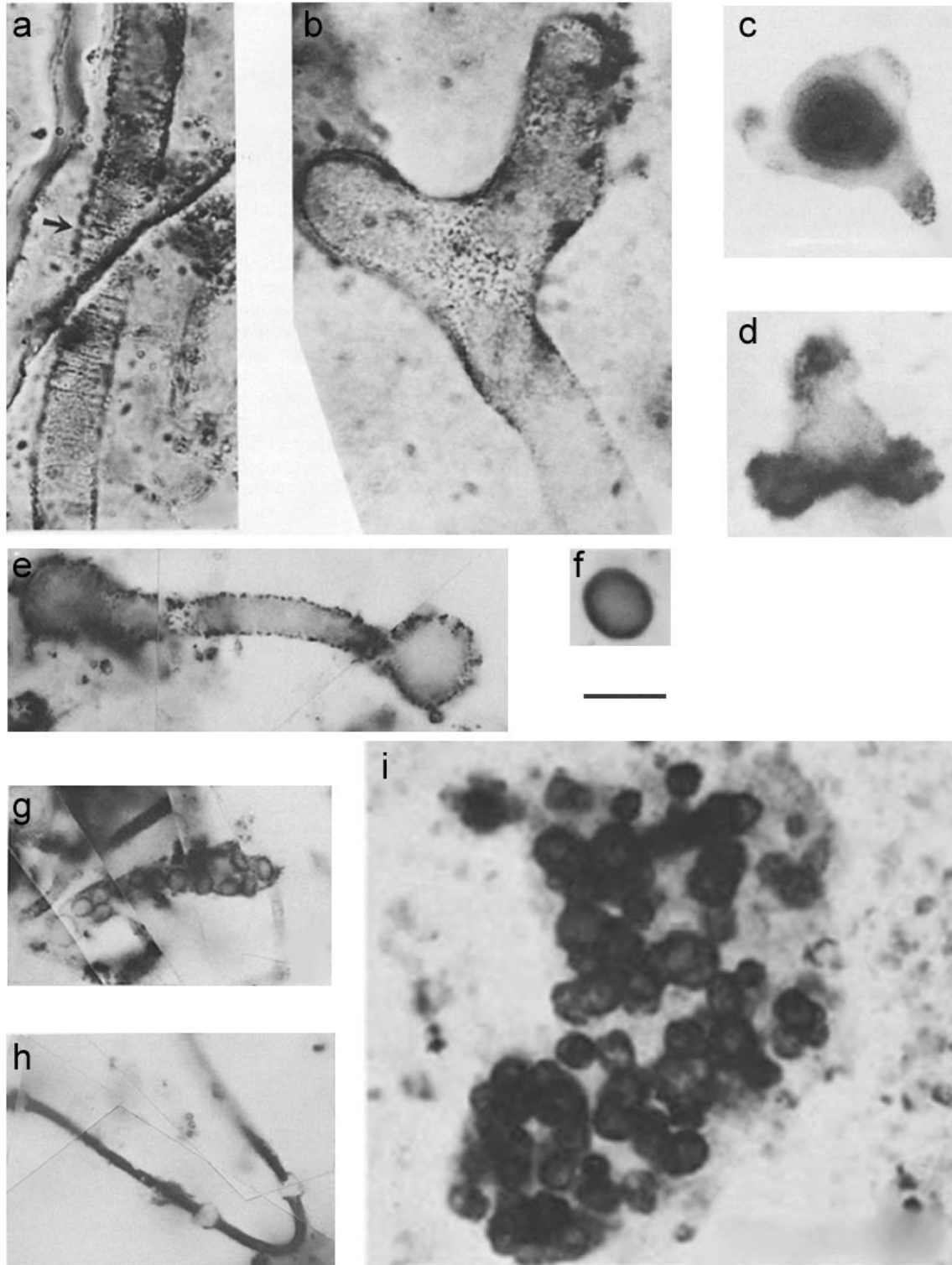


Figure 1.11 Optical microscopy images from several identified Gunflint Chert microorganisms. Scalebar = 10 μm for all specimens except for (i). a) *Animikiea septata*, type specimen from Barghoorn and Tyler (1965); b) *Archaeorestis magna*, type, Sch-W-57-CF-10, 38.9/103.7, 44485; c) *Galaxiopsis melanocentra*, type, FB4, 47.4/93.3, 44484; d) *Exochobrachium triangulum*, Sch-W-CF-11 ; 36.35/100/85, 44483; e) *Xenothrix inconcreta*, Sch-W-CF-11; 29.6/97.5, 44482; f) *Huroniospora*; g) *Thyrmos halis*, Sch-W-CF-11, 37.5/100.0, 44481; h) Trichome of *Gunflintia minuta* with possible heterocysts; i) *Corynbococcus hodgkissii*, Sch-W-CF-11; 35/99.4, 44480, Scalebar = 20 μm . Adapted from Awramik and Barghoorn (1977).

1.6.2 Microfossil Preservation

The Gunflint Chert microfossils usually show exceptional preservation compared with specimens from contemporaneous formations. This level of preservation is, in part, due to the low degree of metamorphic heating experienced by this unit (Shapiro and Konhauser, 2015), with an estimated burial temperature range of 100–130°C (Floran and Papike, 1978; Miyano and Klein, 1986; Winter and Knauth, 1992; Marin et al., 2010), or 150–170°C (Alleon et al., 2016). In addition, although the circulation of oxygenated hydrothermal fluids (Paces and Miller, 1993; Schulz and Cannon, 2007; Shapiro and Konhauser, 2015) may have locally increased the temperature of the site (Floran and Papike, 1978; Winter and Knauth, 1992), they did not induce any significant recrystallization of the microquartz matrix (Marin-Carbonne et al., 2012; Marin-Carbonne et al., 2013).

1.6.3 Biogenicity Debate of Gunflint Microfossils

As fossilized biomolecules may undergo significant degradation before, during or after burial, it may be challenging to determine whether organic microstructures in ancient rocks are biogenic (Schopf and Kudryavtsev, 2012; Alleon et al., 2016). The inevitable degradation of the fossilized specimens due to various factors (pre-and/or post-burial) presents difficulties not only in recovering biomarkers (Bernard and Papineau, 2014; Briggs and Summons, 2014) but also in recognition of morphological and geochemical signatures attributed to abiotic vs. biotic processes (García-Ruiz et al., 2003; McCollom and Seewald, 2006). Furthermore, the older the sample, the more likely fossil remains have been degraded somehow, thus making Precambrian samples subject to intense scrutiny. Also, the likelihood of second-hand contamination of samples cannot

be disregarded when working with microfossils of such age (Rasmussen et al., 2008; Dobrzhinetskaya et al., 2014).

Concerns about abiotic features possibly mimicking truly biotic features may be relevant to some relatively small fossils, such as the filamentous or spherical structures with diameters (or cross-sections) less than 2 μm . However, the relatively large microfossils preserved in the Gunflint Chert that occur alongside the ubiquitous cyanobacterium *Gunflintia* commonly have highly elaborate surface ornaments that essentially preclude the possibility of a non-biotic origin.

1.7 Astrobiological Significance of the Gunflint Chert Microfossils

Parallels exist between the search for life in space and investigations into the origin of life on Earth. Both require decoding evidence left behind from abiotic (physico-chemical) vs. potentially biotic processes (Brasier, 1980; Armstrong and Brasier, 2004) that can often be ambiguous. Not only is the type of studied information shared by both the search for life in outer space and deep in time, but they also share the same characteristic challenges.

One of the main problems both fields possess is that several physico-chemical processes can readily produce structures that closely resemble biogenic ones (Hopkinson et al., 1998; Ball, 1999; Brasier et al., 2006; Ball, 2009; Bailey et al., 2010). That can cause severe misinterpretation of the data and dismiss genuinely biogenic features as abiogenic. In these cases, a morphospace analysis is necessary to reject the null hypothesis of an abiogenic origin for candidate cells, which can be done by following the criteria of the centrality of cell theory (Hardin et al. 2011; Brasier, 2012). Protocols for demonstrating ancient or extraterrestrial life can be used to accomplish this goal. By drawing examples from Earth's geological record, Brasier and Wacey (2012) proposed a protocol

for testing for biogenicity in the early fossil record through meticulous screening of the locality data, fossil morphology, biological affinities, and chemical signals.

In this study, demonstration of biological behaviour or metabolism is considered critical for interpreting the eukaryotic affinity of some Gunflint microfossils. However in the study of early Precambrian fossil records, incomplete data sources usually hamper the screening process because of severe metamorphic and diagenetic alteration of rocks and the associated poor preservation of fossils (Rose et al. 2006; Antcliffe and McLoughlin, 2009).

The aforementioned issues represent the primary challenges of planetary science, paleomicrobiology, and astrobiology. Nevertheless, the advancement in instrumentation is constantly improving, allowing us to perform more accurate analyses. Furthermore, despite being relatively far from being able to directly study extraterrestrial samples and environments, the progress made in these fields allow us to create similar situations in the search for both extinct and extant life on other planetary bodies; such is the case of Mars (e.g., Brasier and Wacey, 2012; Vago et al., 2017; Lukmanov et al., 2018; Lukmanov et al., 2021, Lukmanov et al., 2022). The Gunflint Chert microfossils, similar to studying long-term preservation in the geological record, encourage the possibility of identifying similar structures in extraterrestrial samples, mostly from planets with highly oxidizing atmospheres and iron-rich environments (Schelble et al., 2004; Lukmanov et al., 2018; Lukmanov et al., 2021, Lukmanov et al., 2022).

As we try to find similarities in the processes of identifying extinct life in celestial bodies with a distinct possibility of life, recognizing complex fossil organisms poorly preserved on Earth could be the key to finding the much sought-after evidence of life on the Red Planet.

1.8 Materials and Analytical Methods

1.8.1 Gunflint Chert Samples

This study is based mainly on samples loaned from the Geological Survey of Canada (GSC). Samples were originally collected by the late Hans Hofmann in 1967 (see Hofmann, 1971) from a coastal outcrop of a small outlier (GSC Locality 78417), located approximately 10 km southwest of Schreiber Beach, within Schreiber Channel Provincial Reserve, Ontario, Canada (87°20'48"W, 48°47'50"N). The samples were collected prior to the establishment of the Gunflint Reserve in 1979. Among the loaned samples, sample GSC24380 was used for this study (Fig. 1.6) due to its high content of highly well-preserved microfossils. This sample was then divided into three main bulk pieces labeled as GSC24380, GSC24380d, and GSC24380e from which a total of six thin sections, two per bulk piece, were prepared from the sample. A smaller piece from GSC24380d was taken apart and used for other studies (e.g. SEM and Microprobe). Finally, four SEM studs were created from the remaining material of sample GSC24380d after being lightly etched with hydrofluoric (HF) acid.

1.8.2 Optical Microscopy

Optical microscopy was performed with two different microscopes:

- 1) The Zeiss Axioscope with a 100x oil lens and a 1.6x intermediate lens, achieving a combined 160x optical magnification.
- 2) The Nikon Eclipse LV100 POL microscope at the UWO EPMAL Optical Microscopy Laboratory with a magnification of 100x.

Within the field of optical microscopy, confocal microscopy in particular, possesses several advantages over other conventional methods. One of such advantages is the ability to control the depth of field when imaging. It also offers the possibility of collect serial optical sections, or Z-

sections, from thick specimens. Thus, eliminating or reducing background information away from the focal plane that usually leads to image degradation. To eliminate out-of-focus light when imaging any kind of specimen (even ones with thickness that exceed the immediate plane of focus), the confocal approach takes advantage of spatial filtering techniques (Fellers and Davison, undated).

This technique is ideal for the study of cell biology due to the high-quality images that can be obtained with relative ease from hard-to-image specimens like living cells and tissue, which are commonly prepared and examined through conventional fluorescence microscopy. (Fellers and Davison, undated) For this exact reason, the use of this technique for the study of uni- and multicellular microfossils was chosen, getting images of excellent quality.

Confocal image sequences were acquired manually and processed by using the Extended Depth of Focus (EDF) function of the Nikon NIS Elements imaging software package (ver. 4.1 and ver. 5.02). Thus, a Z-series of confocal images, with approximately equal intervals of focal depth, was combined into a single EDF image. For spherical objects, EDF images of the lower and the upper hemispheres were created separately to avoid overlap of cell surface features of the two hemispheres.

This method was used on the six thin sections created from samples GSC24380 (2), GSC24380d (2), and GSC24380e (2). Each of them was scanned at a relatively small-scale magnification in order to locate the same specimens repeatedly and more easily, followed by a complete scan of the sample through the optical microscope. Images of the best samples were taken, compiled and processed using the EDF software.

1.8.3 Scanning Electron Microscopy (SEM)

Scanning electron microscopy (SEM) with energy dispersive X-ray spectroscopy (EDX) was conducted at the Nanofabrication Facility, Western University (Fig. 1.11). Using a highly focused (primary) electron beam, high resolution images of surface topography can be produced with excellent depth of field. This is mainly due to the generation of many low energy secondary electrons as the beam enters the surface of the sample with an energy range of 0.5–30 kV. Hence, by measuring the secondary electron intensity as a function of the position of the scanning primary electron beam, an image of the sample surface can be constructed. Due to the high spatial resolution and high sensitivity to topographic features on the outermost surface, this analytical method is optimal for the study of microfossils with intricate patterns on their surfaces.

To avoid any external contaminants on the sample – like oil, dirt, etc. – SEM was performed using the LEO (Zeiss) 1540XB FIB/SEM at the ultra-clean Nanofabrication Facility, Western University to obtain BSE images at 1.00 and 5.00 kV. Sample GSC24380d was broken apart in order to obtain smaller pieces (creating four studs) to fit the SEM sample chamber for SEM imaging. The sample of chert to be examined in SEM was lightly etched in HF (5%), then sonicated in deionized water for 15 minutes, and then allowed to dry on a hotplate set at 115°C. The chert was then placed in a beaker of heptane, covered with a watch glass, and allowed to soak for 60 minutes. The sample was then removed and dipped in a second beaker of fresh heptane, which served as the final rinse. The chert was then allowed to air dry overnight in a fume hood. The purpose of the heptane was to de-grease the sample before SEM imaging.

In-situ elemental analysis via Energy Dispersive X-ray (EDX) analysis was performed using the Oxford Instruments X-ray system to generate maps for selected locations of the sample of elements such as carbon (C), oxygen (O), silicon (S), aluminum (Al), sodium (Na), and chlorine (Cl).

1.8.4 Electron Microprobe Analysis (EMPA)

As a non-destructive analytical technique, this tool used to determine the chemical composition of small volumes of solid materials. In principle, it functions similar to the SEM wherein the sample is also bombarded with electrons, causing the emission of x-rays with wavelengths characteristic of each element, thus allowing the analysis of the chemical composition of the sample. These x-rays are classified into two types: wavelength dispersive X-ray spectroscopy (WDS) or energy dispersive X-ray spectroscopy (EDS). Its high-precision, high-accuracy micron- to submicron-scale point analysis with typical detection limits in the 10s–100s of ppm makes this analysis an optimal candidate to obtain high quality images of the microfossils of the Gunflint Chert (Alleon et al., 2016).

Through wavelength dispersive X-ray spectroscopy (WDS) analysis, the chemical composition of thin section samples GSC24380d and GSC24380e was determined with the JEOL JXA-8530F field-emission Electron Microprobe in the Earth and Planetary Materials Analysis (EPMA) Laboratory, Western University. For this analysis, the samples were carbon coated. Backscattered-Electron (BSE) images were obtained with a magnification between 4.00 to 7.00 KX and EHT of 15.0 kV.

1.9 Thesis Structure

- **Chapter 1** —Background information about stratigraphy, paleogeography, paleoclimate and previous studies of the Gunflint biota that are relevant to this study.

- **Chapter 2** — Morphologic analysis of the different types of complex unicellular bodies (CUBs) observed in the Gunflint Chert and interpretation of their biological affinities, supplemented by SEM and geochemical analyses.
- **Chapter 3** — Systematic description of a key CUB species with the best-preserved eukaryotic morphological characteristics.
- **Chapter 4** — Conclusions.

1.10 Goals and Objectives

This study aims to provide more detailed high-resolution images of the “unidentified” microfossils from the Gunflint Chert microbiota, focusing on those that show complex cell morphologies. These morphological data will be used to test the following hypotheses:

1. These complex microfossils are indeed biotic in origin, making them part of the Gunflint Chert microbiota instead of being considered as abiotic processes that appear within the cherty matrix.
2. The microfossils with complex cell surface ultra-structures imply the presence of a cytoskeletal cell wall, an indicator of eukaryotic life forms.

To achieve these research goals stated above, the present thesis will encompass the following approaches and specific objectives:

- Provide an in-depth study of all the complex unicellular bodies (CUBs) and “multicellular” forms, hitherto lumped in the category of “unknown affinities” and investigate their possible affinities to eukaryotes.

- Provide a focused micropaleontological/systematic description of a key CUB form that has continuous geological range from the Paleoproterozoic to the early Cambrian, which will contribute to tracking the evolutionary history of the most eukaryote-like microfossils from the Gunflint Chert, and shed some light on the origin and early evolution of eukaryotes.

References

- Abd El-Rahman, Y., Gutzmer, J., Li, X.H., Seifert, T., Li, C.F., Ling, X.X., and Li, J., 2019, Not all Neoproterozoic iron formations are glaciogenic: Sturtian-aged non-Rapitan exhalative iron formations from the Arabian–Nubian Shield: *Mineralium Deposita*, v. 55, n. 3, p. 577–596.
- Alleon, J., Bernard, S., Le Guillou, C., Marin-Carbonne, J., Pont, S., Beyssac, O., McKeegan, K.D., and Robert, F., 2016, Molecular preservation of 1.88 Ga Gunflint organic microfossils as a function of temperature and mineralogy: *Nature Communications*, v. 7, n. 1, p. 1–11.
- Anbar, A.D., and Knoll, A.H., 2002, Proterozoic ocean chemistry and evolution: a bioinorganic bridge?: *Science*, v. 297, n. 5584, p. 1137–1142.
- Antcliffe, J.B., and McLoughlin, N., 2009, Deciphering Fossil Evidence for the origins of life and the origins of animals: common challenges in different worlds. In *From Fossils to Astrobiology. Records of Life on Earth and the Search for Extraterrestrial Biosignatures*, ed. Springer, Dordrecht, Seckbach, J. and Walsh, M., pp. 211–232.

- Armstrong, H.A., and Brasier, M.D., 2004, *Microfossils*: Blackwell Publishing, Oxford, 2nd edn, p. 304.
- Awramik, S.M., and Barghoorn, E.S., 1977, *The Gunflint microbiota: Precambrian Research*, v.5, p. 121–142.
- Bailey, J.V., Raub, T.D., Meckler, A.N., Harrison, B.K., Rauub, T.M.D., Green, A.M, and Orphan, V.J., 2010, Pseudofossils in relict methane seep carbonates resemble endemic microbial consortia: *Palaeogeography Palaeoclimatology Palaeoecology*, v. 285, p. 131–142.
- Ball, P., 1999, *The self-made tapestry. Pattern Formation in Nature*: Oxford University Press, New York, p. 287.
- Ball, P., 2009, *Branches. Nature's Patterns: A Tapestry in Three Parts*: Oxford University Press, New York, p. 221.
- Barghoorn, E.S., 1971, The oldest fossils. *Scientific American*: v. 224, no. 5, p. 30–43.
- Barghoorn, E.S., and Tyler, S.A., 1965, Microorganisms from the Gunflint Chert: *Science*, v. 147, p. 563–577.
- Barlow, E.V., and Van Kranendonk, M.J., 2018, Snapshot of an early Paleoproterozoic ecosystem: Two diverse microfossil communities from the Turee Creek Group, Western Australia: *Geobiology*, v. 16, n. 5, p. 449–475.
- Bates, R.L., and Jackson, J., 1984, *Dictionary of Geological Terms*, 3rd Ed. American Geological Institute: Doubleday. p. 85. ISBN 0385181019. OCLC 465393210.
- Bau, M., Frei, R., Garbe-Schönberg, D., and Viehmann, S., 2022, High-resolution Ge-Si-Fe, Cr isotope and Th-U data for the Neoproterozoic Temagami BIF, Canada, suggest primary origin

- of BIF bands and oxidative terrestrial weathering 2.7 Ga ago: *Earth and Planetary Science Letters*, v. 589, p. 117579.
- Bekker, A, Slack, J.F., Planavsky, N., Krapez, B., Hofmann, A., Konhauser, K.O., and Rouxel, O.J., 2010, Iron formation: the sedimentary product of a complex interplay among mantle, tectonic, oceanic, and biospheric processes: *Economic Geology*, v. 105, n. 3, p. 467–508.
- Belica, M.E., Piispa, E.J., Meert, J.G., Pesonen, L.J., Plado, J., Pandit, M.K., Kamenov, G.D., and Celestino, M., 2014, Paleoproterozoic mafic dyke swarms from the Dharwar craton; paleomagnetic poles for India from 2.37 to 1.88 Ga and rethinking the Columbia supercontinent: *Precambrian Research*, v. 244, p.100–122.
- Bell, P.J. 2001, Viral eukaryogenesis: was the ancestor of the nucleus a complex DNA virus?: *Journal of Molecular Evolution*, v. 53,n. 3, p. 251–256.
- Benedetto, J.L., 2010, Capítulo 2. El tiempo profundo: El Eón Arcano. El continente de Gondwana a través del tiempo. Una introducción a la Geología Histórica: Academia Nacional de Ciencias. p. 373. ISBN 9789879831373.
- Bernard, S., and Papineau, D., 2014, Graphitic carbons and biosignatures: *Elements*, v. 10, p. 435–440.
- Bispo-Santos, F., D’Agrella-Filho, M.S., Pacca, I.I., Janikian, L., Trindade, R.I., Elming, S.A., Silva, J.A., Barros, M.A., and Pinho, F.E., 2008, Columbia revisited: Paleomagnetic results from the 1790 Ma colider volcanics (SW Amazonian Craton, Brazil): *Precambrian Research*, v. 164, n. 1–2, p.40–49.
- Black, J.G. and Black, L.J., 2018, *Microbiology: principles and explorations*. John Wiley & Sons.

- Blackburn, C.E., 2010, Report on Selected Precambrian Environments in the Province of Ontario for Ontario Parks, Ministry of Natural Resources: Blackburn Geological Services Victoria, B.C., p. 22–40.
- Blatt, H., Middleton, G., and Murray, R., 1980, Origin of sedimentary rocks: Prentice-Hall, p. 576.
- Boggs, S., 2006, Principles of sedimentology and stratigraphy (4th ed.). Upper Saddle River, N.J.: Pearson Prentice Hall. pp. 208–210. ISBN 0131547283.
- Brasier, M.D., 1980, Microfossils: Unwin Hyman, London, p. 193.
- Brasier, M.D., 2012, Secret Chambers: The Inside Story of Cells and Complex Life: Oxford University Press, New York, p. 256.
- Brasier, M.D., and Wacey, D., 2012, Fossils and astrobiology: new protocols for cell evolution in deep time: *International Journal of Astrobiology*, v. 11, n. 4, p. 217–228.
- Brasier, M.D., Antcliffe, J., Saunders, M., and Wacey, D., 2015, Changing the picture of Earth's earliest fossils (3.5-1.9 Ga) with new approaches and new discoveries: *Proceedings of the National Academy of Sciences*, v. 112, p. 4859–4864.
- Brasier, M.D., Green, O.R., Lindsay, J.F., McLoughlin, N., Steele, A., and Stoakes, C., 2005, Critical testing of Earth's oldest putative fossil assemblage from the ~ 3.5 Ga Apex chert, Chinaman Creek, Western Australia: *Precambrian Research*, v. 140, n. 1–2, p. 55–102.
- Brasier, M.D., McLoughlin, N., Green, O.R., and Wacey, D., 2006, A fresh look at the fossil evidence for early Archaean cellular life: *Philosophical Transactions of the Royal Society B*, v. 361, p. 887–902.

- Brennan, D.T., Mahoney, J.B., Li, Z.X., Link, P.K., Evans, N.J., and Johnson, T.E., 2021, Detrital zircon U–Pb and Hf signatures of Paleo-Mesoproterozoic strata in the Priest River region, northwestern USA: A record of Laurentia assembly and Nuna tenure: *Precambrian Research*, v. 367, p.106445.
- Briggs, D.E.G., and Summons, R.E., 2014, Ancient biomolecules: their origins, fossilization, and role in revealing the history of life: *Bioessays*, v. 36, p. 482–490.
- Brocks, J.J., 2012, Molecular fossils and the late rise of oxygenic photosynthesis: EGU General Assembly Conference Abstracts, p. 8419.
- Brocks, J.J., Logan, G.A., Buick, R., and Summons, R.E., 1999, Archean molecular fossils and the early rise of eukaryotes: *Science*, v. 285, no. 5430, p.1033–1036.
- Broderick, T.M., 1920, Economic geology and stratigraphy in the Gunflint iron district, Minnesota: *Economic Geology and the Bulletin of the Society of Economic Geologists*, v. 15, p. 422–452.
- Brown, G.H., 1993, Geology of Oliver Township, District of Thunder Bay: Ministry of Northern Development and Mines, Ontario Geological Survey, Open File Report 5859.
- Byerly, G.R., Lower, D.R., and Walsh, M.M., 1986, Stromatolites from the 3,300–3,500-Myr Swaziland Supergroup, Barberton Mountain Land, South Africa: *Nature*, v. 319 no. 6053, p. 489–491.
- Cairns-Smith, A.G., 1978, Precambrian solution photochemistry, inverse segregation, and banded iron formations: *Nature*, v. 276 p. 0028–0836, 807–808.

- Canfield, D.E., 2005, The Early History of Atmospheric Oxygen: *Earth and Planetary Sciences*, v. 33, p. 1–36.
- Cannon, W.F., 1976, Hard iron ore of the Marquette Range, Michigan: *Economic Geology*, v. 71, p. 1012–1028.
- Cannon, W.F., LaBerge, G.L., Klasner, J.S., and Schulz, K.J., 2008, The Gogebic iron range—A sample of the northern margin of the Penokean fold and thrust belt (No. 1730). US Geological Survey.
- Cannon, W.F., LaBerge, G.L., Klasner, J.S., and Schulz, K.J., 2008, The Gogebic iron range—A sample of the northern margin of the Penokean fold and thrust belt: US Geological Survey, v. 1730.
- Card, K.D., 1990, A review of the Superior province of the Canadian Shield, a product of Archean accretion: *Precambrian Res.*, v. 48, p. 99–156.
- Cloud, P., 1973, Paleogeological Significance of the Banded Iron-Formation: *Economic Geology*, v. 68, n. 7, p. 1135–1143.
- Cloud, P., 1983, Banded iron-formation—a gradualist's dilemma: In *Developments in Precambrian Geology*, v. 6, p. 404–416.
- Cloud, P.E. Jr., 1965, Significance of the Gunflint (Precambrian) microflora: *Science*, v. 148, p. 27–35.
- Cohen, K.M., Finney, S.C., Gibbard, P.L., and Fan, J.-X., 2013; updated 2020, The ICS International Chronostratigraphic Chart; *Episodes*, v. 36, p. 199–204.

- Condie, K.C., 2015, *Earth as an evolving planetary system*: Academic Press. ISBN 9780128036891.
- Cox, G.M., Halverson, G.P., Minarik, W.G., Le Heron, D.P., Macdonald, F.A., Bellefroid, E.J., and Straus, J.V., 2013, Neoproterozoic iron formation: An evaluation of its temporal, environmental and tectonic significance: *Chemical Geology*, v. 362, p. 232–249.
- Craddock, J.P., Rainbird, R.H., Davis, W.J., Davidson, C., Vervoort, J.D., Konstantinou, A., Boerboom, T., Vorhies, S., Kerber, L., and Lundquist, B., 2013, Detrital zircon geochronology and provenance of the Paleoproterozoic Huron (~ 2.4–2.2 Ga) and Animikie (~ 2.2–1.8 Ga) basins, southern Superior Province: *The Journal of Geology*, v. 121, n. 6, p. 623–644.
- Cumberlidge, J.T. and Stone, J.G., 1964, The vulcan iron formation at the groveland mine, iron mountain, Michigan: *Economic Geology*, v. 59, n. 6, p.1094–1106.
- Curran, J., 2012, *Microfossils and Depositional Environment of the Gunflint Iron Formation*: Doctoral Dissertation, GUSTAVUS ADOLPHUS COLLEGE
- Davis, D.W., 2008., Sub-million-year age resolution of Precambrian igneous events by thermal extraction-thermal ionization mass spectrometry Pb dating of zircon: Application to crystallization of the Sudbury impact melt sheet: *Geology*, v. 36, no. 5, p. 383–386.
- Davis, P., 1998, *The Big Picture (Thesis)*: University of Minnesota. p. Assembly of the Superior Province (1), Continental Collision 2.6 Billion Years Ago (2), A Riftine Sequence in the Previously Accreted Terrane (3), Two Crustal Collisions Complete the Penokean Orogeny (4).

- Deflandre, G., 1968, Sur l'existence d~s le Pr~cambrien d'Acritarches du type Acanthomorphae: Eomicrystidium nov. gen. Typification du genre Palaeocryptidium: Comptes rendus de l'Académie des Sciences Paris, v. 266, p. 2385–2389.
- Ding, T.P., Gao, J.F., Tian, S.H., Fan, C.F., Zhao, Y., Wan, D.F., and Zhou, J.X., 2017, The $\delta^{30}\text{Si}$ peak value discovered in middle Proterozoic chert and its implication for environmental variations in the ancient ocean: Scientific Reports, v. 7, no. 1, p. 1–15.
- Dobrzhinetskaya, L., Wirth, R., and Green, H., 2014, Diamonds in Earth's oldest zircons from Jack Hills conglomerate, Australia, are contamination: Earth and Planetary Science Letters, v. 387, p. 212–218.
- Earth and Planetary Materials Analysis Laboratory (EPMAL), undated, Electron Microprobe Laboratory: Available at <https://epma.uwo.ca/about/Electron%20Microprobe.html> (Accessed: 15 April 2020)
- Edhorn, A., 1973, Further investigations of fossils from the Animikie, Thunder Bay, Ontario: Proceedings of the Geologist's Association Canada, v. 25, p. 37–66.
- El Albani, A., Bengtson, S., Canfield, D.E., Bekker, A., Macchiarelli, R., Mazurier, A., Hammarlund, E.U., Boulvais, P., Dupuy, J.J., Fontaine, C., Fürsich, F.T., 2010, Large colonial organisms with coordinated growth in oxygenated environments 2.1 Gyr ago: Nature, v. 466, p. 100–104.
- Evans, D.A., and Mitchell, R.N., 2011, Assembly and breakup of the core of Paleoproterozoic–Mesoproterozoic supercontinent Nuna: Geology, v. 39, n. 5, p.443–446.

- Fallacaro, A. and Calvin, W.M., 2002, Lake Superior Type Banded Iron Formations as an Analog to Mars: In AGU Fall Meeting Abstracts, v. 2002, p. P61D–10
- Fellers, T.J. and Davidson, M.W., undated, National High Magnetic Field Laboratory, 1800 East Paul Dirac Dr., The Florida State University, Tallahassee, Florida, 32310.
- Feulner, G., 2012, The Faint Young Sun Problem: Reviews of Geophysics, v. 50, no. 2.
- Floran, R.J. and Papike, J.J. 1975. Petrology of the Gunflint Iron Formation, Ontario-Minnesota: The low grade rocks. Bulletin of the Geological Society of America, v. 86, p.1169-90.
- Floran, R.J., and Papike, J.J., 1978, Mineralogy and petrology of the Gunflint Iron Formation, Minnesota-Ontario: correlation of compositional and assemblage variations at low to moderate grade: Journal of Petrology, v. 19, p. 215–288.
- Foley, D., 2009, Mineralogy And Metamorphism Of The Stromatolite-Bearing Layers Of The Biwabik Iron Formation (Doctoral dissertation, Gustavus Adolphus College).
- Fox, R.F., 2004, Origin of life and energy: Encyclopedia of Energy, v. 4, p.781–792.
- Fralick, P., Davis, D.W., and Kissin, S.A., 2002, The age of the Gunflint Formation, Ontario, Canada: single zircon U–Pb age determinations from reworked volcanic ash: Canadian Journal of Earth Sciences, v. 39, p. 1085–1091.
- Fralick, P., Planavsky, N., Burton, J., Jarvis, I., Addison, W.D., Barrett, T.J., and Brumpton, G.R., 2017, Geochemistry of Paleoproterozoic Gunflint Formation carbonate: Implications for hydrosphere-atmosphere evolution: Precambrian Research, v. 290, p. 126–146.

- Fralick, P.W., 1988. Microbial biotherms, Lower Proterozoic Gunflint Formation, Thunder Bay, Ontario. In: Geldsetzer, H.H.J., James, N.P., Tebbutt, G.E. (Eds.), *Reefs in Canada and Adjacent Areas*. Canadian Society of Petroleum Geologists, Memoir 13, pp. 24–29.
- Franklin, J.M., Schieders, B.R., and Koopman, E.R., 1991, *Mineral Deposits in the Western Superior Province, Ontario (Field Trip 9)*: Geological Survey of Canada, Open File 2164, p. 105–122.
- Frei, R. and Polat, A., 2013, Chromium isotope fractionation during oxidative weathering—implications from the study of a Paleoproterozoic (ca. 1.9 Ga) paleosol, Schreiber Beach, Ontario, Canada: *Precambrian Research*, v. 224, p. 434–453.
- Frei, R., Gaucher, C., Poulton, S.W., and Canfield, D.E., 2009, Fluctuations in Precambrian atmospheric oxygenation recorded by chromium isotopes: *Nature*, v. 46, n.1(7261), p. 250–253.
- Gabriel, N.W., Papineau, D., She, Z., Leider, A., and Fogel, M.L., 2021, Organic diagenesis in stromatolitic dolomite and chert from the late Palaeoproterozoic McLeary Formation: *Precambrian Research*, v. 354, p.106052.
- García-Ruiz, J.M., Hyde, S.T., Carnerup, A.M., Christy, A.G., Van Kranendonk, M.J., and Welham, N.J., 2003, Self-assembled silica-carbonate structures and detection of ancient microfossils: *Science*, v. 302, p. 1194–1197.
- Goldblatt, C., Lenton, T.M., and Watson, A.J., 2006, The Great Oxidation at 2.4 Ga as a bistability in atmospheric oxygen due to UV shielding by ozone: *Geophysical Research Abstracts*, v. 8, p. 00770.

- Goldich, S.S., Nier, A.O., Baadsgaard, H., Hoffman, J.H., and Krueger, H.W., 1961, The Precambrian geology and geochronology of Minnesota: Minn., Geol. Sum., Bull., v. 4, n. 1, p. 193.
- González-Flores, A.L., Jin, J., Osinski, G.R., and Tsujita, C.J., 2022, Acritarch-like Microorganisms from the 1.9 Ga Gunflint Chert, Canada: *Astrobiology*, v. 22, n. 5, p. 568–578.
- Goodwin, A.M., 1956, Facies relations in the Gunflint iron formation, Ontario: *Economic Geology*, v. 51, no. 6, p. 565–595. doi:10.2113/gsecongeo.51.6.565. ISSN 1554-0774.
- Goodwin, A.M., 1960. Gunflint Iron Formation of the Whitefish Lake area: Ontario Department of Mines Annual Report., 69, p. 41-63.
- Green, J.C., 1996, *Geology on Display, Geology and Scenery of Minnesota's North Shore State Parks*: Minnesota Department of Natural Resources, ISBN 0-9657127-0-2.
- Grey, K., 1994, Stromatolites from the Palaeoproterozoic Earraheedy Group, Earraheedy Basin, Western Australia: *Alcheringa*, v. 18, n. 3, p. 187–218.
- Gross, G.A. 1980, A classification of iron formations based on depositional environments: *The Canadian Mineralogist*, v. 18, p. 215–222.
- Gu, X., 1997, The age of the common ancestor of eukaryotes and prokaryotes: statistical inferences: *Molecular biology and evolution*, v. 14, n. 8, p. 861–866.
- Gumsley, A.P., Chamberlain, K.R., Bleeker, W., Söderlund, U., De Kock, M.O., Larsson, E.R., and Bekker, A., 2017, Timing and tempo of the Great Oxidation Event: *Proceedings of the National Academy of Sciences*, v. 114, n. 8, p. 1811–1816.

- Han, T.M., and Runnegar, B., 1992, Megascopic eukaryotic algae from the 2.1-billion-year-old Negaunee Iron formation: *Science*, v. 257, p. 232–235.
- Hardin, J., Bertoni, G., and Kleinsmith, L.J., 2011, *Becker's World of the Cell*: Pearson Benjamin Cummings, Boston, USA, 8th edn, p. 793.
- Heck, P.R., Huberty, J.M., Kita, N.T., Ushikubo, T., Kozdon, R., and Valley, J.W., 2011, SIMS analyses of silicon and oxygen isotope ratios for quartz from Archean and Paleoproterozoic banded iron formations: *Geochimica et Cosmochimica Acta*, v. 75, n. 20, p. 5879–5891.
- Hem, J.D., Cropper, W.H., Skougstad, M.W., and Oborn, E.T., 1962, *Chemistry of iron in natural water*: Washington, U.S. Govt. Print. Off.
- Hesse, R., 1989, Silica diagenesis: origin of inorganic and replacement cherts: *Earth-Science Reviews*, v. 26, no. 1–3, p. 253–284.
- Hodgskiss, M. S. W., Crockford, P. W., Peng, Y., Wing, B. A., and Horner, T. J., 2019, A productivity collapse to end Earth's Great Oxidation: *PNAS*, v. 116, n. 35, p. 17207–17212.
- Hodgskiss, M.S., Dagnaud, O.M., Frost, J.L., Halverson, G.P., Schmitz, M.D., Swanson-Hysell, N.L., and Sperling, E.A., 2019, New insights on the Orosirian carbon cycle, early Cyanobacteria, and the assembly of Laurentia from the Paleoproterozoic Belcher Group: *Earth and Planetary Science Letters*, v. 520, p. 141–152.
- Hoffman, P.F., 1989, Speculations on Laurentia's first gigayear (2.0 to 1.0 Ga): *Geology*, v. 17, n. 2, p. 135–138.
- Hoffman, P.F., Kaufman, A.J., Halverson, G.P., and Schrag, D.P., 1998, A neoproterozoic snowball earth: *Science*, v. 281, n. 5381, p. 1342–1346.

- Hofmann, H.J., 1971, Polygonomorph acritarchs from the Gunflint Formation (Precambrian):
Journal of Paleontology, v. 45, p. 522–524.
- Hofmann, H.J., 1976, Precambrian microflora, Belcher Islands, Canada: significance and
systematics: Journal of Paleontology, p. 1040–1073.
- Hofmann, H.J., and Jackson, G.D., 1969, Precambrian (aphebian) microfossils from belcher
islands, Hudson Bay: Canadian Journal of Earth Sciences, v. 6, n. 5, p. 1137–1144.
- Holland, H.D., 2006, The oxygenation of the atmosphere and oceans: Philosophical Transactions
of the Royal Society B: Biological Sciences, v. 361, n. 1470, p. 903–915.
- Holm, N.G., 2006, Possible biological origin of banded iron — Formations from hydrothermal
solutions: Origins of Life and Evolution of the Biosphere, v. 17, p. 0169–6149, 229–250.
- Hopkinson, L., Roberts, S., Herrington, R., and Wilkinson, J., 1998, Self organization of
submarine hydrothermal siliceous deposits: evidence from the TAG hydrothermal mound,
26°N Mid Atlantic Ridge: Geology, v. 26, p. 347–350.
- Ilyin, A.V., 2009, Neoproterozoic banded iron formations: Lithology and Mineral Resources, v.
44, n. 1, p. 78–86.
- Ishida, A., Hashizume, K., and Kakegawa, T., 2017, Microbial nitrogen cycle enhanced by
continental input recorded in the Gunflint Formation: Geochemical Perspectives Letters,
v. 4, p.13–18.
- James, H.L., 1954, Sedimentary facies of iron-formation: Economic Geology, v. 49, no. 3, p. 235–
293.

- Jennings, T.A., 2011, Experimental production of bending and radial flake fractures and implications for lithic technologies: *Journal of Archaeological Sciences*, v. 38, no. 12, p. 3644–3651.
- Jirsa, M., and Fralick, P.W., 2010, *Geology of the Gunflint Iron Formation and the Sudbury Impact Layer, Northeastern Minnesota*, Institute on Lake Superior Geology, Field Trip 4.
- Jirsa, M.A., Boerboom, T.J., Green, J.C., Miller, J.D., Morey, G.B., Ojakangas, R.W., Peterson, D.M., and Severson, M.J., 2004, "Field Trip 5 – Classic Outcrops of Northeastern Minnesota": *Proceedings of the 50th Annual Meeting – Part 2. Field Trip Guidebook*. Institute on Lake Superior Geology. p. 129–169.
- Jirsa, M.A., Fralick, P.W., Weiblen, P.W., and Anderson, J.L.B., 2011, Sudbury impact layer in the western Lake Superior region, in Miller, J.D., Hudak, G.J., Wittkop, C., and McLaughlin, P.I., eds., *Archean to Anthropocene: Field Guides to the Geology of the Mid-Continent of North America: Geological Society of America Field Guide 24*, p. 147–169.
- Kappler, A., Pasquero, C., Konhauser, K.O., and Newman, D.K., 2005, Deposition of banded iron formations by anoxygenic phototrophic Fe(II)-oxidizing bacteria: *Geology*, v. 33, p. 0091–7613, 865–868.
- Kasting, J., 1993, Earth's early atmosphere: *Science*, v. 259, n. 5097, p. 920–926.
- Kasting, J.F., and Siefert, J.L., 2002, Life and the evolution of Earth's atmosphere: *Science*, v. 296, n. 5570, p. 1066–1068.

- Katsuta, N., Shimizu, I., Helmstaedt, H., Takano, M., Kawakami, S., and Kumazawa, M., 2012, Major element distribution in Archean banded iron formation (BIF): influence of metamorphic differentiation: *Journal of Metamorphic Geology*, v. 30, n. 5, p. 457–472.
- Kirschvink, J.L., Gaidos, E.J., Bertani, L.E., Beukes, N.J., Gutzmer, J., Maepa, L.N., and Steinberger, R.E., 2000, Paleoproterozoic snowball Earth: Extreme climatic and geochemical global change and its biological consequences: *Proceedings of the National Academy of Sciences*, v. 97, n. 4, p.1400–1405.
- Klein, C., 2005, Some Precambrian banded iron-formations (BIFs) from around the world: Their age, geologic setting, mineralogy, metamorphism, geochemistry, and origins: *American Mineralogist*, v. 90, n. 10, p. 1473–1499.
- Klemic, H., 1970, Iron ore deposits of the United States of America, Puerto Rico, Mexico and Central America: *Survey of World Iron Ore Resources, Occurrence and Appraisal*, Department of Economic and Social Affairs, United Nations, New York, p. 411–477.
- Knauth, L.P., 1979, A model for the origin of chert in limestone: *Geology*, v. 7, no. 6, p. 274–277.
- Knauth, L.P., 2005, Temperature and salinity history of the Precambrian ocean: implications for the course of microbial evolution. In *Geobiology: Objectives, concepts, perspectives*, p. 53–69. Elsevier.
- Knoll, A.H., and Barghoorn, E.S., 1976, A Gunflint-type microbiota from the Duck Creek dolomite, Western Australia: *Origins of life*, v. 7, n. 4, p. 417–423.
- Knoll, A.H., Javaux, E.J., Hewitt, D., and Cohen, P., 2006, Eukaryotic organisms in Proterozoic oceans: *Philosophical Transactions of the Royal Society B*, v. 361, p. 1023–1038.

- Knoll, A.H., Strother, P.K., and Rossi, S., 1988, Distribution and diagenesis of microfossils from the lower Proterozoic Duck Creek Dolomite, Western Australia: *Precambrian research*, v. 38, n. 3, p. 257–279.
- Konhauser, K.O., Lalonde, S.V., Planavsky, N.J., Pecoits, E., Lyons, T.W., Mojzsis, S.J., Rouxel, O.J., Barley, M.E., Rosiere, C., Fralick, P.W., and Kump, L.R., 2011, Aerobic bacterial pyrite oxidation and acid rock drainage during the Great Oxidation Event: *Nature*, v. 478, n. 7369, p. 369–373.
- Kopp, R.E., Kirschvink, J.L., Hilburn, I.A., and Nash, C.Z., 2005, The Paleoproterozoic snowball Earth: A climate disaster triggered by the evolution of oxygenic photosynthesis: *Proceedings of the National Academy of Sciences*, v. 102, p. 11131–11136.
- Korde, K.B., 1958, Concerning several species of fossil blue-green algae: *Mater. Osn. Paleontol.*, v. 2, p. 113–118 (in Russian).
- Krissansen-Totton, J., Arney, G.N., and Catling, D.C., 2018, Constraining the climate and ocean pH of the early Earth with a geological carbon cycle model: *Proceedings of the National Academy of Sciences*, v. 115, no. 16, p. 4105–4110.
- Kump, L.R., and Barley, M.E., 2007, Increased subaerial volcanism and the rise of atmospheric oxygen 2.5 billion years ago: *Nature*, v. 448, p. 1033–1036.
- Lahtinen, R.A.M.M., Korja, A., and Nironen, M., 2005, Paleoproterozoic tectonic evolution: In *Developments in Precambrian Geology*, v. 14, p. 481–531, Elsevier.
- Laird, M., 2017, *Magnetic Petrophysics of the Vulcan Iron Formation (Michigan, USA)*: Open Access Master's Thesis, Michigan Technological University.

- Lane, N., 2016, *The Vital Question: Why is Life the Way it is?*: Profile Books, p. 157–91.
- Laybourn, D.P., 1979, The geology and metamorphism of the Ironwood Iron-Formation, Gogebic Range, Wisconsin.
- Levin, H.L. and King, D.T., 2017, *The Earth through time* (11th edition): John Wiley & Sons, chapter 8, p. 230–246.
- Li, F., Zhu, X., Ding, H., and Zhang, K., 2022, Local hydrothermal sources for Superior-type iron formations: Insights from the Animikie Basin: *Precambrian Research*, v. 377, p. 106736.
- Li, W., Beard, B.L., and Johnson, C.M., 2015, Biologically recycled continental iron is a major component in banded iron formations: *Proceedings of the National Academy of Sciences*, v. 112, n. 27, p. 8193–8198.
- Li, Z.Q., Zhang, L.C., Xue, C.J., Zheng, M.T., Zhu, M.T., Robbins, L.J., Slack, J.F., Planavsky, N.J., and Konhauser, K.O., 2018, Earth's youngest banded iron formation implies ferruginous conditions in the Early Cambrian ocean: *Scientific Reports*, v. 8, n. 1, p. 9970.
- Lopukhin, A.S., 1971, For unification of morphological terminology and diagnostic acritarchs. In: *Dispersal Remnants of Fossil Plants of Kirghizia*, IIIrd. Int. Palynol. Conf., Novosibirsk, Akad. Nauk Kirghizskoi SSR, Frunze, p. 11–35 (in Russian).
- Lopukhin, A.S., 1975. Biofossils of the Precambrian and some problems of their study. In: *Probl. osadoch, geol. dokembriya*. Moscow, Nauka, v. 4, n. 2, p. 169–173 (in Russian).
- Loron, C.C., Halverson, G.P., Rainbird, R.H., Skulski, T., Turner, E.C., and Javaux, E.J., 2021, Shale-hosted biota from the Dismal Lakes Group in Arctic Canada supports an early

- Mesoproterozoic diversification of eukaryotes: *Journal of Paleontology*, v. 95, n. 6, p. 1113–1137.
- Lukmanov, R., Tulej, M., Wiesendanger, R., and Riedo, A., 2018, In-situ detection of biosignatures from 1.9 Ga Gunflint chert with LMS: European Planetary Science Congress p. EPSC2018-392.
- Lukmanov, R.A., Tulej, M., Ligterink, N.F., De Koning, C., Riedo, A., Grimaudo, V., Neubeck, A., Wacey, D., and Wurz, P., 2021, Chemical identification of microfossils from the 1.88-Ga Gunflint chert: Towards empirical biosignatures using laser ablation ionization mass spectrometer: *Journal of chemometrics*, v. 35, n. 10, p. e3370.
- Lukmanov, R.A., Tulej, M., Wiesendanger, R., Riedo, A., Grimaudo, V., Ligterink, N.F., Koning, C.D., Neubeck, A., Wacey, D., and Wurz, P., 2022. Multiwavelength Ablation/Ionization and Mass Spectrometric Analysis of 1.88 Ga Gunflint Chert: *Astrobiology*, v. 22, n. 4.
- Lyons, T.W. and Reinhard, C.T., 2009, Early Earth: Oxygen for heavy-metal fans: *Nature*, v. 461, n. 7261, p. 179–81.
- Lyons, T.W., Reinhard, C.T., and Planavsky, N.J., 2014, The rise of oxygen in Earth's early ocean and atmosphere: *Nature*, v. 506, n. 7488, p.307–315.
- Maliva, R. G., Knoll, A. H., and Simonson, B. M., 2005, Secular change in the Precambrian silica cycle; insights from chert petrology: *Geological Society of America Bulletin*, v. 117, p. 835–845.
- Maliva, R.G. and Siever, R., 1988, Diagenetic replacement controlled by force of crystallization: *Geology*, v. 16, n. 8, p. 688–691.

- Maliva, R.G. and Siever, R., 1989, Nodular chert formation in carbonate rocks: *The Journal of Geology*, v. 97, n. 4, p. 421–433.
- Margulis, L., 1970, *Origin of Eukaryotic Cells*: New Haven, Yale University Press.
- Margulis, L., and Sagan, D., 1986. *Microcosmos: four billion years of microbial evolution*: University of California Press. ISBN 9780520210646.
- Marin, J., Chaussidon, M., and Robert, F., 2010, Microscale oxygen isotope variations in 1.9 Ga Gunflint cherts: assessments of diagenesis effects and implications for oceanic paleotemperature reconstructions: *Geochimica et Cosmochimica Acta*, v. 74, n. 1, p.116–130.
- Marin-Carbonne, J., Chaussidon, M., and Robert, F., 2012, Micrometer-scale chemical and isotopic criteria (O and Si) on the origin and history of Precambrian cherts: implications for paleo-temperature reconstructions: *Geochimica et Cosmochimica Acta*, v. 92, p. 129–147.
- Marin-Carbonne, J., Faure, F., Chaussidon, M., Jacob, D., and Robert, F., 2013, A petrographic and isotopic criterion of the state of preservation of Precambrian cherts based on the characterization of the quartz veins: *Precambrian Research*, v. 231, p. 290–300.
- Martin, W., 2005, Archaeobacteria (Archaea) and the origin of the eukaryotic nucleus: *Current Opinion in Microbiology*, v. 8, n. 6, p. 630–637.
- McCollom, T.M., and Seewald, J. S., 2006, Carbon isotope composition of organic compounds produced by abiotic synthesis under hydrothermal conditions: *Earth and Planetary Science Letters*, v. 243, p. 74–84.

- McSwiggen, P.L., Morey, G.B., and Cleland, J.M., 1995, RI-45 Iron-Formation Protolith and Genesis, Cuyuna Range, Minnesota.
- Miao, L., Moczyłowska, M., Zhu, S., and Zhu, M., 2019, New record of organic-walled, morphologically distinct microfossils from the late Paleoproterozoic Changcheng Group in the Yanshan Range, North China: *Precambrian Research*, v. 321, p. 172–198.
- Michail, S., 2022, Ancient acid rains in the Ediacaran period—An alternative story for sulfate sedimentation: *Precambrian Research*, v. 379, p. 106804.
- Michigan: *The Journal of Geology*, v. 43, n. 2, p.113–132.
- Miller, R. and Dransfield, M., 2011, Airborne Gravity Gradiometry and Magnetics in the Search for Economic Iron Ore Deposits: *Proceedings, Iron Ore 2011 Conference*, Perth, Western Australia, The Australasian Institute of Mining and Metallurgy, Melbourne, p. 109–116.
- Miyano T. and Klein C. 1986, Fluid behavior and phase relations in the system Fe–Mg–Si–C–O–H: applications to high grade metamorphism of iron formation: *Am. J. Sci.*, v. 286, p. 540–575.
- Moorhouse, W.W., 1960, Moorhouse Gunflint Iron Range in the vicinity of Port Arthur: Ontario Department of Mines Annual Report, v. 69, p. 1–40.
- Morey, G.B., 1983, Animikie Basin, Lake Superior region, USA: In *Developments in Precambrian Geology*, v. 6, p. 13–67.
- Morris, R.C. and Horwitz, R.C., 1983, The origin of the iron-formation-rich Hamersley Group of Western Australia — deposition on a platform: *Precambrian Research*, v. 21, n. 3–4, p. 273–297.

Mueller, A.G., 2019, A short review of Precambrian and Phanerozoic sedimentary iron (Mn, P) ore deposits: Maylands W.A. 6051, Australia.

National Center for Biotechnology Information, 2022, Comparison of eukaryotes vs. prokaryotes: Science Primer.

Nordsvan, A.R., Collins, W.J., Li, Z.X., Spencer, C.J., Pourteau, A., Withnall, I.W., Betts, P.G., and Volante, S., 2017, Laurentian crust in northeast Australia: Implications for the assembly of the supercontinent Nuna: *Geology*, v. 46, n. 3, p. 251–254, doi:10.1130/G39980.1.

Oehler, J.H., 1976, Experimental studies in Precambrian paleontology: Structural and chemical changes in blue-green algae during simulated fossilization in synthetic chert: *Geological Society of America Bulletin*, v. 87, p. 117–129.

Ojakangas, R.W., and Matsch, C.L., 1982, *Minnesota's Geology*. Minneapolis: University of Minnesota Press. p. 35–36, 39, 55–57. ISBN 0-8166-0953-5.

Ojakangas, R.W., Morey, G.B., and Southwick, D.L., 2001, Paleoproterozoic basin development and sedimentation in the Lake Superior region, North America: *Sedimentary Geology*, v. 141, p.319–341.

Ojakangas, R.W., Morey, G.B., and Southwick, D.L., 2001. Paleoproterozoic basin development and sedimentation in the Lake Superior region, North America: *Sedimentary Geology*, v. 141, p. 319–341.

- Olson, S.L., Reinhard, C.T., and Lyons, T.W., 2016, Limited role for methane in the mid-Proterozoic greenhouse: *Proceedings of the National Academy of Sciences*, v. 113, n. 41, p.11447–11452.
- Paces, J.B., and Miller, J.D., 1993, Precise U-Pb ages of Duluth Complex and related mafic intrusions, northeastern Minnesota: geochronological insights to physical, petrogenetic, paleomagnetic, and tectonomagmatic processes associated with the 1.1 Ga midcontinent rift system: *Journal of Geophysical Research*, v. 98, p. 13997–14013.
- Pannella, G., 1972, Paleontological evidence on the Earth's rotational history since early Precambrian: *Astrophysics and Space Science*, v. 16, n. 2, p. 212–237.
- Percival, J. A., Sanborn-Barrie, M., Skulski, T., Stott, G. M., Helmstaedt, H., and White, D. J., 2006, Tectonic evolution of the western Superior province from NATMAP and lithoprobe studies: *Can. J. Earth Sci.*, v. 43, p. 1085–1117.
- Percival, J.A. 2007, Eo-to-Mesoarchean terranes of the Superior province and their tectonic context. In van Kranendonk, M. J.; Smithies, R. H.; and Bennett, V. C., eds. *Earth's oldest rocks: Developments in Precambrian Geology* v. 15, Amsterdam, Elsevier, p. 1065–1086.
- Perkins, S., 2009, The iron record of Earth's oxygen . *Science News*, (en inglés) v. 175, p. 1943–1930, 24.
- Pesonen, L., Mertanen, S., Donadini, F., and Salminen, J., 2003, Paleomagnetic configuration of continents during the proterozoic with a special focus on Baltica. In *The Baltic Sea Region: Formation and Deformation of the Crust*, p. 10–13.

- Planavsky, N., Rouxel, O., Bekker, A., Shapiro, R., Fralick, P., and Knudsen, A., 2009, Iron-oxidizing microbial ecosystems thrived in late Paleoproterozoic redox-stratified oceans: *Earth and Planetary Science Letters*, v. 286, n. 1–2, p. 230–242. doi:10.1016/j.epsl.2009.06.033. ISSN 0012-821X.
- Poulton, S.W., and Canfield, D.E., 2011, Ferruginous conditions: a dominant feature of the ocean through Earth's history: *Elements*, v. 7, n. 2, p.107–112.
- Pufahl, P.K., and Fralick, P.W., 2000, Depositional environments of the Paleoproterozoic Gunflint Formation: Thunder Bay, Ontario, Institute of Lake Superior Geology, Annual Meeting, 46th, Proceedings, Field Trip Guidebook, v. 51, Field Trip 4, no pagination.
- Pufahl, P.K., Anderson, S.L., and Hiatt, E.E., 2014, Dynamic sedimentation of Paleoproterozoic continental margin iron formation, Labrador Trough, Canada: Paleoenvironments and sequence stratigraphy. *Sedimentary Geology*, v. 309, p. 48–65.
- Rasmussen, B., Fletcher, I.R., Brocks, J.J., and Kilburn, M.R., 2008, Reassessing the first appearance of eukaryotes and cyanobacteria: *Nature*, v. 455, p. 1101–1105.
- Robbins, L.J., Funk, S.P., Flynn, S.L., Warchola, T.J., Li, Z., Lalonde, S.V., Rostron, B.J., Smith, A.J., Beukes, N.J., de Kock, M.O., and Heaman, L.M., 2019, Hydrogeological constraints on the formation of Palaeoproterozoic banded iron formations: *Nature Geoscience*, v. 12, n. 7, p. 558–563.
- Robert, F., and Chaussidon, M., 2006, A palaeotemperature curve for the Precambrian oceans based on silicon isotopes in cherts: *Nature*, v. 443, n. 7114, p. 969–972.

- Roberts, W.L., Campbell, T.J., and Rapp, G.R. Jr., 1990, *Encyclopedia of Mineralogy*, Second Edition. ISBN 0-442-27681-8.
- Rogers, J.J., and Santosh, M., 2002, Configuration of Columbia, a Mesoproterozoic supercontinent: *Gondwana Research*, v. 5, n. 1, p.5–22.
- Rose, E., McLoughlin, N., and Brasier, M.D., 2006, Ground truth: the epistemology of searching for the earliest life on Earth: *Life As We Know It. Cellular Origin, Life in Extreme Habitats and Astrobiology*, v. 10, pp. 259–286.
- Schelble, R.T., Westall, F., and Allen, C.C., 2004, ~ 1.8 Ga iron-mineralized microbiota from the Gunflint Iron Formation, Ontario, Canada: implications for Mars: *Advances in Space Research*, v. 33, n. 8, p. 1268–1273.
- Schopf, J. W., 1992, Atlas of representative Proterozoic microfossils: In J.W. Schopf, J. W. and Klein, C. (eds.), *The Proterozoic Biosphere: A Multidisciplinary Study*: Cambridge Univ. Press, Cambridge, p. 1055 - 1117
- Schopf, J.W., 1968, Microflora of the Bitter Springs formation, late Precambrian, central Australia: *Journal of Paleontology*, p. 651–688.
- Schopf, J.W., 1987, Precambrian Prokaryotes and Stromatolites: *Series in Geology, Notes for Short Course*, v. 18, p. 20–33.
- Schopf, J.W., 1999, *Cradle of Life: The Discovery of Earth's Earliest Fossils*: Princeton University Press, p. 336, ISBN 0-691-00230-4.
- Schopf, J.W., and Kudryavtsev, A.B., 2012, Biogenicity of Earth's earliest fossils: a resolution of the controversy: *Gondwana Research*, v. 22, p. 761–771.

- Schulz, K.J. and Cannon, W.F., 2007, The Penokean orogeny in the Lake Superior region: *Precambrian Research*, v. 157, n. 1–4, p. 4–25.
- Schulz, K.J., and Cannon, W.F., 2007, The Penokean orogeny in the Lake Superior region: *Precambrian Research*, v. 157, p. 4–25.
- Shapiro, R.S., and Konhauser, K.O., 2015, Hematite-coated microfossils: primary ecological fingerprint or taphonomic oddity of the Paleoproterozoic?: *Geobiology*, v. 13, p. 209–224.
- Shaw, G.H., 2008, Earth's atmosphere – Hadean to early Proterozoic: *Geochemistry*, v. 68, n. 3, p. 235–264.
- Sims, P.K. and Day, W.C., 1993, Great Lakes Tectonic Zone--revisited (No. 1904): US Government Printing Office.
- Slack, J.F. and Cannon, W.F., 2009, Extraterrestrial demise of banded iron formations 1.85 billion years ago: *Geology*, v. 37, n. 11, p. 1011–1014.
- Smith, G.A. and Huckell, B.B., 2005, The geological and geoarchaeological significance of Cerro Pedernal, Rio Arriba County, New Mexico. *Geology of the Chama Basin: New Mexico Geological Society, Guidebook*, v. 56, p. 425–431.
- Sosa Torres, M.E., and Saucedo-Vázquez Juan P, K.P.M., 2015, Chapter 1, Section 2: The rise of dioxygen in the atmosphere. *Sustaining Life on Planet Earth: Metalloenzymes Mastering Dioxygen and Other Chewy Gases: Metal Ions in Life Sciences*, v. 15, p.1–12.
- Surface Science Western, undated, Scanning Electron Microscopy coupled with Energy Dispersive X-ray (SEM/EDX) Spectroscopy: Available at <https://www.surfacesciencwestern.com/analytical-services/scanning-electron->

- microscopy-coupled-with-energy-dispersive-x-ray-semedx-spectroscopy/ (Accessed: 8 May 2019).
- Takemura, M., 2001, Poxviruses and the origin of the eukaryotic nucleus: *Journal of Molecular Evolution*, v. 52, n. 5, p. 419–425.
- Tang, H. and Chen, Y., 2013, Global glaciations and atmospheric change at ca. 2.3 Ga: *Geoscience Frontiers*, v. 4, n. 5, p. 583–596.
- Taylor, T.N. and Taylor, E.L., 1993, *Biology and evolution of fossil plants*: Prentice Hall.
- Thurston, D.R., 1972, Studies on bedded cherts: *Contributions to Mineralogy and Petrology*, v. 36, no. 4, p. 329–334. doi:10.1007/BF00444339. S2CID 128745664.
- Tobin, K.J., 1990, The paleoecology and significance of the Gunflint-type microbial assemblages from the Frere Formation (Early Proterozoic), Nabberu Basin, Western Australia: *Precambrian Research*, v. 47, n. 1–2, p. 71–81.
- Tomitani, A., Knoll, A.H., Cavanaugh, C.M., and Ohno, T., 2006, The evolutionary diversification of cyanobacteria: molecular–phylogenetic and paleontological perspectives: *Proceedings of the National Academy of Sciences*, v. 103, n. 14, p. 5442–5447.
- Torsvik, T.H. and Cocks, L.R.M., 2017, *Earth history and palaeogeography*: Cambridge, United Kingdom, Cambridge University Press. p. 41.
- Tosca, N.J., Macdonald, F.A., Strauss, J.V., Johnston, D.T., and Knoll, A.H., 2011, Sedimentary talc in Neoproterozoic carbonate successions: *Earth and Planetary Science Letters*, v. 306, n. 1–2, p. 11–22.

- Trendall, A.F., 2002, The significance of iron-formation in the Precambrian stratigraphic record. *Precambrian sedimentary environments: A modern approach to ancient depositional systems*, p. 33–66.
- Trendall, A.F., and Blockley, J.G., 2004, Precambrian iron-formation. *The Precambrian earth: tempos and events*: Elsevier, Amsterdam, p. 403–421.
- Vago, J.L., Westall, F., Coates, A.J., Jaumann, R., Korablev, O., Ciarletti, V., Mitrofanov, I., Josset, J.L., De Sanctis, M.C., Bibring, J.P., and Rull, F., 2017, Habitability on Early Mars and the Search for Biosignatures with the ExoMars Rover: *Astrobiology*, v. 17, n. 6–7, p. 471–510.
- Vallini, D.A., Cannon, W.F., and Schulz, K., 2006, Age Constraints for Paleoproterozoic Glaciation in the Lake Superior Region: Detrital Zircon and Hydrothermal Xenotime Ages for the Chocoy Group, Marquette Range Supergroup: *Canadian Journal of Earth Sciences*, v. 43, n. 5, p. 571.
- Van Schmus, W.R., 1976, A Discussion on global tectonics in Proterozoic times-Early and Middle Proterozoic history of the Great Lakes area, North America: *Philosophical Transactions of the Royal Society of London. Series A, Mathematical and Physical Sciences*, v. 280, n. 1298, p. 605–628.
- Wacey, D., Eiloart, K., and Saunders, M., 2019, Comparative multi-scale analysis of filamentous microfossils from the c. 850 Ma Bitter Springs Group and filaments from the c. 3460 Ma Apex chert: *Journal of the Geological Society*, v. 176, n. 6, p. 1247–1260.
- Wacey, D., Menon, S., Green, L., Gerstmann, D., Kong, C., Mcloughlin, N., Saunders, M., and Brasier, M., 2012, Taphonomy of very ancient microfossils from the ~ 3400 Ma Strelley

- Pool Formation and ~ 1900 Ma Gunflint Formation: New insights using a focused ion beam: *Precambrian Research*, v. 220, p. 234–250.
- Wacey, D., Saunders, M., Kong, C., Brasier, A., and Brasier, M., 2016, 3.46 Ga Apex chert ‘microfossils’ reinterpreted as mineral artefacts produced during phyllosilicate exfoliation: *Gondwana Research*, v. 36, p. 296–313.
- Wächtershäuser, G., 2003, From pre-cells to Eukarya – a tale of two lipids: *Molecular Microbiology*, v. 47, n. 1, p. 13–22.
- Wächtershäuser, G., 2006, From volcanic origins of chemoautotrophic life to Bacteria, Archaea and Eukarya: *Philosophical Transactions of the Royal Society of London. Series B, Biological Sciences*, v. 361, n. 1474, p. 1787–1806, discussion p. 1806–1808.
- Walter, M.R., Goode, A.D.T., and Hall, W.D.M., 1976, Microfossils from a newly discovered Precambrian stromatolitic iron formation in Western Australia: *Nature*, v. 261, n. 5557, p. 221–223.
- White, D.A., 1954, *The stratigraphy and structure of the Mesabi Range, Minnesota (Vol. 38)*. University of Minnesota Press.
- Whitmeyer, S. and Karlstrom, K.E., 2007, Tectonic model for the Proterozoic growth of North America: *Geosphere*, v. 3, n. 4, p. 220.
- Wilson, J.P., Fischer, W.W., Johnston, D.T., Knoll, A.H., Grotzinger, J.P., Walter, M.R., McNaughton, N.J., Simon, M., Abelson, J., Schrag, D.P., and Summons, R., 2010, Geobiology of the late Paleoproterozoic Duck Creek Formation, Western Australia: *Precambrian Research*, v. 179, n. 1–4, p. 135–149.

- Winter, B.L., and Knauth, L.P., 1992, Stable isotope geochemistry of cherts and carbonates from the 2.0 Ga Gunflint Iron Formation: implications for the depositional setting, and the effects of diagenesis and metamorphism: *Precambrian Research*, v. 59, p. 283–313.
- Young, G.M., 2014, Did prolonged two-stage fragmentation of the supercontinent Kenorland lead to arrested orogenesis on the southern margin of the Superior province?: *Geoscience Frontiers*, v. 6, n. 3, p. 419–435.
- Zhang, S.H., Zhao, Y., and Santosh, M., 2012, Mid-Mesoproterozoic bimodal magmatic rocks in the northern North China Craton: implications for magmatism related to breakup of the Columbia supercontinent: *Precambrian Research*, v. 222, p.339–367.
- Zhao, G., Sun, M., Wilde, S.A., and Li, S., 2004, A Paleo-Mesoproterozoic supercontinent: assembly, growth and breakup: *Earth-Science Reviews*, v. 67, no. 1–2, p. 91–123.

Chapter 2: Acritarch-like microorganisms from the 1.9 Ga old Gunflint Chert, Canada¹

2.1 Introduction

Microfossils of suspected eukaryotes, both unicellular and multicellular, have been reported from Paleoproterozoic rocks from various locations around the world. Putative eukaryotic biomarkers have been reported from Neoproterozoic drill-core rocks as old as 2.7 Ga, but subsequent study has provided strong evidence for their origin to be a consequence of contamination from drilling (Brocks et al., 1999; Rasmussen et al. 2008; French et al., 2015; Dacks et al., 2016). Some tubular microfossils from rocks of ~2.8–2.7 Ga of South Africa have been attributed, also questionably, to eukaryotes (Każmierczak et al., 2016). Somewhat younger, possible eukaryotic fossils include the macroscopic, whip- to spiral-shaped *Grypania* from the Negaunee Formation of Michigan (originally thought to be ~2.1 Ga by Han and Runnegar, 1992, but later dated at 1874 ± 09 Ma by Schneider et al., 2002) and the more morphologically variable fibro-radial bodies described from the ~2.1 Ga Francevillian Group in Gabon, Africa (El Albani et al., 2010; El Albani et al., 2014; El Albani et al., 2019). Similarly, a eukaryotic affinity has been a matter of debate for the microscopic, cyst-like bodies reported from the Paleoproterozoic, such as those of the Gunflint Chert, Canada (Barghoorn and Tyler, 1965; Cloud 1965; Cloud and Licari, 1968; Licari and Cloud, 1968; Barghoorn, 1971; Edhorn, 1973; Darby, 1974; Kaźmierczak, 1976; Kaźmierczak, 1979; Krumbein, 2010). Although broadly similar to known eukaryotic cells morphologically, such

¹ This chapter is published as an article in *Journal of Astrobiology*: González-Flores, A.L., Jin, J., Osinski, G.R., and Tsujita, C.J., 2022, Acritarch-like Microorganisms from the 1.9 Ga Gunflint Chert, Canada: *Astrobiology*, v. 22, n. 5, p. 568–578.

microfossils have, thus far, failed to reveal well-preserved ultra-cellular structures (especially cross-linked features) one would expect for organic remains of protists (Cavalier-Smith 2002).

Five different microfossils from the Gunflint Chert, which were originally identified as eukaryotes by Edhorn (1973), Darby (1974), and Kaźmierczak (1976, 1979), have since been reconsidered for the following reasons:

- 1) The material described by Edhorn (1973) exhibited poor cellular preservation.
- 2) The presence of a dark spot in the middle of the cellular structure, formerly suspected as evidence of a nucleus or organelles by Edhorn (1973), can be explained as a product of cellular degradation and cytoplasmic coagulation (Golubic, and Hofmann, 1976).
- 3) The bud-like projections in *Huroniospora* (Darby, 1974), which resemble similar features in fungi, can be explained as products of irregular growth patterns in the cell walls of cyanobacteria (Padmaja, 1972; Hirsch, 1974; Krumbein, 2010).
- 4) The resemblance of *Eosphaera* to *Eovolvox*, which was thought to suggest affinities between these forms (Kaźmierczak, 1976), is largely superficial, as *Eosphaera* lacks a well-defined thick inner wall or any evidence of internal daughter colonies (Tappan, 1976).

Importantly, while geochemical data derived from in situ measurements of stable carbon isotopes in pyrobitumen and kerogen do not provide evidence for the presence of eukaryotic biomarkers in rocks 2.7 Ga or older (Rasmussen et al., 2008), biomarkers corroborate the hypothesis that oxygenic cyanobacteria appeared by ~2.15 Ga, followed by the appearance of eukaryotes by ~1.78–1.68 Ga (Summons et al., 1999). Despite the controversies surrounding the reliability of biomarkers and microfossils as evidence for eukaryotic life, cyst-like microfossils have been considered reliable evidence for eukaryotes in rocks between 1.8–1.3 Ga, especially those with a well-preserved cytoskeletal cell wall and complex ornamentation (Meng et al., 2005;

Knoll et al., 2006). Indeed, cyst-like microfossils described from the non-marine deposits of the ~1.2 Ga Torridonian Supergroup of Scotland are currently considered the oldest known protists (Strother et al., 2011). In most cases, however, the identification of these ancient fossils as protists remains a formidable challenge, mainly due to cell body degradation, which renders it difficult, if not impossible, to recognize potential cell nuclei and organelles (if they were indeed present at all). As a result, studies on these forms have typically been made via comparisons of their overall morphology with cyst-like fossils of Phanerozoic age, such as acritarchs, dinoflagellates, or other unicellular algae. With regard to fossil eukaryotes, the diverse and well-preserved acritarch assemblages of Ediacaran rocks of Australia (Willman and Moczyłowska, 2008) provide a good basis for comparison and identification of older acritarchs and cyst-like forms. Such protist cysts are characterized by large cells (30 μm or larger in diameter) with multi-layered walls (often folded and/or wrinkled in preservation), and an outer surface ornamented with a reticulate, polygonal, or other sculptured pattern and prominent hollow processes.

Well known for its diverse microbiota, the richly fossiliferous and usually black to dark-grey rocks of the Gunflint Chert occur in the Gunflint Iron Range along the northern shore of Lake Superior, Canada, from the northern tip of Lake Gunflint (Cook County), Minnesota, to the district of Thunder Bay, Ontario (Fig. 2.1A). Rocks of the Gunflint Iron Range comprise Proterozoic metasedimentary rocks that overlie Archean metasedimentary, metavolcanic and granitic intrusive rocks (Figure 2.1B).

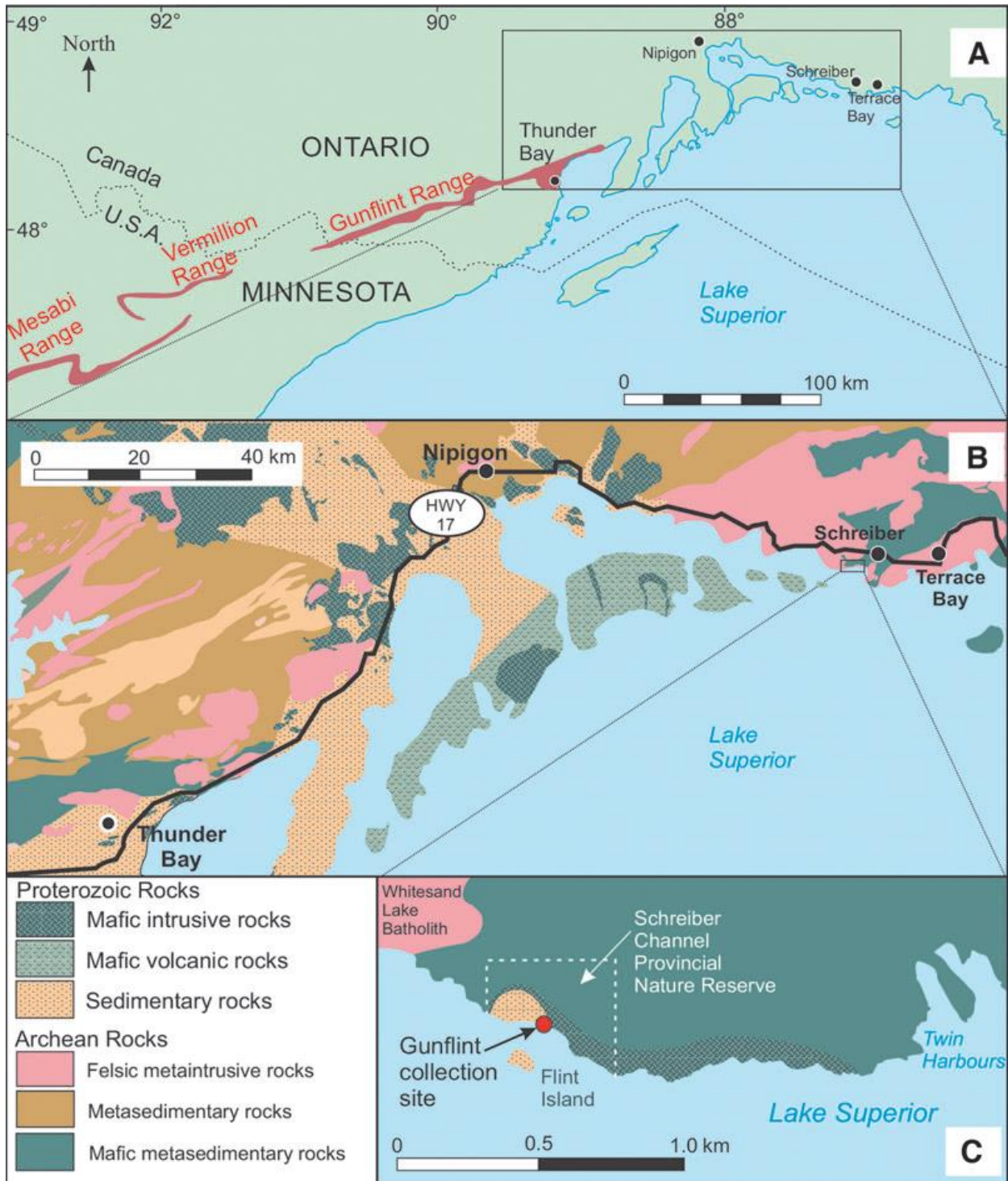


Figure 2.1 Location map of the Gunflint Chert. (A) Map of the northern Lake Superior region showing the Proterozoic Mesabi, Vermillion, and Gunflint iron ranges. (B) Enlarged view of area indicated in (A) at the northern tip of the Gunflint Iron Range, showing the distribution of Proterozoic and Archean rocks. The Gunflint Formation is included in a succession of Proterozoic sedimentary rocks underlain by Archean metamorphic rocks. (C) Enlarged view of area indicated in (B) showing the location of the collection site for Gunflint Chert samples used in this study. The collection site is a coastal outcrop of a small outlier of the Gunflint Chert located within Schreiber Channel Provincial Reserve, approximately 10 km southwest of Schreiber, Ontario (GSC Locality No. 78417, 87-20°48'W, 48-47°50'N). The samples were collected by Hans Hoffmann in 1967 prior to the establishment of the reserve (1979). (A) Modified from Cannon et al. (2008); (B) and (C) modified from Magnus (2015).

Metasedimentary strata of the Paleoproterozoic Animikie Group are divided into three formations. These are, in ascending order, The Kakabeka Conglomerate, the Gunflint Formation, and the Rove Formation. The Gunflint Formation conformably overlies the Kakabeka Conglomerate (Fralick et al., 1995) and, in turn, is overlain conformably by the metamudstones of the Rove Formation (Morey, 1967; Morey, 1969). The lower part of the Gunflint Formation contains the microfossil-rich Gunflint Chert unit, which is the focus of this study. In the discussion below, the term “Gunflint Chert” refers to this specific unit. Nd/Sm dating yielded an age range for this unit to be 2.08–2.11 Ga based on whole rock and 1.86–1.99 Ga for tuffs (Stille and Clauer, 1986; Gerlach et al., 1988; Fralick et al., 2002). The approximate upper age limit of the Gunflint Formation is based on the U-Pb age of 1.87 Ga (Morey, 1969; Fralick et al., 2002) for the upper Gunflint Formation and the overlying Rove Formation. The Gunflint Formation is a 120 m-thick succession of metasedimentary strata that includes siliciclastic, carbonate, chert, and iron formation (taconite) units, with stromatolitic horizons (Fralick et al., 2002). The Gunflint Formation is interpreted to have been deposited on the inner, shallow-water part of a marine platform influenced by strong wave and tidal activity (Wacey et al., 2012).

The exceptional quality of microfossil preservation in the cherty beds of the Gunflint Chert make this unit an important source of Proterozoic fossil data (Wacey et al., 2012). Such preservation is attributed to multiple factors, which include the following: 1) a very low grade of metamorphism (with burial temperatures of ~150°C); 2) the protective attributes of the preservation media (chert and microquartz) against post-depositional damage (Winter and Knauth, 1992; Marin et al., 2010); and 3) hydrothermal circulation of oxygenated fluids that may have caused an increase in temperatures without having induced any recrystallization of the microquartz matrix (Alleon et al., 2016). The best-preserved microfossils yet found in this unit occur in a small

outlier of the Gunflint Chert located on the Lake Superior shoreline southwest of Schreiber, Ontario (Fig. 2.1B,C), where the effects of metamorphism were minimal (Barghoorn and Tyler, 1965).

Microfossils of the Gunflint biota were initially proposed to be the remains of eukaryotes, with affinities that range from unicellular algae to radiolarians (Edhorn, 1973). These claims, however, were later refuted, and the microfossils in question were reinterpreted as prokaryotes (Awramik and Barghoorn, 1977). Although cherts of the Gunflint Chert have not yielded undisputed acritarchs, relatively large organic-walled spherical microfossils, such as *Eosphaera*, have indeed been reported (Barghoorn and Tyler, 1965; Edhorn, 1973). Awramik and Barghoorn (1977) assigned the Gunflint microbiota to sixteen taxa that were variously categorized as cyanophytes, budding bacteria, and organisms of unknown affinities. It is the latter group that is the main focus of this study.

2.2 Materials and Methods

2.2.1 Thin sections

The samples from the Gunflint Chert used in this study are on loan from the Geological Survey of Canada (GSC). Samples were initially collected from an outcrop at the north of Vein Island, located west of Schreiber Beach, Ontario, Canada (Fig. 2.1) by the late Hans Hofmann (GSC Locality No. 78417, 87°20'48"W, 48°47'50"N). This exposure is located in a very small outlier of the Gunflint Chert (Fig. 1C). Among the samples collected from this locality, only sample GSC24380 was used for this study, and a total of six thin sections, numbered GSC24380 (2), GSC24380d (2), and GSC24380e (2), were prepared from the sample.

2.2.2 Optical Microscopy

Optical microscopy involves the passage of visible light transmitted through the sample with a single or multiple lenses to allow an enlarged sample view. The resulting image can be seen through the naked eye, photographed on a photographic plate or, as is the case in this study, digitally captured (Abramowitz and Davidson, 2007; Török and Kao, 2007; Herman and Lemasters, 2012; Mertz, J. 2019).

2.2.2.1 Advantages

This microscopy class is used in many research areas, including microbiology, microelectronics, nanophysics, biotechnology, and pharmaceutical research. It can also be helpful to view biological samples for medical diagnoses, known as histopathology (Davidson and Abramowitz, 2002). In this particular study, this method was chosen due to its easy implementation and the amount of information obtained from the samples, even with a quick observation. Compared to other microscopy methods, the simple preparation of the samples - in contrast to other microscopy methods such as SEM - and the simple operation of the equipment, as well as the software, provide a fast and efficient way to obtain detailed information on the morphology of the object of study, which is crucial for this work.

Another advantage obtained for this study through optical microscopy is observing the microfossils contained in the samples in a three-dimensional way - by moving the sample along the z-axis - as originally preserved—the solid medium. In contrast, other methods discussed later in this study only provide information on the sample's surface. Although they give a clear idea of the texture and geography of the surface, they do not provide information about the three-dimensional shape of the object studied, in this case, the microfossils.

2.2.2.2 Best Suited Materials

Since this technique depends on the transmission of light through the sample to have better image quality, the sample material must have a translucent or transparent matrix. Better results are obtained the more transparent the material is. In the case of materials preserved or embedded in the matrix, they must be at least translucent to observe their particular characteristics.

For this study, the matrix where the target microfossils are preserved is made of chert, which has a high level of transparency, providing it with the optimal characteristics for its analysis by this method.

2.2.2.3 Equipment and Techniques

Optical microscopy was performed on a Zeiss Axioscope with a 100x oil lens and a 1.6x intermediate lens, achieving a 160x optical magnification. Confocal image sequences were acquired manually and processed using the Nikon NIS Elements imaging software package (ver. 4.1) to obtain a series of z-stacked focused images with approximately equal steps in depth, later combined into a single EDF image.

Due to the size of the microfossils to be analyzed, the oil immersion technique and a specialized lens were necessary to obtain better results when capturing images. In light microscopy, oil immersion is a technique used to increase the resolving power of a microscope.

This is accomplished by immersing both the objective lens and the sample in a high refractive index transparent oil, thereby increasing the numerical aperture of the objective lens.

2.2.2.4 Automated vs Manual Processes

Optical microscopes have entered the digital age, and modern microscopes tend to come with a connected computer. The motors automatically move the lens, substage condenser, and imaging system, which are automatically optimized for lighting quality, resolution, and even focus. However, the human element will always be required to supervise the process and verify the results. In some instances, this automated system can play against the study, acquiring unwanted results, or it may simply not be available on all available equipment at the time of the study. In the particular case of this research, this last factor was vital in deciding which method to use when capturing images.

As mentioned in section 2.1.3, only one microscopy set was used. In particular, this equipment lacks the automated function that would provide an even more significant amount of images in the Z-stacking process coupled with high precision in the distance on the z-axis between each photograph. Therefore, two other microscopes with the ability to perform this automated process were considered for this study. However, such equipment lacks the appropriate lenses to provide the optimal resolution to see each microfossil type's specific morphological characteristics. In summary, the decision to use a manual capture method was considered more relevant to obtaining images of higher resolution and quality than images obtained with precise lapses of the distance between them.

Due to the lack of automation, measurements were taken to approximate a constant distance on the Z-axis when capturing images. In addition, millimetre marks were drawn on the microscope knob to guide Z-axis movement at image capture, keeping it as consistent as possible between images.

2.2.3 Sample Preparation

The sample must be prepared according to specific standards for this type of analysis. Thin sections are the most recommended for this kind of method. Although a complicated process or some coating is not necessary as is the case with other microscopies, it is of vital importance to improve the quality of the images that are taken into consideration the following considerations:

2.2.3.1 Sample Thickness

As mentioned in section 2.2.2, transparency is one of the essential qualities for obtaining good quality images in this study, so samples with a wide thickness will reduce the amount of light that goes through the sample. However, if the sample is not too thin, there is a risk of not having enough complete specimens to analyze. Therefore, the thin sections used in this study are 30–50 μm thick.

2.2.4 Imaging Methodology

The following steps were used when photographing the microfossils:

- 1) The first step to perform is scanning all thin sections. Having a copy of these, whether digital or printed, facilitates their registration and helps to keep track of the location of the best specimens in each of the samples.
- 2) We proceed to review each of the thin sections we will be working on, identifying the distribution of the different types of microfossils in the entire sample.
- 3) Once the user is familiar with the contents of the sample, obtain individual images of specimens or particular locations in the sample. This will serve for the counting of specimens per image and the analysis of their distribution.

- 4) Obtain a series of confocal images – from 5 to 15 of these – manually and at tentatively regular intervals of the best specimens for each type in each thin section..
- 5) From the seven thin sections, a total of 900 confocal images were acquired from three of them for this study (samples GSC24380 (2), GSC24380d, GSC24380e).

2.2.5 Image Processing

Image processing was divided into three different steps:

2.2.5.1 Z-stacking

Using the Nikon NIS Elements imaging software package (ver. 4.1), the stacking process of the confocal image series was performed using the program's Z-stacking function, located in the ND Acquisition tab.

For spherical objects, confocal images of the lower and the upper hemispheres were created separately to avoid stacking cell surface features of the two hemispheres.

2.2.5.2 Image Enhancing

Once the images were obtained through the Z-stacking process, the shade and contrast of the images were enhanced using Adobe Photoshop C19. However, as the colour of the matrix varied even within the same sample, being more transparent or more yellowish at times, specific parameters of changes, in contrast, brightness and saturation, were not established in a general way for all images.

2.2.5.3 Pattern Recognition

The distribution of each type of complex unicellular bodies (CUBs) was determined using pixel recognition patterns in Adobe Photoshop C19 to plot them by type and then compare the

population amount of each type per sample. The number of specimens was taken according to the presence of microorganisms within the images taken with 160x magnification, which means that the total area (field of view) of each optical micrograph represents 2475 μm^2 .

In order to conduct automated measurements of CUB sizes and their distribution density, three thin sections were used in this study. 300 extended focal depth (EFD) images were generated from 3358 individual images at 100x magnification for each thin section. The field of view of each EFD image is $88.6 \mu\text{m} \times 72.8 \mu\text{m} = 6450.08 \mu\text{m}^2$. Therefore, the total area examined in detail equals $6450.08 \mu\text{m}^2$ per thin section. Each thin section has an area of $35 \times 55 \text{ mm} = 1925 \text{ mm}^2$ and, therefore, the total photographed and examined area ($6450.08 \mu\text{m}^2$, or 0.00645008 mm^2) is a minimum total thin section area. In the following discussion, regarding distribution patterns of CUBs in the rocks, we only refer to the imaged spot, which tends to have concentrated CUBs, but is highly unlikely to represent the real CUBs distribution in the whole rock.

The histogram of cell size distribution is based on measurements of D1 and D2 of 900 CUBs from images acquired at x100 magnification using a Nikon D2-Ri1 high-resolution digital camera attached to a Nikon Eclipse LV100 POL microscope.

2.2.5.4 Quantitative Analysis

In this study, qualitative and quantitative features derived from the images are compared with relevant morphological characters of acritarchs, known as unicellular eukaryotic fossils.

Based on the images, a qualitative analysis of these was done to identify and differentiate the different types of organisms discussed in the later section.

The measurement of cell diameters of the different bodies was acquired through Nikon NIS Elements imaging software and Adobe Photoshop C19. A total of 900 EDF images were acquired,

with 300 each from three of the most fossiliferous thin sections (GSC24380 (2), GSC24380d, and GSC24380e). Each of such images were derived from a Z-series of 5–17 stacked photos.

In this study, image acquisitions was focused on the relatively large, complex cell bodies. However, filamentous and coccoid bacteria were also imaged on each sample for size and distribution pattern comparisons among the various microfossil forms present. In addition, diameter measurements of individual cells and population-size projections have been done in this study (Fig. 2.4 and Fig. 2.5). Two parameters were defined when measuring the diameter: The Transverse Diameter (DT) and the Longitudinal Diameter (DL). The way both diameters were measured for each specific type of CUBs is shown in Figure 2.2. In most cells, the DL was much greater than the DT due to the elliptical or irregular ellipsoid shape of CUB type 1 and typed 4 (Fig. 2.2A and Fig. 2.2D).

2.2.5.5 *Limitations*

There are some cases where light microscopy is not well suited to the task at hand due to limitations of the technique. For example, aerated discs can be seen at very high magnifications, which are fuzzy discs surrounded by diffraction rings, appearing instead of point objects. Another aspects where optical microscopy is limited compared to other techniques are:

- Does not provide compositional information on the sample.
- The semitransparency of the material causes specimens superimposed on or below them, obscuring many of the features that are the objective of study of this research.

When the limitations of light microscopy are essential, alternative types of microscopy may be more helpful. In addition, this study prompted further questions, namely the elemental composition of the microfossils in the sample. Therefore, as discussed in the sections below, another method

was used to gather more information and complement the data obtained through optical microscopy.

2.2.6 Scanning Electron Microscopy

Scanning electron microscopy (SEM) imaging for sample GSC24380d was performed with the LEO (Zeiss) 1540XB FIB/SEM at the Nanofabrication Facility (University of Western Ontario) at 1.00kV. The sample of chert was lightly etched in HF (5%) then sonicated in deionized water for 15 min and then allowed to dry on a hotplate set at 115°C. The chert was then placed in a beaker of heptane, covered with a watch glass, and allowed to soak for 60 min. The sample was then removed and dipped in a second beaker of fresh heptane, which served as the final rinse. The chert was then allowed to air-dry overnight in a fume hood. The purpose of the heptane was to de-grease the sample before SEM imaging.

The possibility of the observed spherical cellular bodies having been emplaced on the thin sections via sample contamination is precluded by three lines of evidence:

1. Through confocal examination and imaging of the thin sections, the cyst-like bodies documented in this study are unequivocally embedded within the chert (30–50 mm thick), not on either bottom or top surfaces of the thin sections.
2. Some of the spherical bodies co-occur in loose clumps with other Gunflint microorganisms, such as the ubiquitous *cyanobacterium Gunflintia* and small spheres of *Eosphaera*.
3. SEM imaging shows that some of the spherical bodies are filled with microcrystalline quartz that also forms parts of the otherwise cherty (cryptocrystalline) matrix of the rock. This observation of primary preservation of the microorganisms corroborates the

TEM study of the Gunflint Chert by Moreau and Sharp (2004), who demonstrated an organic influence on microquartz precipitation at microfossil-matrix boundaries.

2.3 Results

At least 16 morphospecies of microorganisms have been previously identified from the Gunflint Chert (Awramik, and Barghoorn, 1977). For this study, however, we focus on the larger “complex unicellular bodies” (CUBs) with complex cellular structures, as opposed to their co-occurring, smaller-celled filamentous and coccoid bacteria. As confirmed in this study, the filamentous forms are the most abundant fossils in the Gunflint Chert, with individual cells having diameters of 0.49–0.58 μm and forming filaments up to several hundred μm in length (cf., Barghoorn, and Tyler, 1965). The next most abundant microfossils are coccoid bacteria, characterized by spheroidal to ellipsoidal shape, diameters of 1.0–1.7 μm , variable cell wall thickness, and a pitted or granular surface without protruding processes (see Awramik, 1976). The coccoid forms differ from the CUBs in being much smaller and lacking surface processes or intracellular structures. Based on images from a microfossil-rich chert sample of the Gunflint Chert (GSC 24380), we recognize three types of CUBs and one type of “multicellular” body, as described below.

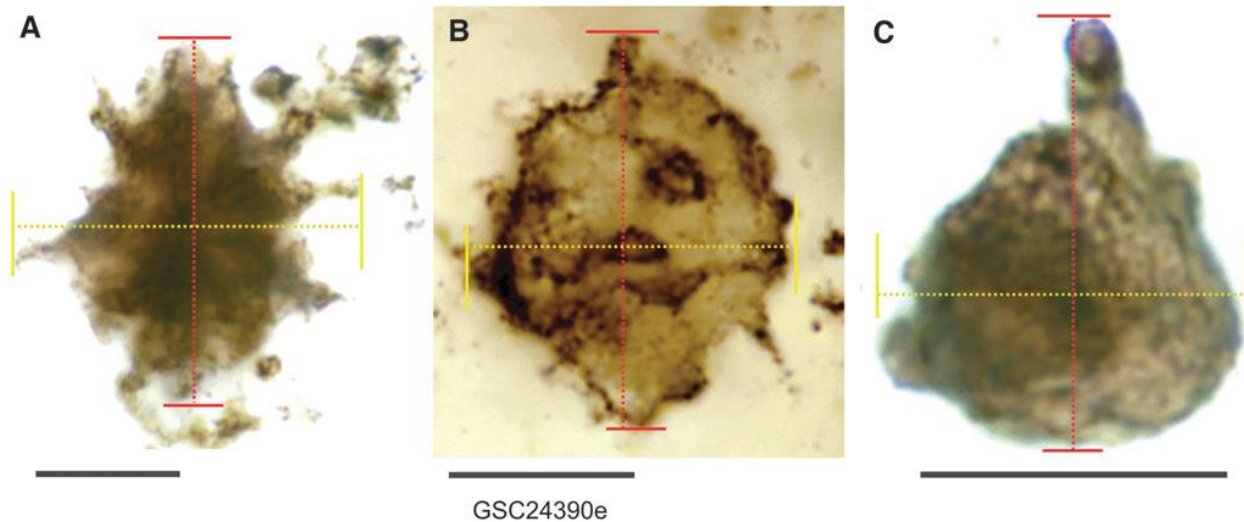


Figure 2.2 Diameter measurements of CUBs. For every CUB type, two diameters were measured: longitudinal diameter (D1, red) refers to the maximum diameter, and transversal diameter (D2, yellow) at perpendicular angle to D1. (A) Measurements of CUB Type 1. (B) Measurements of CUB Type 2. (C) Measurements of CUB Type 3, all from thin section GSC24380e. Scale bar = 10 μm .

2.3.1. CUB Type 1: Spherical cysts with numerous fine processes

These are the best-preserved and most common CUBs examined in this study, with a high level of their original complexity preserved. Their overall shape resembles a star or spoked wheel. Visible between the “spokes” are what appear to be remnants of a thin retractable membrane (Fig. 2.3A–B). Most of the organisms have a central structure, from which long endofilaments radiate outward, forming free hollow-branched processes beyond the membrane (Fig. 2.3A). The web-like membrane between the radiating endofilaments is presumed to be the shrunken remnants of a cell wall. CUB Type 1 cells range in size from 14–25 μm , but most commonly from 18–22 μm (see Fig. 2.6). CUB Type 1 differs from Type 2 and Type 3 in cell structure, especially in that its membrane is supported by thin, radiating, and hollow filaments.

2.3.2. CUB Type 2: Spherical cells with horny pustules

These cells are relatively large spherical bodies that show rather numerous, stubby horns or pustules on the cell surface (Fig. 2.3C–E; see also Appendix A, Item 1). The cysts have an average

diameter of 16–19 μm (Fig. 2.4B). Despite its relatively large size among Gunflint microorganisms, this type does not seem to have been reported in previous studies.

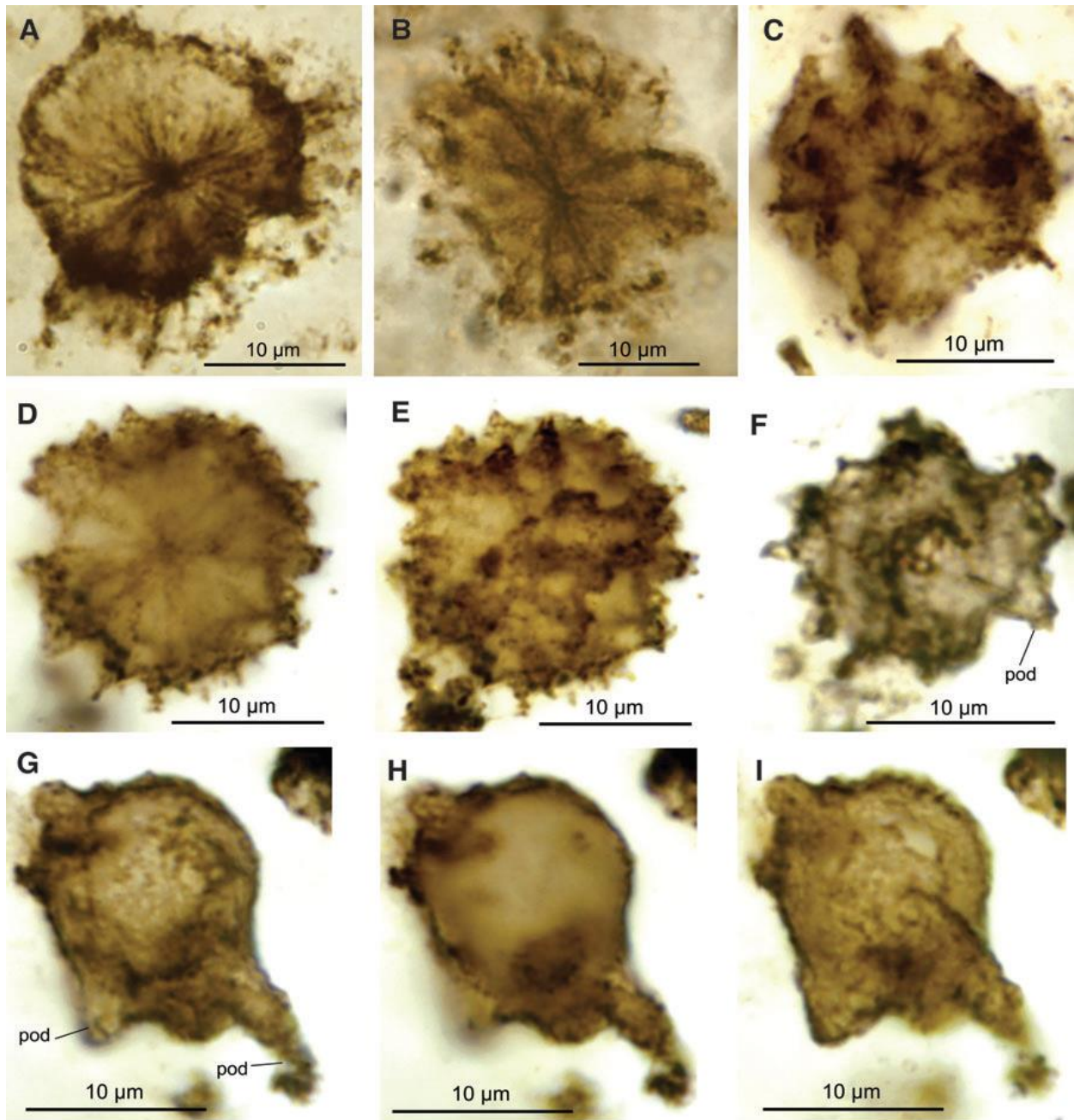


Figure 2.3 Photomicrographs of CUBs. (A, B) CUB Type 1, cells with a spheroidal body bearing radial strands, inter-strand membrane, and delicate processes projecting from cell surface, GSC24380d, thin section no. 2. (C–E) CUB Type 2, two spheroidal cells with numerous hornlike pustules (or podia) projecting from surface, GSC24380e, thin section no. 2. (D) and (E) are extended depth of focus (EDF) images through the “equatorial-center” zone (D) and one hemisphere (E) of the same CUB (see Appendix A, Item 1 for more detailed explanation). (F–I) CUB Type 3, two ovoidal cells with robust podia (labeled “pod”) of uneven sizes; (F) GSC24380d, thin section no. 2; (G–I) GSC24380e, thin section no. 2, three EDF views of the same cell in two hemispheres (G, I) and “equatorial-center zone (H).

CUB Type 2 cells are subspherical and show the smallest variation between D1 and D2 diameters as well as in overall specimen size. They have a transversal diameter range from 16 to 18 μm , and a longitudinal diameter from 16 to 19 μm , with a higher concentration towards the lower end of the size range (around 16 μm for D1 and D2; see Fig. 2.6). In conventional optical microscopy, the cells can be seen to bear radiating “spokes” or strands that merge at the cell centre and extend from the centre to the cell wall. Type 2 CUBs are the second most common in the samples examined, with more than 1700 individuals observed in this study.

2.3.3. CUB Type 3: Irregular cells with robust podia

This cell type is sub-spheroidal to sub-ovoid in shape and bears a relatively small number of large, hollow, variously sized processes or pustules (Fig. 2.3F–I), called “podia” here for simplicity. The longitudinal diameter ranges from 13 to 24 μm , averaging 15.27 μm (Fig. 2.6). Available data indicate that the podia are of variable sizes and irregularly distributed on the cell surface. One particularly well-preserved specimen (Fig. 2.4B) suggests that small processes are common on the cell surface in addition to the large process. The variable length and diameter of the podia, however, may have been due, at least partly, to preservational factors. Some well-preserved podia measure ~ 8 μm in length (Figs. 2.3G–I; 2.4A–C). Some shorter podia are assumed to be remnants of longer structures, as their hollow structure is evident at their broken terminations (Figs. 2.3G–I, 2.4C). Other smaller podia, cylindrical to conical in shape, hollow, range from 2–4 μm in length, up to 1 μm in diameter, and commonly display a rounded or slightly tapering end (e.g. “pod” in Fig. 2.4C).

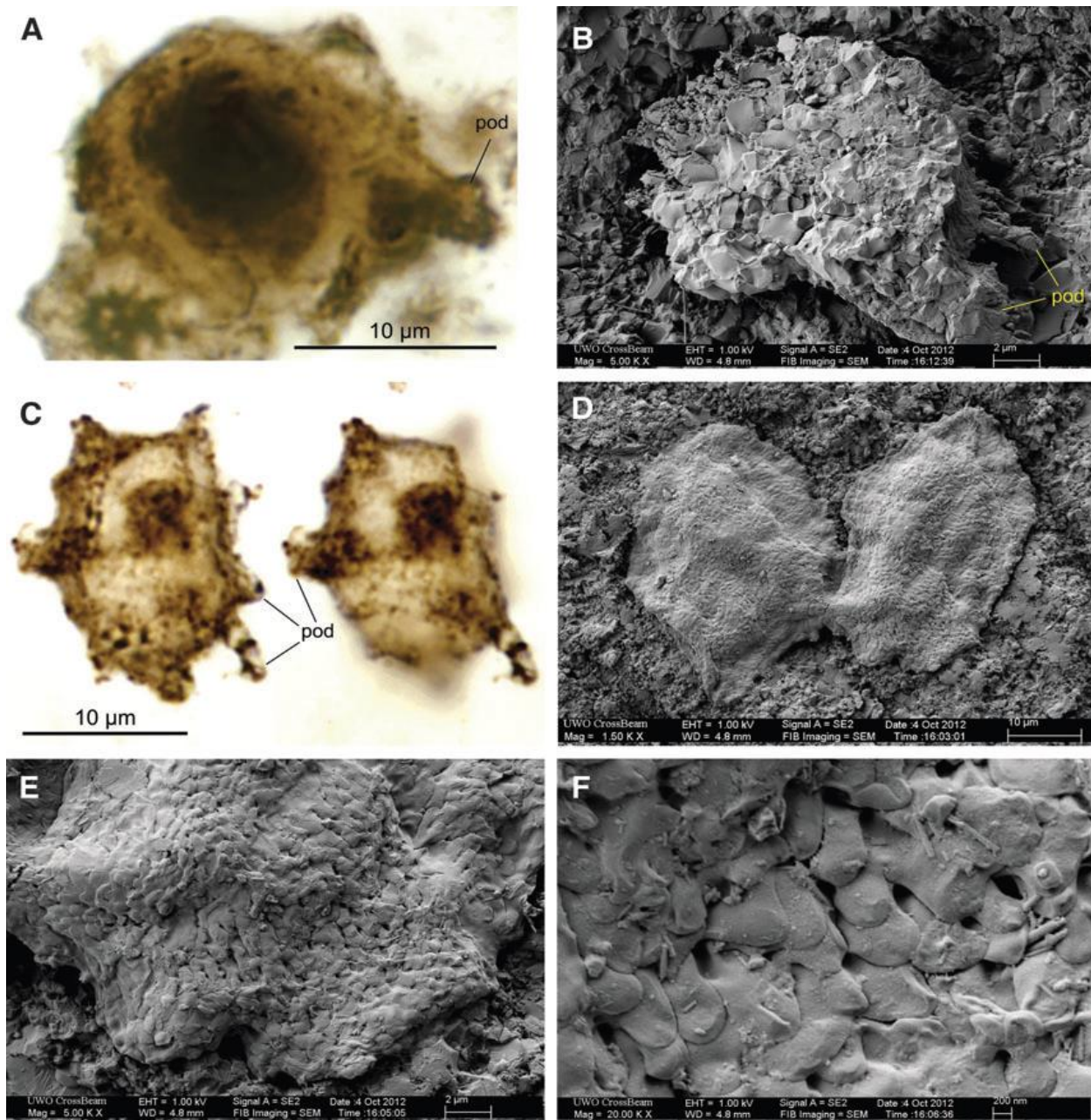


Figure 2.4 Extended depth of focus (EDF) optical and SEM images of CUB Type 3. (A) EDF view of cell with a large central dark body and a robust podium (“pod”), GSC24380d, thin section no. 2. (B) SEM image of internal mold (consisting of microquartz) after light HF etching, showing a large podium and smaller ones (labelled “pod”; note large podium similar to that in Figs. 3G–3I and 4A), GSC24380d, small rock block. (C) Two EDF views (top and bottom sides) of same cell with scale-like ornaments and podia, GSC24380e, thin section 2. (D–F) SEM images of two partly squashed cells (D) similar in shape to (C), and details of their imbricated, scale-like surface ornaments (E, F).

CUB Type 3 cells are translucent like other types but usually darker, making it difficult to discern the internal features as well as those present in the cell membrane that are easier to observe

in the other two types. In overall morphology, some of the CUB Type 3 cells resemble those of *Germinosphaera alveolata* (Miao et al., 2019) from the late Paleoproterozoic Chuanlinggou Formation of China, which were reported recently also from the Mesoproterozoic Fort Confidence Formation, Dismal Lakes Group (1590–1270 Ma) in Arctic Canada (Loron et al., 2021), as having a spheroidal cell body, with a large robust process that is hollow, broad-based, and slightly tapering towards the end. A more striking similarity is the imbricated, scale-like ornaments on the cell surface, present in both the Arctic Canada and Gunflint Chert specimens (compare Loron et al., 2021, Fig. 7.8–7.10, with Fig. 5D–F of this study). The only notable difference is the cell size; the cells from the Mesoproterozoic of Arctic Canada was described by Loron et al. (2021) to have a range of 25.9–57.0 μm , although a small ovoidal specimen they illustrated has a short diameter of $\sim 20 \mu\text{m}$, and a long diameter of $\sim 24 \mu\text{m}$ (excluding the process).

2.3.4. “Multicellular” bodies (MCBs)

This group of microfossils consists of various congregations (i.e., clusters or clumps) of bodies. They appear somewhat darker in colour compared to the other types and have a distinct reticulate pattern visible on the wall of some cells that help differentiate individual bodies within a clump. These clumps may exceed 50 μm along the long axis (e.g., Fig. 2.6A, C, D). Some of the specimens of this type show superposition of the cells at different levels of the Z-axis as well as patterns with a lighter colouration within them, giving the appearance of an amorphous black mass. In some specimens, the cells show a higher degree of integration, resembling a multicellular organism with a uni-serial (Fig. 2.6D) to multi-serial (Fig. 2.6A–C) organization of cells. It is difficult to discern the characteristic podia (as in CUB Type 3) because of the reduction of transparency by overlapping cells, but they may be present in some specimens (e.g., “pod?” in Fig. 2.6B). Crudely

tubular MCBc are commonly 10 to 15 times thicker than their co-occurring, delicate, filamentous bacteria (e.g., Fig. 2.6C–D).

2.4 Discussion

Each of the thin sections examined in this study contain a wide assortment of microorganisms, without any observable patterns of concentration for any given type of CUBs. Individual cells of CUBs examined in this study show variable shapes, with complex ornaments on the cell wall surface. Some characteristics of the CUBs show various degrees of resemblance to certain unicellular protist cell features.

2.4.1. *Eukaryote-like characteristics of the Gunflint CUBs*

In this study, two characteristics of the Gunflint CUBs are considered eukaryote-like: cell size and the presence of complex cell-wall features. Although most bacteria and archaea fall into a size range of 0.5–5.0 μm (Awramik, and Barghoorn, 1977; Shimkets, 1998), some prokaryotes can attain larger sizes. Some Archean microfossils interpreted as cyanobacteria (e.g., Altermann and Kazmierczak, 2003), or simple, biogenic microstructures (Sugitani et al., 2010), for example, can reach 10–40 μm in diameter. Individual cells of CUBs examined in this study have diameters ranging from 13 to 25 μm . This size range is smaller than that of most of the younger acritarch or other eukaryote-like microfossils of Paleo- to Mesoproterozoic age (commonly >50 μm in diameter; e.g., Agić et al., 2017; Miao et al., 2019; Loron et al., 2021), but this smaller size range is well within that of modern unicellular green algae (Kazmierczak, 1976).

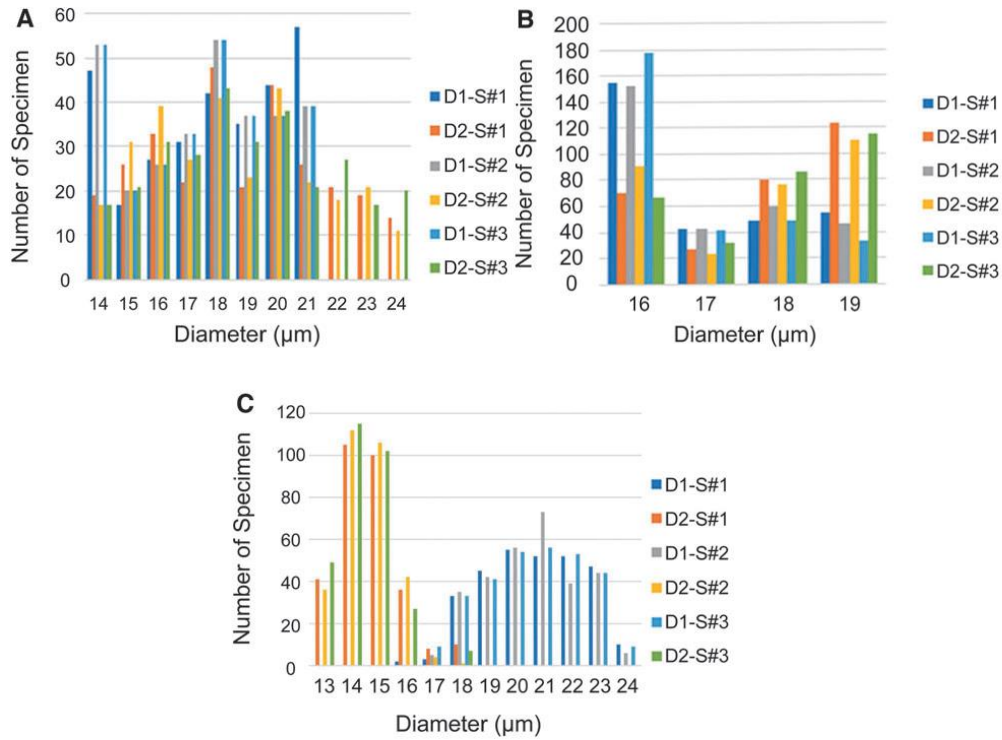


Figure 2.5 Histograms of the distribution of longitudinal and transversal diameters of CUB Types 1–3, based on 900 EDF images of cells acquired at $\times 160$ magnifications from three thin sections (see the Materials and Methods section for details). (A) The diameter distribution of CUB Type 1, ranging from 14 to 24 μm . (B) Diameters for CUB Type 2, the most spherical-like features with values ranging from 16 to 19 μm . (C) Diameters for CUB Type 3, with values ranging from 13 to 24 μm , inclusive of podia.

As noted earlier, the Mesoproterozoic *Germinosphaera* from Arctic Canada with typical eukaryotic features (robust process and scale-like cell wall ornaments) usually have a size of 26–57 μm , but can be as small as ~ 20 μm in diameter (Loron et al., 2021), which overlaps with the size of larger CUBs in this study. A wide range of variation in cell/cyst size within a single species or genus has been observed in much younger organic-walled microorganisms, such as the acritarch *Leiosphaeridia* from the Silurian (Wenlock) of Lithuania (Spiridonov et al., 2017). These authors noted that, within a short geological time of ~ 0.5 Myr, the average cyst diameter of *Leiosphaeridia* differed by about 5 times between cold and warm episodes, with a total range of cyst size from 10 to 150 μm . It is difficult to decipher the climate and ocean water temperature change for the 1.9

Ga Gunflint Chert, but the generally smaller cell size of Gunflint CUBs may have been, in large part, a reflection of their early evolutionary stage, if these microorganisms are indeed eukaryotes.

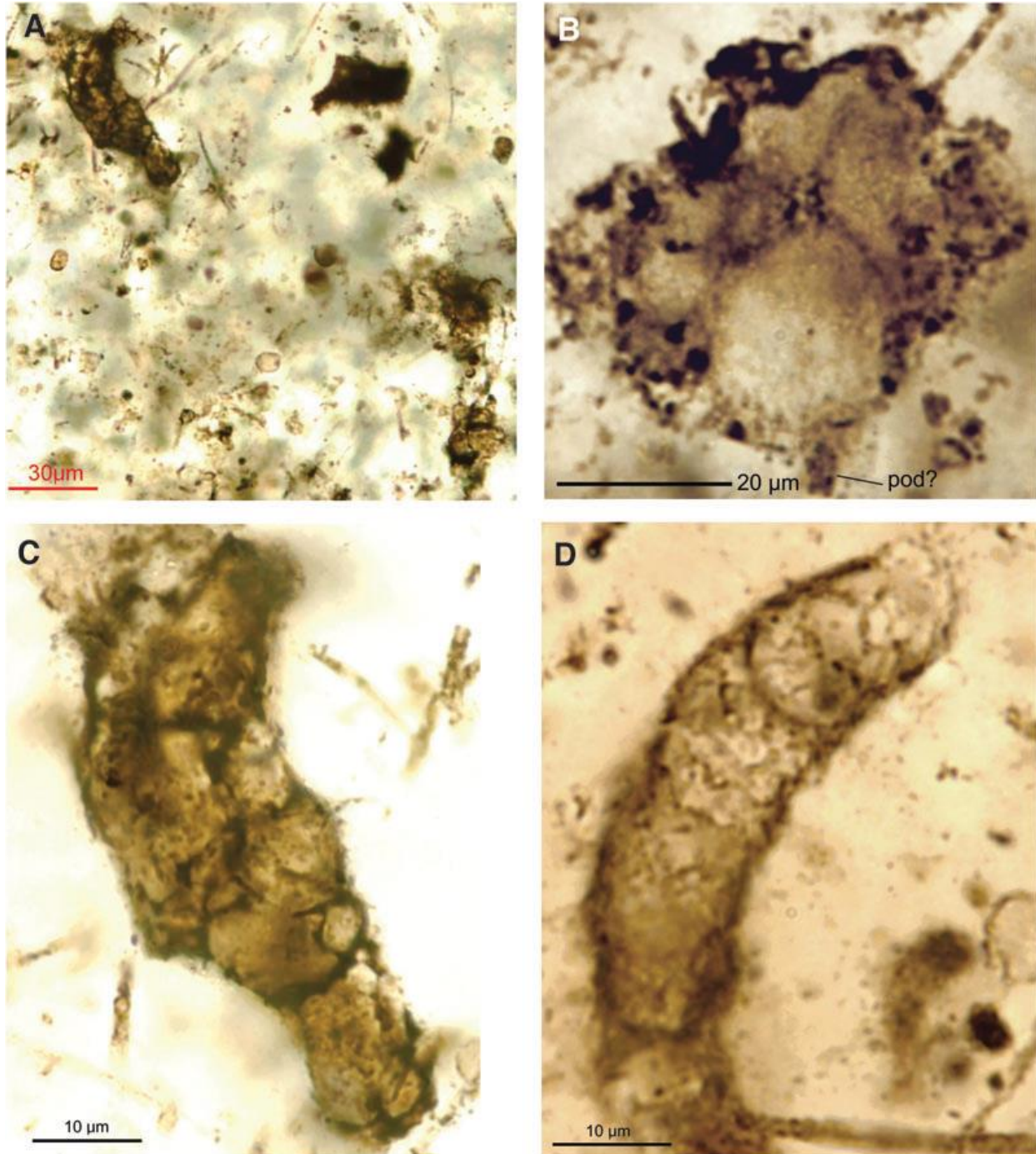


Figure 2.6 Multicellular'' bodies. (A, C) Broken pieces of a rope-like organisms with well-integrated cells of various sizes (C enlarged from upper-left corner of A), with thin, threadlike, filamentous cyanobacteria in the background, GSC24380d, thin section no. 2. (B) Four-celled structure resembling fragment in lower-right corner of (A), GSC24380e, thin section no. 2. (D) Cylindrical form with uniserial, longitudinally stacked cells, GSC24380e, thin section no. 2.

The Gunflint cyst-like cells appear to have had a strong and flexible wall, as indicated by the absence of fractures despite wrinkling and folding (Figs. 2.3–4). The reticulate-patterned surface ornamentation, which include well-defined processes, perforations/pits, ridges, and stubby pustules, large podia, and imbricated scale-like ornaments, are common characteristics of protist cells (e.g. Awramik, and Barghoorn, 1977; Agić et al., 2017;), but are unknown in prokaryotes. These complex organic-walled bodies are regarded by some as possessing truly diagnostic characters of eukaryotes as the formation of these features requires an endomembrane and cytoskeleton, which are known only in eukaryotes (Cavalier-Smith, 2002). Such complex cell-wall structures have been key to the interpretation of Paleo- to Mesoproterozoic eukaryotic microfossils in many recent studies (Agić et al., 2017; Miao et al., 2019; Loron et al., 2021).

Many morphotypes of the complex Gunflint microfossils resemble acritarchs from the Ediacaran strata of the Officer Basin, Australia, studied by Willman and Moczydłowska (2008).

These authors reported a total number of 23 different acritarch species from the Officer Basin. The main differences between these and the Gunflint CUBs is their size and age. The Ediacaran organisms are usually larger than 50 μm in diameter, whereas the CUBs in the Gunflint chert do not exceed 35 μm . However, they share similar morphology as both sets of organisms show a complex wall-surface ornamentation, filamentous structures, and dark spots at their centre (Awramik and Barghoorn, 1977; Darby, 1974; Kaźmierczak, 1979, 1979).

Acritarchs are one of the earliest groups of eukaryotes recognized in the fossil record (Knoll, 2015; Moczydłowska et al., 2011; Butterfield, 2015), and there is some evidence that the complex cells in the Gunflint chert are eukaryotic. For example, Type 1 CUBs have a similar cell shape and surface ornaments to those of *Alicesphaeridium medusoideum* (Willman and Moczydłowska,

2008), although the latter form the Ediacaran of Australia are notably larger in size (>100 μm) and show better developed radial filaments than those of the star-shaped Gunflint microfossils.

CUB Type 1 are the largest and internally complex unicellular bodies among the Gunflint Chert microfossils. The projections (Fig. 2.3A–B) are comparable to the microtubule arrangements in the cellular cytoskeleton of a protist (Menzel and Elsner-Menzel, 1990). The Gunflint biota also contains more delicate radiate structures that lack a well-defined central cell body and are commonly smaller than CUB Type 1 described here. These small star-shaped features most likely represent cyanobacteria, such as *Trichodesmium* (Cloud, 1965; Rubin et al., 2011).

Based on the images obtained in this study, CUB Type 1 also resembles the Mesoproterozoic *Shuiyousphaeridium* from the Beidajian Formation of North China (Meng et al., 2005) and several Ediacaran acritarch genera from the Officer Basin of Australia (Willman and Moczyłowska, 2008), especially in their spherical cell body with numerous, long processes.

Some of the bodies resemble the “desmid-like” or “radiolaria-like” organisms noted by Edhorn (1973). Relatively delicate processes show an irregular texture, thicker proximally, and thinner distally, like those in the Ediacaran acritarch *Tanarium* from Australia (Willman and Moczyłowska, 2008). In some cells, the processes appear to spread into the meshwork (Fig. 2.3A) like those in the Ediacaran acritarch *Appendisphaera* (Willman and Moczyłowska, 2008). In others, the processes appear more robust, with relatively few of these showing the random curvature observed in *Tanarium* from the same Ediacaran assemblage.

In their cell shape, size, and ornamentation, Type 2 CUBs are similar to *Gambierdiscus toxicus*, a modern dinoflagellate (Knoll, 2015). Some specimens show dark-brown bodies with rather clear boundaries inside the cell, which may be preserved nucleus or organelles. Reticulate sculpturing

is visible on the wall of some cells like those observed in BSE images, with regularly spaced pustules, pits, and ridges.

Apart from their relatively small size, some cells of CUB Type 3 with multiple podia on the cell surface (“pod” in Fig. 2.4C) resemble some much younger (Ediacaran) acanthomorph acritarchs (Willman and Moczyłowska, 2008). The prominent single large podium and scale-like cell surface ornaments in some other CUB Type 3 cells (Figs. 2.3G–I; 4A–B) are characteristic of *Germinosphaera alveolata* of late Paleo- to Mesoproterozoic age (see discussion above). All these complex cell-wall structures have been regarded as eukaryotic characteristics (for recent summary, see Agić et al., 2017; Miao et al., 2019; Loron et al., 2021).

2.5 Conclusions

Recent studies have interpreted well-preserved acritarchs and other complex organic-walled microfossils of Proterozoic age as eukaryotes, pushing back the record of these fossils ~1.8 Ga (e.g., Montenari and Leppig, 2003; Willman and Moczyłowska, 2008; Moczyłowska et al., 2011; Butterfield, 2015; Agić et al., 2017; Miao et al., 2019; Loron et al., 2021). Putative eukaryotic microfossils have been reported from the Archean (Każmierczak et al., 2016), although the age is in general agreement with predictions of the genome/molecular timescale (Hedges et al., 2001; Hedges et al., 2004).

The present study on the Gunflint Chert using extended-focal-depth optical microscopy and SEM imaging of the complex unicellular bodies (CUBs) has demonstrated a number of cellular morphologies similar to those of younger Proterozoic microfossils reported to be of eukaryotic affinity.

- 1) Relatively large cell size. The CUBs ranges from 10 to 35 μm in diameter (commonly 13–25 μm), which is considerably larger than the coccoid cyanobacteria in the same samples (usually ~ 5 μm). They are, however, generally smaller than the Proterozoic acritarchs, though the size of larger Gunflint CUBs overlaps with the smaller forms of Mesoproterozoic *Germinosphaera* interpreted by various authors as eukaryote.
- 2) Complex surface ornaments. The reticulate-patterned pits and tubercles and variously shaped processes are not present in the coccoid cyanobacteria in the Gunflint Chert. These cell surface ornaments bear a high degree of similarity to those in acritarchs and other organic-walled microfossils regarded as eukaryotes.
- 3) Intracellular dark bodies. The radiating filaments and well-delimited dark bodies inside the CUB cells may have been the residue of nuclei or organelles.

References

- Abramowitz, M. and Davidson, M.W., 2007, Introduction to microscopy: Molecular Expressions, p. 8–22.
- Agić, H., Moczyłowska, M., and Yin, L., 2015, Diversity of organic-walled microfossils from the early Mesoproterozoic Ruyang Group, North China Craton – A window into the early eukaryote evolution: *Precambrian Research*, v. 297, p. 101–130.
- Agić, H., Moczyłowska, M., and Yin, L., 2017, Diversity of organic-walled microfossils from the early Mesoproterozoic Ruyang Group, North China Craton—A window into the early eukaryote evolution: *Precambrian Research*, v. 297, p. 101–130.

- Alleon, J., Bernard, S., Le Guillou, C., Marin-Carbonne, J., Pont, S., Beyssac, O., McKeegan, K.D., and Robert, F., 2016, Molecular preservation of 1.88 Ga Gunflint organic microfossils as a function of temperature and mineralogy: *Nature Communications*, v. 7, p. 11977.
- Altermann, W., and Kazmierczak, J., 2003, Archean microfossils: a reappraisal of early life on Earth: *Research in Microbiology*, v. 154, p. 611–617
- Awramik, S.M., 1976, Gunflint stromatolites: Microfossil distribution in relation to stromatolite morphology: *Developments in Sedimentology*, Elsevier, v. 20, p. 311–320.
- Awramik, S.M., and Barghoorn, E.S., 1977, The Gunflint microbiota: *Precambrian Research*, v. 5, p. 121–142.
- Barghoorn, E.S., 1971, The oldest fossils: *Scientific American*, v. 224, n. 5, p. 30–43.
- Barghoorn, E.S. and Tyler, S.A., 1965, Microorganisms from the Gunflint Chert: *Science* v. 147, p. 563–577.
- Brocks, J.J., Logan, G.A., Buick, R., and Summons RE., 1999, Archean molecular fossils and the early rise of eukaryotes: *Science*, v. 285, p. 1033–1036.
- Butterfield, N.J., 2015, Early evolution of the Eukaryota: *Palaeontology*, v. 58, n. 1, p. 5–17.
- Cannon, W.F., LaBerge, G.L., Klasner, J.S., and Schulz, K.J., 2008, The Gogebic Iron Range—a sample of the northern margin of the Penokean fold and thrust belt (No. 1730). USGS.
- Cavalier-Smith, T., 2002, The neomuran origin of archaeobacteria, the negibacterial root of the universal tree and bacterial megaclassification: *International Journal of Systematic and Evolutionary Microbiology*, v. 52, p. 7–76.

- Cloud, P.E., 1965, Significance of the Gunflint (Precambrian) microflora: *Science*, v. 148, p. 27–35.
- Cloud, P.E., and Licari, G.R., 1968, Microbiotas of the banded iron formations: *Proceedings of the National Academy of Sciences*, v. 61, no. 3, p. 779.
- Dacks, J.B., Field, M.C., Buick, R., Eme, L., Gribaldo, S., Roger, A.J., Brochier-Armanet, C., and Devos, D.P., 2016, The changing view of eukaryogenesis – fossils, cells, lineages and how they all come together: *Journal of Cell Science*, v. 129, p. 3695–3703.
- Darby, D.G., 1974, Reproductive modes of *Huroniospora microreticulata* from cherts of the Precambrian Gunflint Iron-Formation: *Geological Society of America Bulletin*, v. 85, no. 10, p. 1595–1596.
- Davidson, M.W. and Abramowitz, M., 2002, Optical microscopy: *Encyclopedia of imaging science and technology*, v. 2, n. 1106–1141, p. 120.
- Edhorn, A., 1973, Further investigations of fossils from the Animikie, Thunder Bay, Ontario: *Proceedings of the Geologists' Association*, v. 25, p. 37–66.
- El Albani, A., Bengtson, S., Canfield, D.E., Macchiarelli, R., Mazurier, A., Hammarlund, E.U., Boulvais, P., Dupuy, J.J., Fontaine, C., and Fürsich, F.T., 2010, Large colonial organisms with coordinated growth in oxygenated environments 2.1 Gyr ago: *Nature*, v. 466, p. 100–104.
- El Albani, A., Bengtson, S., Canfield, D.E., Riboulleau, A., Rollion Bard, C., Macchiarelli, R., Ngombi Pemba, L., Hammarlund, E., Meunier, A., Moubiya Mouele, I., and Benzerara,

- K., 2014, The 2.1 Ga Old Francevillian Biota: Biogenicity, Taphonomy and Biodiversity: PLOS ONE, v. 9, no. 6, p. e99438. doi:10.1371/journal.pone.0099438.
- El Albani, A., Mangano, M.G., Buatoid, L.A., Bengtson, S., Riboulleau, A., Bekker, A., Konhauser, K., Lyons, T., Rollion-Bard, C., Bankole, O., and Baghekema, S.G., 2019, Organism motility in an oxygenated shallow-marine environment 2.1 billion years ago: Proceedings of the National Academy of Sciences, v. 116, p. 3431–3436.
- Fralick, P., and Barrett, T.J., 1995, Depositional controls on iron formation associations in Canada. In *Sedimentary Facies Analysis: A Tribute to the Research and Teaching of Harold G.*, edited by G. Plint, Reading, p. 137–156.
- Fralick, P., Davis, D.W., and Kissin, S.A., 2002, The age of the Gunflint Chert, Ontario, Canada: single zircon U–Pb age determinations from reworked volcanic ash: *Canadian Journal of Earth Sciences*, v. 39, p. 1085–1091.
- French, K.L., Hallmann, C., Hope, J.M., Schoon, P.L., Zumberge, J.A., Hoshino, Y., Peters, C.A., George, S.C., Love, G.D., Brocks, J.J., and Buick, R., 2015, Reappraisal of hydrocarbon biomarkers in Archean rocks: *Proceedings of the National Academy of Sciences*, v. 112, p. 5915–5920.
- Gerlach, D.C., Shirey, S.B., and Carlson, R.W., 1988, Nd isotopes in Proterozoic iron formations: evidence for mixed age provenance and depositional variability: *EOS* v. 69, p. 1515.
- Golubic, S., and Hofmann, H.J., 1976, Comparison of Holocene and mid-Precambrian Entophysalidaceae (Cyanophyta) in stromatolitic algal mats: cell division and degradation: *Journal of Paleontology*, p. 1074–1082.

- Han, T.M., and Runnegar, B., 1992, Megascopic eukaryotic algae from the 2.1-billion-year-old Negaunee Iron formation: *Science*, v. 257, p. 232–235.
- Hedges, S.B., Blair, J.E., Venturi, M.L., and Shoe, J.L., 2004, A molecular timescale of eukaryote evolution and the rise of complex multicellular life: *BMC Evolutionary Biology*, v. 4, n. 1, p. 1–9.
- Hedges, S.B., Chen, H., Kumar, S., Hedges, S.B., Chen, H., Kumar, S., Wang, D.Y., Thompson, A.S. and Watanabe, H., 2001, A genomic timescale for the origin of eukaryotes: *BMC Evolutionary Biology*, v. 1, n. 1, p. 1–10.
- Herman, B. and Lemasters, J.J. eds., 2012, *Optical microscopy: emerging methods and applications*: Elsevier.
- Hirsch, P., 1974, Budding bacteria: *Annual Review of Microbiology*, v. 28, n. 1, p. 391–440.
- Hofmann, H.J., 1971, Precambrian fossils, pseudofossils and problematica in Canada: *Geological Survey Canada Bulletin*, v. 189, p. 1–146.
- Kaźmierczak, J., 1976, Devonian and modern relatives of the Precambrian *Eosphaera*: possible significance for the early eukaryotes: *Lethaia*, v. 9, n. 1, p. 39–50.
- Kaźmierczak, J., 1979, The eukaryotic nature of *Eosphaera*-like ferriferous structures from the Precambrian Gunflint Iron Formation, Canada: a comparative study: *Precambrian Research*, v. 9, p. 1–22.
- Kaźmierczak, J., Kremer, B., Altermann, W., and Franchi, I., 2016, Tubular microfossils from 2.8 to 2.7 Ga-old lacustrine deposits of South Africa: A sign for early origin of eukaryotes?: *Precambrian Research*, v.286, p. 180–194.

- Krumbein, W.E., 2010, Gunflint Chert microbiota revisited — Neither stromatolites nor cyanobacteria: In *Microbial Mats*, edited by J. Seckbach and A. Oren, Springer, Dordrecht, p. 53–70.
- Knoll, A.H., 2015, *Life on a Young Planet: The First Three Billion Years of Evolution on Earth*—updated edition: Princeton University Press, p. 296.
- Knoll, A.H., Javaux, E.J., Hewitt, D., and Cohen, P., 2006, Eukaryotic organisms in Proterozoic oceans: *Philosophical Transactions of the Royal Society London B, Biological Sciences*, v. 361, p. 1023–1038.
- Licari, G.R., and Cloud, P.E., 1968, Reproductive structures and taxonomic affinities of some nanofossils from the gunflint iron formation: *Proceedings of the National Academy of Sciences*, v. 59, n. 4, p. 1053.
- Loron, C.C., Halverson, G.P., Rainbird, R.H., Skulski, T., Turner, E.C. and Javaux, E.J., 2021, Shale-hosted biota from the Dismal Lakes Group in Arctic Canada supports an early Mesoproterozoic diversification of eukaryotes: *Journal of Paleontology*, v. 95, n. 6, p. 1113–1137, doi: 10.1017/jpa.2021.45.
- Magnus, W.S., 2015, Gunflint Range. https://en.wikipedia.org/wiki/Gunflint_Range (Accessed October 1, 2021).
- Marin, J., Chaussidon, M., and Robert, F., 2010, Microscale oxygen isotope variations in 1.9 Ga Gunflint cherts: assessments of diagenesis effects and implications for oceanic paleotemperature reconstructions: *Geochimica et Cosmochimica Acta*, v. 74, n. 1, p. 116–130.

- Meng, F.W., Zhou, C.M., Yin, L., Chen, Z., and Yuan, X., 2005, The oldest known dinoflagellates: morphological and molecular evidence from Mesoproterozoic rocks at Yongji, Shanxi Province: *Chinese Science Bulletin*, v. 50, p. 1230–1234.
- Menzel, D., and Elsner-Menzel, C., 1990, The microtubule cytoskeleton in developing cysts of the green alga *Acetabularia*: Involvement in cell wall differentiation: *Protoplasma*, v. 157, n. 1–3, p. 52–63.
- Mertz, J., 2019, *Introduction to optical microscopy*: Cambridge University Press.
- Miao, L., Moczyłowska, M., Zhu, S., and Zhu, M., 2019, New record of organic-walled, morphologically distinct microfossils from the late Paleoproterozoic Changcheng Group in the Yanshan Range, North China: *Precambrian Research*, v. 321, p. 172–198.
- Moczyłowska, M., Landing, E.D., Zang, W., and Palacios, T., 2011, Proterozoic phytoplankton and timing of chlorophyte algae origins: *Palaeontology*, v. 54, n. 4, p. 721–733.
- Montenari, M., and Leppig, U., 2003, The Acritarcha: their classification morphology, ultrastructure and palaeoecological/palaeogeographical distribution: *Paläontol Zeitschrift*, v. 77, p. 173-194.
- Moreau, J.W. and Sharp, T.G., 2004, A transmission electron microscopy study of silica and kerogen biosignatures in 1.9 Ga Gunflint microfossils: *Astrobiology*, v. 4, p. 196–210.
- Morey, G.B., 1967 Stratigraphy and sedimentology of the Middle Precambrian Rove Formation in northeastern Minnesota: *Journal of Sedimentary Research*, v. 37, n. 4, p. 1154–1162.

- Morey, G.B., 1969, The Geology of the Middle Precambrian Rove Formation in northeastern Minnesota. Minnesota Geological Survey: University of Minnesota Digital Conservancy v. 7, p. 1–62.
- Padmaja, T.D., 1972, Studies on coccoid blue-green algae: II. In International Symposium on Taxonomy and Biology of Bluegreen Algae, 1st, Madras, Papers, p. 75–127.
- Rasmussen, B., Fletcher, I.R., Brocks, J.J., and Kilburn, M.R., 2008, Reassessing the first appearance of eukaryotes and cyanobacteria: *Nature*, v. 455, p. 1101–1105.
- Rubin, M., Berman-Frank, I., and Shaked, Y., 2011, Dust- and mineral-iron utilization by the marine dinitrogen-fixer *Trichodesmium*: *Nature Geoscience*, v. 4, p. 529–534.
- Schneider, D.A., Bickford, M.E., Cannon, W.F., Schulz, K.J., and Hamilton, M.A., 2002, Age of volcanic rocks and syndepositional iron formations, Marquette Range Supergroup: implications for the tectonic setting of Paleoproterozoic iron formations of the Lake Superior region: *Canadian Journal of Earth Sciences*, v. 39, n. 6, p. 999–1012.
- Shimkets, L.J., 1998, Structure and Sizes of Genomes of the Archaea and Bacteria. In *Bacterial Genomes: Physical Structure and Analysis*, edited by F.J. de Bruijn, J.R. Lupskin and G.M. Weinstock: Kluwer Academic Publishers, Boston, p. 5–11.
- Spiridonov, A., Venckute-Aleksiene, A., and Radzevičius, S., 2017, Cyst size trends in the genus *Leiosphaeridia* across the Mulde (lower Silurian) biogeochemical event: *Bulletin of Geosciences*, v. 92, p. 391–404.

- Stille, P., and Clauer, N., 1986, Sm–Nd isochron age and provenance of the argillites of the Gunflint iron formation in Ontario, Canada: *Geochimica et Cosmochimica Acta*, v. 50, p. 1141–1146.
- Strother, P.K., Battison, L., Brasier, M.D., and Wellman, C.H., 2011, Earth’s earliest non-marine eukaryotes: *Nature*, v. 473, n. 7348, p. 505–509.
- Sugitani, K., Lepot, K., Nagaoka, T., Mimura, K., Van Kranendonk, M., Oehler, D.Z., and Walter, M.R., 2010, Biogenicity of morphologically diverse carbonaceous microstructures from the ca. 3400Ma Strelley Pool Formation, in the Pilbara Craton, Western Australia: *Astrobiology*, v. 10, n. 9, p. 899–920.
- Summons, R.E., Jahnke, L.L., Hope, J.M., and Logan, G.A., 1999, 2-Methylhopanoids as biomarkers for cyanobacterial oxygenic photosynthesis: *Nature*, v. 400, p. 554–557.
- Tappan, H., 1976, Possible eucaryotic algae (Bangiophyceae) among early Proterozoic microfossils: *Geological Society of America Bulletin*, v. 87, n. 4, p. 633–639.
- Török, P. and Kao, F.J. eds., 2007, *Optical imaging and microscopy: techniques and advanced systems*: Springer, v. 87.
- Wacey, D., Menon, S., Green, L., Gerstmann, D., Kong, C., Mcloughlin, N., Saunders, M., and Brasier, M., 2012, Taphonomy of very ancient microfossils from the ~ 3400 Ma Strelley Pool Formation and ~1900 Ma Gunflint Chert: New insights using a focused ion beam: *Precambrian Research*, v. 220, p. 234–250.

Willman, S., and Moczyłowska, M., 2008, Ediacaran acritarch biota from the Giles 1 drillhole, Officer Basin, Australia, and its potential for biostratigraphic correlation: *Precambrian Research*, v. 162, p. 498–530.

Winter, B.L., and Knauth, L.P., 1992, Stable isotope geochemistry of cherts and carbonates from the 2.0 Ga Gunflint Iron Formation: implications for the depositional setting, and the effects of diagenesis and metamorphism: *Precambrian Research*, v. 59, n. 3–4, p. 283–313.

Chapter 3: *Germinosphaera gunflinta* n. sp. – Protist-like microfossil from the 1.9 Ga Gunflint Chert Formation, northern Ontario, Canada²

3.1 Introduction

Germinosphaera Mikhailova, 1986 is one of the most commonly reported organic-walled microfossils from Proterozoic rocks (for a recent summary, see Loron, 2021). It was originally described from the Neoproterozoic Danshkin Formation of the Siberian Platform, but several species of *Germinosphaera* have subsequently been recognized worldwide. Occurrences reported thus far include: the Paleoproterozoic of North China (Yan, 1995; Miao et al., 2019; Miao et al., 2021; Agić, 2021), Gabon (Amard and Bertrand-Sarfati, 1997; Srivastava and Kumar, 2003), and Siberia (Stanevich et al., 2013); the Mesoproterozoic of North China (Li et al., 2019; Han et al., 2021; Miao et al., 2021), northern USA (Strother and Wellman, 2020), the Siberian Platform (Jankauskas et al., 1989; Veis and Vorob'eva, 1992; Sergeev et al., 1995; Shuvalova et al., 2021), Sweden (Loron et al., 2016a; Loron et al., 2016b; Loron et al., 2017), northern Canada (Loron et al., 2021), and the Democratic Republic of Congo (Baludikay et al., 2016); the Neoproterozoic of Spitsbergen (Butterfield et al., 1994; Butterfield, 2015; Tang et al., 2013; Tang et al., 2015; Knoll et al., 1991), India (Prasad, 2005; Srivastava, 2012), Brazil (Denezine, 2018; Lehn et al., 2019), northwestern Canada (Loron et al., 2019a; Loron et al., 2019b; Butterfield and Rainbird, 1998; Butterfield, 2005b); Russia (Mikhailova, 1986; Vorob'eva et al., 2009; Jankauskas et al., 1989; Veis et al., 2006; Chamov et al., 2010), northern China (Yin and Guan, 1999; Wang, 2021; Yin and Li, 1978; Ouyang et al., 1974), Australia (Zang, 1995; Grey, 2005; Beraldi-Campesi and Retallack, 2016; Retallack et al., 2014; Retallack et al., 2015), and Scotland (Brasier et al., 2017;

² A version of this chapter has been submitted to the Journal of Paleontology and is currently under review.

Battison and Brasier, 2012). In early studies, the genus was identified mostly by its rounded cyst with one prominent process (podium) or more processes (podia). More recently, greater attention was paid to its complex cell-surface ornaments, especially the scale-like microstructures (Loron, 2021). Processes and scale-like ornaments have been considered uniquely eukaryotic characteristics (Agić et al., 2017; Miao et al., 2019; Loron et al., 2021), thus making *Germinosphaera* an important microfossil taxon for investigating the origin and early evolution of eukaryotes because of its abundance and long geological range, from the Paleoproterozoic (~2 Ga) to the latest Neoproterozoic (Ediacaran Period), or even extending into the early Cambrian (Butterfield and Grotzinger, 2012).

Our recent re-examination of the Gunflint Chert Formation (~1.9 Ga) reveals *Germinosphaera* to be an abundant taxon in the well-known Gunflint microbiota as one of three types of complex unicellular bodies (CUBs; González-Flores et al., 2022). In addition to their consistently small cell (cyst) size, the Gunflint forms exhibit the diagnostic characteristics of *Germinosphaera*, namely the distinctive podia and scale-like surface ornaments. The specimens described herein are among the best-preserved material assigned so far to the genus and may potentially reveal important clues to the early evolution of eukaryotes. Other organic-walled microfossils similar to *Germinosphaera* from lower Neoproterozoic rocks in northern Canada have been interpreted as eukaryotes, or some more specifically as fungi (Loron et al., 2019a; Loron et al., 2019b). Similarly, various microfossils from the Gunflint microbiota were also suggested to have a fungal affinity (Krumbein, 2010), although this hypothesis has not attracted much attention. Therefore, the main objectives of this study are to: 1) describe in detail the Gunflint-hosted species of *Germinosphaera*, 2) investigate the size and other morphologic trends of Proterozoic species of *Germinosphaera* and, 3) explore the implications of these characteristics for the evolution of this genus and their eukaryotic affinity.

3.2 Geological Background

The Gunflint Formation of the Animikie Group is exposed along the northern shore of Lake Superior, extending from the Thunder Bay area of Ontario to Cook and Itasca counties of Minnesota (Fig. 2.1).

The Gunflint Formation is a 120 m-thick succession of metasedimentary strata, including siliciclastic, carbonate, stromatolitic chert, and iron formation (taconite) units (Fralick et al., 2002). The Gunflint succession is interpreted to have been deposited on a the shallow marine platform influenced by strong waves and tidal activity (Wacey et al., 2012).

Within the Animikie Group, the Gunflint Formation overlies the Kakabeka Conglomerate (Fralick et al., 1995) and the mudstones of the Rove Formation (Morey, 1967; Morey, 1969). The lower part of the formation is dated at 2.08–2.11 Ga (Stille and Clauer, 1986; Gerlach et al., 1988; Fralick et al., 2002). The unit commonly referred to as the "Gunflint Chert" is a thin (2 m thick) unit of stromatolitic black chert, approximately 60 m above the base of the formation, overlying a thin unit of breccia and sandstone (Barghoorn and Stanley, 1965). The upper age limit of the Gunflint Formation is constrained at approximately 1.87 Ga based on U-Pb dating of the overlying Rove Formation (Morey, 1969; Fralick et al., 2002).

3.3 Material and Methods

Chert samples GSC24380 (2), GSC24380d and GSC24380e from the Gunflint Formation, on loan from the Geological Survey of Canada (GSC), were used for this study. A total of 6 thin sections, three small chert blocks approximately 1.5 x 1.5 x 1 cm, and 4 SEM stud slices were cut from sample GSC24380. The late Hans Hoffman collected the samples in 1976 from an outcrop outlier of the Gunflint Chert on Schreiber Beach, Ontario, Canada (Fig. 2.1).

Conventional optical microscopy was carried out using a Zeiss Axioscope with a 100x oil lens and a 1.6x intermediate lens, achieving a combined optical magnification of 160x. Confocal image sequences were acquired manually, using the Nikon NIS Elements imaging software package (ver. 4.1), resulting in a Z-series (comprising between 5 and 15 in a series depending on the complexity of a given microfossil) of images along with an extended depth of field-view (EDF), with approximately equal steps of focal depths. Each such Z-series was then combined into a single EDF image. For studying the genus *Germinosphaera*, 900 EDF optical images were obtained, with 300 taken per three thin sections GSC24380 (2), GSC24380d and GSC24380e. From the images, qualitative and quantitative analyses were carried out to characterize their size and other morphologic features (e.g., processes and surface ornaments).

For quantitative analysis, measurements of the dimensions of a cyst (main rounded body proper) and its processes (podia) were made separately for both the Gunflint specimens of *Germinosphaera* and those illustrated as photographs in the published literature. Measurements were acquired using the Nikon NIS Elements imaging software and Adobe Photoshop C19. The relationships among numerous specimens and various species of *Germinosphaera* were investigated through multivariate (Principal component) analysis, using the PAST software (Hammer et al., 2001) and Microsoft Excel.

Scanning Electron Microscopy (SEM) Backscattered-Electron (BSE) images for the three blocks of the GSC24380d sample were obtained using the LEO (Zeiss) 1540XB FIB/SEM at Nanofabrication Facility (University of Western Ontario), at a magnification of 2.00 to 5.00 KX and EHT between 1.00 and 5.00 kV. This ultra-clean facility was chosen to avoid any external contamination of the samples. In-situ elemental mapping was performed using the Oxford Instruments x-ray system to measure the concentration pattern of carbon (C), oxygen (O), silicon (S), aluminum (Al), sodium (Na), and chlorine (Cl).

For SEM analysis, the samples were etched in hydrofluoric (HF) acid for 15 to 30 minutes, then carefully drained and rinsed with distilled water to avoid any contamination or removal of exposed organic material from the fossils. After one day of air drying, the samples were coated with a 4 nm thick osmium layer. For the preparation of the 4 SEM stud samples, residual material from HF etching was collected on filter paper and transferred to three of the four studs; for the fourth stud, a small piece of the filter paper containing the residual material was placed on the stud surface.

The chemical composition of the samples was determined through wavelength dispersive X-ray spectroscopy (WDS) analysis using a JEOL JXA-8530F field-emission electron microprobe belonging to the Earth and Planetary Materials Analysis (EPMA) Laboratory (University of Western Ontario). The samples were carbon-coated, and Backscattered-Electron (BSE) images were obtained with a magnification between 4.00 to 7.00 KX and EHT of 15.0 kV.

3.4 Systematic Paleontology

Organic-walled microfossils

Genus *Germinosphaera* Mikhailova (1986) emend. Butterfield in Butterfield et al., 1994

Type species.—*Germinosphaera bispinosa* Mikhailova, 1986, emend. Butterfield, Knoll and Swett, 1994, upper Riphean (Neoproterozoic) deposits of the Siberian Platform, Krasnoyar region, River Uderei, Danshkin Formation, Russia (Mikhailova, 1986; Butterfield et al., 1994).

Remarks.— The type species was from the Neoproterozoic (upper Riphean) Dashka Formation, eastern Siberian Platform, Siberia (Mikhailova, 1986). However, this species was subsequently reported from several other localities, including the Neoproterozoic Svanbergfjellet Formation, Akademikerbreen Group, of Spitsbergen (Butterfield et al., 1994); the Neoproterozoic "upper formation" of the Visingsö Group, Sweden (Loron and Moczydłowska, 2017); the late Mesoproterozoic Escape Rapids Formation and early Neoproterozoic Grassy Bay Formation, Shaler Supergroup, Canada (Loron et al., 2019a; Loron et al., 2019b); the Mesoproterozoic of the Fort Confidence Formation, Dismal Lakes Group, Canada (Loron et al., 2021); the Upper Riphean Dashkin Formation of the Dashkinskaya suite (Jankauskas et al., 1989); the Sirbu Shale of the Upper Bhandar Group, Upper Vindhyan in Son Valley (Prasad, 2005); the Meso-Neoproterozoic Mbuji-Mayi Supergroup, Democratic Republic of Congo (Baludikay et al., 2016); the Meso-Neoproterozoic atar/el Mreiti Group, northwestern Africa (Beghin et al., 2017); the Chuanlinggou Formation, lower Changcheng Group, in the Yanshan Range (Miao et al., 2019); the Mesoproterozoic Xiamaling Formation, North China (Miao et al., 2021); the Tonian

Tongjiazhuang Formation of the Tumen Group, Western Shandong (Li et al., 2019); the Neoproterozoic Sete Lagoas Formation of the Bambuí Group, Brazil (Denezine, 2018); the Maricá, Bom Jardim, and Santa Bárbara outcrops of the Camaqua Basin, Brazil (Lehn et al., 2019); the Meso-Neoproterozoic Deoban Limestone of the Garhwal Lesser Himalaya, India (Srivastava and Kumar, 2003); the Upper Vycheгда Formation of the Timan Ridge, Russian Federation (Vorob'eva et al., 2009); and the Mesoproterozoic Lakhanda Group, Southeastern Siberia (Shuvalova et al., 2021).

Distribution and Age.—Australia, Canada, China, Gabon, India, Spitsbergen, Sweden, Paleoproterozoic to Ediacaran.

Species included (in alphabetical order). The following six species have been assigned to *Germinosphaera*.

Germinosphaera alveolata Miao, Moczyłowski, Zhu and Zhu, 2019. Basal Chuanlinggou Formation, Changcheng Group, late Paleoproterozoic. Subsequently recognized by Loron et al. (2021) from Mesoproterozoic Fort Confidence Formation, Dismal Lakes Group, Canada.

Germinosphaera bispinosa junior synonym of *unispinosa*, according to Butterfield, Knoll and Swett, 1994, Svanbergfjellet Formation, Spitsbergen. Also known from the upper Riphean Dashkin Formation, Siberia (Mikhailova, 1986; Jankauskas et al., 1989); the Mesoproterozoic Lakhanda Group, Southeastern Siberia (Shuvalova et al., 2021); the upper Neoproterozoic Sirbu Shale, India (Prasad, 2005); the Meso-Neoproterozoic Mbuji-Mayi Supergroup, Democratic

Republic of Congo (Baludikay et al., 2016); the Chuanlinggou Formation, North China (Miao et al., 2019; Agić et al., 2021); the Mesoproterozoic Xiamaling Formation, North China (Miao et al., 2021); the Tonian Tongjiazhuang Formation, North China (Li et al., 2019; Han et al., 2021); the Neoproterozoic Sete Lagoas Formation, Brazil (Denezine, 2018); the Camaqua Basin, Southern Brazil (Lehn et al., 2019); Visingsö Group, Sweden (Loron et al., 2017); the Iwower Shaler Supergroup, Northwestern Canada (Loron et al., 2019a; Loron et al., 2019b); the Dismal Lakes Group, Arctic Canada (Loron et al., 2021); the Meso-Neoproterozoic Deoban Limestone, India (Srivastava and Kumar, 2003) and the upper Vycheгда Formation, Russia (Vorob'eva et al., 2009).

Germinosphaera fibrilla Ouyang, Yin and Li, 1974. Butterfield, n. comb. Butterfield et al., 1994 (in Knoll et al., 2006; Butterfield, 2015a; Butterfield, 2015b). Sinian strata of southwest China. Subsequently described from the Neoproterozoic Svanbergfjellet Formation (Akademikerbreen Group) of Spitsbergen.

Germinosphaera guttaformis Yan, 1995 (in Jankauskas et al., 1989). Paleoproterozoic Chuanlinggou Formation, North China. Subsequently described from the Neoproterozoic Svanbergfjellet Formation (Akademikerbreen Group) of Spitsbergen.

Germinosphaera jankauskaii Butterfield, Knoll and Swett, 1994. Neoproterozoic Svanbergfjellet Formation, Spitsbergen.

Germinosphaera tadasii Weiss 1984 (in Butterfield et al. 1994; Butterfield, 2005a). Upper Riphean of the Turukhansk Region. Subsequently recognized by Jankauskas et al., 1989 from the lower Riphean Omakhata Formation of the Uchuro-Maiky District, Siberia.

Germinosphaera unispinosa Mikhailova, 1986, upper Riphean, Russia. Regarded as a senior synonym of *G. bispinosa* by some authors (Butterfield et al., 1994). Also known from the

upper Riphean Dashkin Formation (Jankauskas et al., 1989); the upper Neoproterozoic Sirbu Shale, India (Prasad, 2005); the Neoproterozoic Dongjia Formation, North China (Yin and Guan, 1999); the Alinya Formation (upper Torresian) in the Officer Basin, Australia (Zang, 1995); the upper Visingsö Formation, Sweden (Loron et al., 2016a; Loron et al., 2016b; Loron et al., 2017); the Paleoproterozoic Franceville Group, Gabon (Amard and Bertran-Sarfati, 1997); and the Draken Conglomerate Formation, Spitsbergen (Knoll et al., 1991).

Germinosphaera in open nomenclature.—The following species have been reported in open nomenclature or as “*Germinosphaera*-like” species.

Germinosphaera sp. Yin and Li, 1978. Southwestern China. Subsequently described from upper Tonian volcanoclastic rock from the Shenshan Mélange of the Jiangshan-Shaoxing-Pingxiang Fault, South China (Wang et al., 2021).

Germinosphaera Butterfield and Rainbird, 1998 (in Tang et al., 2013; Tang et al., 2015). Early Neoproterozoic Wynniatt Formation, Victoria Island, northwestern Canada (900–800 Ma).

Germinosphaera-like outgrowth Butterfield, 2005b. Lower Neoproterozoic Wynniatt Formation, Victoria Island, northwestern Canada (900–800 Ma).

Germinosphaera sp. indet. Grey, 2005 (in Beraldi-Campesi and Retallack, 2016; Retallack et al., 2014; Retallack, 2015). ABC Rane Quartzite from the SCYW, South Australia.

Germinosphaera unnamed species Battison and Brasier, 2012 (in Brasier et al., 2017). Cailleach Head (771 Ma) and lower Diabaig (994 Ma) formations of the Torridon Group, Scotland, UK.

Germinosphaera sp. Butterfield and Grotzinger, 2012 (in Allen, 2007). Mid-Ediacaran Naufun Group, and upper Ediacaran to lower Cambrian Ara Group (Huqf Supergroup), Oman.

Germinosphaera sp. Chamov et al., 2010. Upper Riphean, Central Russian Aulacogen and Orsha Depression, East European Platform.

Germinosphaera sp. Li et al., 2019 (in Han, Chen, Li, Pang, Wang, Zhou, Yang, Lyu, Wang, Zhong, Wu, and Yang, 2021). Tongjiazhuang Formation (Tonian), Tumen Group, Western Shandong, North China.

Germinosphaera sp. Veis and Vorob'eva, 1992 (in Sergeev, Knoll and Grotzinger, 1995). Riphaean Ust'-Il'ya and Lower Kotuikan Formations, Anbar Region, Siberia (1483–1459 Ma).

Germinosphaera sp. Srivastava and Kumar, 2003 (in Shukla et al., 2006). Meso–neoproterozoic Deoban Limestone Formation, Garhwal Lesser Himalaya, Uttaranchal.

Germinosphaera (?) Stanevich et al., 2013. Lower Proterozoic Baikal Region, Udokan and Sayany Mountains, Siberia.

“*Germinosphaera*-like” Strother and Wellman, 2020. Nonesuch Formation, Oronto Group, Keweenaw Peninsula of the Upper Peninsula, Michigan, USA.

Germinosphaera gunflinta sp. nov.

Figures 3.1–3.5

2016 “organic microfossil”, Alleon et al., p. 4, fig. 4b.

2022 “CUB [complex unicellular body] Type 3”, González-Flores et al., p. 7, figs. 3G–I, 4A–F.

Holotype.—Sample GSC24380, Thin section GSC24380d (Fig. 3.1). Gunflint Chert Unit, lower Gunflint Formation, Paleoproterozoic. Schreiber Beach, Ontario, Canada.

Figured Paratypes.— GSC24380d (Figs. 3.1a–3.1h; 3.2a–3.2f; 3.3a–3.3f; 3.4a–3.4f; 3.5a; 3.6a–3.6e; 3.7a), GSC24380e (Figs. 3.1i, 3.1j, 3.6f). Same locality and stratigraphic horizon as holotype (Fig. 3.1).

Type locality.— Schreiber Beach, North of Lake Superior, Ontario, Canada.

Type stratum.— Gunflint Chert unit, lower Gunflint Formation.

Material.— A total of 7 thin sections were prepared from one of the samples (GSC24380).

Diagnosis.—(emended) Slightly elongate-oval to spheroidal cyst with one main process (podium) and occasionally one or two secondary processes (podia) extending gradually from the cyst wall. The process varies from being distally tapering to thickening.

Description.—The cyst proper is small, with a range of 9–20 μm in diameter (avg = 15.27 μm ; standard deviation = 1.06 μm), subspherical to ovoidal shape (Figs. 3.1a–f), with an organic wall thickness of approximately 500 nm. Radiating threads or small rounded bodies may be present inside the cyst, with similar material and optical properties as the cyst wall (Fig. 3.1g).

Processes (podia): The large main podium commonly extends from an elongated end of the cyst, up to 10 μm in length (average = 6.3 μm), with a relatively broad base (up to 4 μm in diameter) at the junction with the cyst wall, tapering gradually towards the distal end (Fig. 3.1a, c, d). The length of secondary processes has a range of 1–8 μm . The processes are centrally hollow tubes but may be filled by chert or other sediments (Fig. 3.2a, b, f).

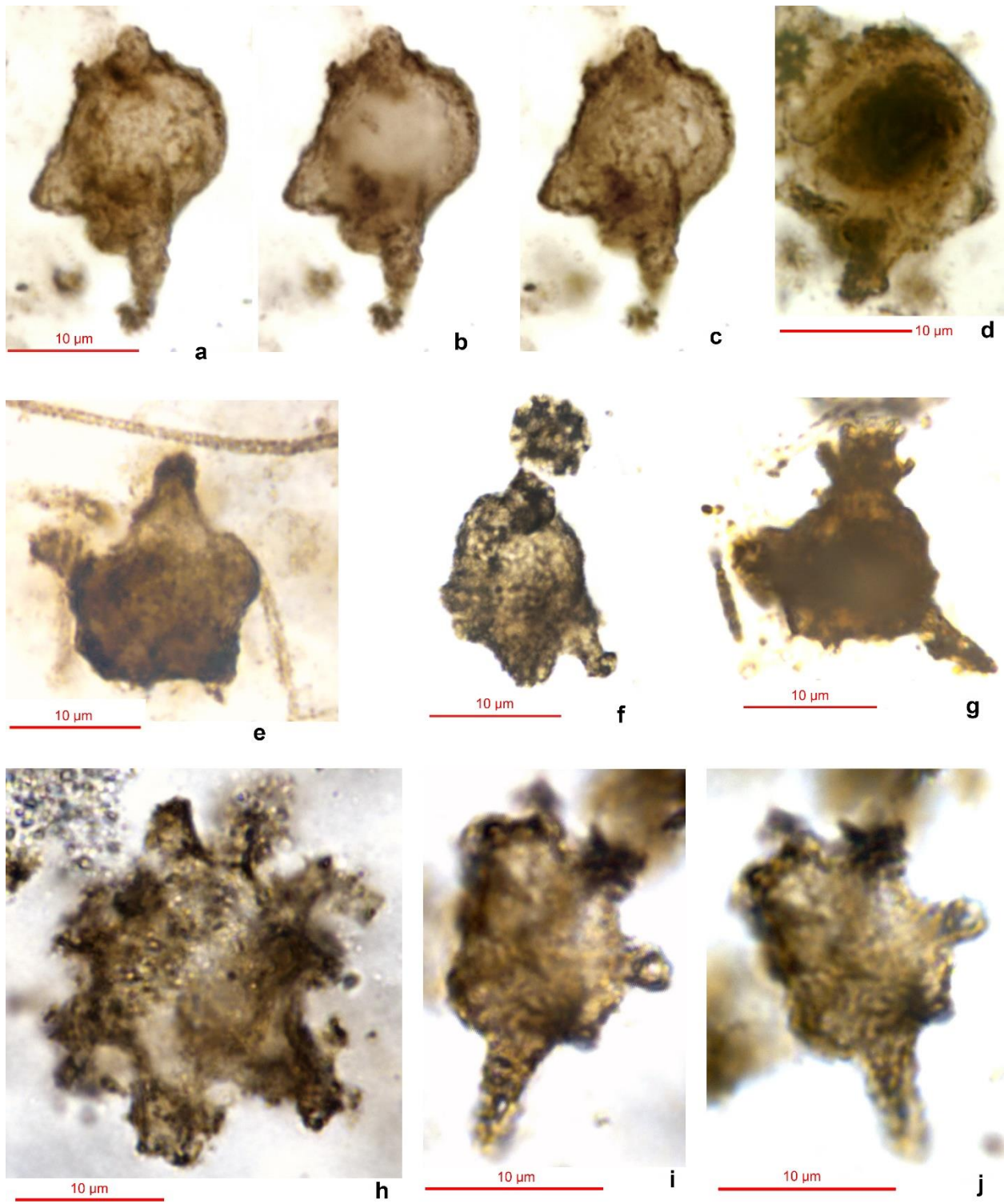


Figure 3.1 *Germinosphaera gunflinta* n. sp. Optical images generated from extended depth of focus (EDF) Z-series, sample GSC 24380, Gunflint Formation, Schreiber Beach, northwestern Ontario. (1–3) holotype, GSC 24380e-02-02, thin section no. 2, views of left hemisphere, equatorial plane, and right hemisphere of same specimen. (4) paratype, GSC 24380d-02-06, thin section no. 2, cell with large dark body in centre. (5) paratype, GSC 24380d-005, thin section no. 2, cell with two robust podia; note associated filaments of *Gunflintia*. (6) paratype, GSC 24380d-011, thin section no. 2, cell with two large podia (top podium broken); not

reticulate-patterned tubercles on cell surface. (7) paratype, GSC 24380d-001, thin section no. 2, cell with two large podia (top podium branching). (8) paratype, GSC 24380d-004, thin section no. 2, variant with multiple robust podia. (9, 10) paratype, GSC 24380e-001, thin section no. 2, views of left and right hemispheres of cell with one prominent podium and multiple shorter podia; note reticulate tubercles and curly ridges on cell surface (compare with SEM images in Figs. 4.6, 5.4, 5.5, 6.6).

Surface ornaments: The surface ornaments may be scale-like in SEM images (Fig. 3.3a–d) or pustular (Fig. 3.4a–e) in conventional optical images, best-developed cysts, but also observed on large processes. Individual scales/pustules range from 0.6–0.8 μm in diameter, but some may appear as branching clusters of 2–4 pustules, and some pustules terminate in a sharp tip or spine (Fig. 3.1g, i, j).

Diagnosis.—(emended) Slightly elongate-oval to spheroidal cyst with one main process (podium) and occasionally one or two secondary processes (podia) extending gradually from the cyst wall. The process varies from being distally tapering to thickening.

Description.—The cyst proper is small, with a range of 9–20 μm in diameter (avg = 15.27 μm ; standard deviation = 1.06 μm), subspherical to ovoidal shape (Figs. 3.1a–f), with an organic wall thickness of approximately 500 nm. Radiating threads or small rounded bodies may be present inside the cyst, with similar material and optical properties as the cyst wall (Fig. 3.12).

Processes (podia): The large main podium commonly extends from an elongated end of the cyst, up to 10 μm in length (average = 6.3 μm), with a relatively broad base (up to 4 μm in diameter) at the junction with the cyst wall, tapering gradually towards the distal end (Fig. 3.1a, c, d). The length of secondary processes has a range of 1–8 μm . The processes are centrally hollow tubes but may be filled by chert or other sediments (Fig. 3.2a, b, f).

Surface ornaments: The surface ornaments may be scale-like in SEM images (Fig. 3.3a–d) or pustular (Fig. 3.4a–e) in conventional optical images, best-developed cysts, but also observed on

large processes. Individual scales/pustules range from 0.6–0.8 μm in diameter, but some may appear as branching clusters of 2–4 pustules, and some pustules terminate in a sharp tip or spine (Fig. 3.1g, i, j).

Remarks.—*Germinosphaera gunflinta* resembles other congeneric species in its spheroidal cyst and one prominent podium but differs in its consistently smaller size. However, its maximum size (21.8 μm) overlaps with the minimum size reported for many other species. Aside from 2.0 Ga *G. unispinosa* reported by Amard and Bertrand-Sarfati (1997), which has a rather poor state

In the Gunflint material, the scale/pustules appear to be hollow inside, composed of a soft, flexible, originally organic wall, and they sit on a similar cyst wall. When etched out from the chert, the cyst and pustule walls collapsed and flattened. However, their original 3-D shapes are sometimes preserved in internal mounds of porous chert, matching the outline and shape of *G. gunflinta* bodies recognized by optical microscopy (Figs. 3.1a, 3.3a-f, 3.4c and 3.4f). Similar scale-like or pustular ornaments have also been observed in *G. alveolata* (Miao et al., 2019; Loron et al., 2021), with individual scales of relatively similar sizes, averaging 1.83 μm in diameter for *G. alveolata*, and 1.75 for *G. gunflinta*.

G. gunflinta has a similar number (up to three, including the dominant podium) of the processes as *G. unispinosa*, *G. bispinosa* and *G. fibrilla*. As in many occurrences of *G. unispinosa* and *G. bispinosa*, the dominant podium attains a diameter varying from one-half to one-quarter of the cyst diameter and a more variable-length from shorter to much longer than the cyst diameter. Unlike the other two species, however, the podium in the new species has a variable diameter along its length, from distally tapering (most commonly) to swelling (Fig. 3.1e, 3.1g). Some specimens of the new species resemble those of *G. fibrilla* in having three processes, but the processes of *G. gunflinta* are much more robust but less regularly spaced on the cyst body.

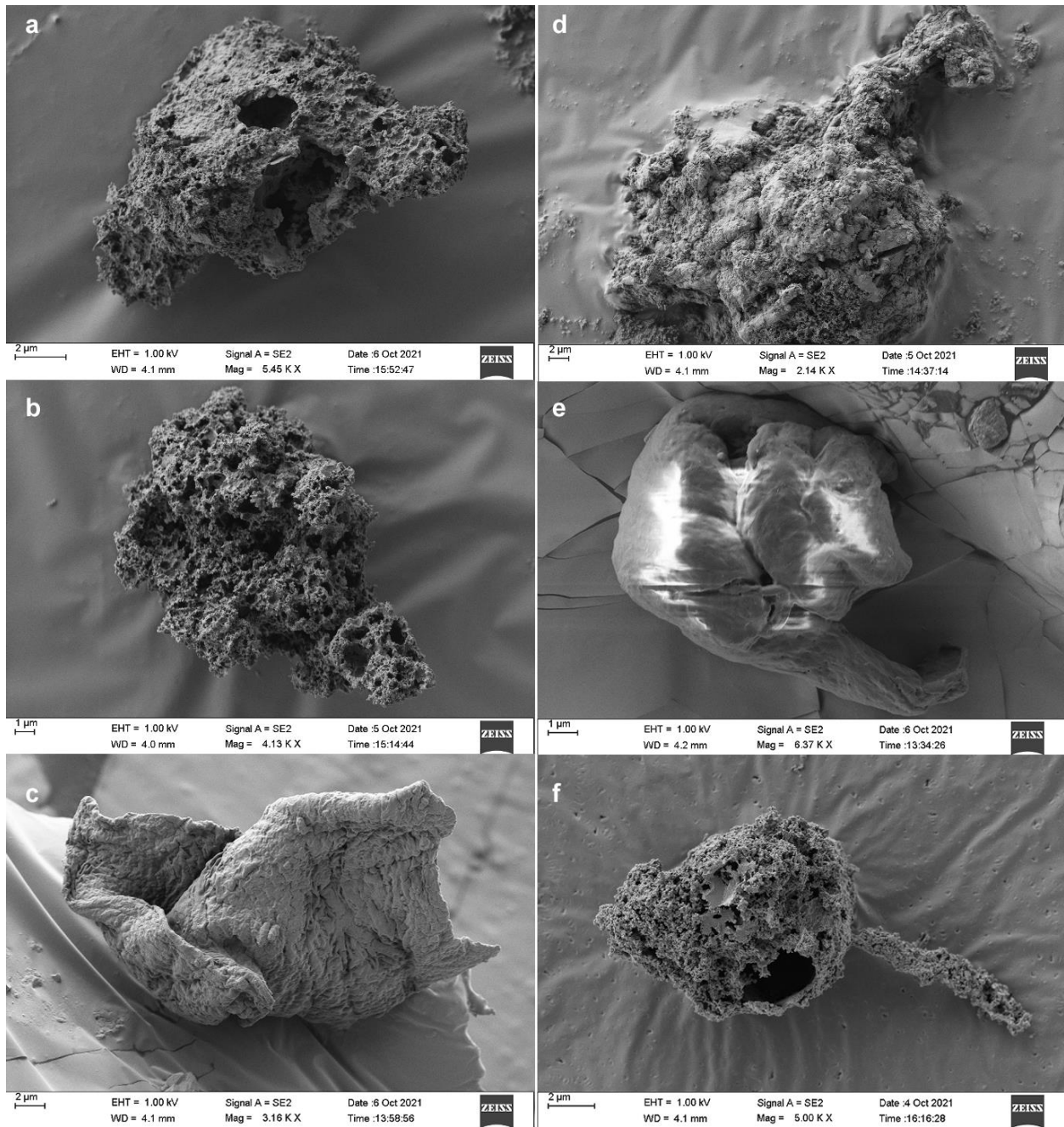


Figure 3.2 Scanning Electron Microscopy (SEM) Backscattered-Electron (BSE) images of *Germinosphaera gunflinta* filtered residual material after light HF etching, sample GSC24380d. (a) specimen with a central body and two podia on opposing sides, stud no. 1. (b) specimen showing a single small podia, stud no.1. (c) folded specimen showing scale-like ornaments on its surface. (d-e) specimen displaying light folding and bumped surface texture with single thin podia, stud no. 2. (f) cell with partially void cyst and single thin podia. Scalebar depicted individually for each specimen.

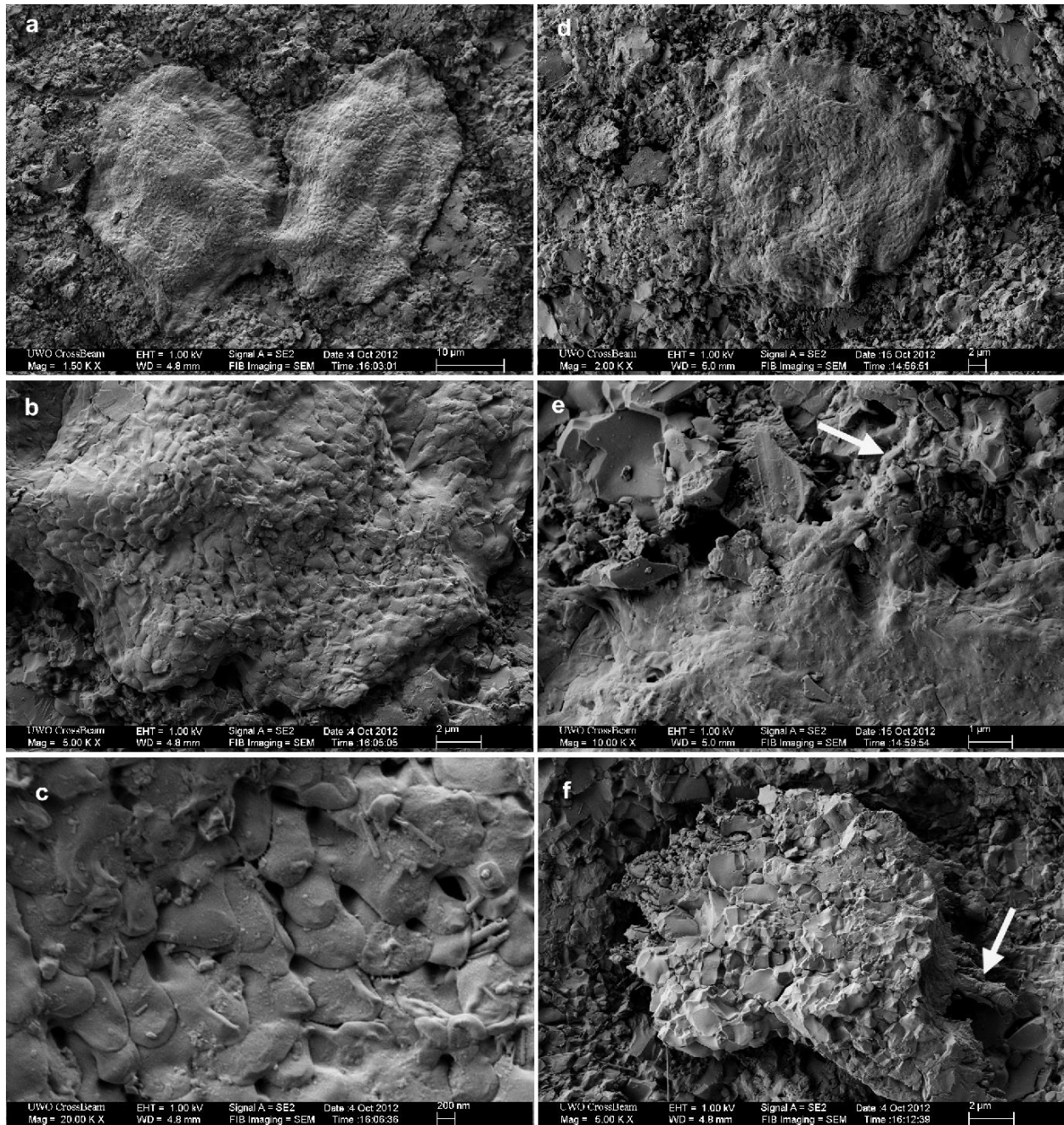


Figure 3.3 SEM images of *Germinosphaera gunflinta* after light HF etching, sample GSC24380d. (a) images of two partly squashed cells. (b-c) magnifications of Fig. 7a showing scale-like surface ornaments. (d) single specimen with scale-like surface texture. (e) magnification of Fig. 7d depicting the texture difference between the matrix and the specimen. (f) internal mold (consisting of microquartz), showing a large podia. Scalebar depicted individually for each specimen (González-Flores et al., 2022).

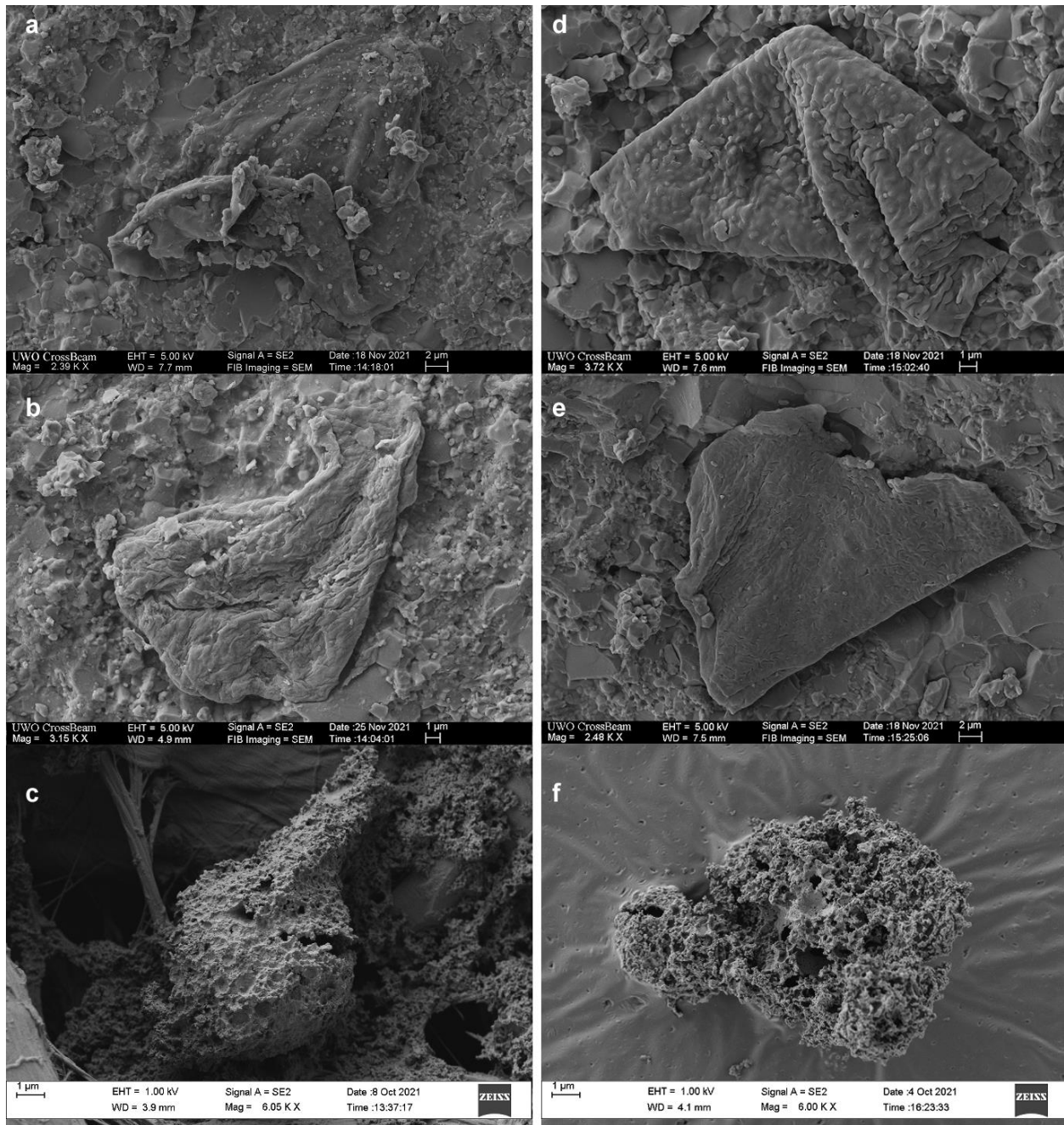


Figure 3.4 SEM images of small bulk sample (a, b, d, e) and studs made from its filtered residual material (c, f) after light HF etching, sample GSC24380d. (a, b, d, e) folded specimen with, bumpy texture and complex surface ornaments, small bulk sample. (c) specimen over filtered paper matrix showing a single small podia, stud no. 4. (f) specimen displaying two small podia with wither distal diameter, stud no. 3. Scalebar depicted individually for each specimen.

Geochemical Analysis.— In addition to identifying the surface ornaments of the cells through the SEM, the elemental mappings revealed a clear difference in the cell composition compared to the

matrix in which it is found. As shown in Figure 3.5, three elemental maps of carbon (C), silicon (Si) and oxygen (O) were made on a specific part of the sample containing both the matrix and one of the specimens. The three maps reflect the silhouette of the cell, indicating the presence of Si and O only in the matrix (Fig. 3.5b, 3.5d), while carbon is more present inside the cell (Fig. 3.5c).

Confirming the presence of carbon on the cell wall, electron microprobe (EMP) studies show similar results (Fig. 3.6, 3.7). In Figure 3.7, we can see that the lightest elements, denoted in dark colours, are concentrated in the rim of the cell, as well as in its internal structures, while the heaviest elements, shown in white and bright tones, appear only as small white dots inside the cell.

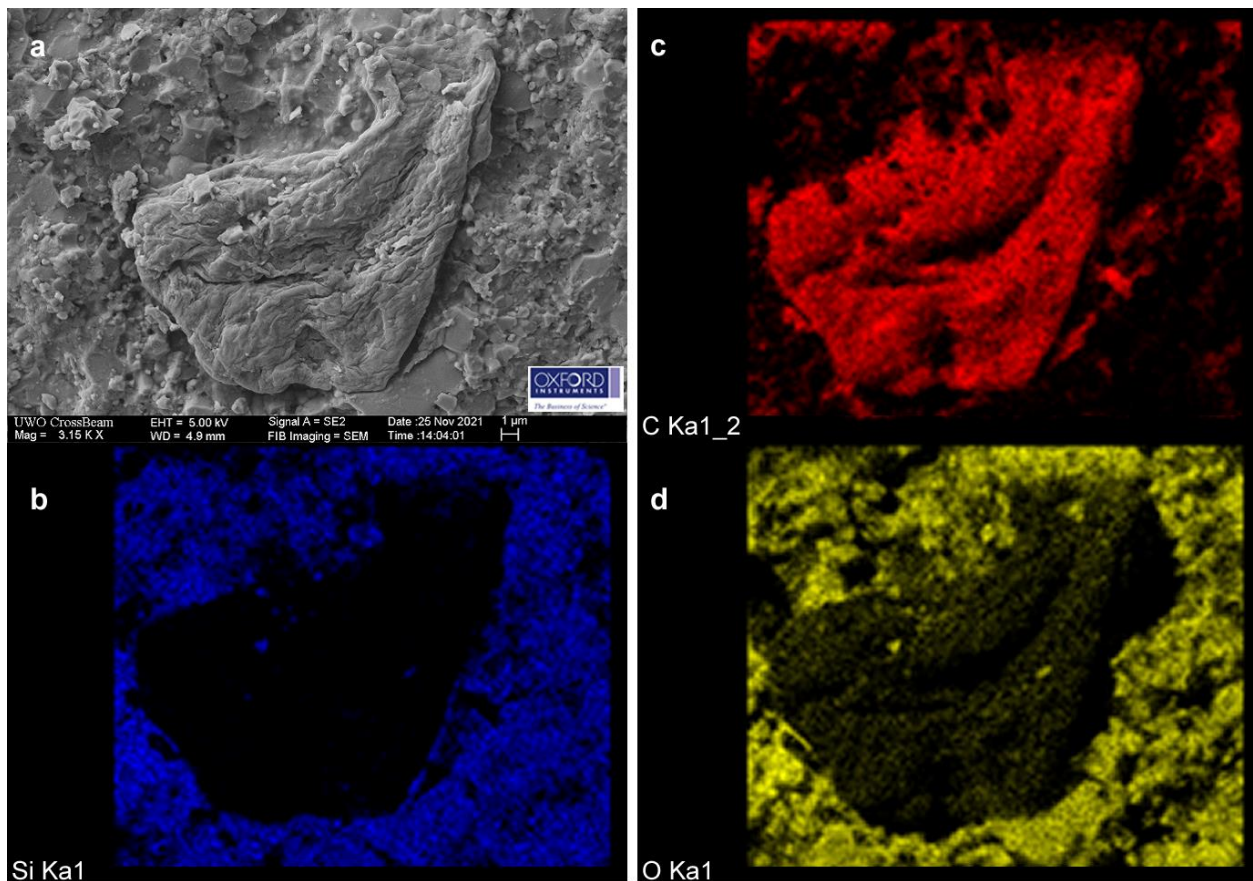


Figure 3.5 In-situ elemental maps of specimen from Figure 3.4b, GSC24380d, small bulk sample. (a) folded specimen with, bumpy texture, complex surface ornaments and single podia with larger distal diameter. (b-d) Element maps of carbon (C), silicon (Si), and oxygen (O) displaying the clear shape of the cell.

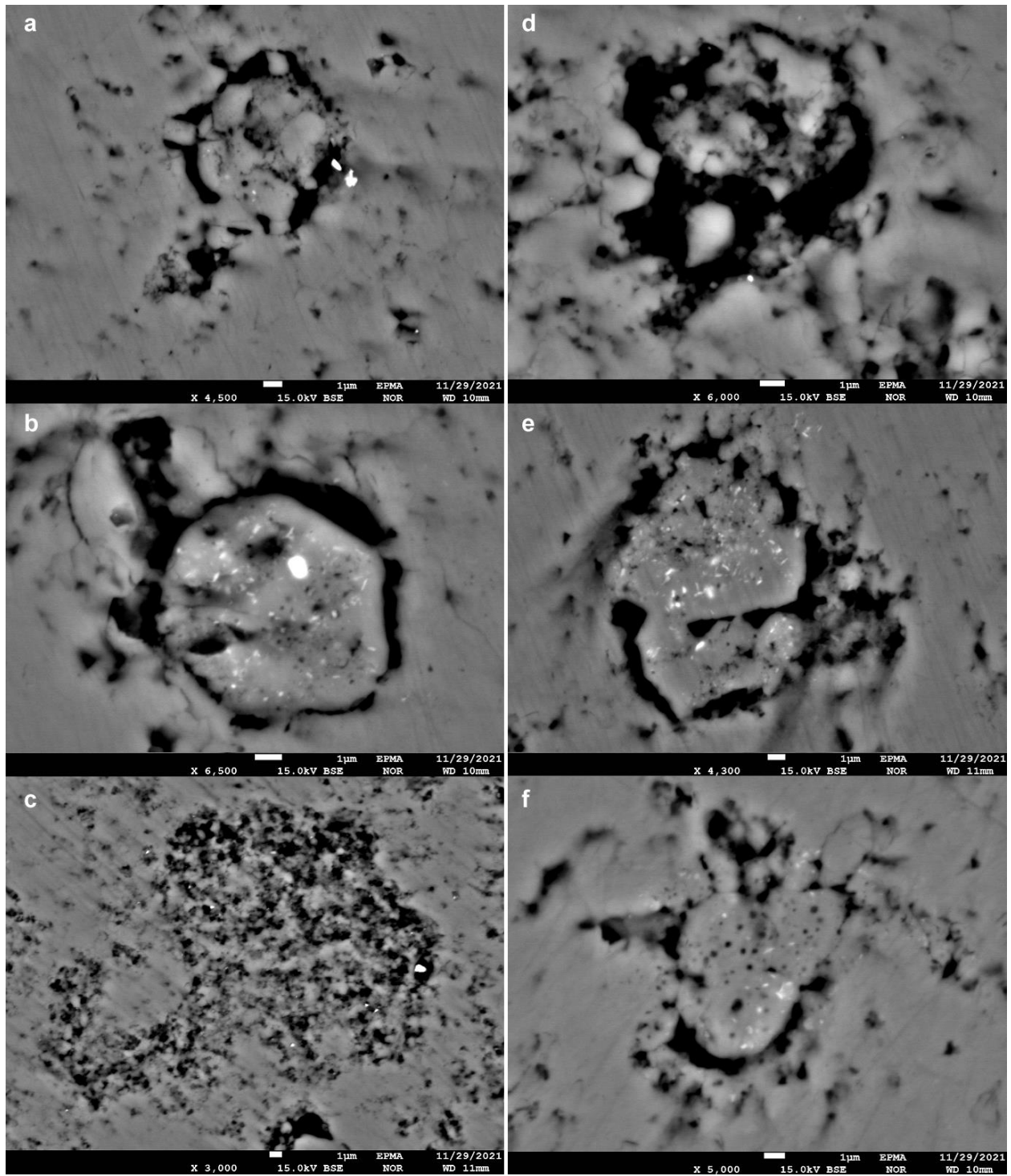


Figure 3.6 Backscattered-Electron (BSE) field-emission electron microprobe (EPM) images from thin sections GSC24380d and GSC24380e, magnification between 4.00 – 7.00 KX and 15.0 kV EHT. (a) GSC24380d_35; (b) GSC24380d_81; (c) GSC24380d_115; (d) GSC24380d_53; (e) GSC24380d_97; (f) GSC24380e_5. Scalebar of 1µm.

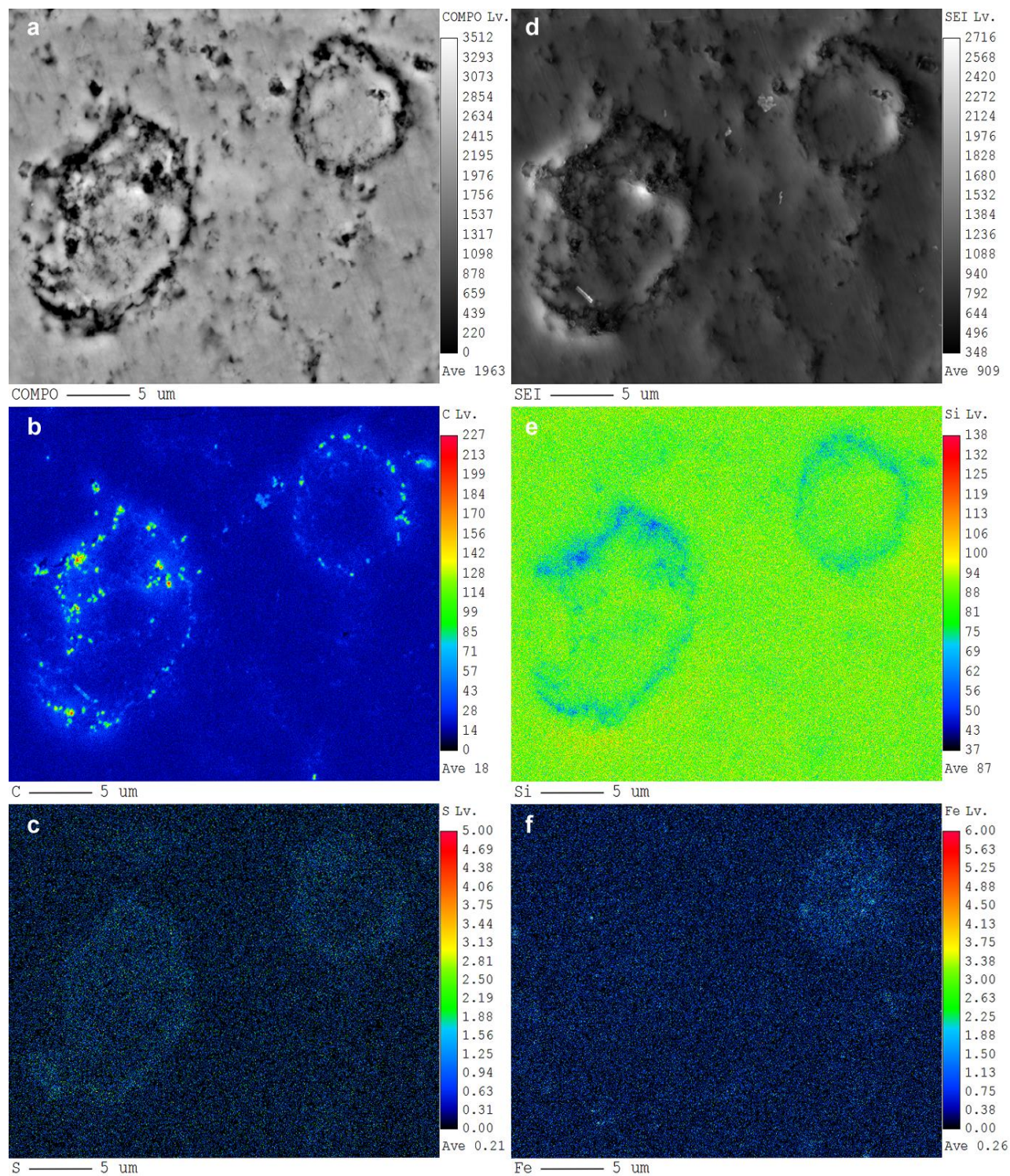


Figure 3.7 Field-emission electron microprobe (EPM) wavelength dispersive X-ray spectroscopy (WDS) element maps. (a) composition (COMPO) mode image from thin sections GSC24380d; (b)WDS Carbon map; (c) WDS Sulfur map; (d) secondary electron image (SEI) image; (e) WDS Silicon map; (f) WDS Iron map. Scalebar of 5μm.

The wavelength dispersive X-ray spectroscopy (WDS) element maps of Carbon (Fig. 3.7b) and Silicon (Fig. 3.7e) present similarities with the results presented by the SEM, where the cell wall, as well as internal structures, denote the presence of carbon with colours ranging from light blue to red (Fig. 3.7b), and with a lack of silicon in the cell wall denoted by dark blue colours (Fig. 3.7e). Confirming the presence of carbon on the cell wall, electron microprobe (EMP) studies show similar results (Fig. 3.6, 3.7). In Figure 3.7, we can see that the lightest elements, denoted in dark colours, are concentrated in the rim of the cell, as well as in its internal structures, while the heaviest elements, shown in white and bright tones, appear only as small white dots inside the cell. The wavelength dispersive X-ray spectroscopy (WDS) element maps of Carbon (Fig. 3.7b) and Silicon (Fig. 3.7e) present similarities with the results presented by the SEM, where the cell wall, as well as internal structures, denote the presence of carbon with colours ranging from light blue to red (Fig. 3.7b), and with a lack of silicon in the cell wall denoted by dark blue colours (Fig. 3.7e).

3.5 Results and Discussion

In the Gunflint Chert, *Germinosphaera gunflinta* sp. nov. is one of the largest and most common type of unicellular organisms. However, it was not identified in an earlier study (e.g., Awramik and Barghoorn, 1977). To investigate the phylogenetic relationships and evolutionary significance of *G. gunflinta*, a comprehensive literature survey of 66 publications was carried out to compile a dataset on the size of cysts, the number and length of podia, and the geological age of 146 figured specimens of other congeneric species. These specimens were combined with 49 well-preserved specimens of *G. gunflinta* to generate a dataset (see Table 1, appendix B) for quantitative analyses to compare the similarities and differences and the overall morphological

trends among the various morphospecies, using bivariate and multivariate analyses. A bivariate plot explores the range of cell sizes against the geological age of all known species of *Germinosphaera* (Fig. 3.8). A principal component (multivariate) analysis is used to investigate the relationships among these specimens based on their cell size, the length of the podia, and the number of podia per specimen (Fig. 3.9).

3.5.1 Analysis of cell size over time in *Germinosphaera* from Paleoproterozoic to Ediacaran

In this analysis, a bivariate plot was created using the average age of the geological formation in which each specimen occurs, based on the minimum and maximum age of the formation if an exact geological age was not provided. In Fig. 3.8, the cyst size represents an average of the maximum and minimum diameter. The length of podia/processes was not included in the measurement of cyst size because the podia tend to be extremely variable even among members of the same species of similar age.

Fig. 3.8 shows a clear increase in cyst size from the late Paleoproterozoic (Orosirian, 1.9–2.0 Ga), with maximum sizes attaining 20.5 μm in *G. gunflinta*, to the latest Ediacaran (542 Ma), with sizes up to 333.3 μm . Another trend in the plot is the increased range of cyst sizes with geological age, from a variation of ~ 16 μm between the minimum and maximum sizes of various forms of *Germinosphaera* during the Orosirian to a range of 229 μm among Ediacaran species. Finally, the smallest Neoproterozoic specimens are similar in size and shape to the largest ones belonging to the Paleoproterozoic (including *G. gunflinta*), suggesting a morphological continuity and continued evolution among various species of *Germinosphaera*.

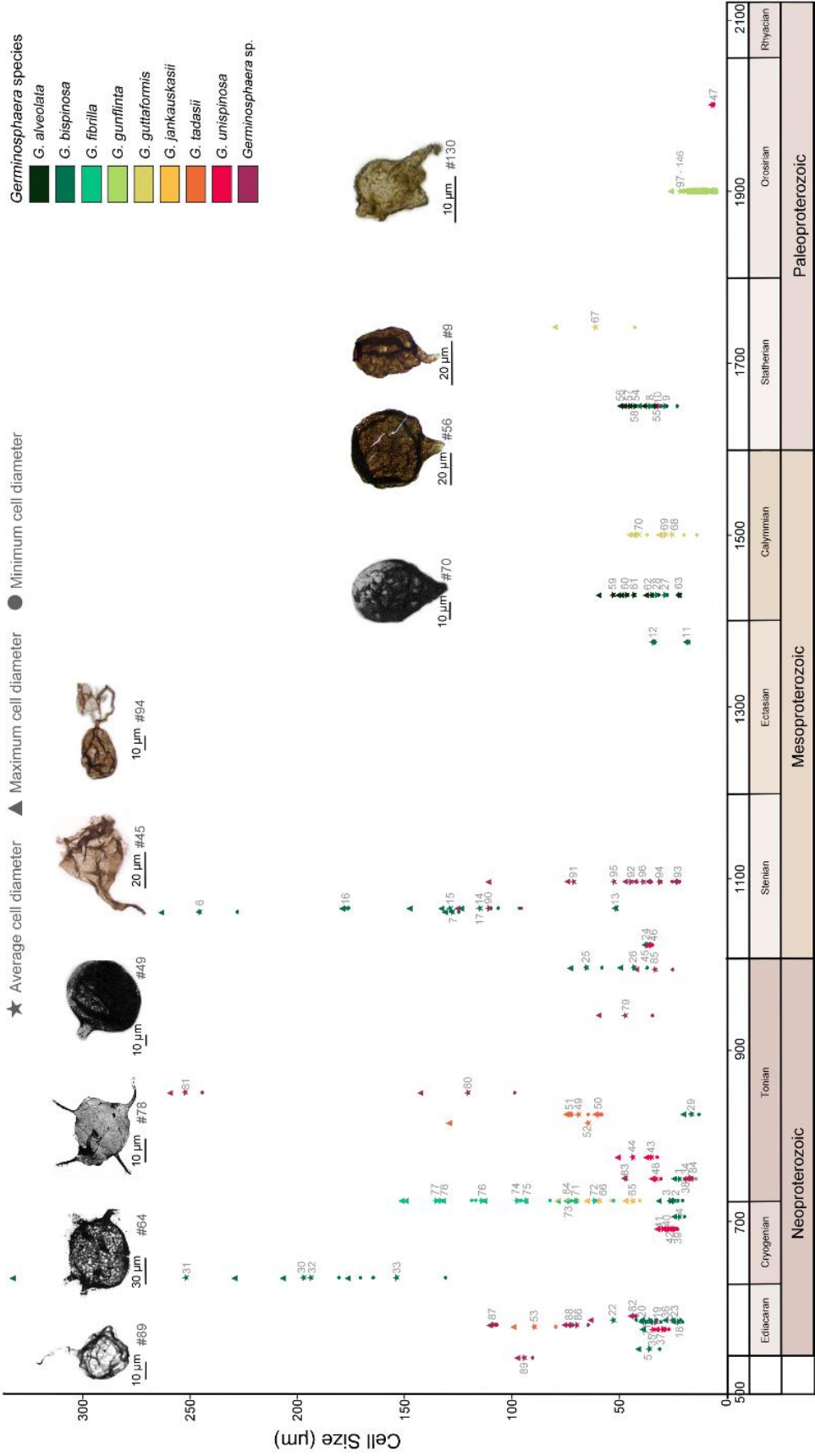


Figure 3.8 Average age versus measured cell diameters plot for 146 specimens from collected database on the genus *Germinosphaera*. Age average was calculated from the minimum and maximum age from the respective formation of each specimen when specific age was not provided. Different colours depict the species distribution through time and different scattered-point symbols indicate the different diameters that were measured. Last 49 numbers indicate the different diameters measured for the *G. gunflinta* sp. nov.

Regarding species diversification within *Germinosphaera*, Figure 3.8 shows that *G. bispinosa* was the most widespread species throughout the Proterozoic (from the end of the Statherian to the end of the Ediacaran). In contrast, each of the other species seems to have a more limited geological range. For example, *G. alveolata* and *G. unispinosa* are confined mostly to the Paleoproterozoic and the Meso-Neoproterozoic, respectively. For *G. guttaformis*, *G. fibrilla*, *G. tadasii* and *G. jankauskasiai*, the sample size is too small to generalize temporal distribution trend. For more detailed information refer to Appendix B, Item 2.

3.5.2 Multivariate analysis of morphological characters of *Germinosphaera*

Multiple variables (measurements of morphological characters) include the following:

1. MaxD – maximum diameter of cyst
2. MinD – minimum diameter of cyst
3. PL1 – main podium length
4. PBD1 – main podium base diameter
5. PDED1 – main podium distal end diameter
6. PL2 – secondary podium length #2
7. PBD2 – secondary podium base diameter #2
8. PDED2 – secondary podium distal end diameter #2
9. PL3 – secondary podium length #3
10. PBD3 – secondary podium base diameter #3
11. PDED3 – secondary podium distal end diameter #3
12. PL4 – secondary podium length #4

13. PBD4 – secondary podium base diameter #4

14. PDED4 – secondary podium distal end diameter #4

Each of the 14 characters was measured for every individual specimen reported within the compiled database, including direct measurements of the Gunflint specimens and measurements derived from publications of other species. A principal component analysis was conducted from the compiled measurements, treating the data matrix as variance-covariance with the following eigenvalues of the variables as displayed in Table 3.1.

Table 3.1. Eigenvalues of variables in the principal component analysis.

PC	Eigenvalue	% variance
1 (MaxD)	5487.89	79.309
2 (MinD)	858.436	12.406
3 (PL1)	236.046	3.4113
4 (PBD1)	161.573	2.335
5 (PDED1)	72.3434	1.0455
6 (PL2)	60.5284	0.87474
7 (PBD2)	18.3957	0.26585
8 (PDED2)	12.2258	0.17668
9 (PL3)	7.19904	0.10404
10 (PBD3)	3.56879	0.051575
11 (PDED3)	0.918915	0.01328
12 (PL4)	0.303503	0.0043861
13 (PBD4)	0.181077	0.0026169
14 (PDED4)	0.0137212	0.00019829

The result of the multivariate analysis is depicted in the PCA scatterplot (Fig. 3.9). The 146 points, representing the 146 measured specimens, are ordinated based on the similarities and differences and their relative Eigenvalues of MaxD, MinD, PL#, PBD#, PDED#, etc. For more detailed information refer to Appendix B, Item 3.

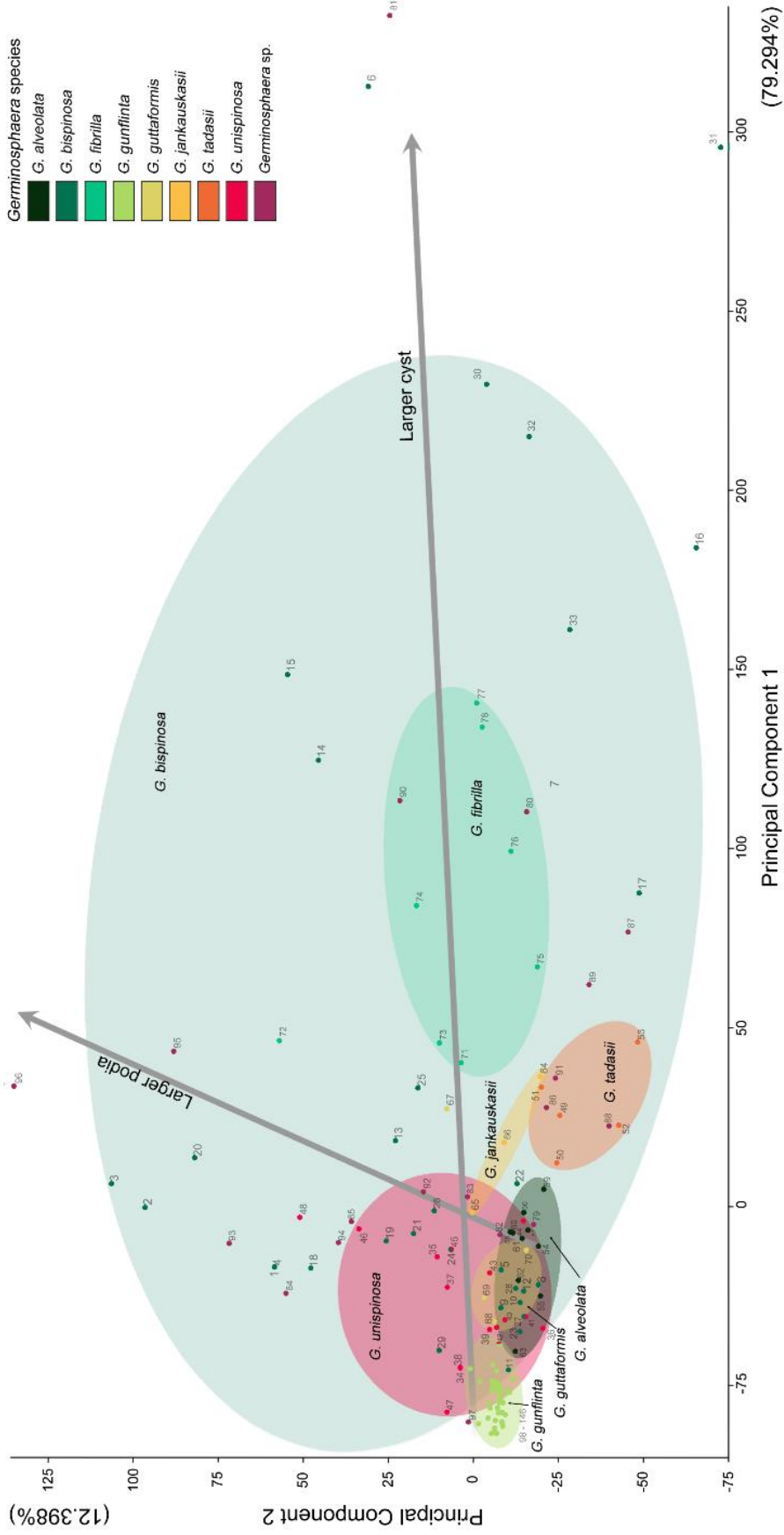


Figure 3.9 Size multivariate plot for 146 specimens from collected database on the genus *Germinosphaera*. Each dot depicts the combined value of 14 different criteria measured for each cell. The dots are colour coded to depict the different species of the genus. The circles on the back display the overlap between different species and the arrows mark the different trends identified from this analysis. They only include the most representative specimens of the sample.

Individually, every species included in this study is represented in the plot by a specific colour, and each of the points in the plot is colour-coded by species. In addition to the unique colour of the points, elliptical outlines were used to delimit the species groupings to show the degrees of separation and overlap among them.

As seen in the scatterplot (Fig. 3.9), the following trends can be generalized:

- 1) Cyst size. From left to right and parallel to the x-axis, a trend of increasing cyst size can be recognized, from the smallest at the left end of the spectrum (MaxD = 5.64 μm ; specimen #135; GSC24380e-039) to the largest on the right (MaxD = 264 μm ; specimen #81; see also Butterfield, 2005b).
- 2) Podia size. Unparallel to the y-axis, specimens in the lower-left part of the plot have smaller podia or lack secondary podia. In contrast, those towards the upper-right part of the graph have longer podia in proportion to the size of the cyst.
- 3) Relationships between the trends of cyst/podium size and species. Each species is marked by an ellipsoid outline in the PCA scatter plot. Understandably, the sample size based on figured specimens in the literature is usually small. Therefore, it may or may not represent a given species' true range of size variations. Despite this data limitation, it can be noted that the “species circles” of *G. gunflinta*, based on first-hand measurements of samples, and *G. unispinosa*, represented by relatively large numbers of specimens in the analysis, are confined to a relatively small and largely discrete area in the PCA plot, indicating that they are well-defined and distinguishable species. In contrast, *G. bispinosa* is also represented by a large sample size but scattered over a much larger area in the graph. Based on information from published illustrations, *G. alveolata* appears to be a well-defined species, despite the samples being derived from widely separate geographic regions.

The other species in the analysis, such as *G. tadasii*, *G. guttaformis*, *G. fibrilla* and *G. jankauskasii*, are represented by rather limited samples, which may have contributed to their small and distinct circles. It is important to note that all other species, except for the new species, fall within the large circle of *G. bispinosa*. This appears to support the earlier notion of Butterfield et al. (1994) that *G. Bispinosa* and *G. unispinosa* are not different species but rather one and the same.

3.5.3 Significance of *Germinosphaera gunflinta* sp. nov

The oldest eukaryotic organisms with complex morphology have been recognized convincingly in the fossil record of the late Paleoproterozoic (~1.6 Ga; for a summary, see Butterfield, 2015b; Javaux and Lepot, 2018). As an organic-walled microfossil ranging fairly continuously from the middle Paleoproterozoic to the early Cambrian, *Germinosphaera* can now shed more light on the early evolution of eukaryotes. Several recent studies (e.g., Agić et al., 2017; Loron et al., 2021) have shown that a diverse group of Mesoproterozoic organic-walled forms, such as *Dictyosphaera* (Xing and Liu, 1973), *Germinosphaera*, and *Gigantosphaeridium* (Agić et al., 2015), have complex cell-surface ornaments, including reticulate-patterned sculptures, scale-like pustules, in addition to various processes, which are typical of unicellular eukaryotes. Some Mesoproterozoic microfossils similar to *Germinosphaera*, such as *Ourasphaera* Loron et al., 2019b, were interpreted as fungi (Loron et al., 2019a). In previous studies, all Gunflint microfossils were regarded mostly as prokaryotes mainly because of the relatively small size and unknown surface ornaments. However, affinities to eukaryotes (e.g. Kaźmierczak, 1979) or, more specifically, to fungi (Krumbein, 2010) have been proposed. The various developed podia (long processes) in many forms of *Germinosphaera* figured in the literature have some degree of morphological resemblance to the connecting filaments in *Ourasphaera* (Loron et al., 2019b, fig.

1). Most of the podia in *G. gunflinta* show distal breakage, implying they were originally longer hollow tubules, but no T-junctions have been observed in *Ourasphaera*.

A thorough investigation of one of the Gunflint forms, *G. gunflinta*, revealed two crucial characteristics. First, its diameter range of 5–22 μm , whereas being the lowest among all congeneric species, clearly has its larger end of the spectrum overlapping with the smaller end of several other species, such as *G. unispinosa* and *G. bispinosa*, ranging from late Paleoproterozoic to the Ediacaran (Yan, 1995; Amard and Bertrand-Sarfati, 1997; Srivastava and Kumar, 2003; Miao et al., 2019; Agić, 2021).

There was a continuous increase in cyst size from the middle Paleoproterozoic *G. gunflinta* to the other species in the late Paleoproterozoic and early Mesoproterozoic, suggesting an evolutionary continuity in cyst size within *Germinosphaera* (Figs. 3.8, 3.9). There is a significant size jump within the species of *Germinosphaera* around 1100 Ga. Although the real cause is still unknown, there are two most likely hypotheses: 1) there was an environmental event during that time that cause the increase in size of every single *Germinosphaera* species, or 2) there was a general lack of fossil record of the genus around this time interval, thus producing an artifact of abrupt increase in cell size.

Second, *G. gunflinta* shares eukaryotic-like characteristics with other congeneric species, as well as with other eukaryote-like genera, such as the presence of multiple processes (podia), scale-like pustules on the cyst surface, and wrinkles/folds of the cyst surface (Compare Figs. 3.2–4 of this study with Agić et al., 2017, figs. 4A–C, 6A–C; Miao et al., 2019, figs. 8k–l, 10. g–g1; Loron et al., 2021, fig. 4.5, 7.8–7.10). The continuity in cyst size and surface ornaments is strong evidence that the eukaryote-like *Germinosphaera* can be traced back to the Gunflint biota.

3.6 Conclusions

Through morphological analysis of 146 specimens of *Germinosphaera*, including those of *G. gunflinta* sp. nov. from the Gunflint Formation and existing species illustrated in previous literature, the following conclusions can be drawn:

- 1) Among the long lineage of *Germinosphaera* ranging from middle Paleoproterozoic to early Cambrian, *G. gunflinta* sp. nov. is the oldest representative that shows well-preserved surface ornaments such as a large podium and secondary processes and scale-like pustules.
- 2) There is an evolutionary continuity from the *G. gunflinta* to younger congeneric species of late Paleoproterozoic–Mesoproterozoic age in terms of increasing cyst size (from an average of 13 μm to over 100 μm in diameter) and development of complex surface ornaments (processes, large podia, reticulate sculpture, scale-like pustules, etc.). Such continuity suggests that the *Germinosphaera* lineage, commonly regarded as a eukaryote, can convincingly be traced to the 1.9 Ga Gunflint Chert. This provides important new data for studying the early evolution of eukaryotes.
- 3) There is a dramatic increase in the maximum cyst size of *Germinosphaera* around 1.1 Ga. The cause of this drastic increase in cell size is poorly understood and requires future investigation.

References

Agić, H., 2021, Origin and Early Evolution of the Eukaryotes: Perspectives from the Fossil Record: In *Prebiotic Chemistry and the Origin of Life*, p. 255–289. Springer, Cham.

- Agić, H., Moczyłowska, M., and Yin, L.M., 2015, Affinity, life cycle, and intracellular complexity of organic-walled microfossils from the Mesoproterozoic of Shanxi, China: *Journal of Paleontology*, v. 89, n. 1, p. 28–50.
- Agić, H., Moczyłowska, M., and Yin, L., 2017, Diversity of organic-walled microfossils from the early Mesoproterozoic Ruyang Group, North China Craton—A window into the early eukaryote evolution: *Precambrian Research*, v. 297, p. 101–130.
- Allen, P.A., 2007, The Huqf Supergroup of Oman: basin development and context for Neoproterozoic glaciation: *Earth-Science Reviews*, v. 84, n. 3–4, p. 139–185.
- Alleon, J., Bernard, S., Le Guillou, C., Marin-Carbonne, J., Pond, S., et al., 2016, Molecular preservation of 1.88 Ga Gunflint organic microfossils as a function of temperature and mineralogy. *Nature Communications*, 7:11977 doi: 10.1038/ncomms11977.
- Amard, B., and Bertrand-Sarfati, J., 1997, Microfossils in 2000 Ma old cherty stromatolites of the Franceville Group, Gabon: *Precambrian Research*, v. 81, n. 3–4, p. 197–221.
- Awramik, S.M., and Barghoorn, E.S., 1977, The Gunflint microbiota: *Precambrian Research*, v. 5, p. 121–142.
- Baludikay, B.K., Storme, J.Y., François, C., Baudet, D., and Javaux, E.J., 2016, A diverse and exquisitely preserved organic-walled microfossil assemblage from the Meso–Neoproterozoic Mbuji-Mayi Supergroup (Democratic Republic of Congo) and implications for Proterozoic biostratigraphy: *Precambrian Research*, v. 281, p. 166–184.

- Barghoorn, E.S., and Tyler, S.A., 1965, Microorganisms from the Gunflint Chert: These structurally preserved Precambrian fossils from Ontario are the most ancient organisms known: *Science*, v. 147, n. 3658, p. 563–575.
- Battison, L., and Brasier, M.D., 2012, Remarkably preserved prokaryote and eukaryote microfossils within 1 Ga-old lake phosphates of the Torridon Group, NW Scotland: *Precambrian Research*, v. 196, p. 204–217.
- Beghin, J., Storme, J.Y., Blanpied, C., Gueneli, N., Brocks, J.J., Poulton, S.W., and Javaux, E.J., 2017, Microfossils from the late mesoproterozoic–early neoproterozoic atar/el Mreïti group, Taoudeni basin, Mauritania, northwestern Africa: *Precambrian Research*, v. 291, p. 63–82.
- Beraldi-Campesi, H., and Retallack, G.J., 2016, Terrestrial ecosystems in the Precambrian. In *Biological soil crusts: An organizing principle in drylands*, p. 37–54. Springer Cham.
- Brasier, A.T., Culwick, T., Battison, L., Callow, R.H.T., and Brasier, M.D., 2017, Evaluating evidence from the Torridonian Supergroup (Scotland, UK) for eukaryotic life on land in the Proterozoic: *Geological Society London Special Publications*, v. 448, n. 1, p. 121–144.
- Butterfield, N.J., 2005a, Reconstructing a complex early Neoproterozoic eukaryote, Wynnatt Formation, arctic Canada: *Lethaia*, v. 38, n. 2, p. 155–169.
- Butterfield, N.J., 2005b, Probable proterozoic fungi: *Paleobiology*, v. 31, n. 1, p. 165–182.
- Butterfield, N.J., 2015a, Proterozoic photosynthesis—a critical review: *Palaeontology*, v. 58, n. 6, p. 953–972.
- Butterfield, N.J., 2015b, Early evolution of the Eukaryota: *Palaeontology*, v. 58, n. 1, p. 5–17.

- Butterfield, N.J., and Grotzinger, J.P., 2012, Palynology of the Huqf Supergroup, Oman: Geological Society London Special Publications, v. 366, n. 1, p. 251–263.
- Butterfield, N.J., and Rainbird, R.H., 1998, Diverse organic-walled fossils, including “possible dinoflagellates,” from the early Neoproterozoic of arctic Canada.: *Geology*, v. 26, n. 11, p. 963–966.
- Butterfield, N.J., Knoll, A.H., and Swett, K., 1994, Paleobiology of the neoproterozoic svanbergfjellet formation, Spitsbergen: *Lethaia*, v. 27, n. 1, p. 76–76.
- Chamov, N.P., Kostyleva, V.V., and Veis, A.F., 2010, Structure of the Precambrian sedimentary cover and upper part of the basement in the Central Russian aulacogen and Orsha depression (East European Platform): *Lithology and Mineral Resources*, v. 45, n. 1, p. 56–88.
- Denezine, M., 2018, Microfósseis orgânicos da Formação Sete Lagoas, município de Januária, estado de Minas Gerais, Brasil: taxonomia e análise bioestratigráfica.
- Fralick, P., and Barrett, T.J., 1995 Depositional controls on iron formation associations in Canada. In *Sedimentary Facies Analysis: A Tribute to the Research and Teaching of Harold G*, edited by G. Plint, Reading, p. 137–156.
- Fralick, P., Davis, D.W., and Kissin, S.A., 2002, The age of the Gunflint Chert, Ontario, Canada: single zircon U–Pb age determinations from reworked volcanic ash: *Canadian Journal of Earth Sciences*, v. 39, p. 1085–1091.
- Gerlach, D.C., Shirey, S.B., and Carlson, R.W., 1988, Nd isotopes in Proterozoic iron formations: evidence for mixed age provenance and depositional variability: *EOS*, v. 69, p. 1515.

- González-Flores, A.L., Jin, J., Osinski, G.R., and Tsujita, C.J., 2022, Acritarch-like Microorganisms from the 1.9 Ga Gunflint Chert, Canada: *Astrobiology*, v. 22, n. 5, p. 568–578.
- Grey, K., 2005, Ediacaran palynology of Australia: *Australasian Palaeontological Memoirs*, v. 31, p. 439.
- Hammer, Ø., Harper, D.A.T., and Ryan, P.D., 2001, PAST: paleontological statistics software package for education and data analysis. *Palaeontologia Electronica*, v. 4, n. 1, p. 9. (http://palaeo-electronica.org/2001_1/past/issue1_01.htm)
- Han, C.M., Chen, L., Li, G.J., Pang, K., Wang, W., Zhou, G.Z., Yang, F.J., Lyu, W.G., Wang, K., Zhong, Z.H. and Wu, C.X., 2021, First record of organic-walled microfossils from the Tonian Shiwangzhuang Formation of the Tumen Group in western Shandong, North China: *Palaeoworld*, v. 30, n. 2, p. 208–219.
- Jankauskas, T.V., Mikhailova, N.S., and Hermann, T.N., 1989, Mikrofosilii dokembriya SSSR [Precambrian Microfossils of the USSR]. *Trudy Instituta Geologii i Geochronologii Dokembriya SSSR Akademii Nauk: Leningrad*, p. 188.
- Javaux, E.J., and Lepot, K., 2018, The Paleoproterozoic fossil record: implications for the evolution of the biosphere during Earth's middle-age: *Earth-Science Reviews*, v. 176, p. 68–86.
- Kaźmierczak, J., 1979, The eukaryotic nature of *Eosphaera*-like ferriferous structures from the Precambrian Gunflint Iron Formation, Canada: A comparative study: *Precambrian Research*, v. 9, n. 1–2, p. 1–22.

- Knoll, A.H., Swett, K., and Mark, J., 1991, Paleobiology of a Neoproterozoic tidal flat/lagoonal complex: the Draken Conglomerate Formation, Spitsbergen: *Journal of Paleontology*, p. 531–570.
- Knoll, A.H., Javaux, E.J., Hewitt, D., and Cohen, P., 2006, Eukaryotic organisms in Proterozoic oceans: *Philosophical Transactions of the Royal Society B Biological Sciences*, v. 361, n. 1470, p. 1023–1038.
- Krumbein, W.E., 2010, Gunflint Chert microbiota revisited – neither stromatolites, nor cyanobacteria, in Seckbach, J., and A. Oren, A., eds., *Microbial Mats: Modern and Ancient Microorganisms in Stratified Systems, Cellular Origin, Life in Extreme Habitats and Astrobiology*, no. 14, p. 53–70. New York, Springer Science.
- Lehn, I., Horodyski, R.S., and Paim, P.S.G., 2019, Marine and non-marine strata preserving Ediacaran microfossils: *Scientific Reports*, v. 9, n. 1, p. 1–8.
- Li, G., Pang, K., Chen, L., Zhou, G., Han, C., Yang, L., Wang, W., Yang, F., and Yin, L., 2019, Organic-walled microfossils from the Tonian Tongjiazhuang Formation of the Tumen Group in western Shandong, North China Craton and their biostratigraphic significance: *Gondwana Research*, v. 76, p. 260–289.
- Loron, C.C., 2016a, Biodiversity of Organic-Walled Eukaryotic Microfossils from the Tonian Visingsö Group, Sweden.
- Loron, C.C., and Moczyłowska, M., 2016b, New record of organic-walled microfossils of algal and some uncertain affinities from the Tonian Visingsö Group in southern Sweden.

- Loron, C.C., and Moczyłowska, M., 2017, Tonian (Neoproterozoic) eukaryotic and prokaryotic organic-walled microfossils from the upper Visingsö Group, Sweden: *Palynology*, v. 42, n. 2, p. 220–254.
- Loron, C.C., François, C., Rainbird, R.H., Turner, E.C., Borensztajn, S., and Javaux, E.J., 2019a Early fungi from the Proterozoic era in Arctic Canada: *Nature*, v. 570, n. 7760, p. 232–235.
- Loron, C.C., Rainbird, R.H., Turner, E.C., Greenman, J.W., and Javaux, E.J., 2019b, Organic-walled microfossils from the late Mesoproterozoic to early Neoproterozoic lower Shaler Supergroup (Arctic Canada): diversity and biostratigraphic significance. *Precambrian Research*, v. 321, p. 349–374.
- Loron, C.C., Halverson, G.P., Rainbird, R.H., Skulski, T., Turner, E.C., and Javaux, E.J., 2021 Shale-hosted biota from the Dismal Lakes Group in Arctic Canada supports an early Mesoproterozoic diversification of eukaryotes: *Journal of Paleontology*, v. 95, n. 6, p. 1113–1137.
- Miao, L., Moczyłowska, M., Zhu, S., and Zhu, M., 2019, New record of organic-walled, morphologically distinct microfossils from the late Paleoproterozoic Changcheng Group in the Yanshan Range, North China: *Precambrian Research*, v. 321, p. 172–198.
- Miao, L., Moczyłowska, M., and Zhu, M., 2021, A diverse organic-walled microfossil assemblage from the Mesoproterozoic Xiamaling Formation, North China: *Precambrian Research*, v. 360, p. 106–235.
- Mikhailova, N.S., 1986, New finds of the microfossils from the Upper Riphean deposits of the Krasnoyarsk region: *Current Problems of Modern Paleoalgology*, p. 31–37.

- Morey, G.B., 1967, Stratigraphy and Sedimentology of the Middle Precambrian Rove Formation in Northeastern Minnesota: *Journal of Sedimentary Research*, v. 37, n. 4, p. 1154–1162.
- Morey, G.B., 1969, The Geology of the Middle Precambrian Rove Formation in northeastern Minnesota: Minnesota Geological Survey. University of Minnesota Digital Conservancy, v. 7, p. 1–62.
- Ouyang, S., Yin, L., and Li, Z., 1974, The Cambrian paleospores. In: *A Handbook of the Stratigraphy and Paleontology in Southwest China*: Science Press Beijing, p. 114:123 (in Chinese).
- Prasad, B., Uniyal, S.N., and Asher, R., 2005, Organic-walled microfossils from the Proterozoic Vindhyan Supergroup of Son Valley, Madhya Pradesh, India.
- Retallack, G.J., 2014, Precambrian life on land: *Paleobotanist*, v. 63, n. 1, p. 1–15.
- Retallack, G.J., 2015, Acritarch evidence for an Ediacaran adaptive radiation of Fungi: *Botanica Pacifica: a journal of plant science and conservation*, v. 4, n. 2, p. 19–33.
- Sergeev, V.N., Knoll, A.H., and Grotzinger, J.P., 1995, Paleobiology of the mesoproterozoic Billyakh group, anabar uplift, northern Siberia: *Journal of Paleontology*, v. 69, n. S39, p. 1–37.
- Shukla, M., Babu, R., Singh, V.K., and Sharma, M.A., 2006, *Catalogue of Precambrian Palaeobiology from India*.
- Shuvalova, J.V., Nagovitsin, K.E., Duda, J.P., and Parkhaev, P.Y., 2021, Early Eukaryotes in the Lakhanda Biota (Mesoproterozoic, Southeastern Siberia)—Morphological and

- Geochemical Evidence: In *Doklady Biological Sciences* v. 500, n. 1, p. 127–132. Pleiades Publishing.
- Srivastava, P., and Kumar, S., 2003, New microfossils from the Meso-Neoproterozoic Deoban Limestone, Garhwal Lesser Himalaya, India.
- Srivastava, P., 2012. Ediacaran discs from the Jodhpur Sandstone, Marwar Supergroup, India: a biological diversification or taphonomic interplay.
- Stanevich, A.M., Postnikov, A.A., Kornilova, T.A., Terleev, A.A., and Popov, N.V., 2013, Bacterial, fungal, and algal microfossils in the Lower Proterozoic Baikal region of Siberia (Udokan and Sayany Mountains): *Journal of Paleontology*, v. 47, n. 9, p. 977–983.
- Stille, P., and Clauer, N., 1986, Sm–Nd isochron age and provenance of the argillites of the Gunflint iron formation in Ontario, Canada: *Geochimica et Cosmochimica Acta*, v. 50, p. 1141–1146.
- Strother, P.K., and Wellman, C.H., 2020, The Nonesuch Formation Lagerstätte: a rare window into freshwater life one billion years ago: *Journal of the Geological Society*, v. 178, n. 2.
- Tang, Q., Pang, K., Xiao, S., Yuan, X., Ou, Z., and Wan, B., 2013, Organic-walled microfossils from the early Neoproterozoic Liulaobei Formation in the Huainan region of North China and their biostratigraphic significance: *Precambrian Research*, v. 236, p. 157–181.
- Tang, Q., Pang, K., Yuan, X., Wan, B., and Xiao, S., 2015, Organic-walled microfossils from the Tonian Gouhou Formation, Huaibei region, North China Craton, and their biostratigraphic implications: *Precambrian Research*: v. 266, p. 296–318.

- Veis, A.F. and Vorob'eva, N.G., 1992, Riphean and Vendian Microfossils of the Anabar Massif: *Izvestiya of the Academy of Sciences of the U.S.S.R.*, n.1, p. 114–130.
- Veis, A.F., Vorob'eva, N.G., and Golubkova, E.Y., 2006 The early Vendian microfossils first found in the Russian Plate: Taxonomic composition and biostratigraphic significance: *Stratigraphy and Geological Correlation*, v. 14, n. 4, p. 368–385.
- Vorob'eva, N.G., Sergeev, V.N., and Knoll, A.H., 2009, Neoproterozoic microfossils from the northeastern margin of the East European Platform: *Journal of Paleontology*, v. 83, n. 2, p. 161–196.
- Wacey, D., Menon, S., Green, L., Gerstmann, D., Kong, C., Mcloughlin, N., Saunders, M., and Brasier, M., 2012, Taphonomy of very ancient microfossils from the ~ 3400 Ma Strelley Pool Formation and ~1900 Ma Gunflint Chert: New insights using a focused ion beam *Precambrian Research*, v. 220, p. 234–250.
- Wang, L., Zhang, K., Lin, S., He, W., and Yin, L., 2021, Origin and age of the Shenshan tectonic mélange in the Jiangshan-Shaoxing-Pingxiang Fault and late Early Paleozoic juxtaposition of the Yangtze Block and the West Cathaysia terrane, South China: *Bulletin*, v. 134, n. 1–2, p. 113–129.
- Weiss, A.F., 1984, Mikrofossilii iz verkhnego rifeya Turukhanskogo rajona. [Microfossils from the Upper Riphean of the Turukhansk region. *Paleontol J*, v. 2, p. 98–104.]: *Paleontologicheskij Zhurnal*, v. 2, p. 102–108.
- Xing, Y. and Liu, K., 1973, On Sinian microflora in Yenliao region of China and its geographic significance. *Acta Geologica Sinica*, 1, pp.1-64.

- Yin, L., and Guan, B., 1999, Organic-walled microfossils of Neoproterozoic Dongjia Formation, Lushan County, Henan Province, North China: *Precambrian Research*, v. 94, n. 1–2, p. 121–137.
- Yin, L.M., and Li, Z.P., 1978, Precambrian microfossils of Southwest China, with reference to their stratigraphical significance. *Memoirs of Nanjing Institute of Geology and Palaeontology* [in Chinese with English summary]: Academia Sinica, v. 10, p. 41–108.
- Yan, Y., 1995, Shale facies microfloras from lower Changcheng system in Kuancheng, Hebei and comparison with those of neighboring areas. *Wei ti gu Sheng wu xue bao: Acta Micropalaeontologica Sinica*, v. 12, n. 4, p. 349–373.
- Zang, W.L., 1995, Early Neoproterozoic sequence stratigraphy and acritarch biostratigraphy, eastern Officer Basin, South Australia: *Precambrian Research*, v. 74, n. 3, p. 119–175.

Chapter 4: Conclusion

4.1 Conclusions

The oldest well-recognized, acritarch-like, eukaryotic microfossils have been dated to around 1.6 Ga (Miao et al., 2019). Despite the existence of older microfossils with morphological features that are characteristic of eukaryotes (Montenari and Leppig, 2003; Willman and Moczyłowska, 2008; Moczyłowska et al., 2011; Butterfield, 2015; Agić et al., 2017; Miao et al., 2019; Loron et al., 2021), their state of preservation has often led to debatable interpretations. Furthermore, the generally well-preserved microbiota from the ~1.9 Ga Gunflint Chert has also suffered cellular degradation, making it impossible to recognize membrane-bounded nuclei or organelles (even if the biota contained fossil eukaryotic cells).

In this study, an extended depth of focus (EDF) imaging technique was used in combination with scanning electron microscopy (SEM) and electron microprobe analysis (EMA) to study the Gunflint Chert microfossils. This led to the recognition of three new types of microfossils with eukaryote-like morphology, collectively termed Complex Unicellular Bodies (CUBs; González-Flores et al., 2022), which generally have a cell size more remarkable than the co-occurring (and previously known) prokaryotic fossil organisms (Barghoorn and Tyler, 1965; Awramik and Barghoorn, 1977; Barghoorn, 1971; Edhorn, 1973; Schopf, 1968).

The three types of CUBs recognized in this study are as follows:

- CUB Type 1: Spherical cysts with numerous radially arranged thin processes similar to those in some acritarchs and dinoflagellates (Fig. 2.2a).

- CUB Type 2: Spherical cells with numerous horny pustules and reticulate cell-wall sculpturing such as perforations, pits, and ridges (Fig. 2.2b).
- CUB Type 3: Spheroidal to irregular cells with single or multiple robust podia, tubercles, ridges, and scale-like surface ornaments (Fig. 2.2c).

Larger organisms composed of congregations of multiple bodies referred to in this study as "multicellular bodies" (Fig. 2.6) are also present within the Gunflint Chert microbiota. A more in-depth study is needed for this group of fossils to understand their prokaryotic or eukaryotic affinity.

The Gunflint CUBs share several characteristics with younger Proterozoic microfossils that have been interpreted as eukaryotes. These include the following:

1. **Cell size.** Ranging from 10 to 35 μm in diameter (larger than the co-occurring coccoid cyanobacteria that are usually $\sim 5 \mu\text{m}$ in diameter), the Gunflint CUBs are generally smaller than the younger Proterozoic acritarchs (Fig. 3.9). They do, however, overlap in size with the smaller forms of Mesoproterozoic–Neoproterozoic *Germinosphaera* interpreted by various authors as eukaryotes (Miao et al., 2019, Loron et al., 2021; Butterfield et al., 1994; Jankauskas et al., 1989; Mikhailova, 1986).
2. **Surface ornaments.** Reticulate-patterned tubercles, scale-like ornaments, folded ridges, and variously shaped processes bear a high degree of similarity to those observed in acritarchs and other organic-walled microfossils regarded as eukaryotes (Miao et al., 2019; Loron et al., 2021).
3. **Intracellular dark bodies.** Radiating filaments and well-delimited dark bodies inside the CUB cells may be the preserved residues of intracellular structures such as nuclei or organelles.

Among the three types of CUBs of the Gunflint microbiota, CUB Type 3 was identified as a new species of *Germinosphaera*, *G. gunflinta*, characterized by a rounded cyst with thick walls, one or more robust podia and scale-like surface ornaments. A comprehensive morphological analysis of 146 specimens of *Germinosphaera* worldwide (including *G. gunflinta* and eight other species), ranging from the Paleoproterozoic (~2.0 Ga) to the Ediacaran, reveals several morphological trends:

1. The oldest representative within the *Germinosphaera* genus is *G. gunflinta* sp. nov. It possesses the characteristic features of this genus such as a sizeable robust podium, secondary processes, and scale-like pustules. Well-preserved surface ornaments that several other species from this genus display are also present on this newly identified species.
2. There is an apparent morphological and evolutionary continuity for this genus that starts with its oldest and newly identified member, *G. gunflinta*. This continuity moves through younger congeneric species of late Paleoproterozoic–Mesoproterozoic age belonging to the same genus. This continuity may suggest that the *Germinosphaera*'s eukaryotic lineage can be traced to the 1.9 Ga Gunflint Chert.
3. The dramatic increase in the maximum cyst size of *Germinosphaera* around 1.1 Ga is still poorly understood, as its cause remains still unknown and requires further investigation outside of the specs of this work.

4.2 Future Work

4.2.1 In-depth Taxonomic Study of the Remaining CUB types

Among the three types of CUBs, only Type 3 has been systematically studied and recognized as a new species of *Germinosphaera*. The other two types remain to be studied in greater taxonomic depth.

CUB Type 1 (Fig. 4.1a) has membrane-supported, radially arranged hollow filaments. Similar to those observed in the younger acritarch *Alicesphaeridium medusoideum* (see Willman and Moczyłowska, 2008), although the latter from the Ediacaran of Australia is notably larger in overall size (>100 μm) and shows better developed radial filaments (Fig. 4.1b).

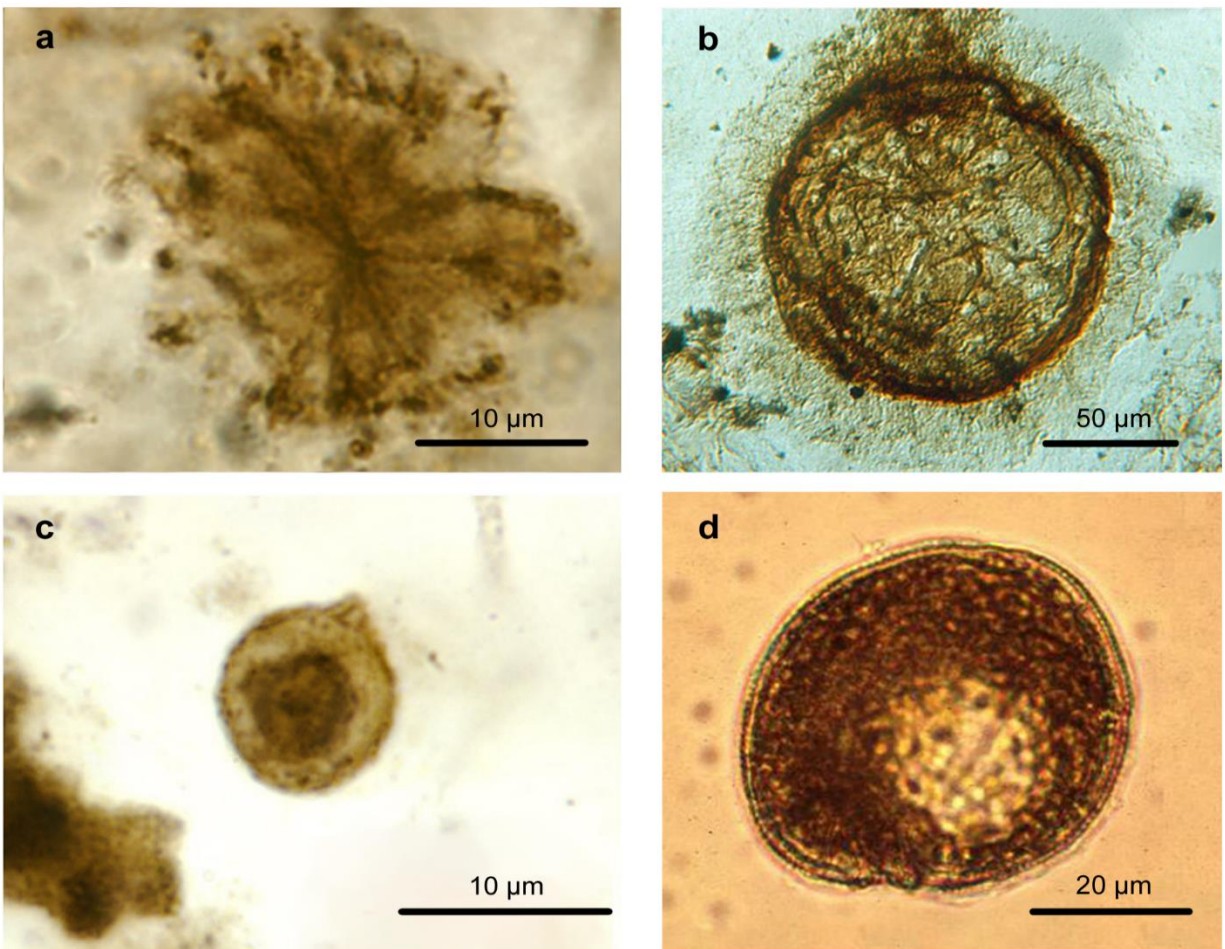


Figure 4.1 a) Optical image of CUB Type 1, sample GSC24380d_213; b) Optical image of *Alicesphaeridium medusoideum* from Willman and Moczyłowska (2008); c) Optical image of CUB Type 1, sample GSC24380e_290; d) Optical image of *Gambierdiscus toxicus* from Knoll, (2015). Scalebar = 10 μm for (a) and (c), 20 μm for (d), and 50 μm for (b).

CUB Type 2 has a spherical cell with horny pustules with reticulate cell-wall sculpturing such as perforations, pits, and ridges (Fig. 4.1c). The cell shape, size, and ornamentation are similar to *Gambierdiscus toxicus* (Fig. 4.1d), a modern dinoflagellate (Knoll, 2015).

4.2.2 Gunflint Multicellular Structures

This study examined "multicellular bodies" only superficially (Fig. 4.2a). Some comprise relatively loose cell aggregates (i.e., clusters or clumps of clearly individual cells), whereas others show much more tightly fused or integrated cells. Some of the loose aggregates show similarity to colonies of modern unicellular green algae *Chlorococcum* (e.g. *Chlorococcum vacuolatum*) and *Chlorosarcinopsis* (e.g. *Chlorosarcinopsis gelatinosa*) (Stanier and Cohen-Bazire, 1977) (Fig. 4.2b-c).

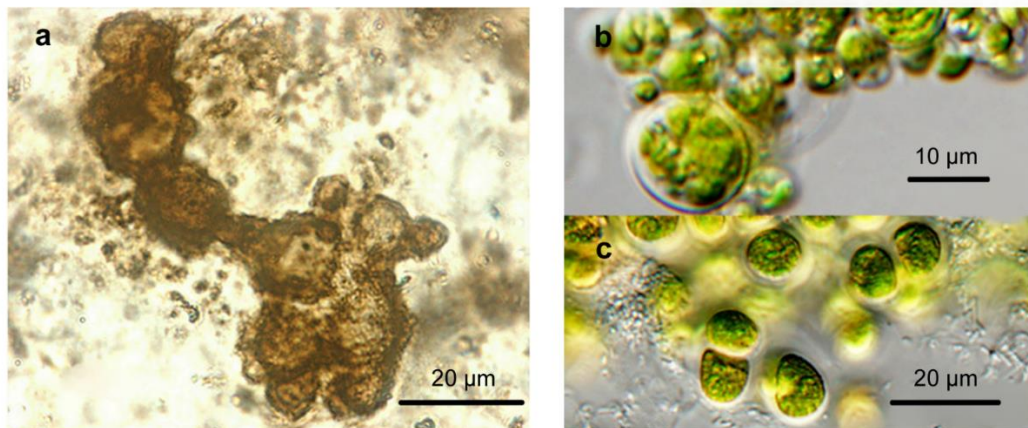


Figure 4.2 a) Optical image of Multicellular Body of sample GSC24380d_217. b) Optical images of *Chlorococcum vacuolatum* and c) *Chlorosarcinopsis gelatinosa* from Stanier and Cohen-Bazire (1977). Scalebar = 10 µm for (b) and 20 µm for (a) and (c).

4.3 Significance of the Study

The results of this study have several significant implications:

- First, the common occurrence of complex unicellular bodies (CUBs) in the Gunflint biota suggests that simple eukaryotes were already diverse and abundant 1.9 billion years ago.

- The high level of diversity of Gunflint CUBs also suggests that the origin of eukaryotes most likely predates the Gunflint Chert. The Gunflint fossil data corroborate the molecular timescale of eukaryote evolution, which suggests significant eukaryotic divergence of eukaryotes around 1.9 Ga but the origin of basal eukaryotes may well be as early as 2.6 Ga as suggested by Bromham and Penny (2003), Ho and Duchene (2014) and Dos Reis et al. (2016).
- There are also significant implications on the field of astrobiology. Firstly, in its facies association with the Gunflint BIF, the Gunflint chert microbiota is one of the best possible terrestrial analogs on the search of extinct life on another planets (Lukmanov et al., 2022). In this respect, Mars is one of the best candidates to find such kind of traces in future studies. BIFs in general have been suggested as a suitable analog (Fallacaro and Calvin, 2006; Allen et al., 2001; Lukmanov et al., 2022) since iron oxides and silicates precipitate as an aqueous mineral phase that is perfect for trapping any microbiota present during the precipitation process.
- Being able to identify the microbiota in the Gunflint chert offers the potential of extrapolating the technics used for biomarker tracing and morphological characterization to space exploration. Moreover, understanding the living and preservation conditions for the Gunflint microorganisms offers a useful example for other candidate planetary bodies with habitable zones.

References

Agić, H., Moczyłowska, M., and Yin, L., 2017, Diversity of organic-walled microfossils from the early Mesoproterozoic Ruyang Group, North China Craton—A window into the early eukaryote evolution: *Precambrian Research*, v. 297, p. 101–130.

- Allen, C.C., Westall, F., and Schelble, R.T., 2001, Importance of a martian hematite site for astrobiology: *Astrobiology*, v. 1, p. 111–123.
- Awramik, S.M., and Barghoorn, E.S., 1977, The Gunflint microbiota: *Precambrian Research*, v.5, p. 121–142.
- Barghoorn, E.S., 1971, The oldest fossils. *Scientific American*: v. 224, no. 5, p. 30–43.
- Barghoorn, E.S., and Tyler, S.A., 1965, Microorganisms from the Gunflint Chert: *Science*, v. 147, p. 563–577.
- Bromham, L. and Penny, D., 2003, The modern molecular clock: *Nature Reviews Genetics*, v. 4, n. 3, p. 216–224.
- Butterfield, N.J., 2015, Early evolution of the Eukaryota: *Palaeontology*, v. 58, n. 1, p. 5–17.
- Butterfield, N.J., Knoll, A.H., and Swett, K., 1994, Paleobiology of the neoproterozoic svanbergfjellet formation, Spitsbergen: *Lethaia*, v. 27, n. 1, p. 76–76.
- Dos Reis, M., Donoghue, P.C., and Yang, Z., 2016, Bayesian molecular clock dating of species divergences in the genomics era: *Nature Reviews Genetics*, v. 17, n. 2, p. 71–80.
- Edhorn, A., 1973, Further investigations of fossils from the Animikie, Thunder Bay, Ontario: *Proceedings of the Geologist's Association Canada*, v. 25, p. 37–66.
- Fallacaro, A. and Calvin, W.M., 2006, Spectral properties of Lake Superior banded iron formation: application to martian hematite deposits: *Astrobiology*, v. 6, n. 4, p. 563–580.
- González-Flores, A.L., Jin, J., Osinski, G.R., and Tsujita, C.J., 2022, Acritarch-like Microorganisms from the 1.9 Ga Gunflint Chert, Canada: *Astrobiology*, v. 22, n. 5, p. 568–578.

- Ho, S.Y. and Duchêne, S., 2014, Molecular-clock methods for estimating evolutionary rates and timescales: *Molecular ecology*, v. 23, n. 24, p. 5947–5965.
- Jankauskas, T.V., Mikhailova, N.S., and Hermann, T.N., 1989, Mikrofosilii dokembriya SSSR [Precambrian Microfossils of the USSR]. *Trudy Instituta Geologii i Geochronologii Dokembriya SSSR Akademii Nauk: Leningrad*, p. 188.
- Knoll, A.H., 2015, *Life on a Young Planet: The First Three Billion Years of Evolution on Earth*: Princeton University Press, Princeton, NJ.
- Loron, C.C., Halverson, G.P., Rainbird, R.H., Skulski, T., Turner, E.C., and Javaux, E.J., 2021, Shale-hosted biota from the Dismal Lakes Group in Arctic Canada supports an early Mesoproterozoic diversification of eukaryotes: *Journal of Paleontology*, v. 95, n. 6, p. 1113–1137.
- Lukmanov, R.A., Tulej, M., Wiesendanger, R., Riedo, A., Grimaudo, V., Ligterink, N.F., de Koning, C., Neubeck, A., Wacey, D., and Wurz, P., 2022, Multiwavelength Ablation/Ionization and Mass Spectrometric Analysis of 1.88 Ga Gunflint Chert: *Astrobiology*, v. 22, n. 4, p. 369–386.
- Miao, L., Moczyłowska, M., Zhu, S., and Zhu, M., 2019, New record of organic-walled, morphologically distinct microfossils from the late Paleoproterozoic Changcheng Group in the Yanshan Range, North China: *Precambrian Research*, v. 321, p. 172–198.
- Mikhailova, N.S., 1986, New finds of the microfossils from the Upper Riphean deposits of the Krasnoyarsk region: *Current Problems of Modern Paleoalgology*, p. 31–37.

- Moczyłowska, M., Landing, E.D., Zang, W., and Palacios, T., 2011, Proterozoic phytoplankton and timing of chlorophyte algae origins: *Palaeontology*, v. 54, n. 4, p. 721–733.
- Montenari, M., and Leppig, U., 2003, The Acritarcha: their classification morphology, ultrastructure and palaeoecological/palaeogeographical distribution: *Paläontol Zeitschrift*, v. 77, p. 173-194.
- Schopf, J.W., 1968, Microflora of the Bitter Springs formation, late Precambrian, central Australia: *Journal of Paleontology*, p. 651–688.
- Stanier, R.Y. and Cohen-Bazire, G., 1977, Phototrophic prokaryotes: the cyanobacteria: *Annual review of microbiology*, v. 31, n. 1, p. 225–274.
- Willman, S., and Moczyłowska, M., 2008, Ediacaran acritarch biota from the Giles 1 drillhole, Officer Basin, Australia, and its potential for biostratigraphic correlation: *Precambrian Research*, v. 162, p. 498–530.

Appendices

A. Optical Microscope CUB types' of measurements and plots for samples GSC24380 (2), GSC24380d and GSC24380e

This appendix contains the data used for the analysis of the different types of CUB's on Chapter 2. On each Item, every plot depicts a single type of CUB carefully catalogued from 3 different thin sections: GSC24380 (2), GSC24380d and GSC24380e.

Item 1. Extended focal depth optical imaging process.

In this study, images of the Gunflint Chert microfossils were acquired using a Zeiss Axioscope. Maximum magnification was achieved with a 100x oil lens and a 1.6x intermediate lens, obtaining a combined 160x optical magnification, which applies to nearly all the images presented in this paper. At this magnification, it is impossible to bring every part of a microfossil (with a diameter ranging from 13 to 25 μm in diameter) into focus with a single photograph. To obtain a completely focused image, the extended depth of focus (EDF) imaging technique was adopted, using the Nikon NIS Elements imaging software package (ver. 4 or ver. 5). With this technique, a series of z-stacked individual images were acquired at approximately equal-distance focal steps. For spheroidal objects, for example, between 5 and 15 “confocal” images were acquired, depending on the complexity of morphological features that need to be incorporated.

From the individual confocal images, various combinations of images representing the lower hemisphere, equatorial zone, and upper hemispheres of a spheroidal object can be combined into new, single “focused images”, as these combinations help avoid stacking or overlapping cell surface features of the two hemispheres. For the images used in Fig. 3 (D and E; GSC24380e, thin

section no. 2) in the main paper, for example, a total of 12 individual confocal images (Suppl-Fig. 1A–L) were obtained for a CUB Type 2 object; image L is a combination of A–C, showing the morphological features of one “polar area”; image N (see also Fig. 3B in the main paper) is a combination of D–G, representing the “equatorial zone” through the center of the object; image O combines A–G to illustrate one hemisphere, whereas image P (see also Fig. 3C in the main paper) combines G–L to show the other hemisphere. The overall darkness and contrast were adjusted using Adobe Photoshop or Corel PhotoPaint.

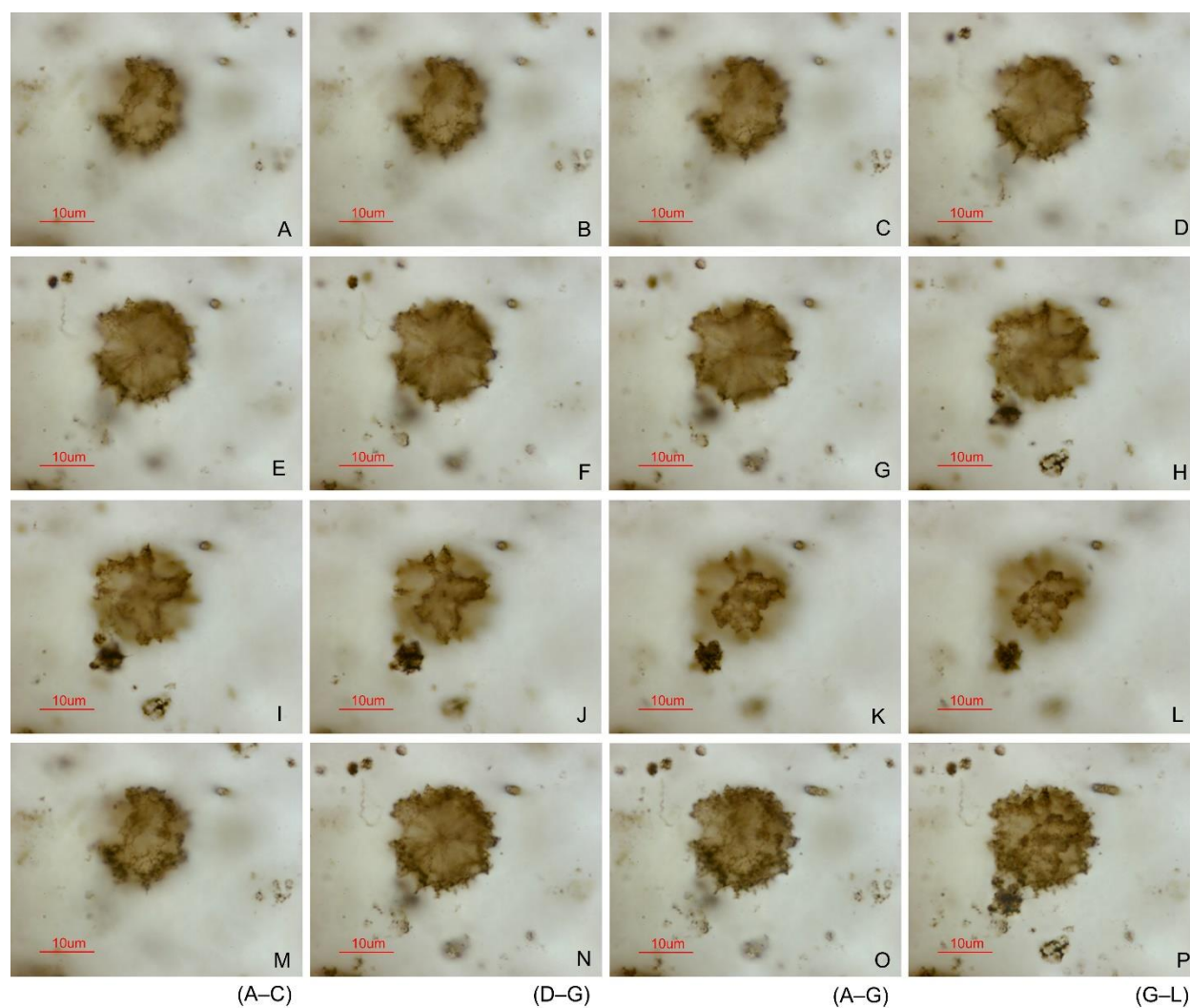


Figure A.1.1. **a-p**) series of z-stacked optical individual images from sample GSC24380e. For corresponding description see text in Appendix A, Item 1.

Item 2. Diameter measurements plots for thin section GSC24380 (2).

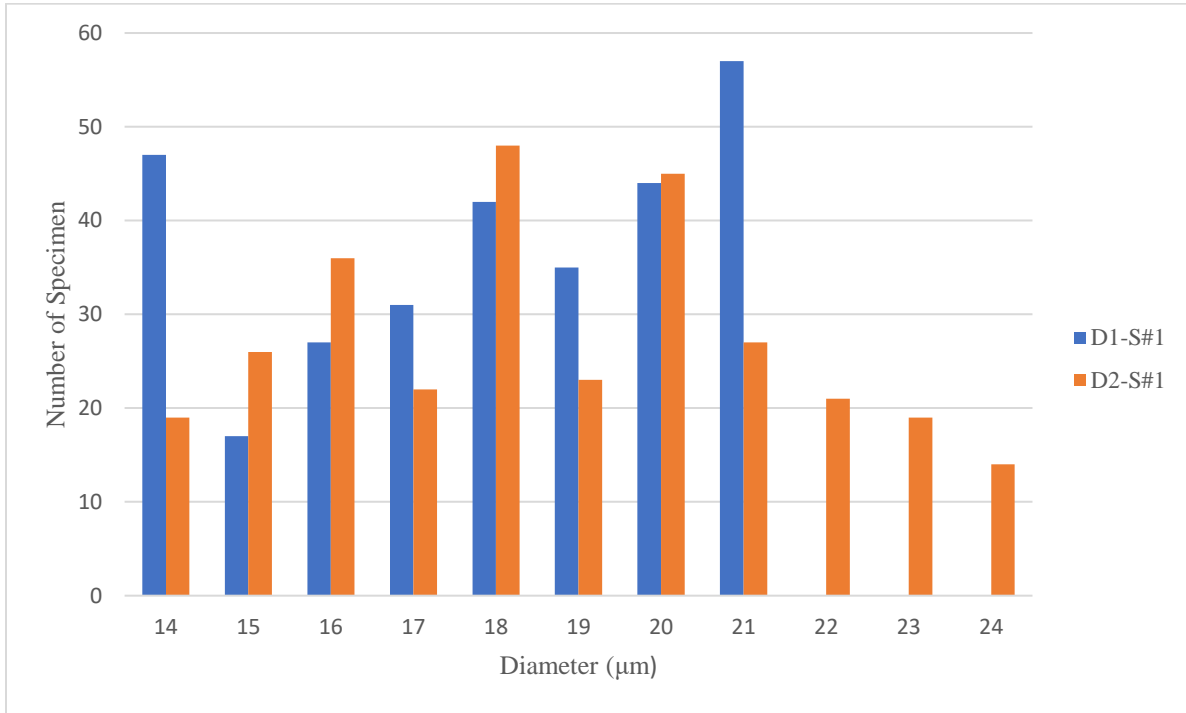


Figure A.2.1. Plot depicting the amount of specimens that have a similar maximum (D1) and minimum diameters (D2) in a sample pool of 300 of CUB type 1.

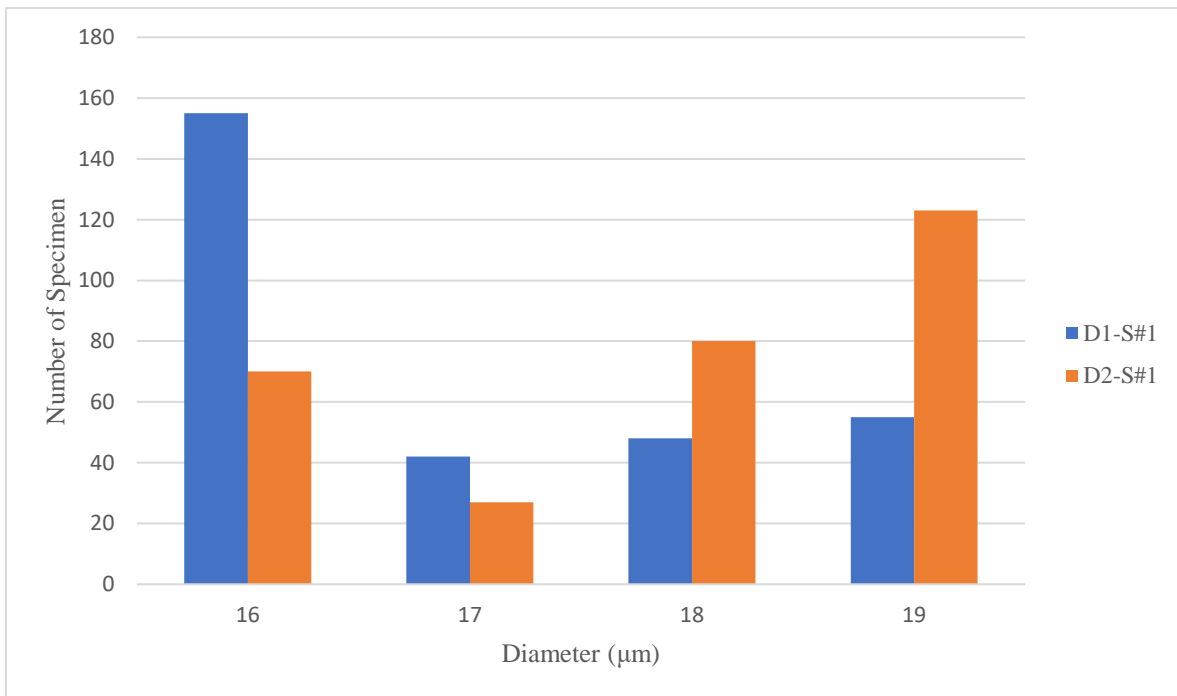


Figure A.2.2. Plot depicting the amount of specimens that have a similar maximum (D1) and minimum diameters (D2) in a sample pool of 300 of CUB type 2.

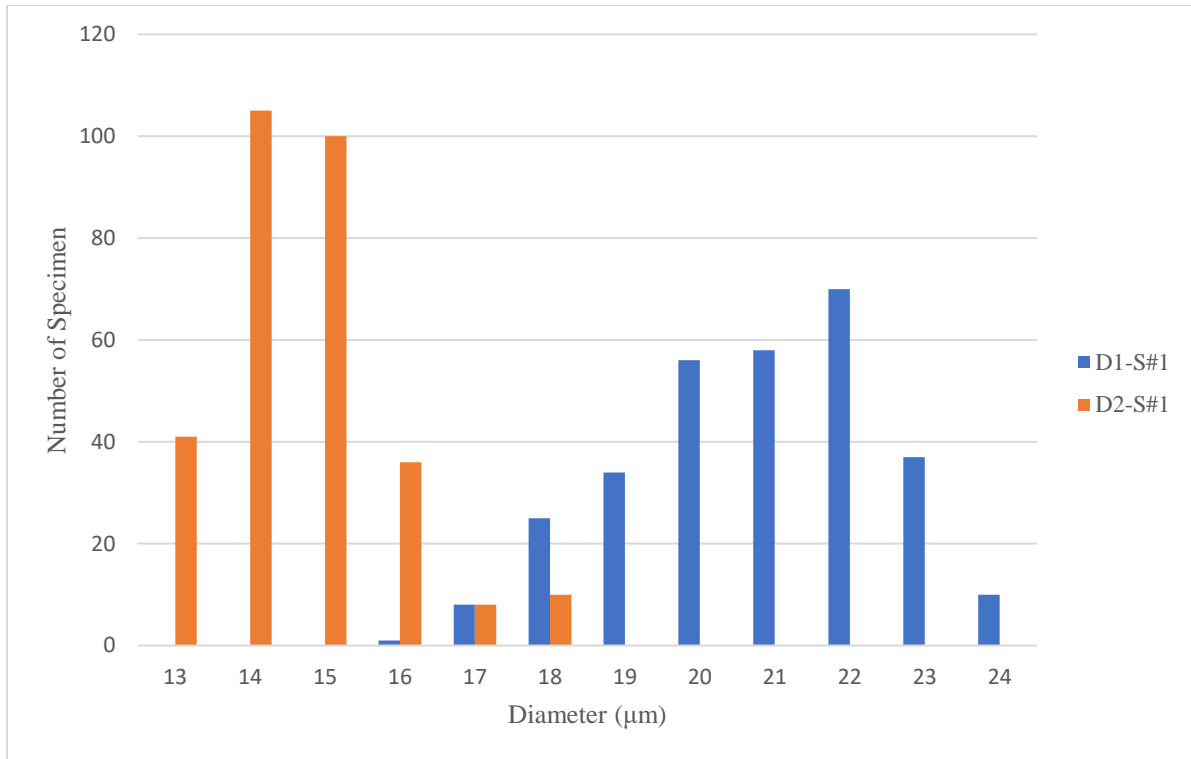


Figure A.2.3. Plot depicting the amount of specimens that have a similar maximum (D1) and minimum diameters (D2) in a sample pool of 300 of CUB type 3.

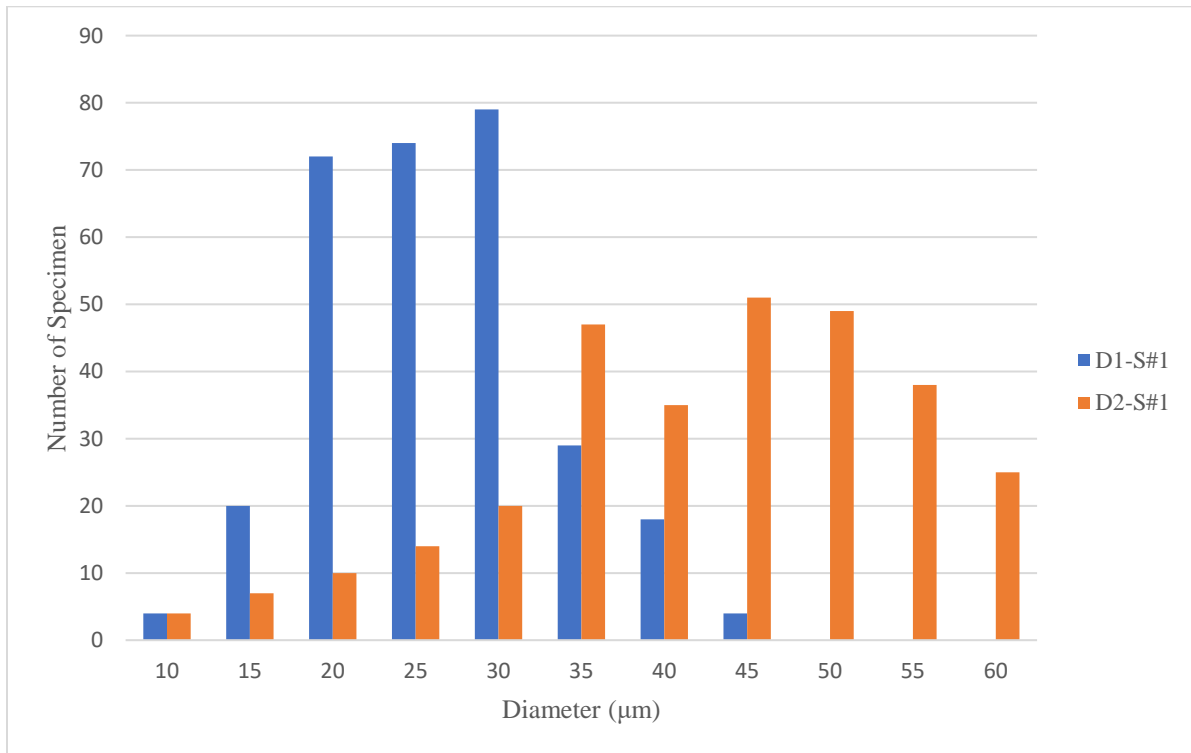


Figure A.2.4. Plot depicting the amount of specimens that have a similar maximum (D1) and minimum diameters (D2) in a sample pool of 300 of Multicellular Bodies.

Item 3. Diameter measurements plots for thin section GSC24380d.

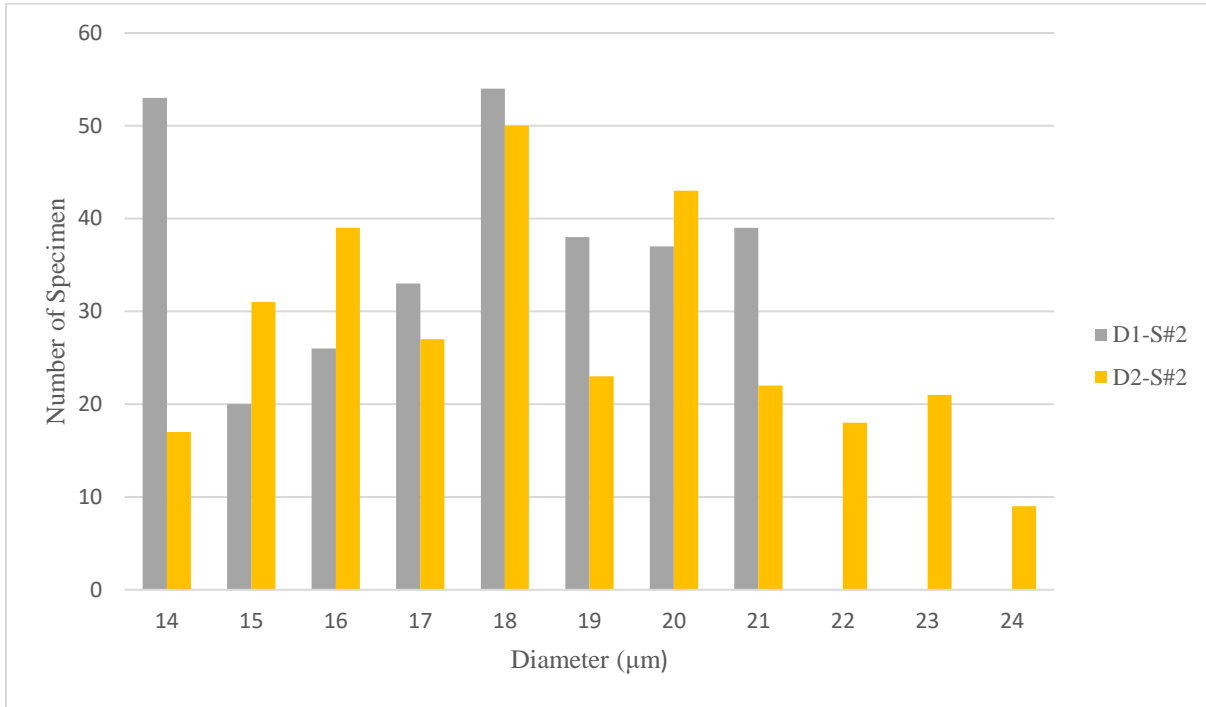


Figure A.3.1. Plot depicting the amount of specimens that have a similar maximum (D1) and minimum diameters (D2) in a sample pool of 300 of CUB type 1.

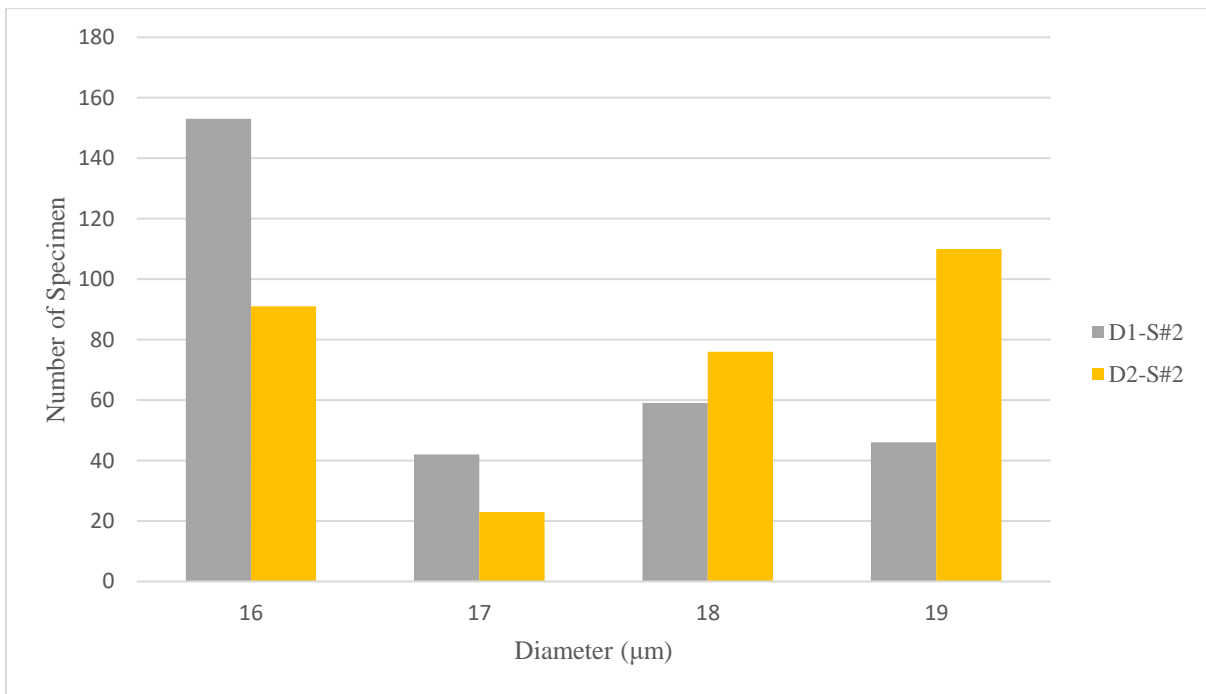


Figure A.3.2. Plot depicting the amount of specimens that have a similar maximum (D1) and minimum diameters (D2) in a sample pool of 300 of CUB type 2.

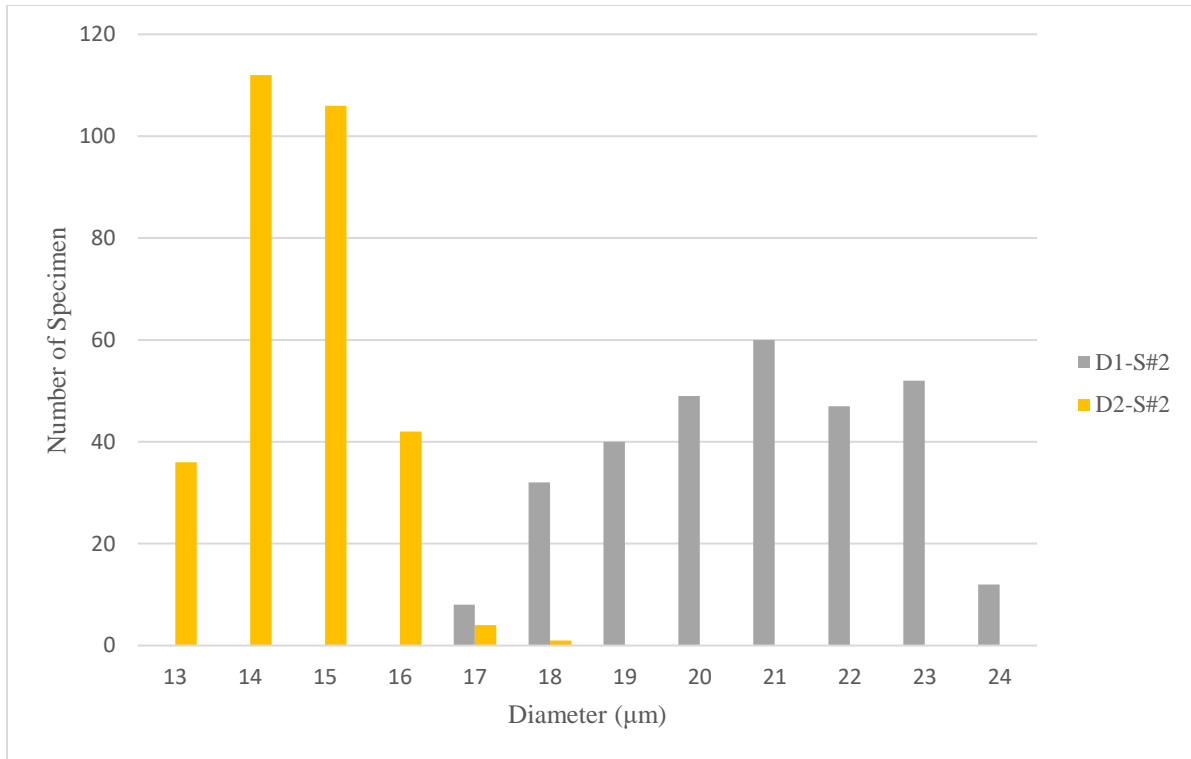


Figure A.3.3. Plot depicting the amount of specimens that have a similar maximum (D1) and minimum diameters (D2) in a sample pool of 300 of CUB type 3.

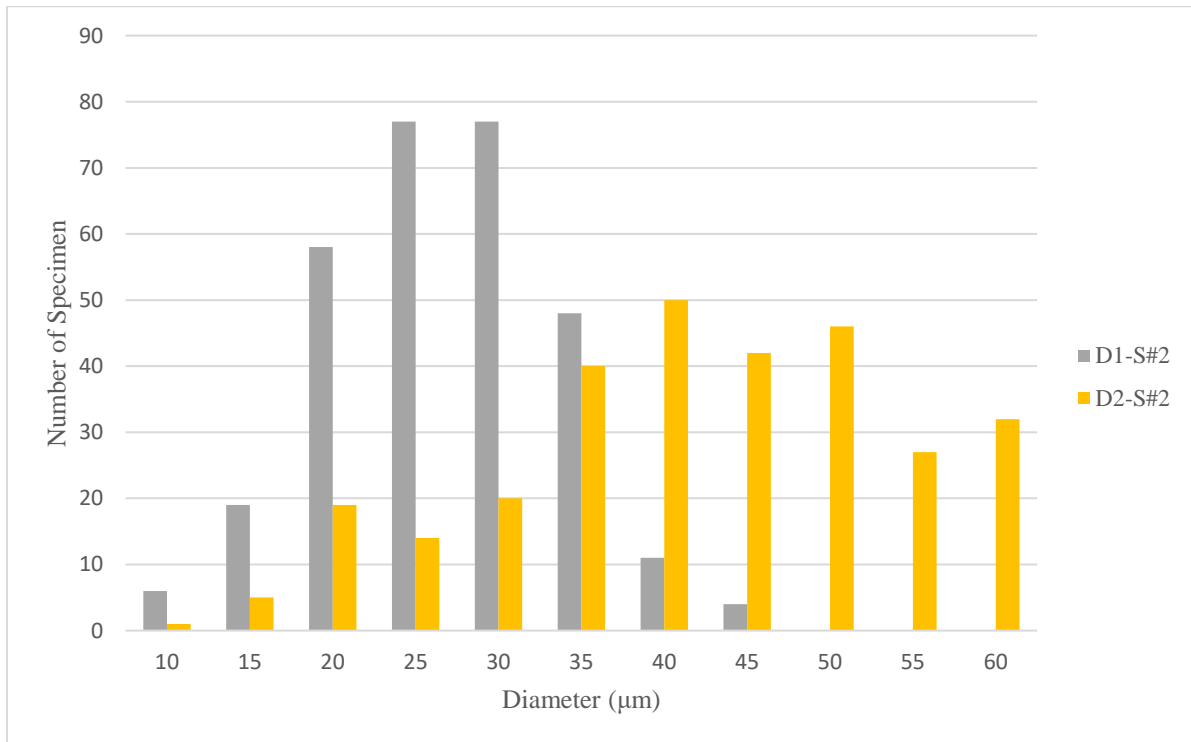


Figure A.3.4. Plot depicting the amount of specimens that have a similar maximum (D1) and minimum diameters (D2) in a sample pool of 300 of Multicellular Bodies.

Item 4. Diameter measurements plots for thin section GSC24380e.

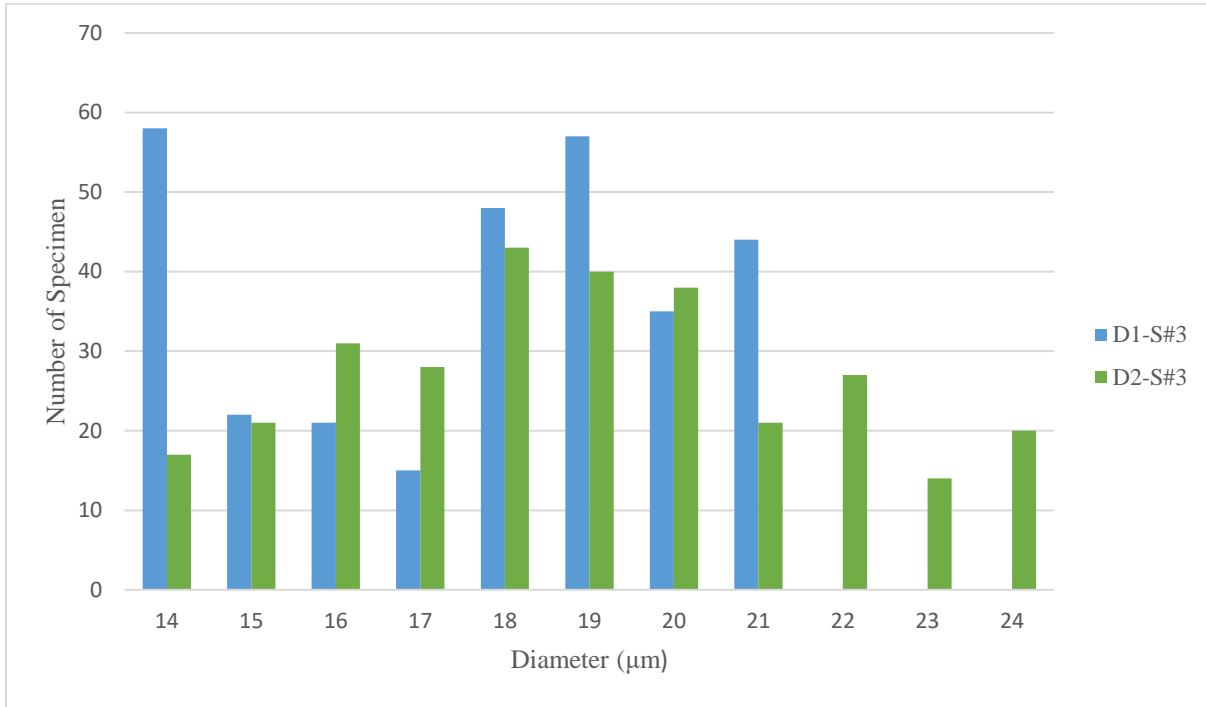


Figure A.4.1. Plot depicting the amount of specimens that have a similar maximum (D1) and minimum diameters (D2) in a sample pool of 300 of CUB type 1.

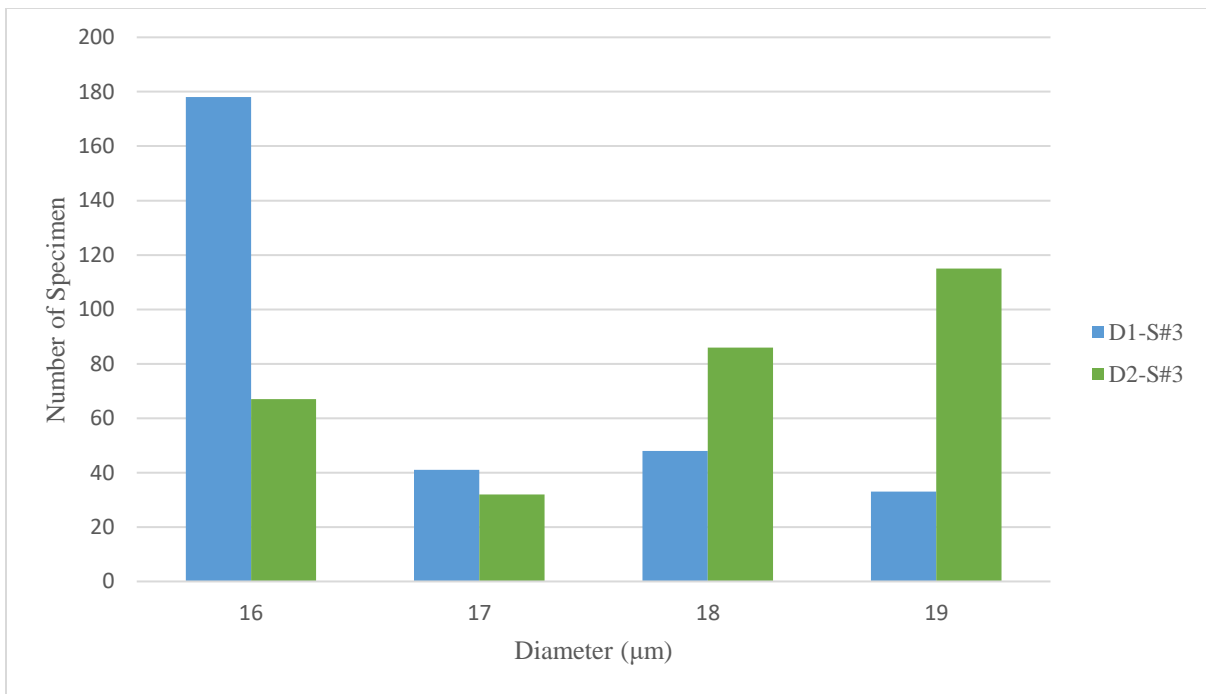


Figure A.4.2. Plot depicting the amount of specimens that have a similar maximum (D1) and minimum diameters (D2) in a sample pool of 300 of CUB type 2.

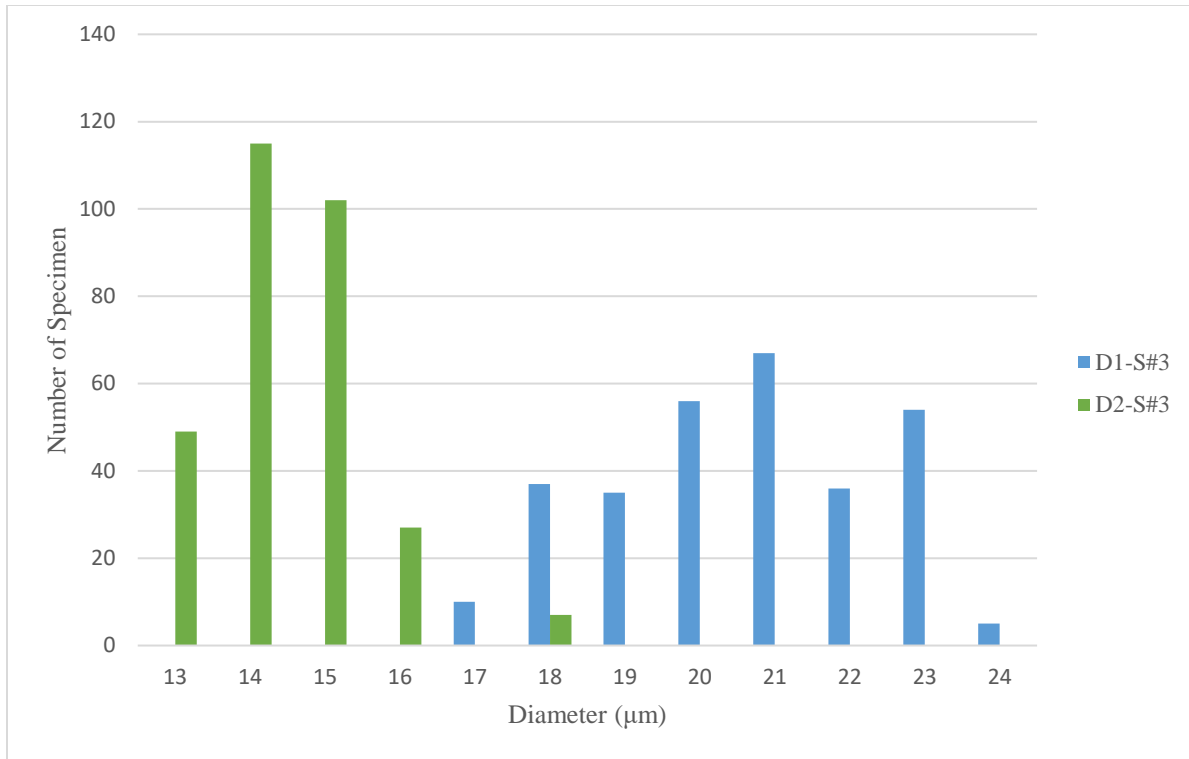


Figure A.4.3. Plot depicting the amount of specimens that have a similar maximum (D1) and minimum diameters (D2) in a sample pool of 300 of CUB type 3.

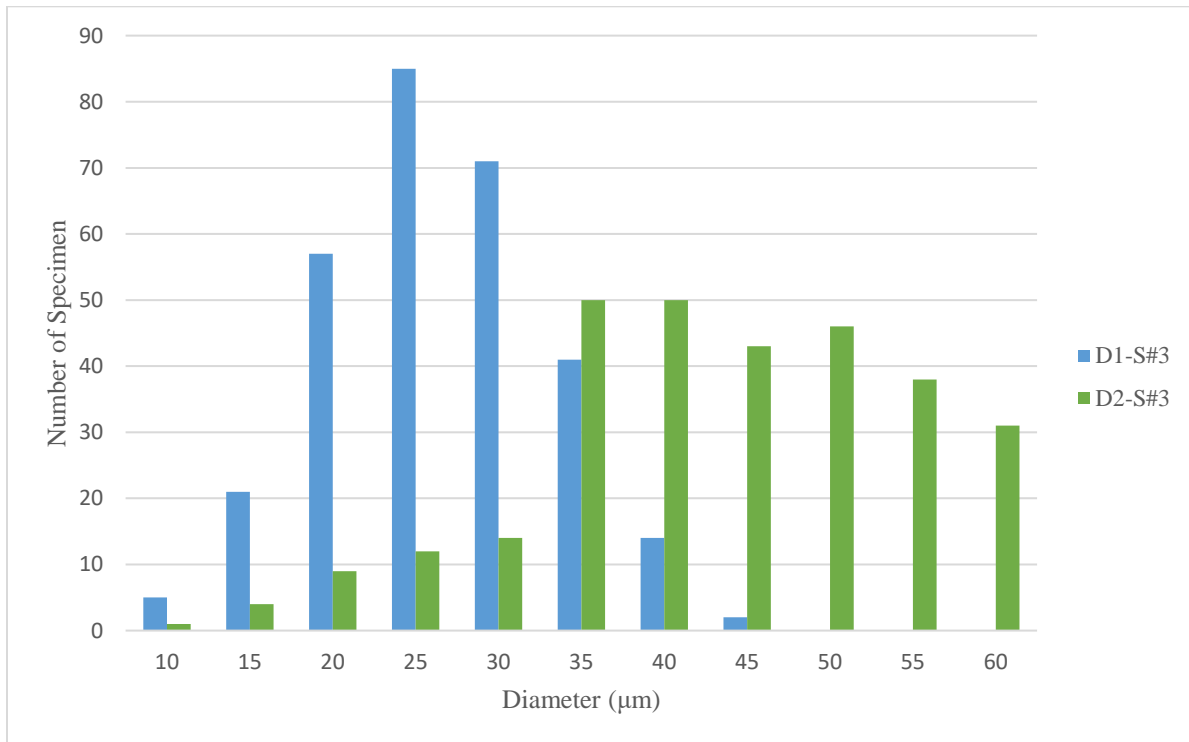


Figure A.4.4. Plot depicting the amount of specimens that have a similar maximum (D1) and minimum diameters (D2) in a sample pool of 300 of Multicellular Bodies.

B. Optical Microscope measurements of *Germinosphaera* specimen.

This appendix contains the data used for the analysis of *Germinosphaera* species on Chapter 3. It is divided into 3 items with several charts for a clearer depiction of the data.

On each Item, every table shows the same information categories for each species. Each specie is color coded to facilitate their identification. The specimen number assigned on the table is the one corresponding to the plots used in both analysis of Items 2 and 3 of Appendix B. The color coded ages indicate the eon each specimen belongs to; green for Paleoproterozoic formations, blue for Mesoproterozoic and red for Neoproterozoic ones. For the abbreviations on tables from item 3, please refer to section 3.5.2.

Item 1. Germinosphaera specimen extracted from bibliography and samples GSC24380, GSC24380d and GSC24380e

Table B1.1 Specimen data for *Germinosphaera bispinosa*.

<i>Germinosphaera</i> species	Specimen number	Specimen name	Average Age (Ma)	Stratigraphic Unit	Locality	References
<i>bispinosa</i>	1	Fig. 6 No. 882/2	750	Dashkin Formation, Upper Riphean	Yakutia, East Siberian Platform, Krasnoyarsk region, River Uderei, Dashkin Suite	Mikhailova, 1986
	2	Fig. 16(D) HUPC 62794; 86-G-62-28 (O-19-2)	725	Svanbergfjellet Formation	Spitsbergen	Butterfield et al., 1994; Tang et al., 2013; Tang et al., 2015
	3	Fig. 16(E) HUPC 62795; 86-G-62-14 (J-41-2)				
	4	Table, Fig. 6 (Mikhailova, 1986a) XLVII, Fig. 2	705.9	Dashkin Formation, Upper Riphean, Dashkinskaya suite	Yenisei Ridge, Siberia	Jankauskas et al., 1989

5	P1.11.3; DMH-A, EFR R 52/2	552	Sirbu Shale, Upper Bhandar Group, Upper Vindhyan	Son Valley, Madhya Pradesh, India	Prasad et al., 2005
6	Fig. 6(A) 65066/W-44-1	1061	Meso–Neoproterozoic Mbuji-Mayi Supergroup	Democratic Republic of Congo	Baludikay et al., 2016
7	Fig. 6(C) 65066/Z-57-1				
8	Fig. 5(d) PB22503, chl-cq 0502, W/29/3-4	1650	Chuanlinggou Formation, Changzhoucun-Qingshanling section	North China	Miao et al., 2019; Agić, 2021
9	Fig. 5(e) PB22504, chl-cq 0514, Y/33/1-2				
10	Fig. 5(f) PB22505, chl-cq 0506, K/24/4				
11	Fig. 5(d) PB23591, xm-tl2-04120, U/40/1	1375	Mesoproterozoic Xiamaling Formation		Miao et al., 2021
12	Fig. 5(e) PB23592, xm-tl2-04112, R/24				
13	Fig. 10(C) TM10-(54+4.5)-93; LY-Y20	1065	Tonian Tongjiazhuang Formation, Tumen Group	Western Shandong, North China	Li et al., 2019; Han et al., 2021
14	Fig. 10(D) TM10-(54+4.5)-53; LY-Y20				
15	Fig. 10(E) TM21-20; LY-Y20				
16	Fig. 10(F) TM(1-8)-3Y28-3; LY-3Y28				
17	Fig. 10(G) TM(1-8)-4Y37-1; LY-4Y37				
18	Fig. 11(A) EF: W43/2	583.5	Neoproterozoic Sete Lagoas Formation, Bambuí Group	Brazil	Denezine, 2018
19	Fig. 11(B) EF: S26				
20	Fig. 11(C) EF: O28/3				
21	Fig. 3(G) ULVG 12509		Maricá outcrop, Camaqua Basin	Southern Brazil	Lehn et al., 2019
22	Fig. 3(I) ULVG 12506		Bom Jardim outcrop, Camaqua Basin		

	23	Fig. 3(J) ULVG 12515		Santa Bárbara outcrop, Camaqua Basin		
	24	P1.(3) Finder C38; P1.3 PMU-V14-4 (C38)	1022.5	Visingsö upper formation, Visingsö Group,	Sweden	Loron et al., 2016b
	25	Fig. 8 (E) 74639-F41,4; 15RAT-021A1	996	lower Shaler Supergroup	Northwestern Canada	Loron et al., 2019a; Loron et al., 2019b
	26	Fig. 8 (F) 74713-C50; 15RAT-021A1				
	27	Fig. 4 (4) 76801-h28,4	1430	Dismal Lakes Group	Arctic Canada	Loron et al., 2021
	28	Fig. 4 (5) DLFC-25				
	29	P6.1 Db1-15, 51.6/17.7	825	Meso-Neoproterozoic Deoban Limestone	Garhwal Lesser Himalaya, India	Srivastava and Kumar, 2003
	30	Fig. 13(13) 62N2-73 (2605,5) p.1, 14700-375	635	Upper Vycheгда Formation, Timan Ridge	Northeastern Margin of the East European Platform, Russian Federation	Vorob'eva et al., 2009
	31	Fig. 13(14) 62N2-7 (2605,5) p.6, 14700-37				
	32	Fig. 13(15) 62N2-57 (2605,5) p.1, 14700-267				
	33	Fig. 13(17) 62N2-66 (2605,5) p.4, 14700-320				

Table B1.2 Specimen data for *Germinosphaera* species *unispinosa* and *tadasii*.

<i>Germinosphaera</i> species	Specimen number	Specimen name	Average Age (Ma)	Stratigraphic Unit	Locality	References
<i>unispinosa</i>	34	Table, Fig. 5 (Mikhailova, 1986a) XLVII, Fig. 1	750	Dashkin Formation, Upper Riphean, Dashkinskaya suite	Yenisei Ridge, Siberia	Jankauskas et al., 1989
	35	P1. 10.3; DMH-A, EFR S 56/4	575	Nagod Limestone, Bhandar Group, Upper Vindhyan	Son Valley, Madhya Pradesh, India	Prasad et al., 2005
	36	P1.11.1; DMH-A, EFR N 43				
	37	P1.11.2; DMH-A, EFR Q 37/2				

	38	Fig. 5 No. 882/1	750	Dashkin Formation, Upper Riphean	Yakutia, East Siberian Platform, Krasnoyarsk region, River Uderei, Dashkin Suite	Mikhailova, 1986
	39	Fig. 5 (2) Slide 91-5-27-2-3, Z4/37	692	Neoproterozoic Dongjia Formation, Jiunodong Section	Lushan County, Henan Province, North China	Yin and Guan, 1999
	40	Fig. 5 (4) Slide 91-5-27-3-1, Q1/39				
	41	Fig. 5 (6) Slide 91-5-27-3-2, L1/37				
	42	Fig. 5 (9) Slide 91-5-27-2-4, M3/48				
	43	Fig. 26(K) 5341RS309-10, N44-1	775	Upper Torrenian, Alinya Formation, Officer Basin	South Australia	Zang, 1995
	44	Fig. 26(L) 5341RS309-8, F33				
	45	P1.(C) Finder C38; P1.3 PMU-V14-4 (C38)	1022.5	Visingsö upper formation, Visingsö Group	Sweden	Loron et al., 2016a; Loron et al., 2016b
	46	P1.(D) Finder X39				Loron et al., 2016a
	47	Fig. 5S FV26/A, coord. 0/120, micrograph 46/29	2000	Franceville Group	Gabon	Amard and Bertrand-Sarfati, 1997; Srivastava and Kumar, 2003
	48	Fig. 19(6) P-4353-13A, V54/4, HUHPC #62409	750	Draken Conglomerate Formation	Spitsbergen	Knoll et al., 1991
<i>tadasii</i>	49	GII AH CCCP No. 8032-2, tab. XLVII, Fig. 3	825	Omakhata Formation, Lower Riphean	Uchuro-Maiky District	Jankauskas et al., 1989
	50	GII AH CCCP No. 8032-2, tab. XLVII, Fig. 4				
	51	GII AH CCCP No. 8032-2, tab. XLVII, Fig. 5				
	52	Fig. 3; 4825-4820	815	Yshkemes Formation, Yshkemes-Vapol assemblage	Riphean–Lower Vendian deposits, Russia	Weiss, 1984; Veis et al., 2006
	53	Fig. 3; 2907-2900	577.5	Vychevda Formation		

Table B1.3 Specimen data for *Germinosphaera* species *alveolata*, *jankauskasii*, and *guttaformis*.

<i>Germinosphaera</i> species	Specimen number	Specimen name	Average Age (Ma)	Stratigraphic Unit	Locality	References
<i>alveolata</i>	54	Fig. 5(g) PB22506, chl-cq 0501, Q/36	1650	Lowermost Chuanlinggou Formation, Changcheng Group	North China	Miao et al., 2019
	55	Fig. 5(h) PB22507, chl-cq 0504, Z/41				
	56	Fig. 5(i) PB22508, chl-cq 0506, Q/32				
	57	Fig. 5(j) PB22509, chl-cq 0602, W/28				
	58	Fig. 5(k) PB22510, chl-cq 0517, N/39				
	59	Fig. 7 (4) 76091- n29,3	1430	Dismal Lakes Group	Arctic Canada	Loron et al., 2021
	60	Fig. 7 (5) 76522- r59				
	61	Fig. 7 (6) 76804- n37				
	62	Fig. 7 (7) 76092- h45				
63	Fig. 7 (8) DLFC- 25					
<i>jankauskasi</i>	64	Fig. 16(A) HUPC 627 1 5; 86-G- 62-12M (L-31-3)	725	Svanbergfjellet Formation	Spitsbergen	Butterfield et al., 1994
	65	Fig. 16(B) HUPC 62792; 86-G-62- 30M (J-33-1)				
	66	Fig. 16(C) HUPC 62793; 86-G-62- 155M (N-35-I)				
<i>guttaformis</i>	67	Ax.12	1741	Lower Changcheng System	Kuancheng, Hebei, North China	Yan, 1995
	68	IGGD AH CCCP No. 1360/3, tab. XLVII, Fig. 6	1500	Chernorechen Formation, Upper Riphean	Irarsky District, Sukharikha River, iberia	Jankauskas et al., 1989
	69	IGGD AH CCCP No. 1360/3, tab. XLVII, Fig. 7				
	70	IGGD AH CCCP No. 1360/3, tab. XLVII, Fig. 8				

Table B1.4 Specimen data for *Germinosphaera fibrilla* and unidentified species.

<i>Germinosphaera</i> species	Specimen number	Specimen name	Average Age (Ma)	Stratigraphic Unit	Locality	References
<i>fibrilla</i>	71	Fig. 17(A) HUPC 62799; 86-G-62-97M (L-38-3)	725	Svanbergfjellet Formation	Spitsbergen	Butterfield et al., 1994; Butterfield, 2015
	72	Fig. 17(B) HUPC 62800; 86-G-62-24M (H-31-2)				
	73	Fig. 17(C) HUPC 62801; 86-G-62-27M (O-38-4)				
	74	Fig. 17(D) HUPC 62802; 86-G-62-23M (O-30-3)				
	75	Fig. 17(E) HUPC 62803; 86-G-62-25M (N-28-3)				
	76	Fig. 17(F) HUPC 62804; 86-G-62-100M (O-29-3)				
	77	Fig. 17(G) HUPC 62805; 86-G-62-28M (O-30-0)				
	78	Fig. 17(H) HUPC 62806; 86-G-62-33M (K-36-3)				
<i>Brocholaminaria Germinosphaera</i> sp.	79	Fig. S3 Additional Data Repository	940	Late Tonian Volcanic Sedimentary rock from the Shenshan Mélange	Jiangshan-Shaoxing-Pingxiang Fault, South China	Wang et al., 2021
<i>Germinosphaera</i>	80	Fig. 3 (E) Member 2	850	Wynniatt Formation	Victoria Island, northwestern Canada	Butterfield and Rrainbird, 1998; Tang et al., 2013; Tang et al., 2015
<i>Germinosphaera</i> -like outgrowth	81	Fig. 2(D)X.41243 (VI21-4m-U59)	850	Wynniatt Formation	Victoria Island, northwestern Canada	Butterfield, 2005a; Butterfield, 2005b
<i>Germinosphaera</i> sp. indet.	82	Fig. 3.3(g)	590	ABC Range Quartzite	SCYW la bore, South Australia	Grey, 2005; Beraldi-Campesi and Retallack 2016; Retallack et al. 2014; Retallack et al., 2015
<i>Germinosphaera</i> unnamed specie	83	Fig. 15(d) CAI-2e	751	Cailleach Head Formation, Cailleach Head, Torridon Group	Scotland, UK	Brasier et al., 2017; Battison and Brasier 2012
<i>Germinosphaera</i> unnamed specie	84	Fig. 15(e) CAI-2e				
<i>Germinosphaera</i> unnamed specie	85	Fig. 15(f) DIA-13mac	994	Diabaig Formation, Lower Diabaig, Torridon Group		

<i>Germonosphaera</i> sp.	86	Fig. 3 Dhahir-1, 1319 m	580	Mid-Ediacaran Naufun Group, Huqf Supergroup	Oman	Butterfield and Grotzinger, 2012; Allen, 2007
<i>Germonosphaera</i> sp.	87	Fig. 3 Dhahir-1, 1319 m				
<i>Germonosphaera</i> sp.	88	Fig. 3 Dhahir-1, 1319 m				
<i>Germinosphaera</i> spp.	89	Fig. 3 A1 Afeef-1, 4032 m		Late-Ediacaran/early Cambrian Ara Group, Huqf Supergroup		
<i>Germinosphaera</i> sp.	90	Fig. 10(A) TM20-04; LY-Y20	1065	Tonian Tongjiazhuang Formation, Tumen Group	western Shandong, North China	Li et al., 2019; Han et al., 2021
<i>Germinosphaera</i> -like	91	Fig. 2(r)	1096	Nonesuch Formation, Oronto Group	Keweenaw Peninsula of the Upper Peninsula, Michigan, USA	Strother and Wellman, 2020
<i>Germinosphaera</i> -like	92	Fig.3 (d)				
<i>Germinosphaera</i> -like	93	Fig. 3(e)				
<i>Germinosphaera</i>	94	Fig.3 (f)				
<i>Germinosphaera</i> -like	95	Fig. 3(g)				
<i>Germinosphaera</i> -like	96	Fig.3 (i)				

Table B1.1 Specimen data for *Germinosphaera gunflinta*.

<i>Germinosphaera</i> species	Specimen number	Specimen name	Average Age (Ma)	Stratigraphic Unit	Locality	References
<i>gunflinta</i>	97	GSC24380 (2)-061	1900	Gunflint Chert Unit, lower Gunflint Formation	Schreiber Beach, Ontario, Canada	González-Flores et al., 2022
	98	GSC24380 (2)-109				
	99	GSC24380 (2)-187				
	100	GSC24380d-004				
	101	GSC24380d-017				
	102	GSC24380d-019				
	103	GSC24380d-031				
	104	GSC24380d-093				
	105	GSC24380d-120				
	106	GSC24380d-156				
	107	GSC24380d-157				
	108	GSC24380d-179				
	109	GSC24380d-202				
	110	GSC24380d-215				
111	GSC24380d-222					

112	GSC24380d-226			
113	GSC24380d-227			
114	GSC24380d-230			
115	GSC24380d-231			
116	GSC24380d-233			
117	GSC24380d-239			
118	GSC24380d-241			
119	GSC24380d-247			
120	GSC24380d-258			
121	GSC24380d-266			
122	GSC24380d-270			
123	GSC24380d-274			
124	GSC24380d-281			
125	GSC24380d-283			
126	GSC24380d-296			
127	GSC24380d-345			
128	GSC24380d-380			
129	GSC24380d-500			
130	GSC24380d-574			
131	GSC24380e-001			
132	GSC24380e-009			
133	GSC24380e-013			
134	GSC24380e-032			
135	GSC24380e-039			
136	GSC24380e-080			
137	GSC24380e-088			
138	GSC24380e-091			
139	GSC24380e-108			
140	GSC24380e-132			
141	GSC24380e-280			
142	GSC24380e-308			
143	GSC24380e-310			
144	GSC24380e-546			
145	GSC24380e-555a			
146	GSC24380e-555b			

Item 2. Dataset for Figure 3.8, Age vs Size plot

Table B2.1 Maximum, minimum, average diameter and average age for specimens of *Germinosphaera bispinosa*.

<i>Germinosphaera</i> species	Specimen number	Specimen name	Average Age (Ma)	Average D (µm)	Max D (µm)	Min D (µm)
<i>bispinosa</i>	1	Fig. 6 No. 882/2	750	22.5	25	20
	2	Fig. 16(D) HUPC 62794; 86-G-62-28 (O-19-2)	725	25	27	23
	3	Fig. 16(E) HUPC 62795; 86-G-62-14 (J- 41-2)		26.5	32	21
	4	Table, Fig. 6 (Mikhailova, 1986a) XLVII, Fig. 2	705.9	22.5	25	20
	5	P1.11.3; DMH- A, EFR R 52/2	552	36.58	41.58	31.58
	6	Fig. 6(A) 65066/W-44-1	1061	246	264	228
	7	Fig. 6(C) 65066/Z-57-1		128.335	131.67	125
	8	Fig. 5(d) PB22503, chl- cq 0502, W/29/3-4	1650	36.095	41.46	30.73
	9	Fig. 5(e) PB22504, chl- cq 0514, Y/33/1-2		29.02	34.63	23.41
	10	Fig. 5(f) PB22505, chl- cq 0506, K/24/4		31.95	34.63	29.27
	11	Fig. 5(d) PB23591, xm- tl2-04120, U/40/1	1375	18.655	19.33	17.98

	12	Fig. 5(e) PB23592, xm- tl2-04112, R/24		34.385	35.06	33.71
	13	Fig. 10(C) TM10- (54+4.5)-93; LY-Y20	1065	51.925	52.31	51.54
	14	Fig. 10(D) TM10- (54+4.5)-53; LY-Y20		115	133.33	96.67
	15	Fig. 10(E) TM21-20; LY- Y20		129	148	110
	16	Fig. 10(F) TM(1-8)-3Y28- 3; LY-3Y28		177.965	179.66	176.27
	17	Fig. 10(G) TM(1-8)-4Y37- 1; LY-4Y37		115.385	124.1	106.67
	18	Fig. 11(A) EF: W43/2		583.5	23.12	25.27
	19	Fig. 11(B) EF: S26	33.655		36.06	31.25
	20	Fig. 11(C) EF: O28/3	38.045		40.58	35.51
	21	Fig. 3(G) ULVG 12509	36.38		39.66	33.1
	22	Fig. 3(I) ULVG 12506	53		63.6	42.4
	23	Fig. 3(J) ULVG 12515	25.5		29	22
	24	P1.(3) Finder C38; P1.3 PMU-V14-4 (C38)	1022.5	37.605	38.6	36.61
	25	Fig. 8 (E) 74639-F41,4; 15RAT-021A1	996	65.78	73.04	58.52
	26	Fig. 8 (F) 74713-C50; 15RAT-021A1		43.635	50	37.27
	27	Fig. 4 (4) 76801-h28,4	1430	29.31	35.52	23.1
	28	Fig. 4 (5) DLFC-25		32.93	37.93	27.93

	29	P6.1 Db1-15, 51.6/17.7	825	16.94	20.65	13.23
	30	Fig. 13(13) 62N2-73 (2605,5) p.1, 14700-375	635	197.5	230	165
	31	Fig. 13(14) 62N2-7 (2605,5) p.6, 14700-37		252.08	333.33	170.83
	32	Fig. 13(15) 62N2-57 (2605,5) p.1, 14700-267		194.045	207.14	180.95
	33	Fig. 13(17) 62N2-66 (2605,5) p.4, 14700-320		154.165	177.08	131.25

Table B2.2 Maximum, minimum, average diameter and average age for specimens of *Germinosphaera unispinosa* and *tadasii*.

<i>Germinosphaera</i> species	Specimen number	Specimen name	Average Age (Ma)	Average D (µm)	Max D (µm)	Min D (µm)
<i>unispinosa</i>	34	Table, Fig. 5 (Mikhailova, 1986a) XLVII, Fig. 1	750	19	17.5	14.58
	35	P1. 10.3; DMH-A, EFR S 56/4	575	34.7	39.4	30
	36	P1.11.1; DMH-A, EFR N 43		29.75	30.5	29
	37	P1.11.2; DMH-A, EFR Q 37/2		30.18	32.9	27.46
	38	Fig. 5 No. 882/1	750	19	17.5	14.58
	39	Fig. 5 (2) Slide 91-5-27-2-3, Z4/37	692	25.2	26.4	24
	40	Fig. 5 (4) Slide 91-5-27-3-1, Q1/39		28.4	29.6	27.2

	41	Fig. 5 (6) Slide 91-5-27-3-2, L1/37		30	32.8	27.2
	42	Fig. 5 (9) Slide 91-5-27-2-4, M3/48		26	28.8	23.2
	43	Fig. 26(K) 5341RS309-10, N44-1	775	35.48	38.06	32.9
	44	Fig. 26(L) 5341RS309-8, F33		44.03	51.61	36.45
	45	P1.(C) Finder C38; P1.3 PMU-V14-4 (C38)	1022.5	37.605	38.6	36.61
	46	P1.(D) Finder X39		35.895	36.92	34.87
	47	Fig. 5S FV26/A, coord. 0/120, micrograph 46/29	2000	6.875	7.5	6.25
	48	Fig. 19(6) P-4353-13A, V54/4, HUHPC #62409	750	33.22	35.25	31.19
<i>tadasii</i>	49	GII AH CCCP No. 8032-2, tab. XLVII, Fig. 3	825	69.375	73.75	65
	50	GII AH CCCP No. 8032-2, tab. XLVII, Fig. 4		60	61.67	58.33
	51	GII AH CCCP No. 8032-2, tab. XLVII, Fig. 5		73.75	75	72.5
	52	Fig. 3; 4825-4820	815	65	130	130
	53	Fig. 3; 2907-2900	577.5	90	100	80

Table B2.3 Maximum, minimum, average diameter and average age for specimens of *Germinosphaera alveolata*, *jankauskasiai*, and *guttaformis*.

<i>Germinosphaera</i> species	Specimen number	Specimen name	Average Age (Ma)	Average D (µm)	Max D (µm)	Min D (µm)
<i>alveolata</i>	54	Fig. 5(g) PB22506, chl-cq 0501, Q/36	1650	43.05	45.61	40.49
	55	Fig. 5(h) PB22507, chl-cq 0504, Z/41		33.535	38.78	28.29
	56	Fig. 5(i) PB22508, chl-cq 0506, Q/32		48.295	49.76	46.83
	57	Fig. 5(j) PB22509, chl-cq 0602, W/28		45.49	48.05	42.93
	58	Fig. 5(k) PB22510, chl-cq 0517, N/39		43.245	49.9	36.59
	59	Fig. 7 (4) 76091-n29,3	1430	53.275	60	46.55
	60	Fig. 7 (5) 76522-r59		47.07	50.69	43.45
	61	Fig. 7 (6) 76804-n37		43.45	49.66	37.24
	62	Fig. 7 (7) 76092-h45		35.175	38.28	32.07
	63	Fig. 7 (8) DLFC-25		22.41	22.93	21.89
<i>jankauskasiai</i>	64	Fig. 16(A) HUPC 627 1 5; 86-G-62-12M (L-31-3)	725	74.4	79.2	69.6
	65	Fig. 16(B) HUPC 62792; 86-G-62-30M (J-33-1)		44.1	47.4	40.8
	66	Fig. 16(C) HUPC 62793; 86-G-62-155M (N-35-l)		59.7	65.4	54
<i>guttaformis</i>	67	Ax.12	1741	61.5	80	43

	68	IGGD AH CCCP No. 1360/3, tab. XLVII, Fig. 6	1500	25.785	31.57	20
	69	IGGD AH CCCP No. 1360/3, tab. XLVII, Fig. 7		28.925	43.57	14.28
	70	IGGD AH CCCP No. 1360/3, tab. XLVII, Fig. 8		41.36	45.45	37.27

Table B2.4 Maximum, minimum, average diameter and average age for specimens of *Germinosphaera fibrilla* and unidentified species.

<i>Germinosphaera</i> species	Specimen number	Specimen name	Average Age (Ma)	Average D (µm)	Max D (µm)	Min D (µm)
<i>fibrilla</i>	71	Fig. 17(A) HUPC 62799; 86-G-62-97M (L-38-3)	725	70.755	94.34	47.17
	72	Fig. 17(B) HUPC 62800; 86-G-62-24M (H-31-2)		62.015	71.15	52.88
	73	Fig. 17(C) HUPC 6280 1 ; 86-G-62-27M (O-38-4)		74.015	75	73.03
	74	Fig. 17(D) HUPC 62802; 86-G-62 -23M O-30-3)		98.075	113.46	82.69
	75	Fig. 17(E) HUPC 62803; 86-G-62-25M (N-28-3)		93.75	113.46	74.04
	76	Fig. 17(F) HUPC 62804; 86-G-62 - 100M (O-29-3)		114.42	132.69	96.15

	77	Fig. 17(G) HUPC 62805; 86-G-62-28M (0-30-0)		135.575	151.92	119.23
	78	Fig. 17(H) HUPC 62806; 86-G-62-33M (K-36-3)		133.655	150	117.31
<i>Brocholaminaria</i> <i>Germinosphaera</i> sp.	79	Fig. S3 Additional Data Repository	940	47.5	60	35
<i>Germinosphaera</i>	80	Fig. 3 (E) Member 2	850	121.11	143.12	99.1
<i>Germinosphaera</i> - like outgrowth	81	Fig. 2(D)X.41243 (VI21-4m- U59)	850	252.295	259.94	244.65
<i>Germinosphaera</i> sp. indet.	82	Fig. 3.3(g)	590	43.945	45.26	42.63
<i>Germinosphaera</i> unnamed specie	83	Fig. 15(d) CAI- 2e	751	47.725	48.18	47.27
<i>Germinosphaera</i> unnamed specie	84	Fig. 15(e) CAI- 2e		17.645	18.82	16.47
<i>Germinosphaera</i> unnamed specie	85	Fig. 15(f) DIA- 13mac	994	33.89	42.22	25.56
<i>Germonosphaera</i> sp.	86	Fig. 3 Dhahir- 1, 1319 m	580	70.37	75.93	64.81
<i>Germonosphaera</i> sp.	87	Fig. 3 Dhahir- 1, 1319 m		109.26	111.11	107.41
<i>Germonosphaera</i> sp.	88	Fig. 3 Dhahir- 1, 1319 m		73.16	74.1	72.22
<i>Germinosphaera</i> spp.	89	Fig. 3 A1 Afeef-1, 4032 m		94.445	98.15	90.74
<i>Germinosphaera</i> sp.	90	Fig. 10(A) TM20-04; LY- Y20	1065	111	126	96
<i>Germinosphaera</i> - like	91	Fig. 2(r)	1096	71.58	111.58	31.58
<i>Germinosphaera</i> - like	92	Fig.3 (d)		45	47.78	42.22
<i>Germinosphaera</i> - like	93	Fig. 3(e)		23.33	24.44	22.22
<i>Germinosphaera</i>	94	Fig.3 (f)		31.315	36.84	25.79

<i>Germinosphaera</i> -like	95	Fig. 3(g)		52.775	74.44	31.11
<i>Germinosphaera</i> -like	96	Fig.3 (i)		39.23	43.08	35.38

Table B2.5 Maximum, minimum, average diameter and average age for specimens of *Germinosphaera gunflinta*.

<i>Germinosphaera</i> species	Specimen number	Specimen name	Average Age (Ma)	Average D (µm)	Max D (µm)	Min D (µm)
<i>gunflinta</i>	97	GSC24380 (2)-061	1900	6.29	7.44	5.13
	98	GSC24380 (2)-109		17.05	18.72	15.38
	99	GSC24380 (2)-187		12.31	12.56	12.05
	100	GSC24380d-004		9.36	10.26	8.46
	101	GSC24380d-017		13.08	13.59	12.56
	102	GSC24380d-019		17.31	18.72	15.89
	103	GSC24380d-031		11.03	11.54	10.51
	104	GSC24380d-093		21.80	26.15	17.44
	105	GSC24380d-120		13.47	14.62	12.31
	106	GSC24380d-156		11.28	12.82	9.74
	107	GSC24380d-157		13.08	13.85	12.31
	108	GSC24380d-179		11.80	12.82	10.77
	109	GSC24380d-202		12.69	14.1	11.28
	110	GSC24380d-215		15.02	15.03	15.02
111	GSC24380d-222	15.22	16.03	14.41		
112	GSC24380d-226	14.94	15.43	14.45		

	113	GSC24380d-227		15.33	16.13	14.53
	114	GSC24380d-230		14.79	15.27	14.30
	115	GSC24380d-231		15.48	16.27	14.69
	116	GSC24380d-233		14.81	15.48	14.14
	117	GSC24380d-239		15.08	15.96	14.20
	118	GSC24380d-241		14.55	14.70	14.40
	119	GSC24380d-247		14.55	15.09	14.00
	120	GSC24380d-258		14.85	15.04	14.65
	121	GSC24380d-266		14.41	15.23	13.58
	122	GSC24380d-270		15.27	15.75	14.80
	123	GSC24380d-274		14.57	14.79	14.35
	124	GSC24380d-281		15.21	15.35	15.08
	125	GSC24380d-283		15.37	16.19	14.55
	126	GSC24380d-296		15.00	16.67	13.33
	127	GSC24380d-345		13.33	14.35	12.31
	128	GSC24380d-380		10.77	11.79	9.74
	129	GSC24380d-500		10.64	11.28	10
	130	GSC24380d-574		10.39	11.28	9.49
	131	GSC24380e-001		12.31	13.59	11.03
	132	GSC24380e-009		6.93	7.18	6.67
	133	GSC24380e-013		9.74	10.51	8.97
	134	GSC24380e-032		8.08	10.77	5.38

	135	GSC24380e-039		5.64	6.41	4.87
	136	GSC24380e-080		6.03	6.41	5.64
	137	GSC24380e-088		6.41	7.69	5.13
	138	GSC24380e-091		6.16	6.41	5.9
	139	GSC24380e-108		8.33	8.97	7.69
	140	GSC24380e-132		8.46	8.97	7.95
	141	GSC24380e-280		14.75	17.44	12.05
	142	GSC24380e-308		10.00	10.77	9.23
	143	GSC24380e-310		18.08	20.51	15.64
	144	GSC24380e-546		7.95	7.95	7.95
	145	GSC24380e-555a		10.13	11.53	8.72
	146	GSC24380e-555b		8.47	8.72	8.21

Item 3. Dataset for Figure 3.9 Multivariate plot

Table B3.1 Multivariate values of specific measurements for specimens of *Germinosphaera bispinosa*.

G. sp.	S. #	MaxD (µm)	MinD (µm)	PL1 (µm)	PBD1 (µm)	PDED1 (µm)	PL2 (µm)	PBD2 (µm)	PDED2 (µm)	PL3 (µm)	PBD3 (µm)	PDED3 (µm)	PL4 (µm)	PBD4 (µm)	PDED4 (µm)
<i>bispinosa</i>	1	25	20	80	3	1.5	8	2.5	1.5	0	0	0	0	0	0
	2	27	23	121.5	5.8	5	0	0	0	0	0	0	0	0	0
	3	32	21	133	8	6.5	0	0	0	0	0	0	0	0	0
	4	25	20	80	3	1.5	8	2.5	1.5	0	0	0	0	0	0
	5	41.58	31.58	16.32	3.68	2.11	13.68	3.68	2.63	0	0	0	0	0	0
	6	264	228	158	72	10.8	0	0	0	0	0	0	0	0	0
	7	131.7	125	44.17	36.67	16.67	0	0	0	0	0	0	0	0	0
	8	41.46	30.73	4.87	6.83	5.12	0	0	0	0	0	0	0	0	0
	9	34.63	23.41	13.17	9.76	1.46	0	0	0	0	0	0	0	0	0
	10	34.63	29.27	8.29	7.32	2.44	0	0	0	0	0	0	0	0	0
	11	19.33	17.98	5.39	5.4	2.7	0	0	0	0	0	0	0	0	0
	12	35.06	33.71	8.1	9.44	3.15	0	0	0	0	0	0	0	0	0
	13	52.31	51.54	56.15	22.31	23.85	0	0	0	0	0	0	0	0	0
	14	133.3	96.67	111.7	48	18.33	0	0	0	0	0	0	0	0	0
	15	148	110	128	46	26	0	0	0	0	0	0	0	0	0
	16	179.7	176.3	22.03	77.97	55.93	0	0	0	0	0	0	0	0	0
	17	124.1	106.7	11.28	21.54	18.46	0	0	0	0	0	0	0	0	0
	18	25.27	20.97	68.82	9.14	1.61	22.04	15.59	5.38	12.9	4.84	2.42	0	0	0
	19	36.06	31.25	50	10.1	0.48	29.81	5.77	3.85	0	0	0	0	0	0
	20	40.58	35.51	112.3	6.52	0.72	0	0	0	0	0	0	0	0	0
	21	39.66	33.1	43.45	18.62	7.59	0	0	0	0	0	0	0	0	0
	22	63.6	42.4	20	12	2.4	0	0	0	0	0	0	0	0	0
	23	29	22	5.33	9.7	9.3	0	0	0	0	0	0	0	0	0
	24	38.6	36.61	32.2	8.81	2.03	0	0	0	0	0	0	0	0	0
	25	73.04	58.52	56.52	6.09	3.48	0	0	0	0	0	0	0	0	0
	26	50	37.27	40.91	4.64	1.82	0	0	0	0	0	0	0	0	0
	27	35.52	23.1	6.21	3.45	3.79	0	0	0	0	0	0	0	0	0
	28	37.93	27.93	10.34	11.38	6.21	7.24	9.31	5.52	0	0	0	0	0	0
	29	20.65	13.23	26.45	7.74	4.19	0	0	0	0	0	0	0	0	0
	30	230	165	100	37.5	25	0	0	0	0	0	0	0	0	0
	31	333.3	170.8	58.33	37.5	25	0	0	0	0	0	0	0	0	0
	32	207.1	181	83.33	23.81	9.52	23.81	33.33	26.19	0	0	0	0	0	0
	33	177.1	131.3	52.08	50	20.83	43.75	27.08	20.83	0	0	0	0	0	0

Table B3.2 Multivariate values of specific measurements for specimens of *Germinosphaera unispinosa* and *tadasii*.

G. sp.	S. #	MaxD (µm)	MinD (µm)	PL1 (µm)	PBD1 (µm)	PDED1 (µm)	PL2 (µm)	PBD2 (µm)	PDED2 (µm)	PL3 (µm)	PBD3 (µm)	PDED3 (µm)	PL4 (µm)	PBD4 (µm)	PDED4 (µm)
<i>unispinosa</i>	34	17.5	14.58	19.25	3.5	1.17	0	0	0	0	0	0	0	0	0
	35	39.4	30	35.53	7.65	4.41	0	0	0	0	0	0	0	0	0
	36	30.5	29	0	0	0	0	0	0	0	0	0	0	0	0
	37	32.9	27.46	30.05	6.22	1.04	0	0	0	0	0	0	0	0	0
	38	17.5	14.58	19.25	3.5	1.17	0	0	0	0	0	0	0	0	0
	39	26.4	24	14.4	4.8	2.4	0	0	0	0	0	0	0	0	0
	40	29.6	27.2	11.2	2.4	1.6	0	0	0	0	0	0	0	0	0
	41	32.8	27.2	5.6	3.2	3.2	0	0	0	0	0	0	0	0	0
	42	28.8	23.2	12.8	3.2	2.4	0	0	0	0	0	0	0	0	0
	43	38.06	32.9	19.35	9.68	0.65	0	0	0	0	0	0	0	0	0
	44	51.61	36.45	16.77	6.45	6.45	0	0	0	0	0	0	0	0	0
	45	38.6	36.61	32.2	8.81	2.03	0	0	0	0	0	0	0	0	0
	46	36.92	34.87	60.08	4.1	1.54	0	0	0	0	0	0	0	0	0
	47	7.5	6.25	18.93	1.79	1.42	0	0	0	0	0	0	0	0	0
48	35.25	31.19	77.29	8.14	6.1	0	0	0	0	0	0	0	0	0	
<i>tadasii</i>	49	73.75	65	13.75	12.5	10	0	0	0	0	0	0	0	0	0
	50	61.67	58.33	10	15	11.67	0	0	0	0	0	0	0	0	0
	51	75	72.5	21.25	12.5	13.75	0	0	0	0	0	0	0	0	0
	52	130	0	0	0	0	0	0	0	0	0	0	0	0	0
	53	100	80	0	0	0	0	0	0	0	0	0	0	0	0

Table B3.3 Multivariate values of specific measurements for specimens of *Germinosphaera alveolata*, *jankauskasi*, and *guttaformis*.

G. sp.	S. #	MaxD (µm)	MinD (µm)	PL1 (µm)	PBD1 (µm)	PDED1 (µm)	PL2 (µm)	PBD2 (µm)	PDED2 (µm)	PL3 (µm)	PBD3 (µm)	PDED3 (µm)	PL4 (µm)	PBD4 (µm)	PDED4 (µm)
<i>alveolata</i>	54	45.61	40.49	7.8	12.2	9.27	0	0	0	0	0	0	0	0	0
	55	38.78	28.29	2.93	9.66	9.02	0	0	0	0	0	0	0	0	0
	56	49.76	46.83	14.63	18.05	5.85	0	0	0	0	0	0	0	0	0
	57	48.05	42.93	12.2	13.17	6.83	0	0	0	0	0	0	0	0	0
	58	49.9	36.59	17.07	14.15	7.32	0	0	0	0	0	0	0	0	0
	59	60	46.55	11.38	14.48	13.45	0	0	0	0	0	0	0	0	0
	60	50.69	43.45	14.48	11.38	6.21	0	0	0	0	0	0	0	0	0
	61	49.66	37.24	13.45	8.28	8.28	0	0	0	0	0	0	0	0	0

	62	38.28	32.07	10.34	12.41	7.24	0	0	0	0	0	0	0	0	0
	63	22.93	21.89	5	8.1	2.76	0	0	0	0	0	0	0	0	0
<i>jankauskasi</i>	64	79.2	69.6	22.2	10.8	7.2	15.6	10.8	6	14.4	9.6	12	13.2	9.6	7.8
	65	47.4	40.8	28.8	6.6	6.72	19.8	7.2	7.8	20.4	6	12	15.6	8.4	8.4
	66	65.4	54	26.4	9	7.2	17.4	7.8	6	15.84	8.4	6	0	0	0
<i>guttaformis</i>	67	80	43	46.7	10	6.7	0	0	0	0	0	0	0	0	0
	68	31.57	20	13.68	8.42	5.26	0	0	0	0	0	0	0	0	0
	69	43.57	14.28	19.29	6.43	2.14	0	0	0	0	0	0	0	0	0
	70	45.45	37.27	10.91	13.63	5.45	0	0	0	0	0	0	0	0	0

Table B3.4 Multivariate values of specific measurements for specimens of *Germinosphaera fibrilla* and unidentified species.

G. sp.	S. #	MaxD (µm)	MinD (µm)	PL1 (µm)	PBD1 (µm)	PDED1 (µm)	PL2 (µm)	PBD2 (µm)	PDED2 (µm)	PL3 (µm)	PBD3 (µm)	PDED3 (µm)	PL4 (µm)	PBD4 (µm)	PDED4 (µm)
<i>fibrilla</i>	71	94.34	47.17	47.17	9.43	5.66	0	0	0	0	0	0	0	0	0
	72	71.15	52.88	96.15	13.46	5.76	76.92	5.76	5.76	0	0	0	0	0	0
	73	75	73.03	51.92	7.69	5.76	50	7.69	5.76	38.46	5.76	5.76	0	0	0
	74	113.5	82.69	73.07	18.26	7.69	0	0	0	0	0	0	0	0	0
	75	113.5	74.04	33.65	13.46	5.76	17.88	7.69	5.76	0	0	0	0	0	0
	76	132.7	96.15	50.96	9.61	3.83	38.46	9.61	3.83	0	0	0	0	0	0
	77	151.9	119.2	71.15	25	7.69	55.76	15.38	5.19	59.61	19.23	4.81	57.7	11.53	3.84
	78	150	117.3	69.23	9.61	7.69	30.77	8.65	5.38	63.46	15.38	5.76	63.5	11.54	3.85
No ID	79	60	35	12.5	0	0	0	0	0	0	0	0	0	0	0
	80	143.1	99.1	49.54	3.67	3.67	47.71	3.67	5.5	42.2	7.34	3.67	41.3	5.5	3.67
	81	259.9	244.7	152.9	113.2	97.86	0	0	0	0	0	0	0	0	0
	82	45.26	42.63	20	6.84	2.11	0	0	0	0	0	0	0	0	0

83	48.18	47.27	31.82	12.73	13.64	0	0	0	0	0	0	0	0	0
84	18.82	16.47	74.12	9.41	5.88	0	0	0	0	0	0	0	0	0
85	42.22	25.56	62.22	12.22	16.67	0	0	0	0	0	0	0	0	0
86	75.93	64.81	18.52	11.11	3.7	0	0	0	0	0	0	0	0	0
87	111.1	107.4	11.11	18.52	5.56	0	0	0	0	0	0	0	0	0
88	74.1	72.22	0	0	0	0	0	0	0	0	0	0	0	0
89	98.15	90.74	16.67	20.37	12.96	14.81	29.63	14.81	0	0	0	0	0	0
90	126	96	84	44	30	14	4	4	16	12	6	36	16	10
91	111.6	31.58	20	11.58	6.32	0	0	0	0	0	0	0	0	0
92	47.78	42.22	44.44	14.44	16.67	0	0	0	0	0	0	0	0	0
93	24.44	22.22	94.44	10	6.67	0	0	0	0	0	0	0	0	0
94	36.84	25.79	64.74	3.68	1.58	0	0	0	0	0	0	0	0	0
95	74.44	31.11	127.8	15.56	11.11	0	0	0	0	0	0	0	0	0

	96	43.08	35.38	169.2	4.62	7.69	0	0	0	0	0	0	0	0	0
--	----	-------	-------	-------	------	------	---	---	---	---	---	---	---	---	---

Table B3.5 Multivariate values of specific measurements for specimens of *Germinosphaera gunflinta*.

G. sp.	S. #	MaxD (µm)	MinD (µm)	PL1 (µm)	PBD1 (µm)	PDED1 (µm)	PL2 (µm)	PBD2 (µm)	PDED2 (µm)	PL3 (µm)	PBD3 (µm)	PDED3 (µm)	PL4 (µm)	PBD4 (µm)	PDED4 (µm)
<i>gunflinta</i>	97	7.44	5.13	12.1	2.05	2.05	0	0	0	0	0	0	0	0	0
	98	18.7	15.4	3.33	5.13	3.08	0	0	0	0	0	0	0	0	0
	99	12.6	12.1	4.87	5.38	4.62	0	0	0	0	0	0	0	0	0
	100	10.3	8.46	3.85	6.67	4.87	3.08	5.13	4.62	0	0	0	0	0	0
	101	13.6	12.6	5.38	5.89	1.28	4.1	7.18	4.1	2.56	3.85	2.05	0	0	0
	102	18.7	15.9	8.46	6.67	4.62	0	0	0	0	0	0	0	0	0
	103	11.5	10.5	7.69	4.36	4.359	0	0	0	0	0	0	0	0	0
	104	26.2	17.4	10.3	6.15	3.59	8.97	10.3	9.49	0	0	0	0	0	0
	105	14.6	12.3	8.21	4.62	2.82	3.59	4.1	2.56	0	0	0	0	0	0
	106	12.8	9.74	4.87	5.89	2.82	4.36	6.92	6.15	0	0	0	0	0	0
	107	13.9	12.3	7.44	6.92	2.82	6.92	8.72	6.41	0	0	0	0	0	0
	108	12.8	10.8	3.85	5.38	2.56	3.33	4.1	0.77	0	0	0	0	0	0
	109	14.1	11.3	5.12	5.89	2.82	4.87	5.12	4.36	0	0	0	0	0	0
	110	15	15	8.69	7.95	4.62	0	0	0	0	0	0	0	0	0
	111	16	14.4	8.27	6.92	3.59	0	0	0	0	0	0	0	0	0
	112	15.4	14.5	3.18	1.59	2.31	0	0	0	0	0	0	0	0	0
	113	16.1	14.5	6.49	2.82	2.82	0	0	0	0	0	0	0	0	0
	114	15.3	14.3	7.77	5.9	4.87	0	0	0	0	0	0	0	0	0
	115	16.3	14.7	7.44	3.59	3.85	0	0	0	0	0	0	0	0	0
	116	15.5	14.1	4.31	1.54	1.28	0	0	0	0	0	0	0	0	0
	117	16	14.2	7.58	4.36	5.64	2.01	2.05	1.79	0	0	0	0	0	0
	118	14.7	14.4	6.4	1.54	1.79	3.85	1.77	2.56	0	0	0	0	0	0
	119	15.1	14	7.23	3.85	1.79	3.13	1.54	1.28	0	0	0	0	0	0
	120	15	14.7	6.13	3.33	1.54	1.12	1.03	0.77	4.01	1.28	2.05	0	0	0
	121	15.2	13.6	7.65	2.05	3.33	0	0	0	0	0	0	0	0	0
	122	15.8	14.8	7.78	3.08	2.56	0	0	0	0	0	0	0	0	0
	123	14.8	14.4	7.91	3.85	1.03	0	0	0	0	0	0	0	0	0
	124	15.4	15.1	3.66	0.77	1.03	0	0	0	0	0	0	0	0	0
125	16.2	14.6	8.37	5.13	4.87	0	0	0	0	0	0	0	0	0	
126	16.7	13.3	15.6	10.8	6.92	3.33	6.41	1.03	2.82	4.1	3.85	0	0	0	
127	14.4	12.3	11.8	7.95	8.97	7.69	7.18	5.13	0	0	0	0	0	0	
128	11.8	9.74	5.13	4.87	0.77	0	0	0	0	0	0	0	0	0	

129	11.3	10	3.59	1.28	1.54	0	0	0	0	0	0	0	0	0
130	11.3	9.49	7.18	3.59	0.78	0	0	0	0	0	0	0	0	0
131	13.6	11	4.62	3.33	1.28	0	0	0	0	0	0	0	0	0
132	7.18	6.67	4.1	2.82	1.79	0	0	0	0	0	0	0	0	0
133	10.5	8.97	4.36	4.62	1.54	1.54	2.56	1.28	0	0	0	0	0	0
134	10.8	5.38	6.92	3.08	1.28	0	0	0	0	0	0	0	0	0
135	6.41	4.87	4.62	2.31	1.28	0	0	0	0	0	0	0	0	0
136	6.41	5.64	3.08	2.82	1.54	0	0	0	0	0	0	0	0	0
137	7.69	5.13	8.97	2.05	5.13	0	0	0	0	0	0	0	0	0
138	6.41	5.9	3.85	2.05	2.31	1.28	1.54	1.79	0	0	0	0	0	0
139	8.97	7.69	2.56	2.56	1.54	1.28	1.54	1.28	0	0	0	0	0	0
140	8.97	7.95	4.62	2.56	1.03	0	0	0	0	0	0	0	0	0
141	17.4	12.1	8.46	3.85	1.03	0	0	0	0	0	0	0	0	0
142	10.8	9.23	2.31	3.08	3.85	0	0	0	0	0	0	0	0	0
143	20.5	15.6	10.3	5.9	5.64	0	0	0	0	0	0	0	0	0
144	7.95	7.95	2.05	2.05	1.79	0	0	0	0	0	0	0	0	0
145	11.5	8.72	3.59	3.33	1.79	0	0	0	0	0	0	0	0	0
146	8.72	8.21	2.56	2.56	1.03	2.31	0.77	0.77	2.31	4.1	2.05	1.79	4.1	2.31

C. Scanning Electron Microscopy (SEM) maps from sample GSC24380d

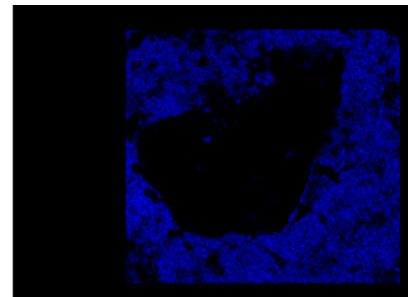
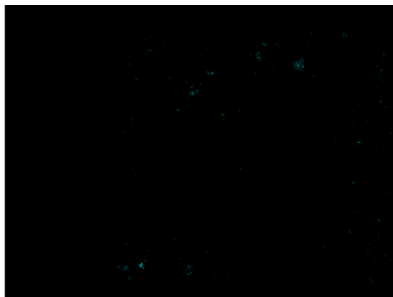
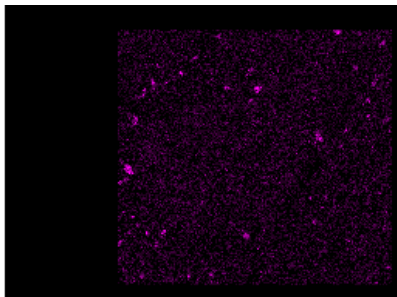
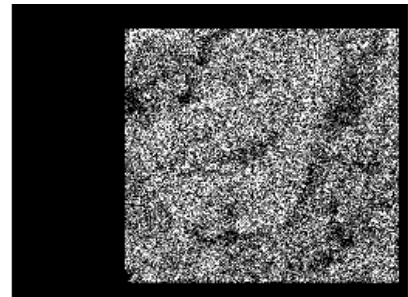
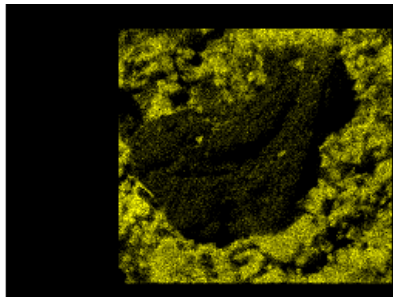
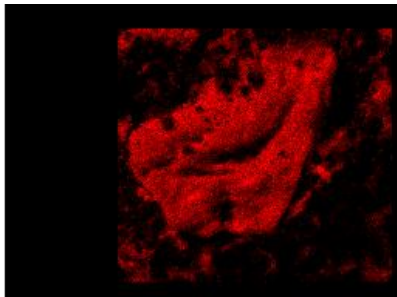
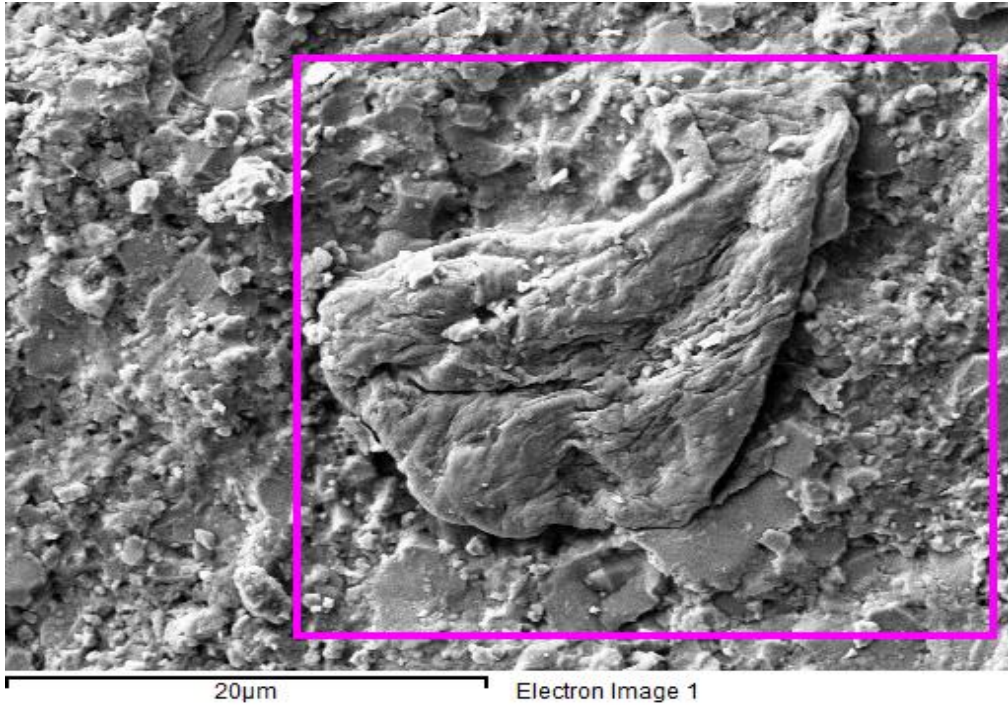
This appendix contains *Germinosphaera gunflinta* n. sp. SEM images along with their corresponding element maps of multiple cells of different locations in sample GSC 24380d, a small chert block, Gunflint Formation, Schreiber Beach, northwestern Ontario.

All free cells were treated priorly with an HF-etching and are encrusted by chert matrix.

For a detailed analysis of the maps refer to section 3. 4.

Item 1. GSC24380d element maps

Sample GSC24380d_Location 1



Spectrum processing :

Peaks possibly omitted : 3.300, 3.484 keV

Processing option : All elements analyzed (Normalised)

Number of iterations = 5

Standard :

C CaCO₃ 1-Jun-1999 12:00 AM

O SiO₂ 1-Jun-1999 12:00 AM

Na Albite 1-Jun-1999 12:00 AM

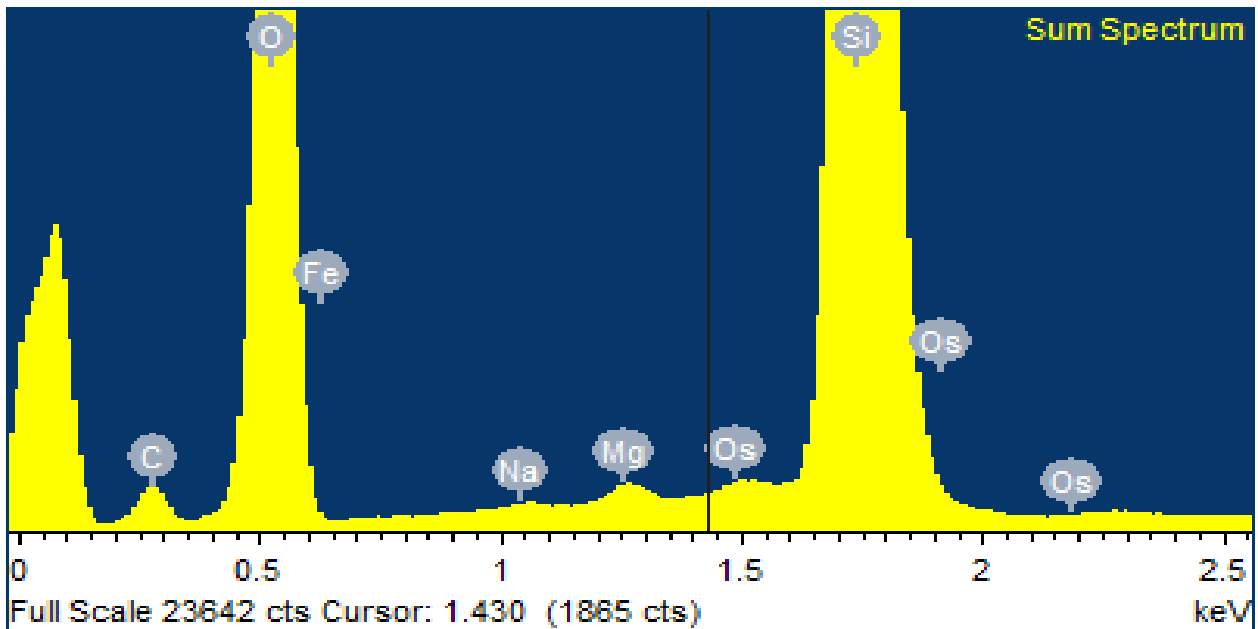
Mg MgO 1-Jun-1999 12:00 AM

Si SiO₂ 1-Jun-1999 12:00 AM

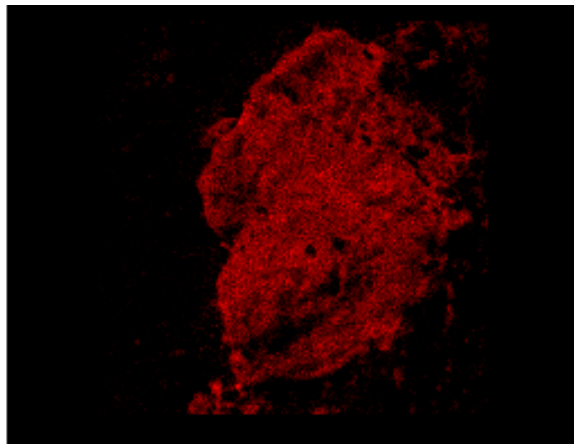
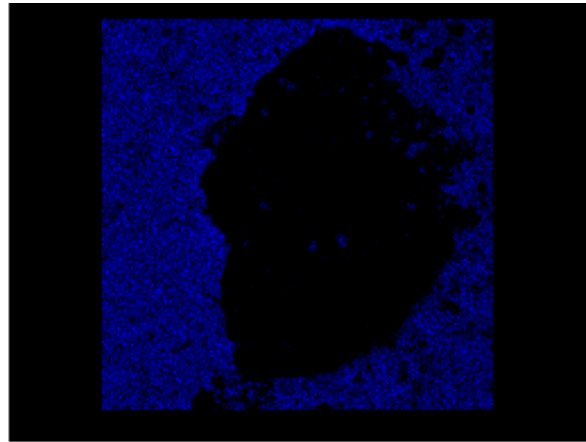
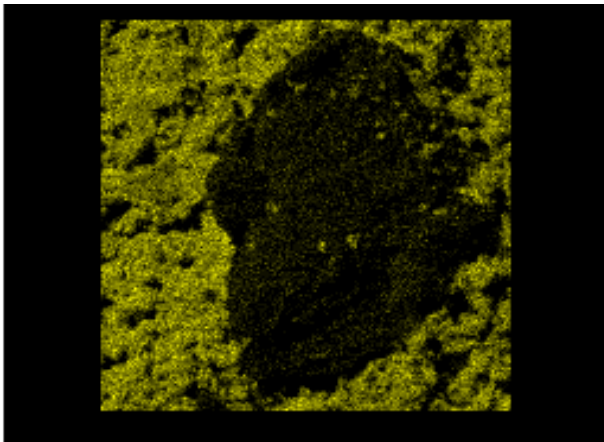
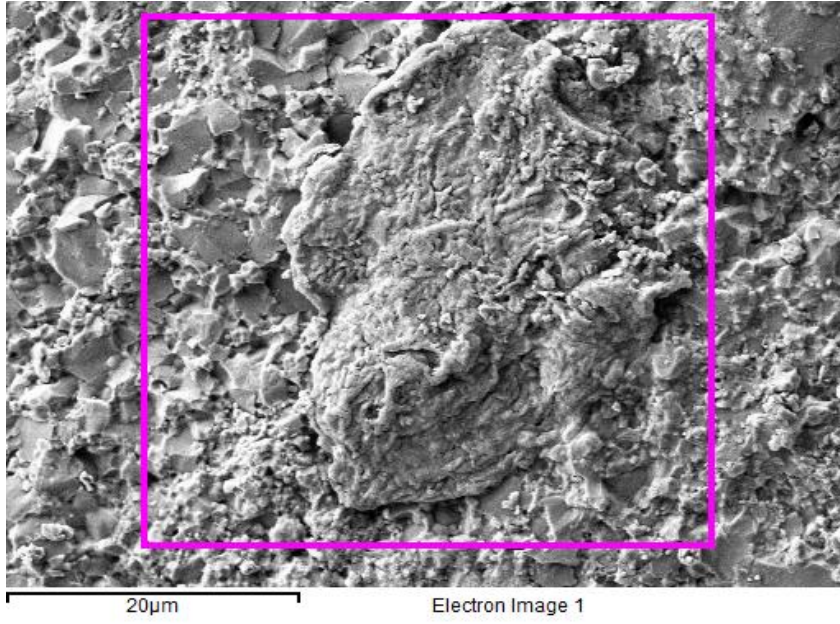
Fe Fe 1-Jun-1999 12:00 AM

Os Not defined 1-Jun-1999 12:00 AM

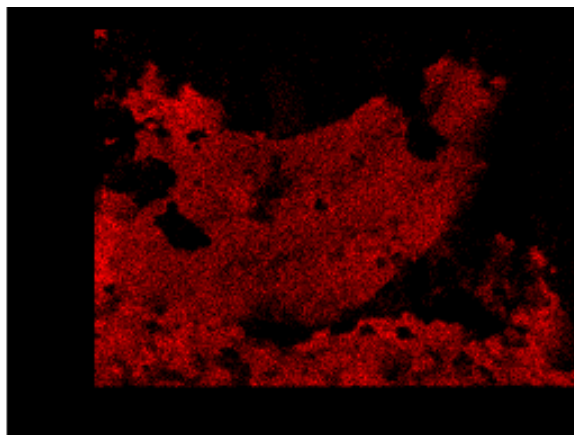
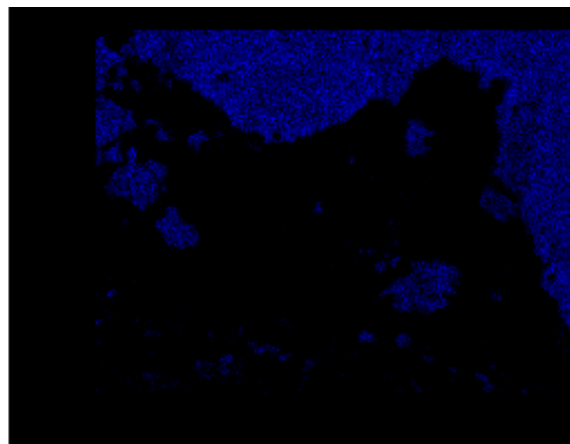
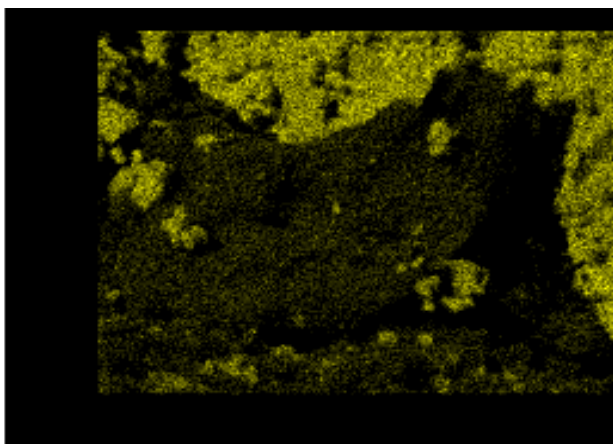
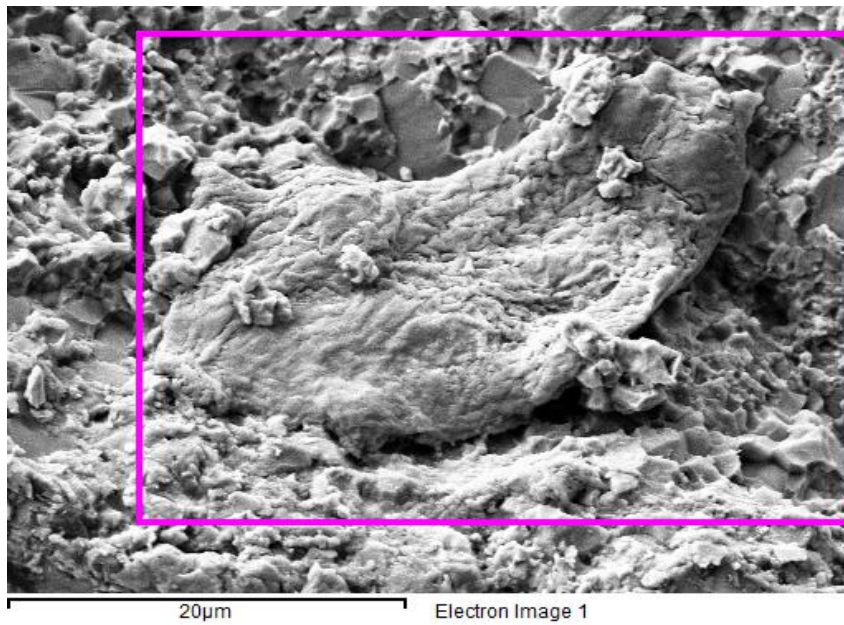
Element	Weight%	Atomic%
C K	9.07	14.14
O K	51.29	59.99
Na K	0.09	0.07
Mg K	0.25	0.19
Fe K	0.16	0.05
Si K	38.21	25.46
Totals	100.00	



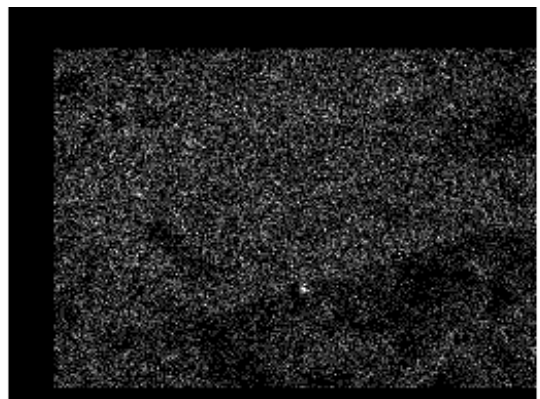
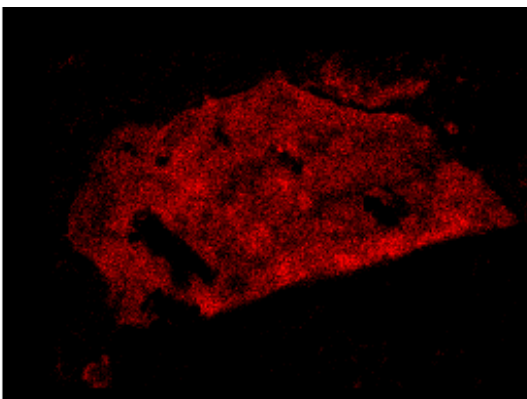
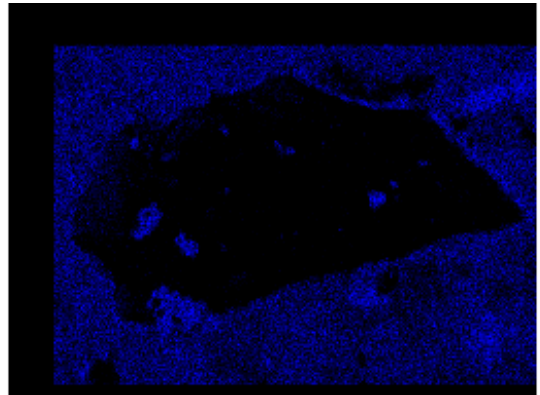
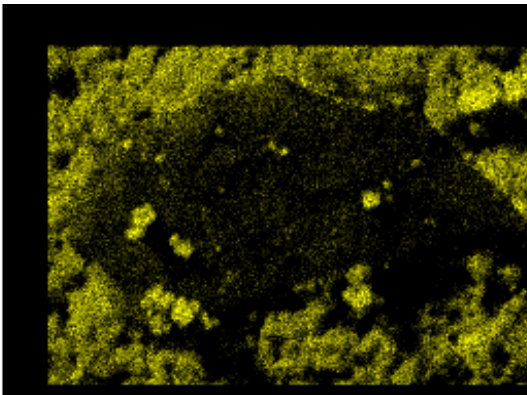
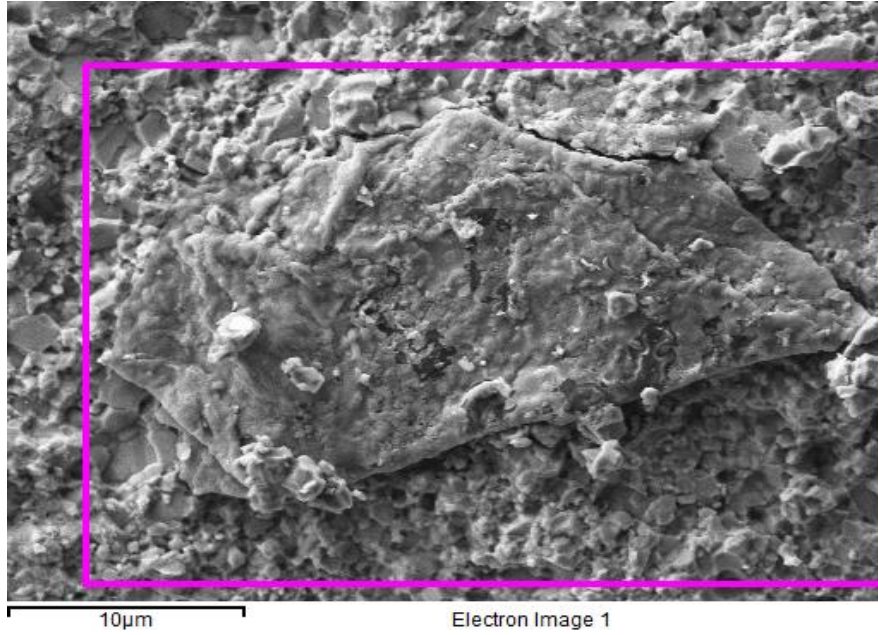
Sample GSC24380d_Location 2



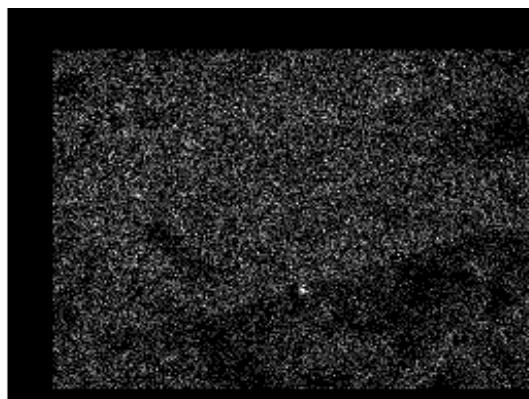
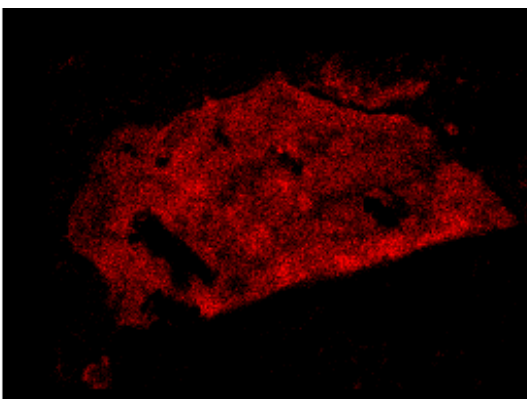
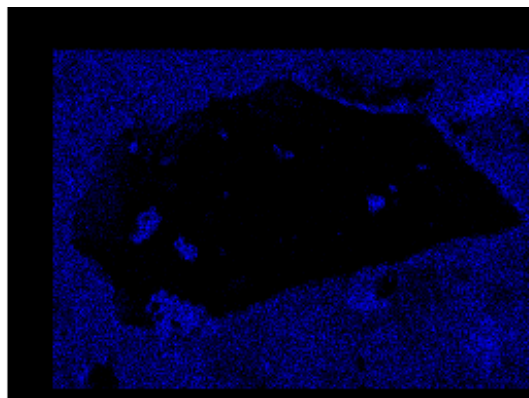
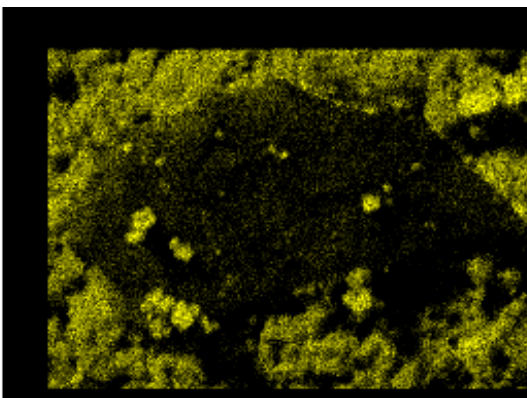
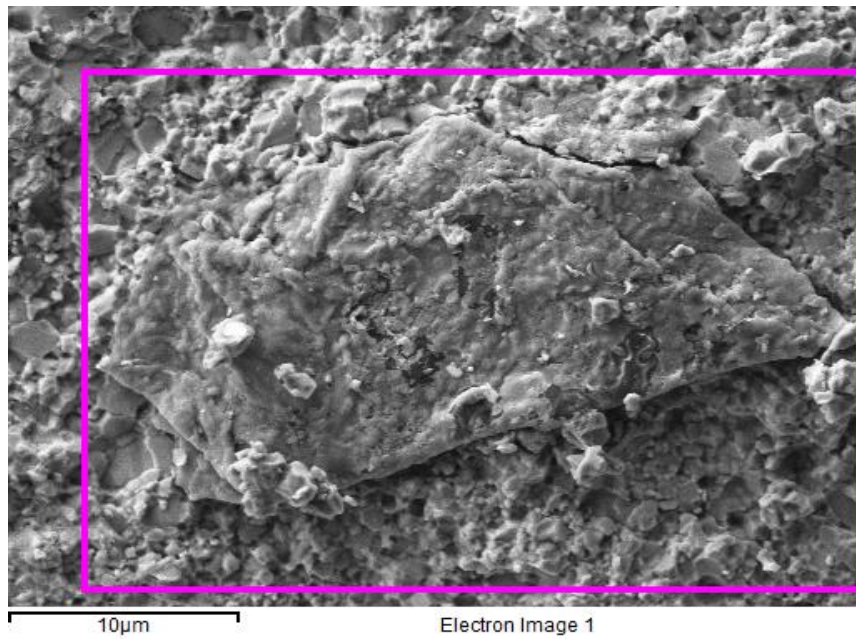
Sample GSC24380d_Location 3



Sample GSC24380d_Location 4



Sample GSC24380d_Location 5



D. Electron Microprobe (EMP) WDS maps

This appendix contains field-emission electron microprobe (EPM) wavelength dispersive X-ray spectroscopy (WDS) element maps along with their corresponding composition (COMPO) mode and secondary electron image (SEI) images for different types of CUBs.

Each of the 4 items in this appendix displays the images and mapping for an individual specimen of sample GSC24380d's thin section. For more information about the detailed analysis please refer to sections 3.4.

Item 1. Sample GSC24380d-27 maps

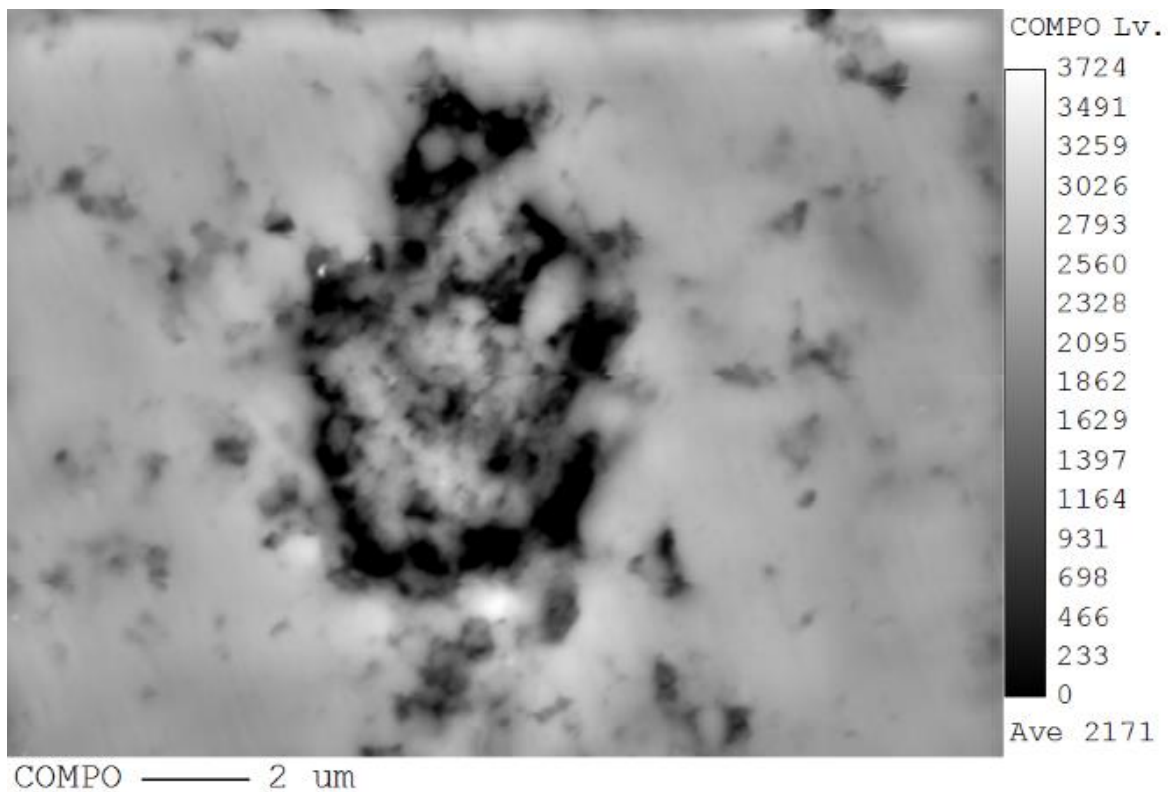


Figure D.1.1. Field-emission electron microprobe (EPM) composition (COMPO) mode image for CUB type 3.

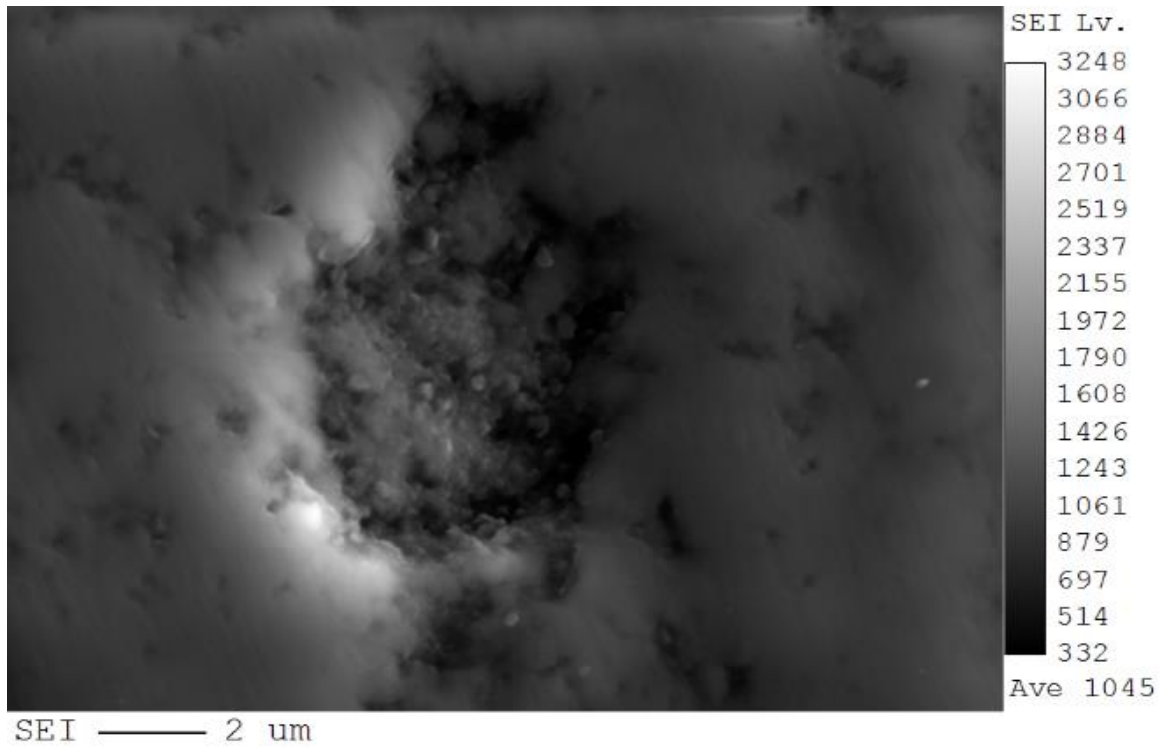


Figure D.1.2. Field-emission electron microprobe (EPM) secondary electron image (SEI) for CUB type 3.

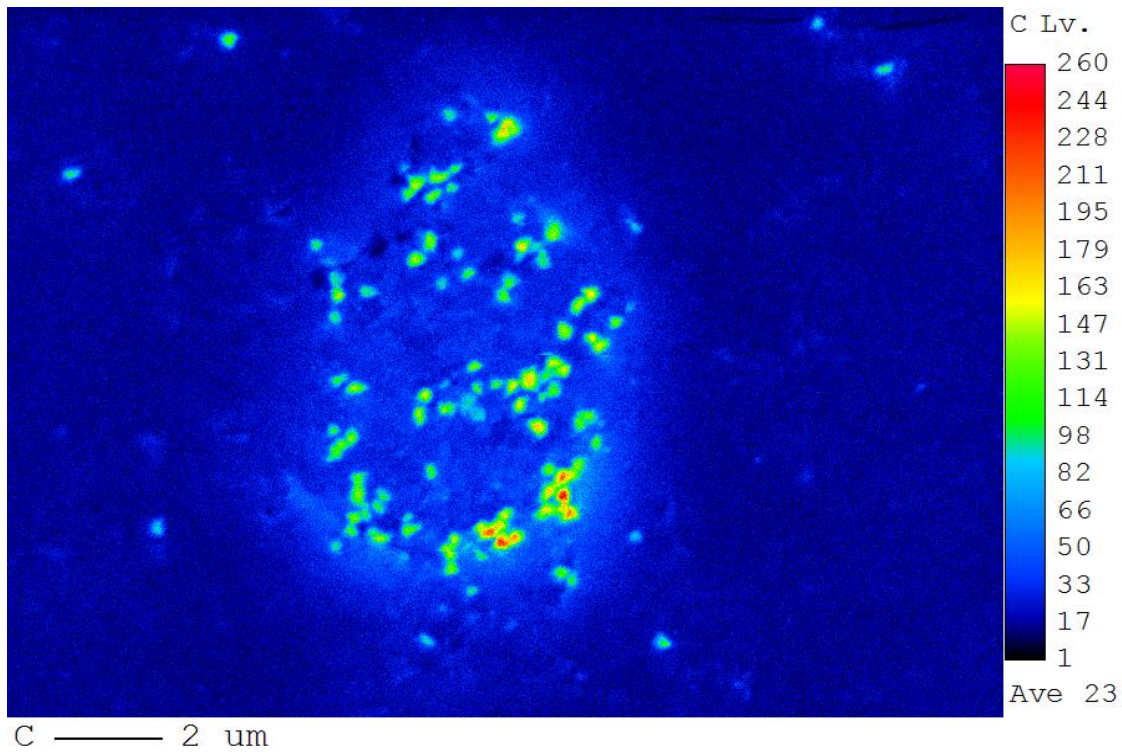


Figure D.1.3. Field-emission electron microprobe (EPM) wavelength dispersive X-ray spectroscopy (WDS) carbon element map for CUB type 3.

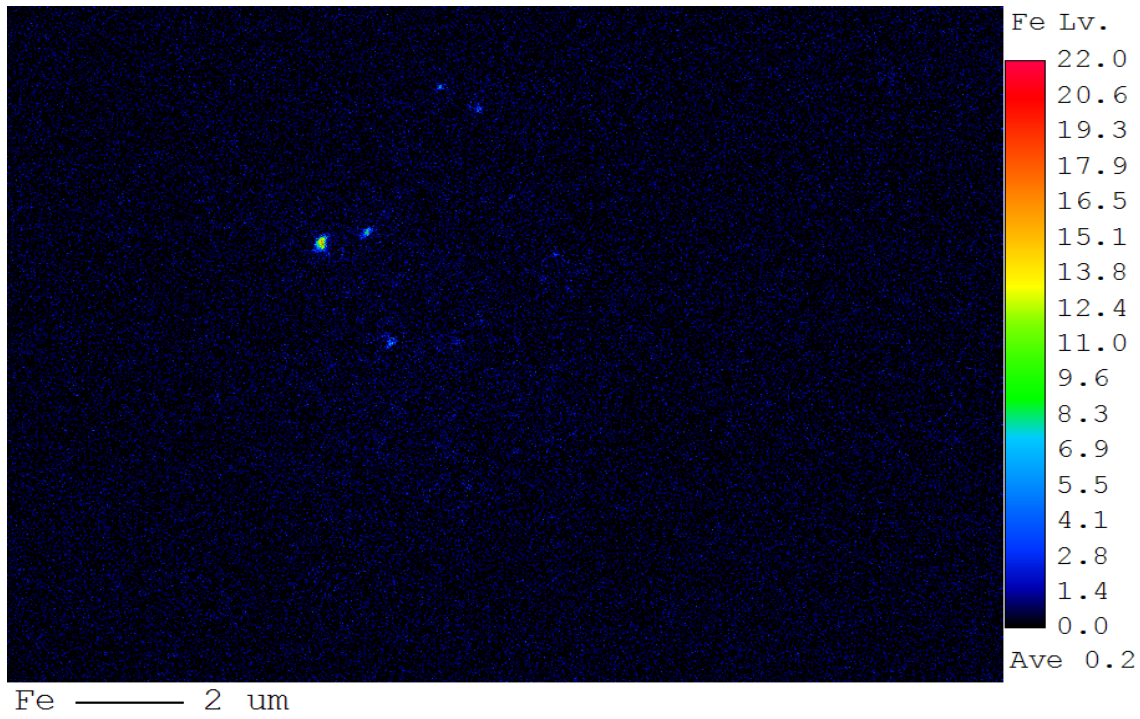


Figure D.1.4. Field-emission electron microprobe (EPM) wavelength dispersive X-ray spectroscopy (WDS) iron element map for CUB type 3.

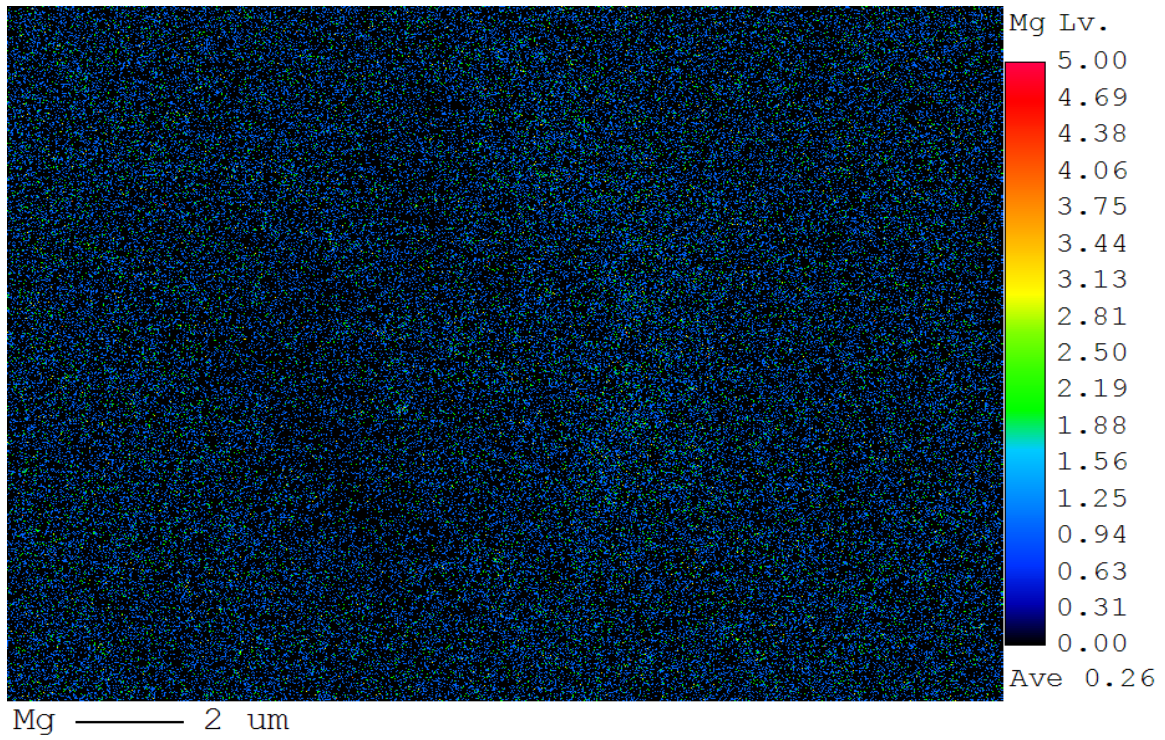


Figure D.1.5. Field-emission electron microprobe (EPM) wavelength dispersive X-ray spectroscopy (WDS) magnesium element map for CUB type 3.

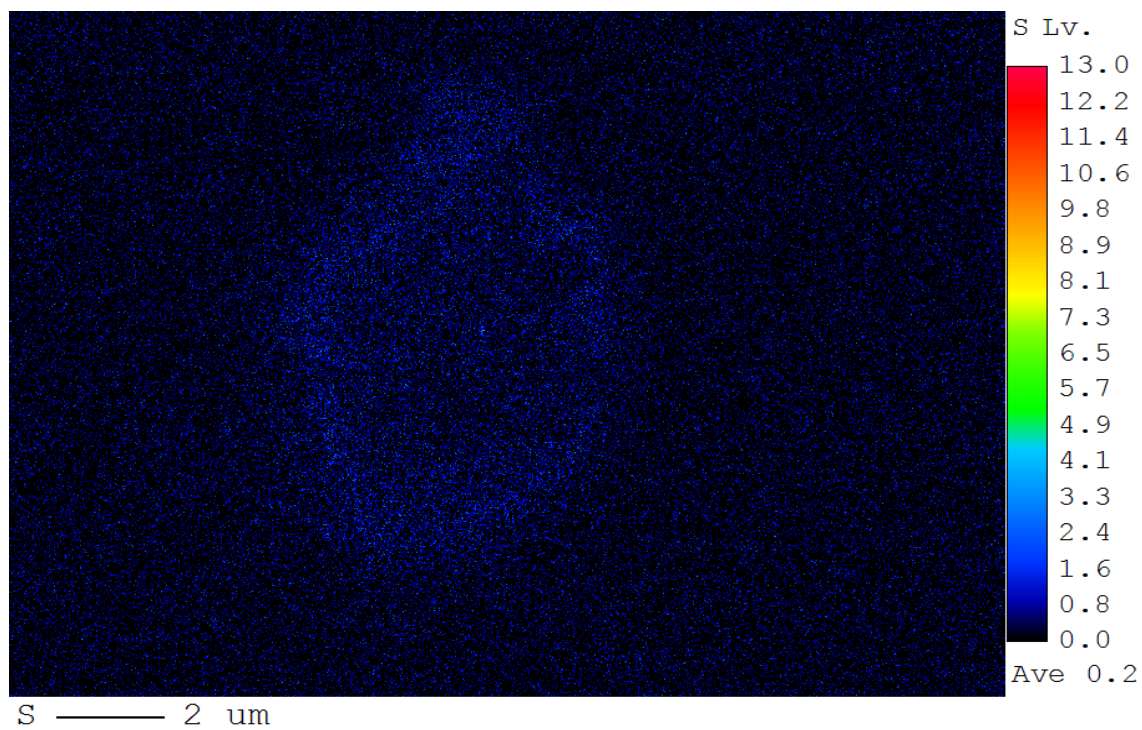


Figure D.1.6. Field-emission electron microprobe (EPM) wavelength dispersive X-ray spectroscopy (WDS) sulfur element map for CUB type 3.

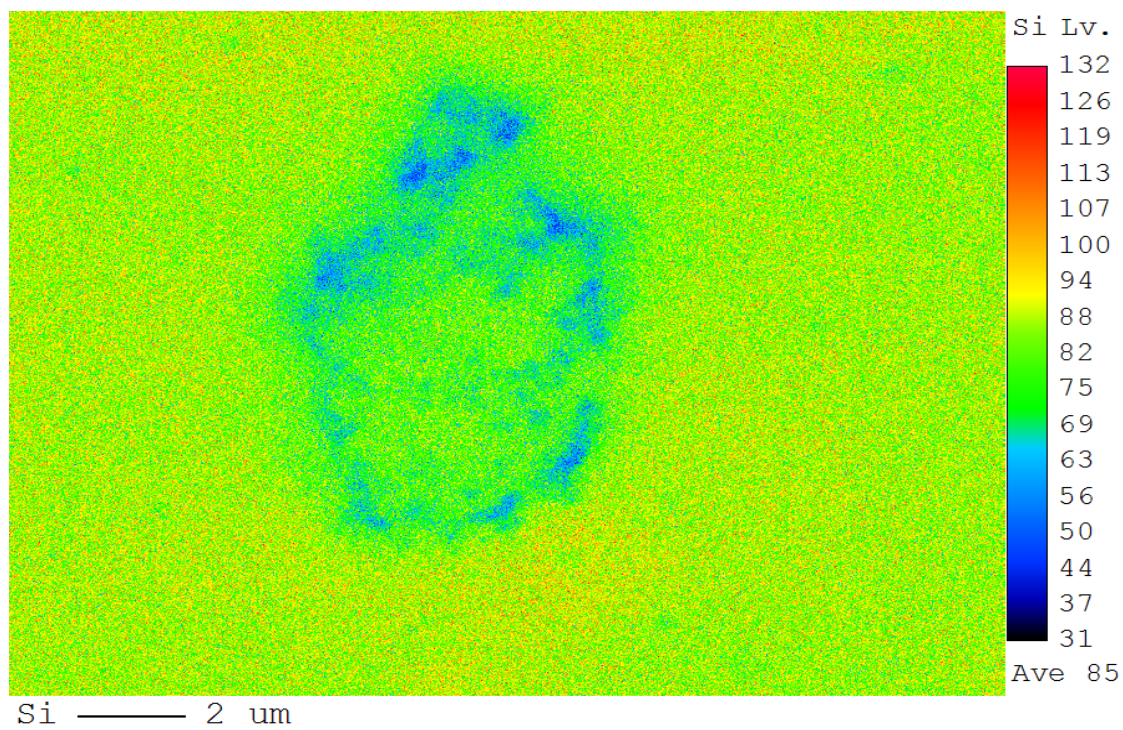


Figure D.1.7. Field-emission electron microprobe (EPM) wavelength dispersive X-ray spectroscopy (WDS) silicon element map for CUB type 3.

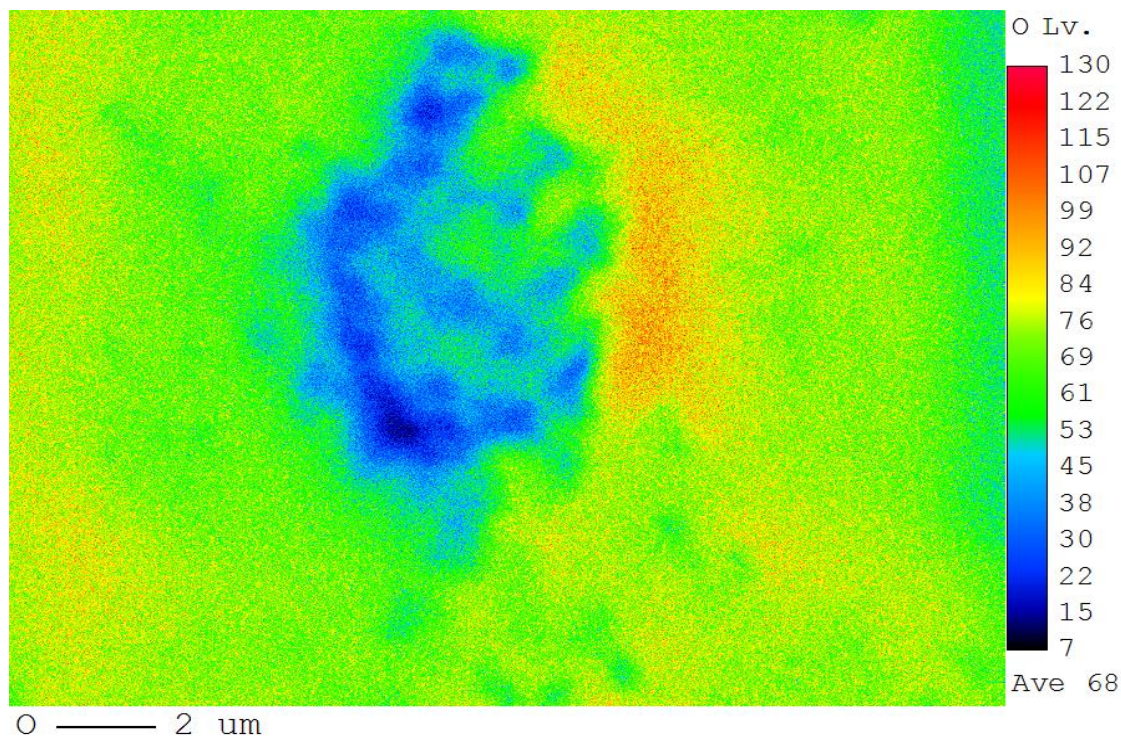


Figure D.1.8. Field-emission electron microprobe (EPM) wavelength dispersive X-ray spectroscopy (WDS) Oxygen element map for CUB type 3.

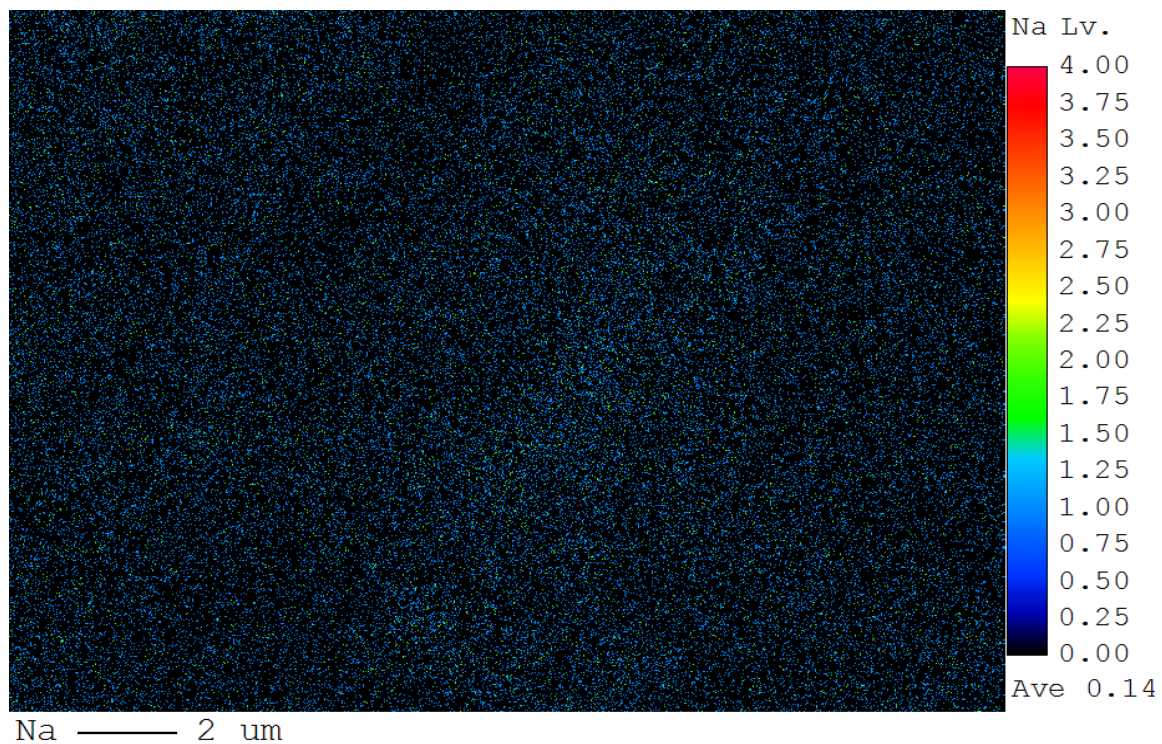


Figure D.1.9. Field-emission electron microprobe (EPM) wavelength dispersive X-ray spectroscopy (WDS) sodium element map for CUB type 3.

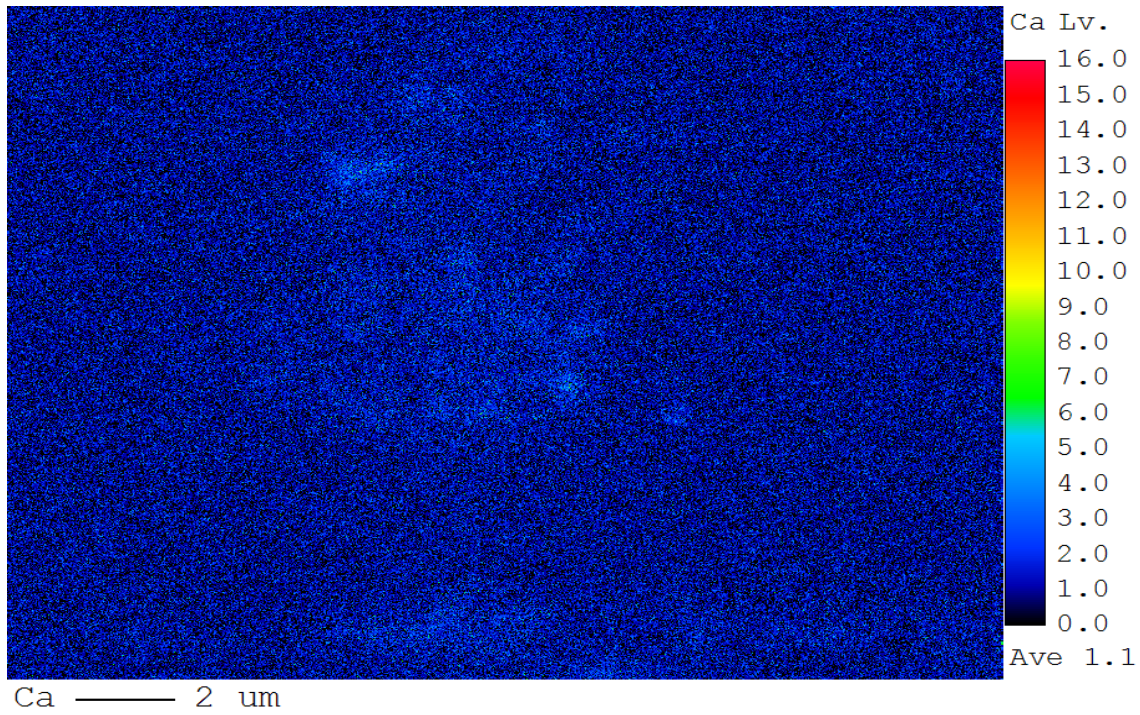


Figure D.1.10. Field-emission electron microprobe (EPM) wavelength dispersive X-ray spectroscopy (WDS) calcium element map for CUB type 3.

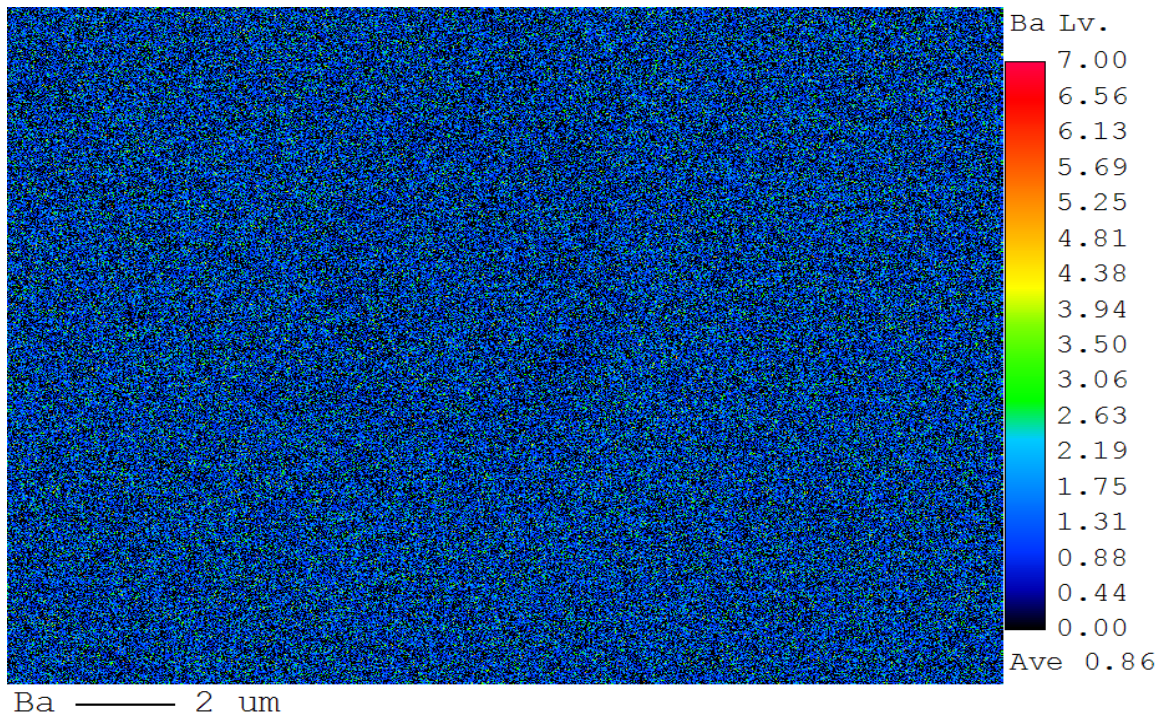


Figure D.1.11. Field-emission electron microprobe (EPM) wavelength dispersive X-ray spectroscopy (WDS) barium element map for CUB type 3.

Item 2. Sample GSC24380d-31 maps

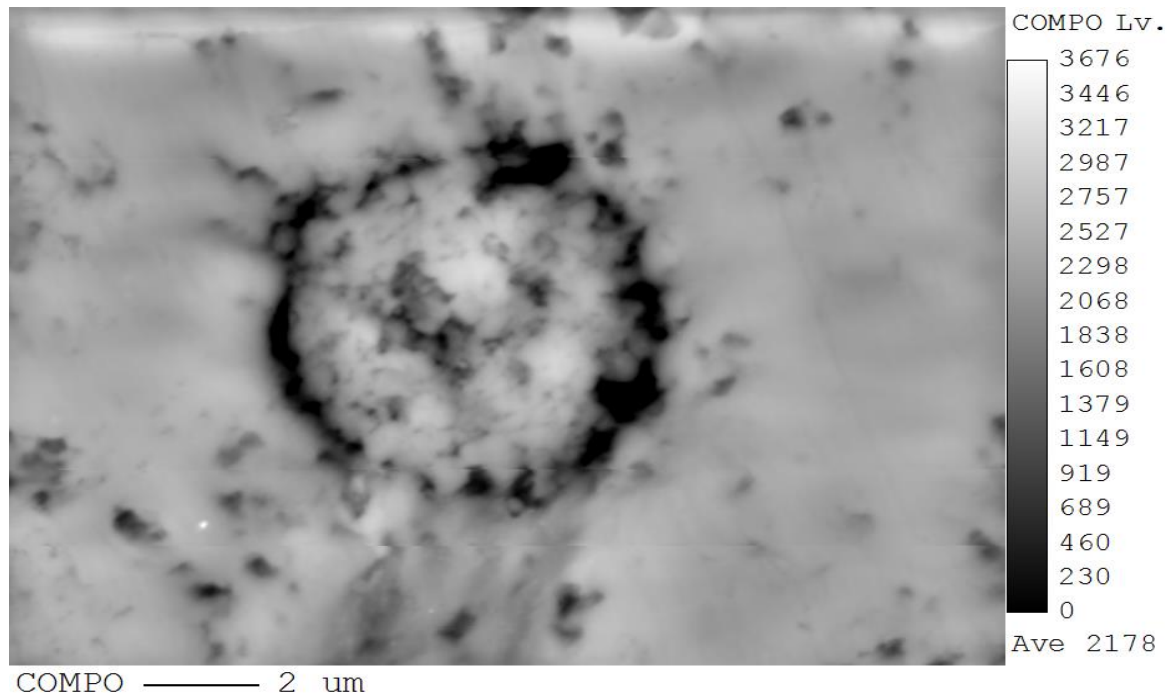


Figure D.2.1. Field-emission electron microprobe (EPM) composition (COMPO) mode image for CUB type 2.

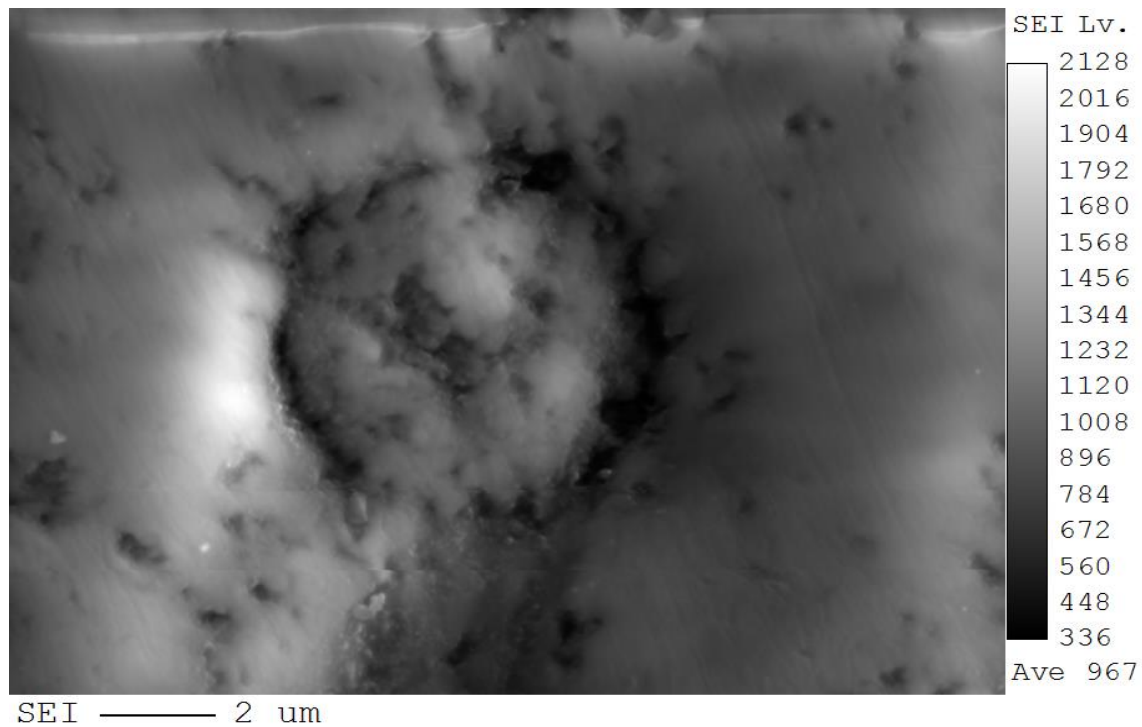


Figure D.2.2. Field-emission electron microprobe (EPM) secondary electron image (SEI) for CUB type 2.

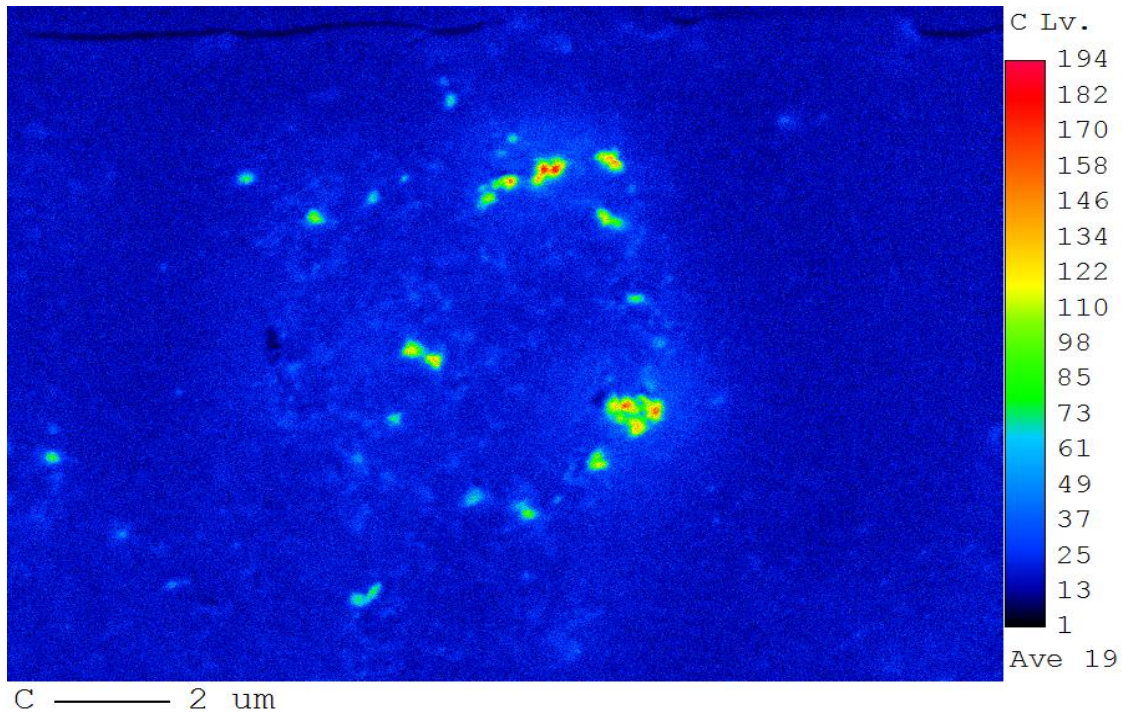


Figure D.2.3. Field-emission electron microprobe (EPM) wavelength dispersive X-ray spectroscopy (WDS) carbon element map for CUB type 2.

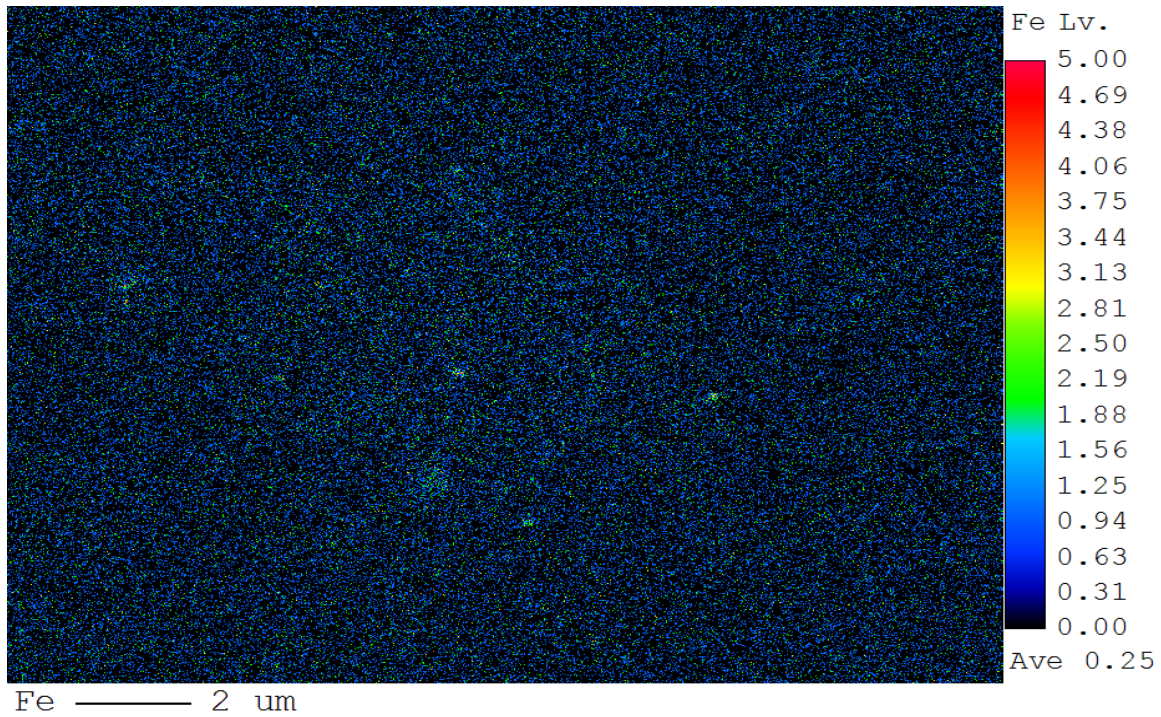


Figure D.2.4. Field-emission electron microprobe (EPM) wavelength dispersive X-ray spectroscopy (WDS) iron element map for CUB type 2.

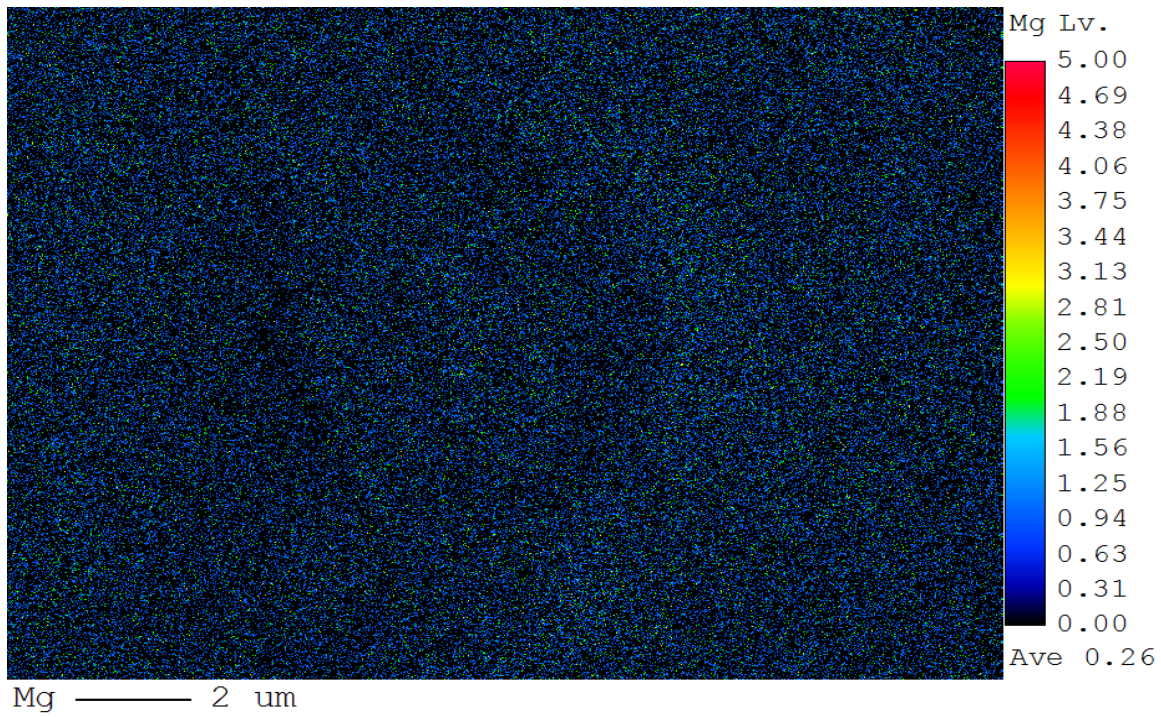


Figure D.2.5. Field-emission electron microprobe (EPM) wavelength dispersive X-ray spectroscopy (WDS) magnesium element map for CUB type 2.

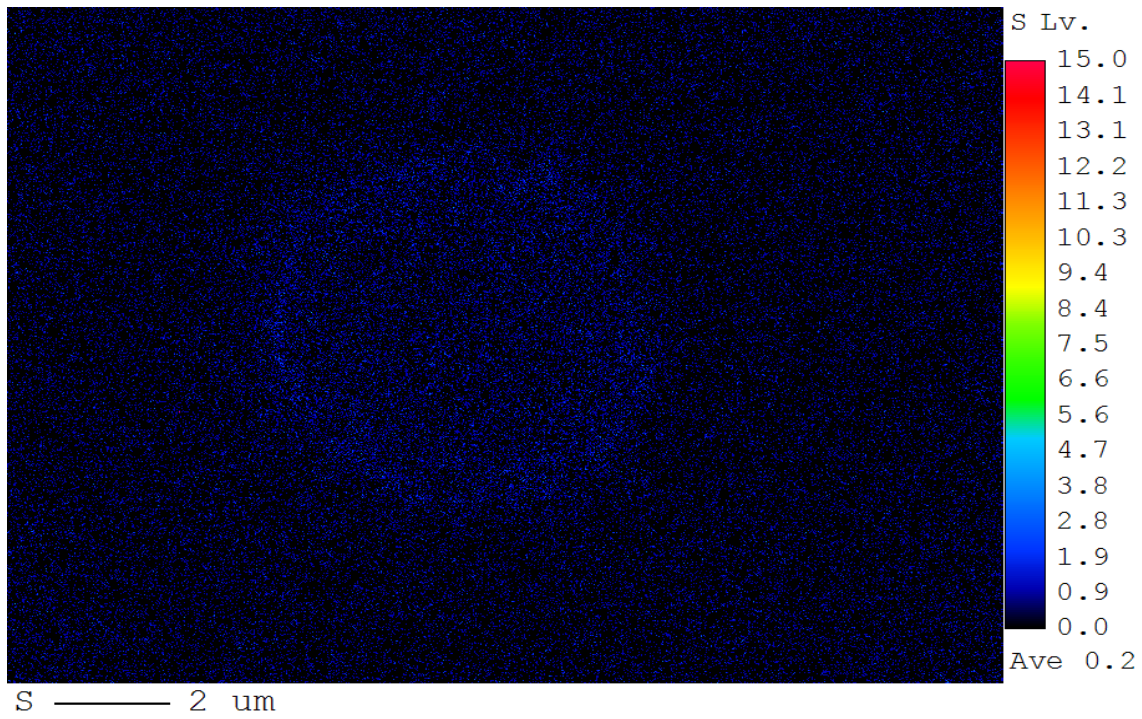


Figure D.2.6. Field-emission electron microprobe (EPM) wavelength dispersive X-ray spectroscopy (WDS) sulfur element map for CUB type 2.

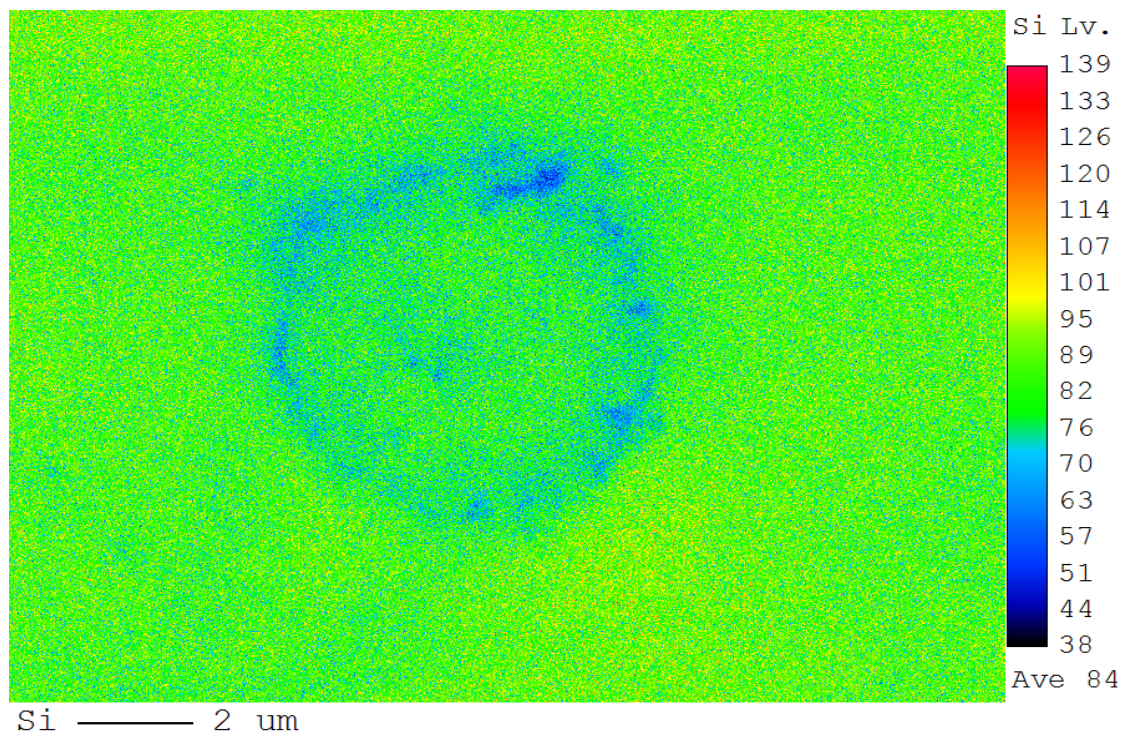


Figure D.2.7. Field-emission electron microprobe (EPM) wavelength dispersive X-ray spectroscopy (WDS) silicon element map for CUB type 2.

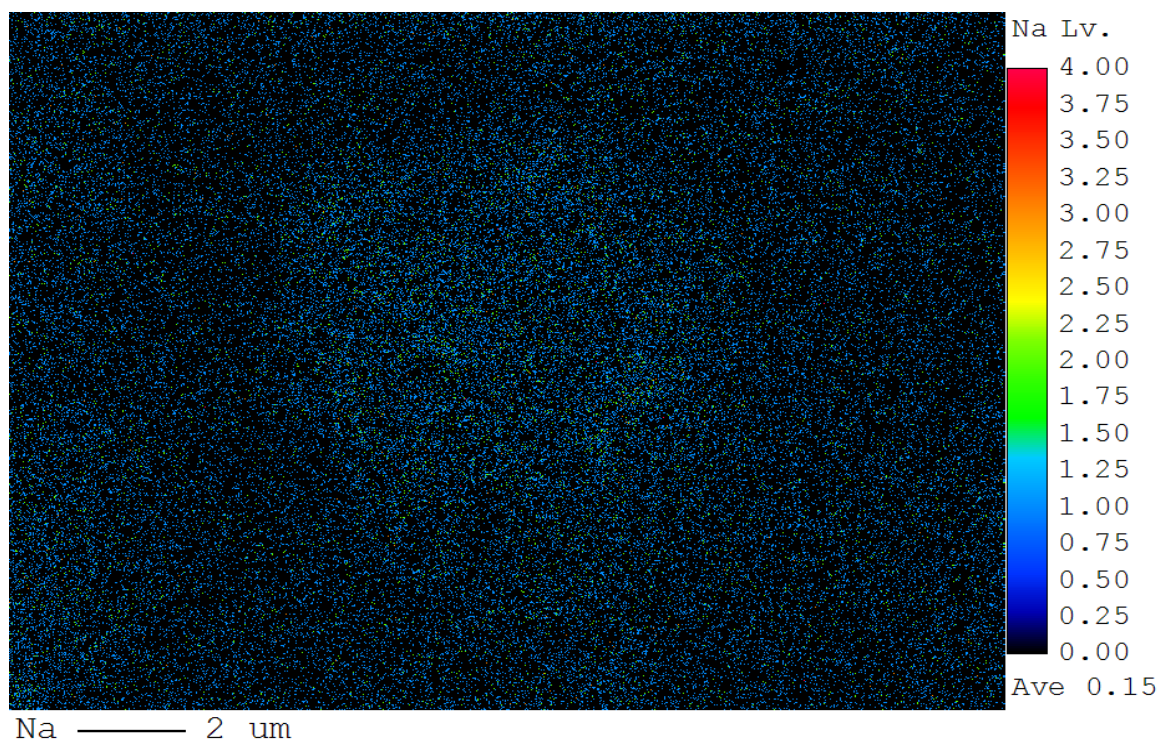


Figure D.2.8. Field-emission electron microprobe (EPM) wavelength dispersive X-ray spectroscopy (WDS) Oxygen element map for CUB type 2.

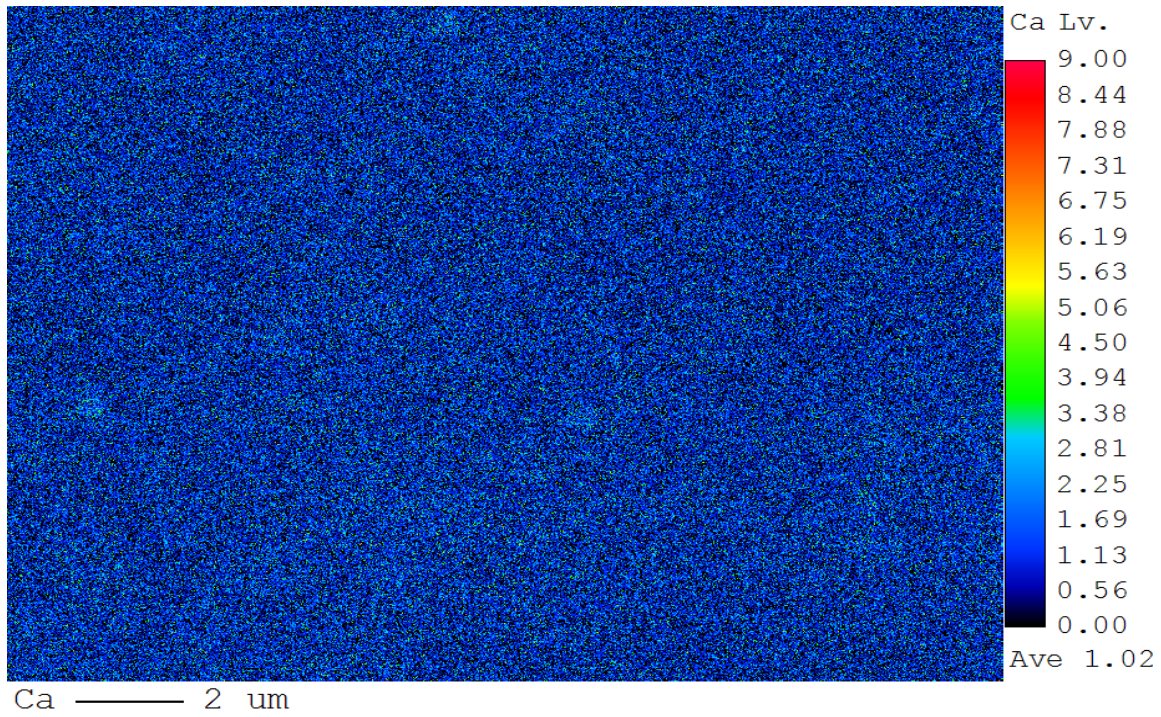


Figure D.2.9. Field-emission electron microprobe (EPM) wavelength dispersive X-ray spectroscopy (WDS) sodium element map for CUB type 2.

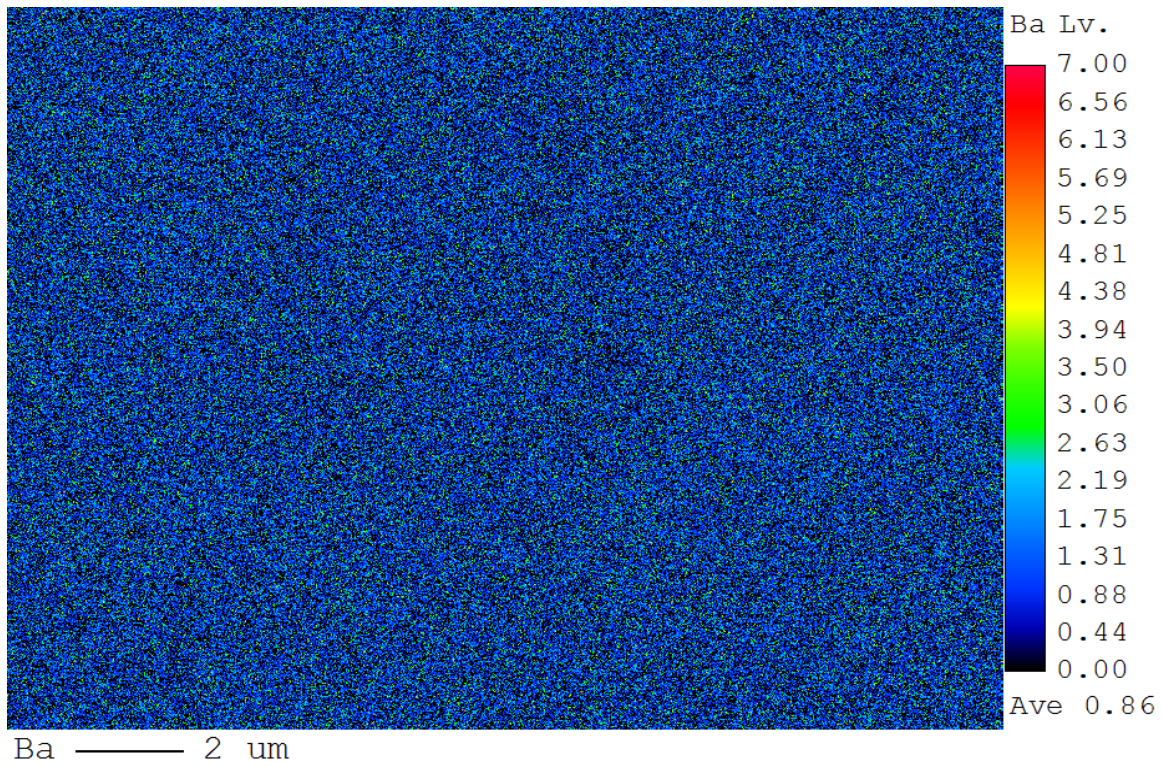


Figure D.2.10. Field-emission electron microprobe (EPM) wavelength dispersive X-ray spectroscopy (WDS) calcium element map for CUB type 2.

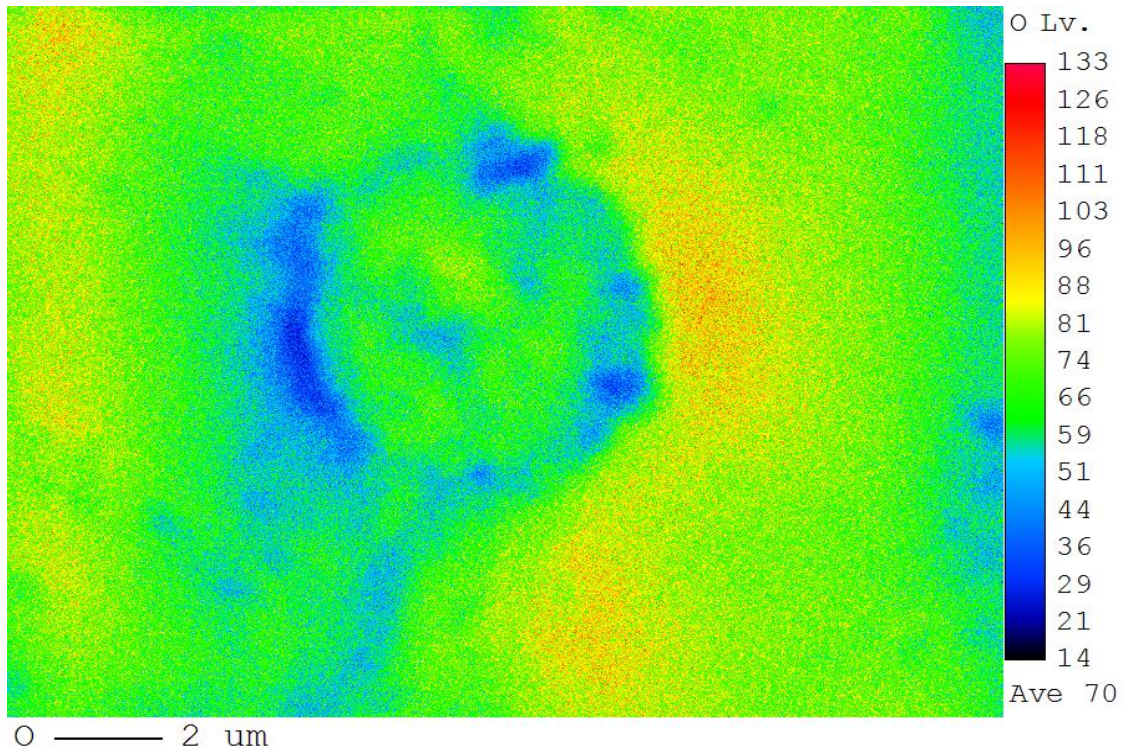


Figure D.2.11. Field-emission electron microprobe (EPM) wavelength dispersive X-ray spectroscopy (WDS) barium element map for CUB type 2.

Item 3. Sample GSC24380d-36 maps

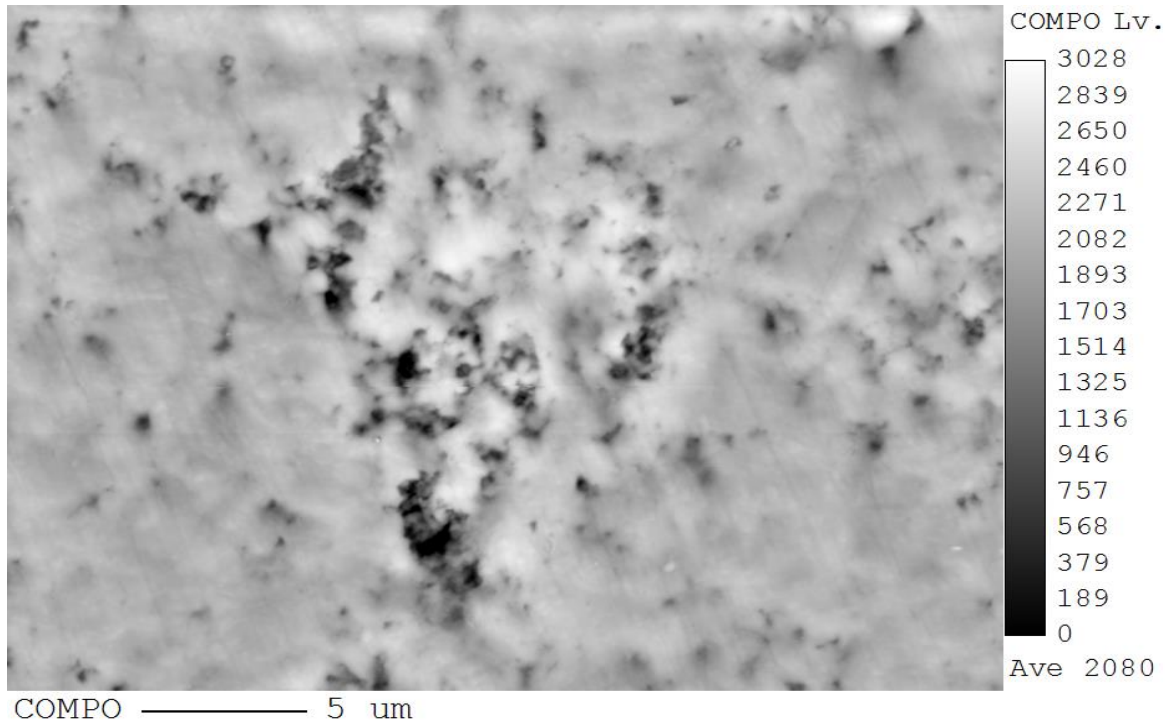


Figure D.3.1. Field-emission electron microprobe (EPM) composition (COMPO) mode image for CUB type 3.

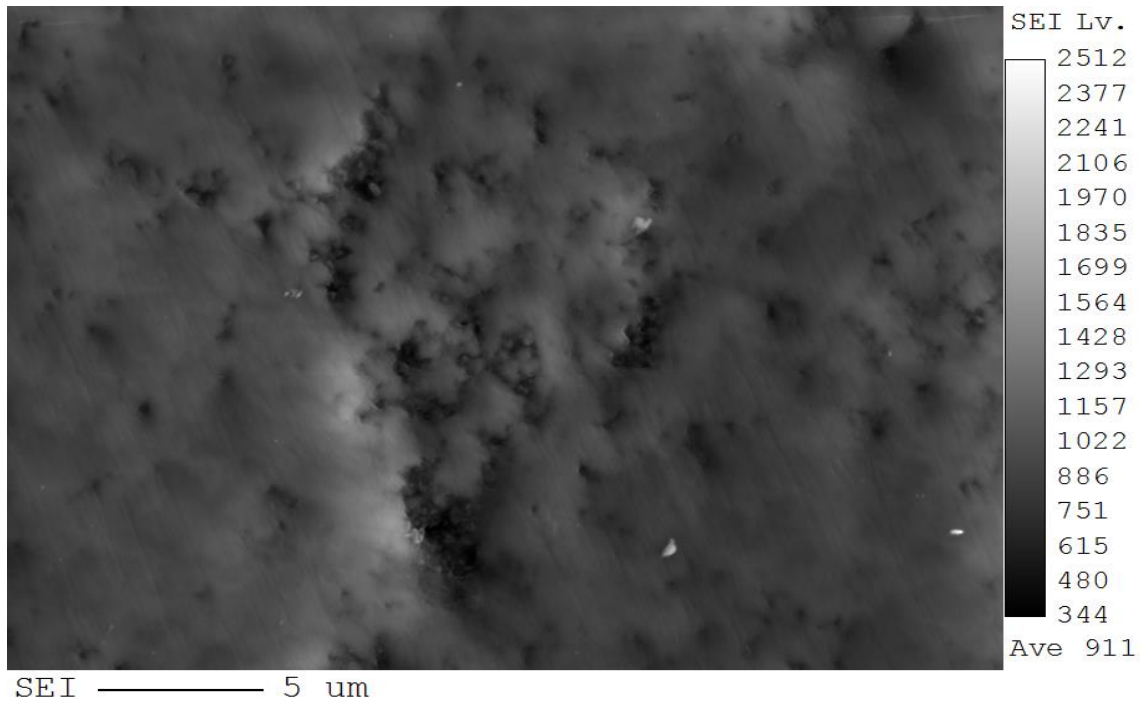


Figure D.3.2. Field-emission electron microprobe (EPM) secondary electron image (SEI) for CUB type 3.

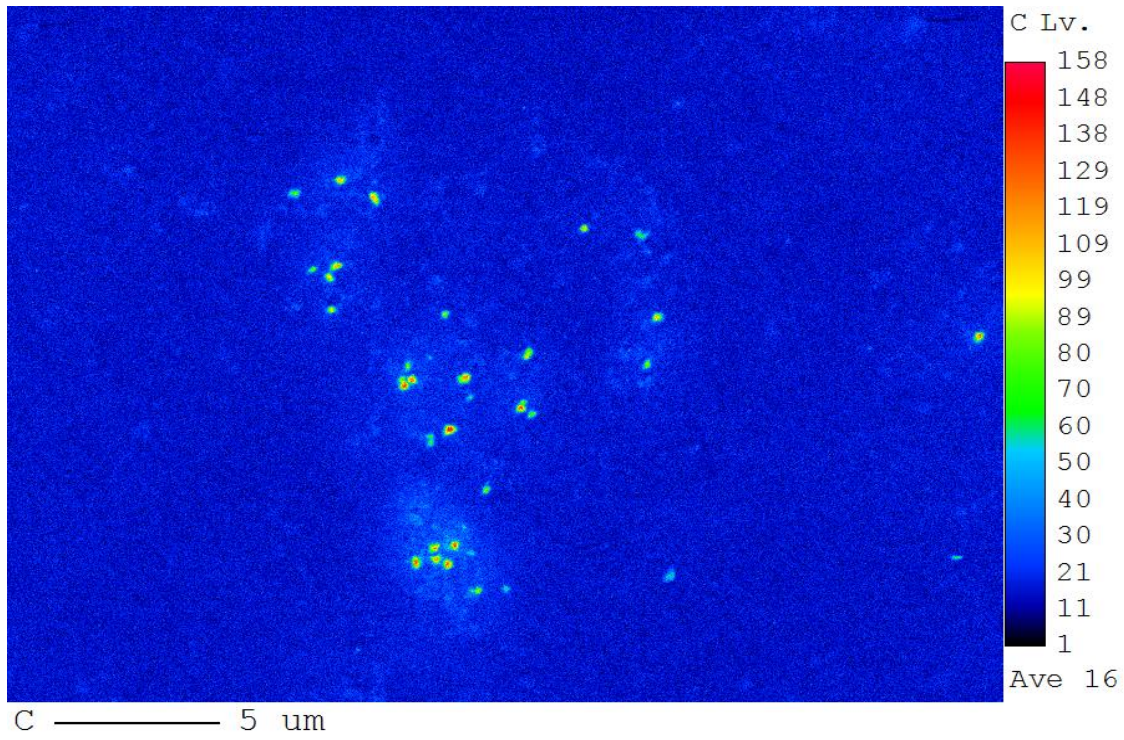


Figure D.3.3. Field-emission electron microprobe (EPM) wavelength dispersive X-ray spectroscopy (WDS) carbon element map for CUB type 3.

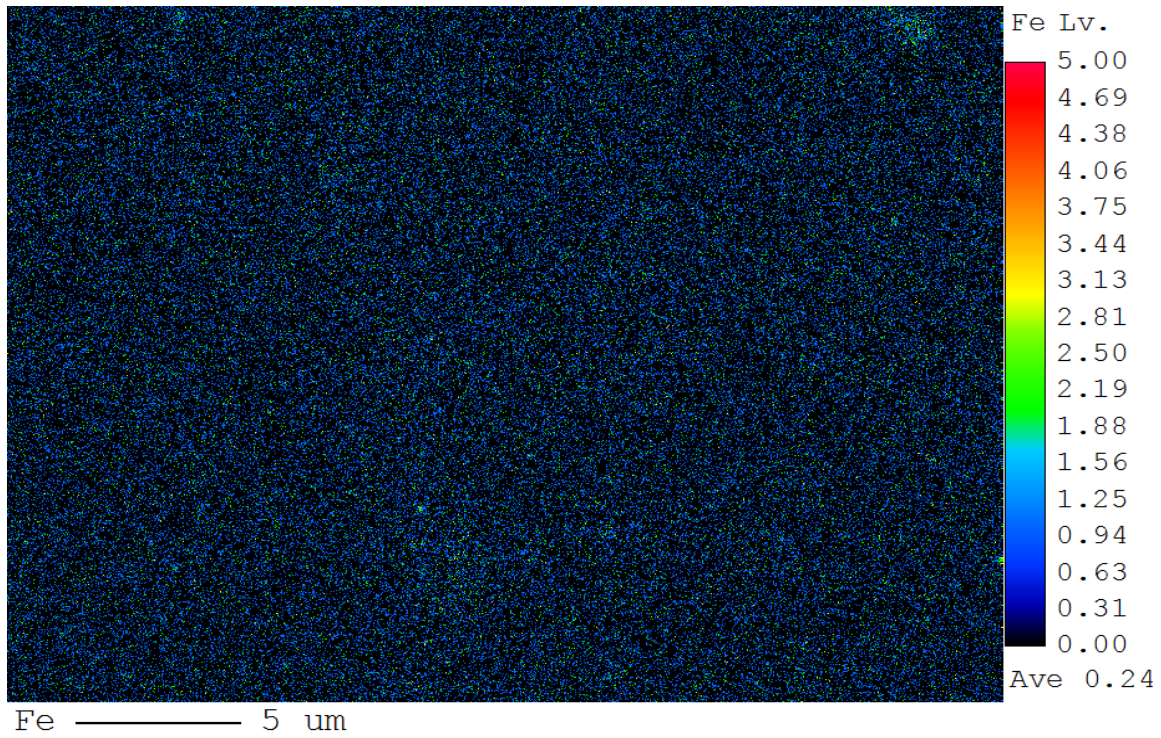


Figure D.3.4. Field-emission electron microprobe (EPM) wavelength dispersive X-ray spectroscopy (WDS) iron element map for CUB type 3.

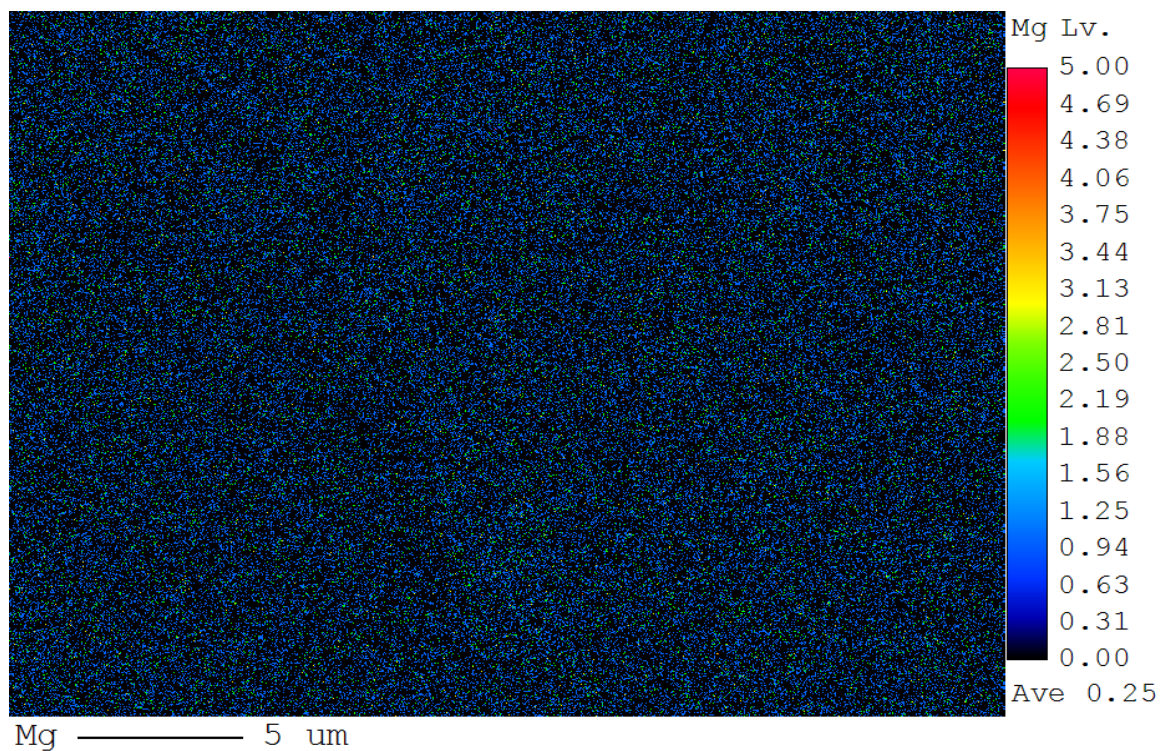


Figure D.3.5. Field-emission electron microprobe (EPM) wavelength dispersive X-ray spectroscopy (WDS) magnesium element map for CUB type 3.

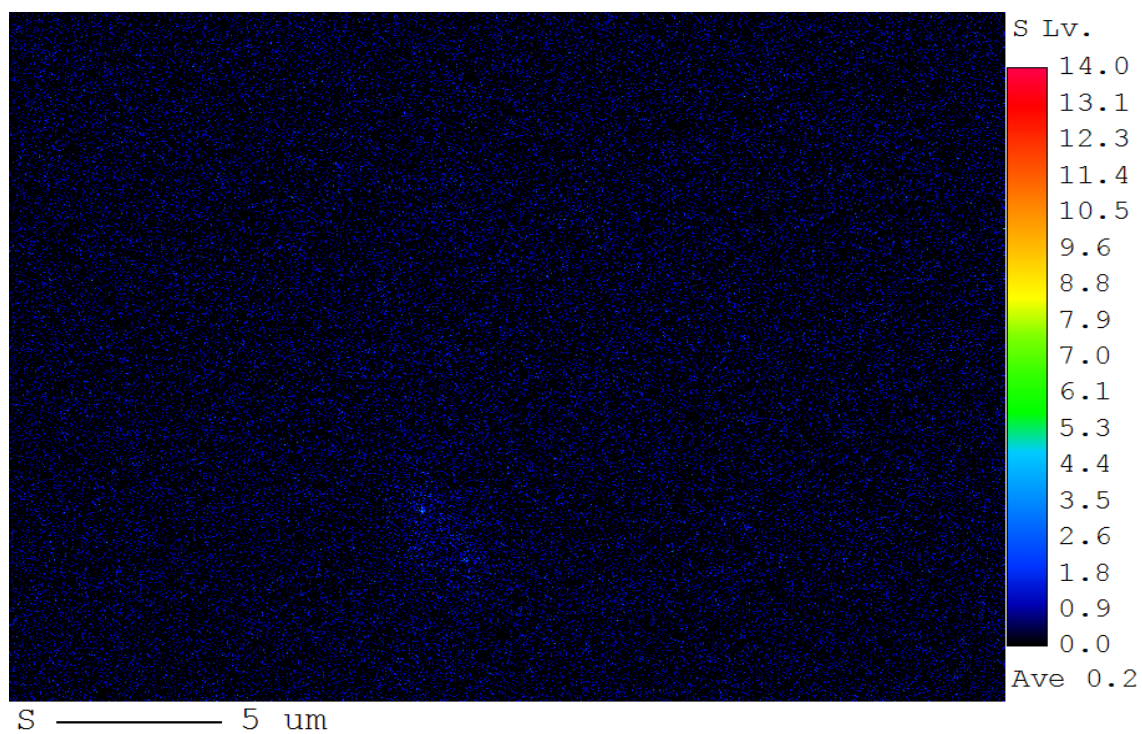


Figure D.3.6. Field-emission electron microprobe (EPM) wavelength dispersive X-ray spectroscopy (WDS) sulfur element map for CUB type 3.

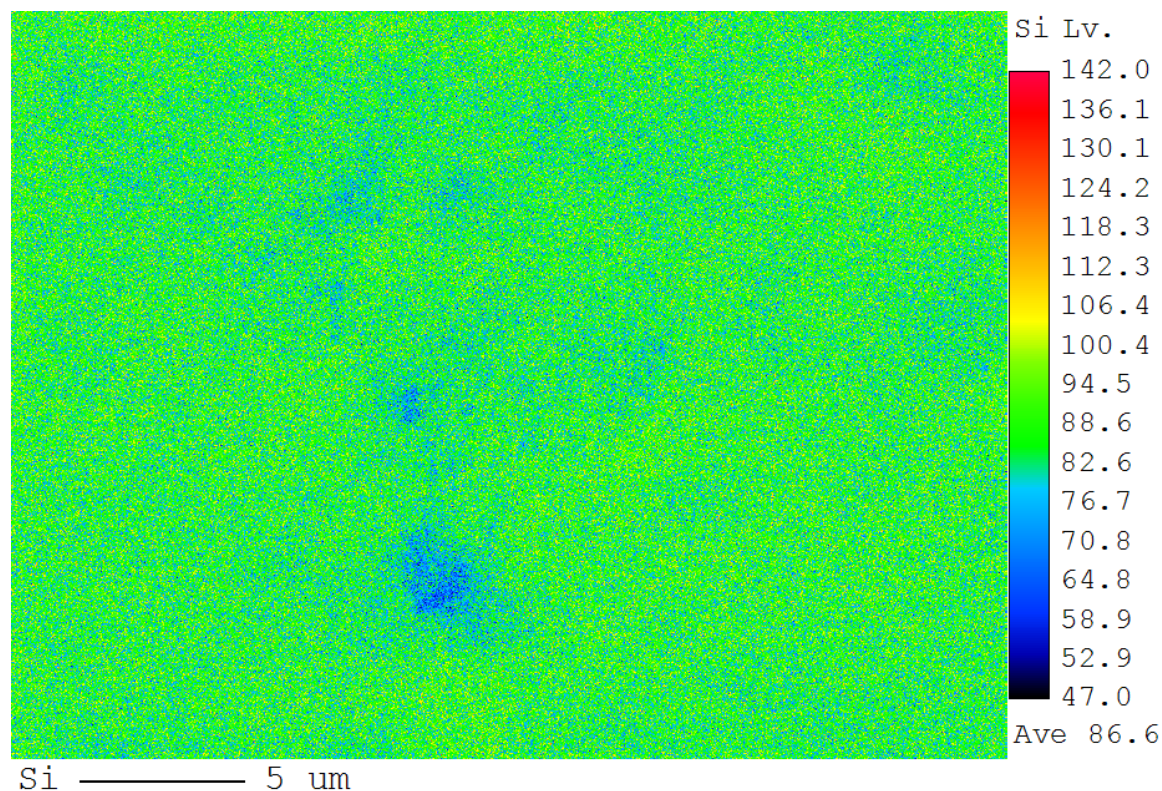


Figure D.3.7. Field-emission electron microprobe (EPM) wavelength dispersive X-ray spectroscopy (WDS) silicon element map for CUB type 3.

E. Other analytical methods

This appendix contains the data obtained for several methods that were also tested during this research project. The lack of mention of these methods on the main sections of this thesis is due to different reason that are explained within the items listed below.

Item 1. Laser Raman Spectroscopy (LRS)

In this analytical method molecular polarization changes are required for Raman scattering to take place. Upon striking a molecule, photons are scattered elastically (Rayleigh scattering) and inelastically (Raman scattering), generating Stoke's and anti-Stokes lines (Surface Science Western, undated). In Raman spectroscopy, there's no limit to a sample's shape and size as the

scattering process allows samples of any shape and size to be examined. Even material amounts down to $\sim 1 \mu\text{m}$ can be studied through this method. It's due to this characteristic that this technique was selected in order to study the small specimens within the Gunflint Chert samples (Alleon et al., 2016; Brasier et al., 2015; Schopf et al., 2002; Wacey et al., 2013).

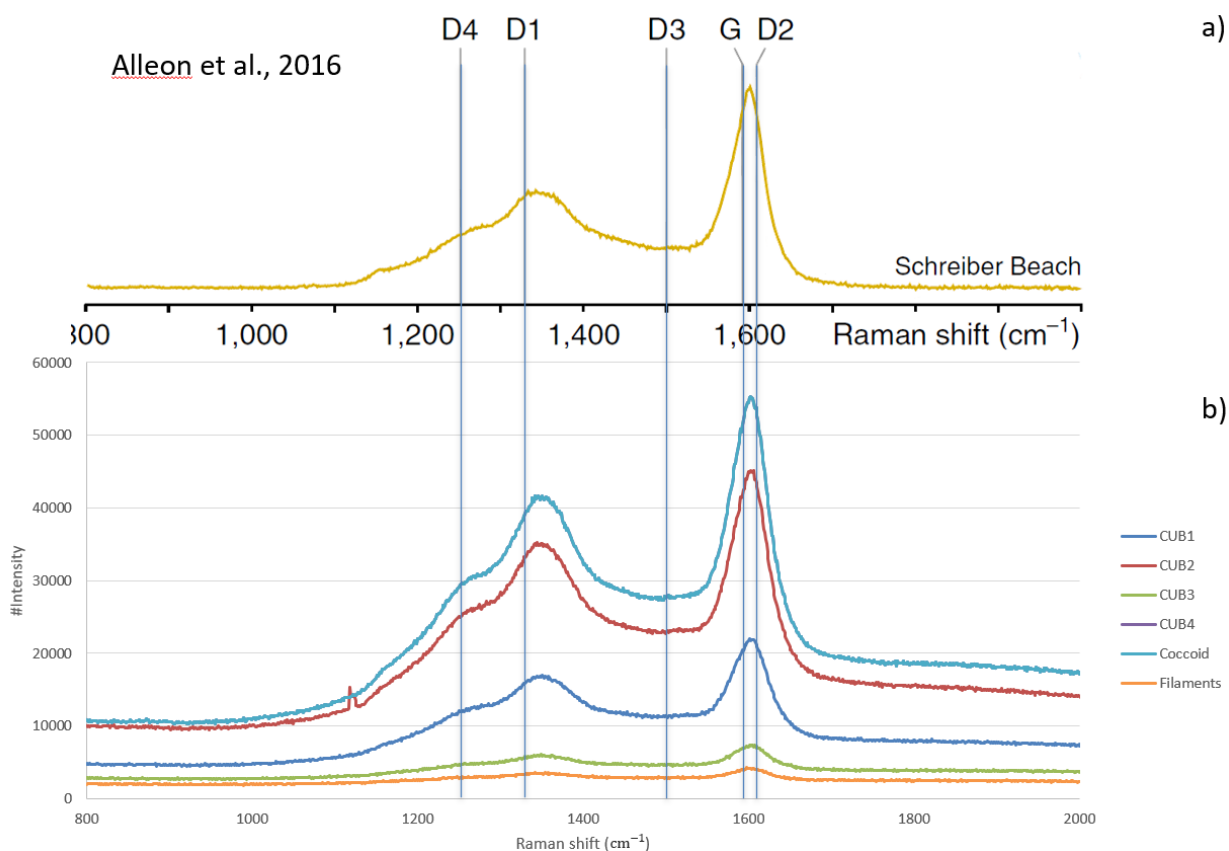


Figure E.1. Raman spectra for samples of Schreiber Beach, Ontario Canada. a) Representative Raman spectra from microfossils of Schreiber Beach locality from Alleon et al., 2016. b) Raman spectra from different types of microorganisms of the Gunflint chert microbiota, including all CUB types as well as coccooid and filamentous organisms. Both charts show spectra typical for disordered carbons with “defect” composite bands G (G + D2), D (D1 + D4) and D3. Its physical and chemical significance remains ambiguous.

The results obtained from this method match the ones presented by Alleon et al. (2016), which were also done on Gunflint chert samples from a nearby locality also at Schreiber Beach, Ontario, Canada. Both Alleon's and this project's results are shown on figure E.1a and E.1b respectively.

For thin sections GSC24380, GSC24380d, and GSC24380e laser Raman spectroscopy analysis was carried out in thirty different spots pertaining to each type of CUB. No sample preparation was needed for this method, just to ensure that the thin sections were clean and free of any coating, lens oil, fingerprints or dust. Using an Argon laser with wavelength 633 nm and 50 mW of power of the Renishaw InVia Reflex Raman Spectrometer at Surface Science Western (Fig. 1.10), it was possible to analyze the different types of CUBs present in the samples despite their small size.

As shown on the figures and previously stated by Alleon et al., cherts from the Gunflint formations have a homogenous composition in terms of carbon structure. This in turn explains why different kinds of microfossils species from the same formation display a similar Raman spectrum (Fig. E.1b). Yet, small differences within the respective intensities and concentrations of the spectra can be noticed from one organism to another.

Even if this analysis' results were an undoubted success, they weren't included on this thesis main manuscript due to its focus. This work heavily focuses on the morphology this organisms have instead of deepening on their geochemistry and biosignatures. Further work on this topics needs to be done and this result should be considered as an encouraging start.

Item 2. Micro-XRF, Micro-CT and Synchrotron analyses

Three other analytical methods where used in this study, but unfortunately, not one of them yielded any useful results that would contribute in any way to this works goals and objectives. The analytical methods that were used are the following:

- Micro X-ray Fluorescence (MICRO-XRF)

This analytical method works by the recollection of characteristic secondary X-rays that a particular material emits when it has been excited by being bombarded with high-energy X-rays. It provides detailed elemental and chemical analysis of the sample, being useful for the identification different materials as well as for research in the fields of geochemistry, forensics, archeology and art.

Thin sections of the Gunflint chert were analyzed by a Bruker M4 Tornado micro-XRF instrument from the Earth and Planetary Materials Analysis Laboratory (EPMA) at Western. It required no sample preparation and was intended to provided elemental composition points of 1) the matrix, 2) cell wall and 3) internal structures of the Gunflint microfossils, as well as elemental mapping at micron scale.

Unfortunately, the micron scale that this equipment in particular had wasn't enough for the analysis to be concluded in a satisfactory way. As shown in figure E.2.1, the magnification this equipment worked with – 100 μm – wasn't high enough for the Gunflint microfossils to be analyzed or to even show up on the image.

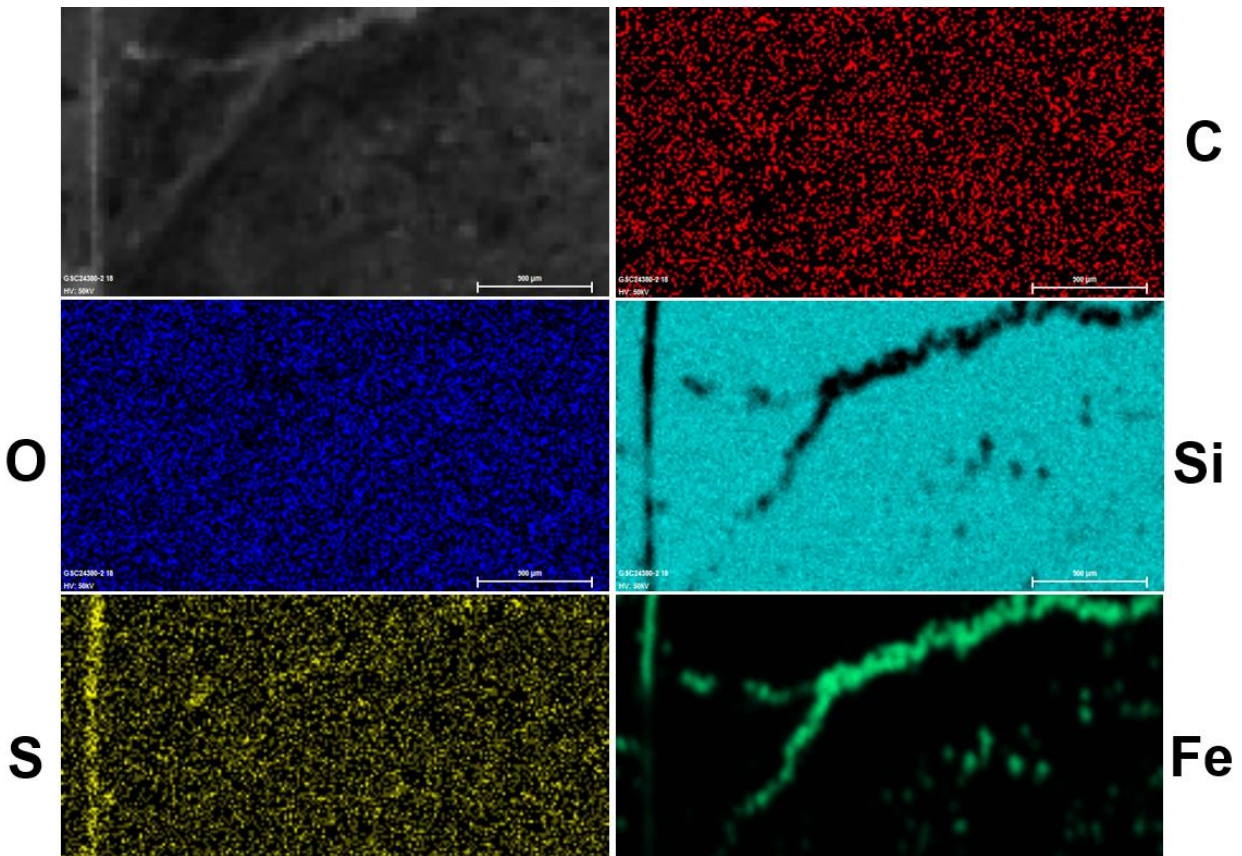


Figure E.2.1. Micro-XRF maps of the Gunflint chert thin section GSC24380d from the EPMA Laboratory at Western University. Compo image as well as carbon, oxygen, silicon, sulfur and iron maps at a 100 µm are unable to show the 9-25 µm microfossils from this sample.

- X-ray Micro-Computed Tomography (MICRO-CT)

This is a non-destructive technique that takes 3D images by using highly energetic X-ray beams to create a series of grayscale 2D projections that varies depending of the volumen's internal density and the atomic number of the elements within the imaged material. These projections are later reconstructed to create a virtual 3D model.

This analysis was performed on a piece of the bulk sample GSC24380 of the Gunflint chert by a Zeiss Xradia 410 Versa Micro-CT instrument with a Minimum

spatial resolution of 0.9 μm and a minimum voxel size of 100 nm at larger working distances at Surface Science Western.

In this case, as this technique is based on differences in density to be shown on the greyscale, there wasn't a lot that can be seen as there is no great difference between the composition of the matrix and the microfossils (Fig. E.2.1a). Also, as it was the case with the Micro-XRF, the magnification the equipment can reach, wasn't high enough to be able to spot the microfossils within the sample (Fig. E.2.1c).

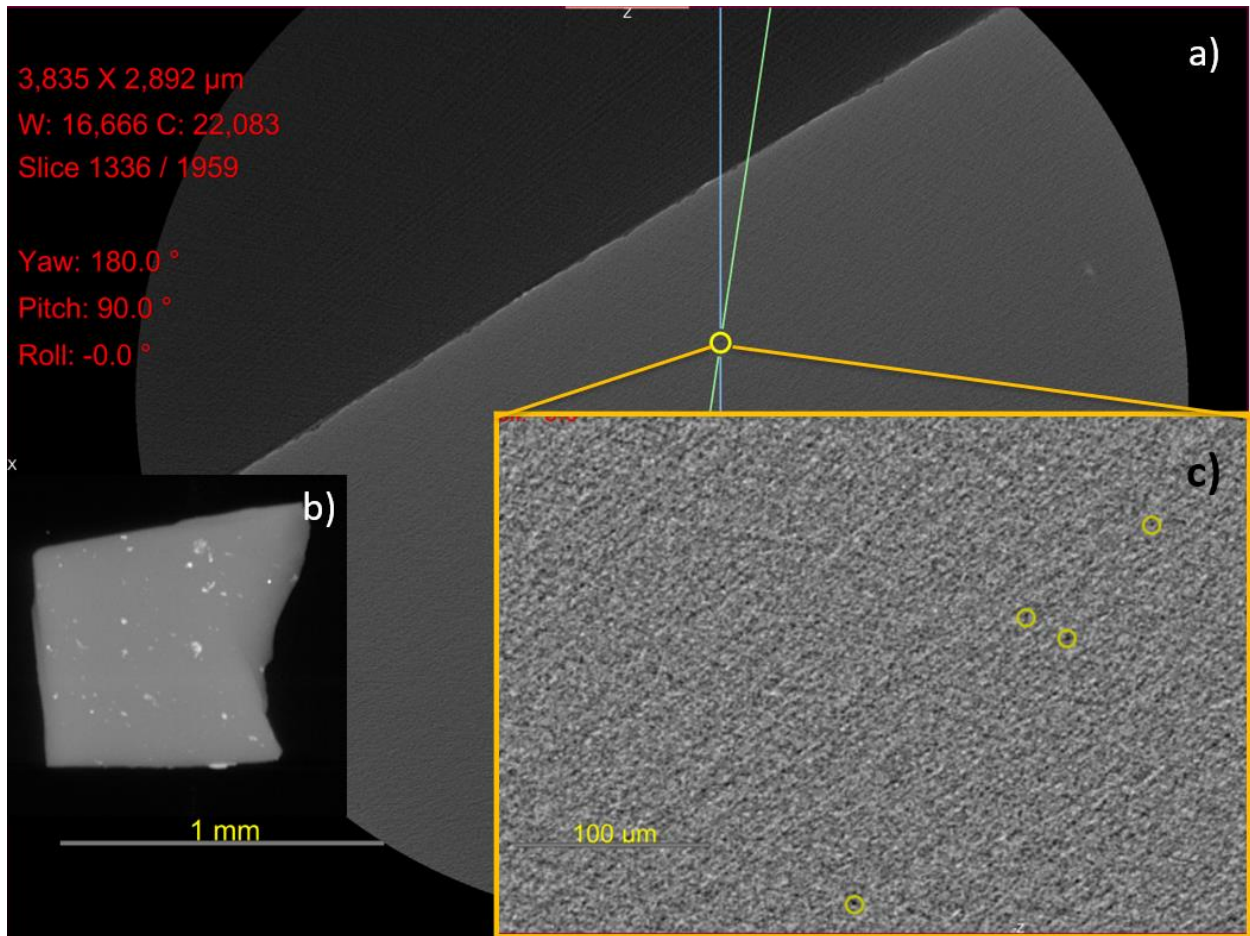


Figure E.2.2. Micro-CT images of a bulk piece of Gunflint chert sample GSC24380. a) 1mm magnification of a flat face of the sample where small dark gray dots can be slightly seen, one is marked inside a yellow circle. b) Virtual 3D model of the entirety of the sample piece, light spots depicting higher density inclusions within the chert. c) Magnification of circled section on image

E.2.1a, at a scale of 100 μm , small darkened structures that appear to have similar morphology and size to the CUBs identified in this study can be seen but not appreciated in great detail.

- **Synchrotron X-ray Tomography**

This technique enables the examination of the internal structure of materials at submicron spatial resolution. It is a powerful technique for investigating the internal structure of objects and can be applied to many different fields of research such as materials sciences, life sciences, etc. For this technique to work, the object to be analyzed has to be rotating and located in an X-ray beam's path. This will create projections that can be measured by a detector. Through the recompilation of these projections, a virtual 3D representation of the measured object can be created but, as the imaged projections typically suffer from noise, it is often carried to the reconstructed images. This noise can be reduced by either increasing the exposure time or the photon flux that affects the measured object.

Two pieces of bulk sample GSC24380 of the Gunflint chert were sent to be analyzed remotely (due to the 2021 pandemic lockdown) through the Advance Photon Source (APS) at the Argonne National Laboratory in Chicago Illinois. As it was the case with the Micro-CT analysis, synchrotron analysis was also limited by the size of the microfossils within the sample. Figure E.2.3 shows one of the faces of the analyzed sample, depicting darker spots with similar structures and size to the CUBs identified in this study, but as the magnification didn't allow to see them clearly, there is no way for us to get any useful information from them.



Figure E.2.3. Synchrotron image of a bulk piece of Gunflint chert sample GSC24380, where small, darkened structures that appear to have similar morphology and size to the CUBs identified in this study can be seen but not appreciated in great detail.

All these analytical methods could work in a nearby future when the level of magnification/resolution improves on each of these equipments. Further investigation on its usefulness can be proven after changes on the instrumentation can be made.

References

- Agić, H., 2021, Origin and Early Evolution of the Eukaryotes: Perspectives from the Fossil Record: In *Prebiotic Chemistry and the Origin of Life*, p. 255–289. Springer, Cham.
- Alleon, J., Bernard, S., Le Guillou, C., Marin-Carbonne, J., Pont, S., Beyssac, O., McKeegan, K.D., and Robert, F., 2016, Molecular preservation of 1.88 Ga Gunflint organic microfossils as a function of temperature and mineralogy: *Nature Communications*, v. 7, n. 1, p. 1–11.
- Amard, B., and Bertrand-Sarfati, J., 1997, Microfossils in 2000 Ma old cherty stromatolites of the Franceville Group, Gabon: *Precambrian Research*, v. 81, n. 3–4, p. 197–221.

- Baludikay, B.K., Storme, J.Y., François, C., Baudet, D., and Javaux, E.J., 2016, A diverse and exquisitely preserved organic-walled microfossil assemblage from the Meso–Neoproterozoic Mbuji-Mayi Supergroup (Democratic Republic of Congo) and implications for Proterozoic biostratigraphy: *Precambrian Research*, v. 281, p. 166–184
- Beraldi-Campesi, H., and Retallack, G.J., 2016, Terrestrial ecosystems in the Precambrian. In *Biological soil crusts: An organizing principle in drylands*, p. 37–54. Springer Cham.
- Brasier, M.D., Antcliffe, J., Saunders, M., and Wacey, D., 2015, Changing the picture of Earth’s earliest fossils (3.5–1.9 Ga) with new approaches and new discoveries: *Proceedings of the National Academy of Sciences*, v. 112, p. 4859–4864.
- Brasier, A.T., Culwick, T., Battison, L., Callow, R.H.T., and Brasier, M.D., 2017, Evaluating evidence from the Torridonian Supergroup (Scotland, UK) for eukaryotic life on land in the Proterozoic: *Geological Society London Special Publications*, v. 448, n. 1, p. 121–144.
- Battison, L., and Brasier, M.D., 2012, Remarkably preserved prokaryote and eukaryote microfossils within 1 Ga-old lake phosphates of the Torridon Group, NW Scotland: *Precambrian Research*, v. 196, p. 204–217.
- Butterfield, N.J., Knoll, A.H., and Swett, K., 1994, Paleobiology of the neoproterozoic svanbergfjellet formation, Spitsbergen: *Lethaia*, v. 27, n. 1, p. 76–76.
- Butterfield, N.J., and Rainbird, R.H., 1998, Diverse organic-walled fossils, including “possible dinoflagellates,” from the early Neoproterozoic of arctic Canada.: *Geology*, v. 26, n. 11, p. 963–966.

- Butterfield, N.J., 2005a, Reconstructing a complex early Neoproterozoic eukaryote, Wynniatt Formation, arctic Canada: *Lethaia*, v. 38, n. 2, p. 155–169.
- Butterfield, N.J., 2005b, Probable proterozoic fungi: *Paleobiology*, v. 31, n. 1, p. 165–182.
- Butterfield, N.J., and Grotzinger, J.P., 2012, Palynology of the Huqf Supergroup, Oman: *Geological Society London Special Publications*, v. 366, n. 1, p. 251–263.
- Butterfield, N.J., 2015, Early evolution of the Eukaryota: *Palaeontology*, v. 58, n. 1, p. 5–17.
- Chamov, N.P., Kostyleva, V.V., and Veis, A.F., 2010, Structure of the Precambrian sedimentary cover and upper part of the basement in the Central Russian aulacogen and Orsha depression (East European Platform): *Lithology and Mineral Resources*, v. 45, n. 1, p. 56–88.
- Denezine, M., 2018, Microfósseis orgânicos da Formação Sete Lagoas, município de Januária, estado de Minas Gerais, Brasil: taxonomia e análise bioestratigráfica.
- González-Flores, A.L., Jin, J., Osinski, G.R., and Tsujita, C.J., 2022, Acritarch-like Microorganisms from the 1.9 Ga Gunflint Chert, Canada: *Astrobiology*, v. 22, n. 5, p. 568–578.
- Grey, K., 2005, Ediacaran palynology of Australia: *Australasian Palaeontological Memoirs*, v. 31, p. 439.
- Han, C.M., Chen, L., Li, G.J., Pang, K., Wang, W., Zhou, G.Z., Yang, F.J., Lyu, W.G., Wang, K., Zhong, Z.H. and Wu, C.X., 2021, First record of organic-walled microfossils from the Tonian Shiwangzhuang Formation of the Tumen Group in western Shandong, North China: *Palaeoworld*, v. 30, n. 2, p. 208–219.

- Jankauskas, T.V., Mikhailova, N.S., and Hermann, T.N., 1989, Mikrofosilii dokembriya SSSR [Precambrian Microfossils of the USSR]. Trudy Instituta Geologii i Geochronologii Dokembria SSSR Akademii Nauk: Leningrad, p. 188.
- Knoll, A.H., Swett, K., and Mark, J., 1991, Paleobiology of a Neoproterozoic tidal flat/lagoonal complex: the Draken Conglomerate Formation, Spitsbergen: *Journal of Paleontology*, p. 531–570.
- Lehn, I., Horodyski, R.S., and Paim, P.S.G., 2019, Marine and non-marine strata preserving Ediacaran microfossils: *Scientific Reports*, v. 9, n. 1, p. 1–8.
- Li, G., Pang, K., Chen, L., Zhou, G., Han, C., Yang, L., Wang, W., Yang, F., and Yin, L., 2019, Organic-walled microfossils from the Tonian Tongjiazhuang Formation of the Tumen Group in western Shandong, North China Craton and their biostratigraphic significance: *Gondwana Research*, v. 76, p. 260–289.
- Loron, C.C., 2016a, Biodiversity of Organic-Walled Eukaryotic Microfossils from the Tonian Visingsö Group, Sweden.
- Loron, C.C., and Moczyłowska, M., 2016b, New record of organic-walled microfossils of algal and some uncertain affinities from the Tonian Visingsö Group in southern Sweden.
- Loron, C.C., and Moczyłowska, M., 2018, Tonian (Neoproterozoic) eukaryotic and prokaryotic organic-walled microfossils from the upper Visingsö Group, Sweden: *Palynology*, v. 42, n. 2, p. 220–254.

- Loron, C.C., Rainbird, R.H., Turner, E.C., Greenman, J.W., and Javaux, E.J., 2018, Implications of selective predation on the macroevolution of eukaryotes: evidence from Arctic Canada. *Emerging Top Life Sciences*, v. 2, n. 2, p. 247–255.
- Loron, C.C., François, C., Rainbird, R.H., Turner, E.C., Borensztajn, S., and Javaux, E.J., 2019a Early fungi from the Proterozoic era in Arctic Canada: *Nature*, v. 570, n. 7760, p. 232–235.
- Loron, C.C., Rainbird, R.H., Turner, E.C., Greenman, J.W., and Javaux, E.J., 2019b, Organic-walled microfossils from the late Mesoproterozoic to early Neoproterozoic lower Shaler Supergroup (Arctic Canada): diversity and biostratigraphic significance. *Precambrian Research*, v. 321, p. 349–374.
- Miao, L., Moczyłowska, M., Zhu, S., and Zhu, M., 2019, New record of organic-walled, morphologically distinct microfossils from the late Paleoproterozoic Changcheng Group in the Yanshan Range, North China: *Precambrian Research*, v. 321, p. 172–198.
- Miao, L., Moczyłowska, M., and Zhu, M., 2021, A diverse organic-walled microfossil assemblage from the Mesoproterozoic Xiamaling Formation, North China: *Precambrian Research*, v. 360, p. 106–235.
- Mikhailova, N.S., 1986, New finds of the microfossils from the Upper Riphean deposits of the Krasnoyarsk region: *Current Problems of Modern Paleoalgology*, p. 31–37.
- Ouyang, S., Yin, L., and Li, Z., 1974, The Cambrian paleospores. In: *A Handbook of the Stratigraphy and Paleontology in Southwest China*: Science Press Beijing, p. 114:123 (in Chinese).

- Prasad, B., Uniyal, S.N., and Asher, R., 2005, Organic-walled microfossils from the Proterozoic Vindhyan Supergroup of Son Valley, Madhya Pradesh, India.
- Retallack, G.J., 2014, Precambrian life on land: *Paleobotanist*, v. 63, n. 1, p. 1–15.
- Retallack, G.J., 2015, Acritarch evidence for an Ediacaran adaptive radiation of Fungi: *Botanica Pacifica: a journal of plant science and conservation*, v. 4, n. 2, p. 19–33.
- Schopf, J.W., Kudryavtsev, A.B., Agresti, D.G., Wdowiak, T.J., and Czaja, A.D., 2002, Laser-Raman imagery of Earth's earliest fossils: *Nature*, v. 416, n. 6876, p. 73–76.
- Sergeev, V.N., Knoll, A.H., and Grotzinger, J.P., 1995, Paleobiology of the mesoproterozoic Billyakh group, anabar uplift, northern Siberia: *Journal of Paleontology*, v. 69, n. S39, p. 1–37.
- Shuvalova, J.V., Nagovitsin, K.E., Duda, J.P., and Parkhaev, P.Y., 2021, Early Eukaryotes in the Lakhanda Biota (Mesoproterozoic, Southeastern Siberia)—Morphological and Geochemical Evidence: In *Doklady Biological Sciences* v. 500, n. 1, p. 127–132. Pleiades Publishing.
- Srivastava, P., and Kumar, S., 2003, New microfossils from the Meso-Neoproterozoic Deoban Limestone, Garhwal Lesser Himalaya, India.
- Stanevich, A.M., Postnikov, A.A., Kornilova, T.A., Terleev, A.A., and Popov, N.V., 2013, Bacterial, fungal, and algal microfossils in the Lower Proterozoic Baikal region of Siberia (Udokan and Sayany Mountains): *Journal of Paleontology*, v. 47, n. 9, p. 977–983.
- Strother, P.K., and Wellman, C.H., 2021, The Nonesuch Formation Lagerstätte: a rare window into freshwater life one billion years ago: *Journal of the Geological Society*, v. 178, n. 2.

- Tang, Q., Pang, K., Xiao, S., Yuan, X., Ou, Z., and Wan, B., 2013, Organic-walled microfossils from the early Neoproterozoic Liulaobei Formation in the Huainan region of North China and their biostratigraphic significance: *Precambrian Research*, v. 236, p. 157–181.
- Tang, Q., Pang, K., Yuan, X., Wan, B., and Xiao, S., 2015, Organic-walled microfossils from the Tonian Gouhou Formation, Huaibei region, North China Craton, and their biostratigraphic implications: *Precambrian Research*: v. 266, p. 296–318.
- Veis, A.F. and Vorob'eva, N.G., 1992, Riphean and Vendian Microfossils of the Anabar Massif: *Izvestiya of the Academy of Sciences of the U.S.S.R.*, n.1, p. 114–130.
- Veis, A.F., Vorob'eva, N.G., and Golubkova, E.Y., 2006 The early Vendian microfossils first found in the Russian Plate: Taxonomic composition and biostratigraphic significance: *Stratigraphy and Geological Correlation*, v. 14, n. 4, p. 368–385.
- Vorob'eva, N.G., Sergeev, V.N., and Knoll, A.H., 2009, Neoproterozoic microfossils from the northeastern margin of the East European Platform: *Journal of Paleontology*, v. 83, n. 2, p. 161–196.
- Wacey, D., McLoughlin, N., Kilburn, M.R., Saunders, M., Cliff, J.B., Kong, C., Barley, M.E., and Brasier, M.D., 2013, Nanoscale analysis of pyritized microfossils reveals differential heterotrophic consumption in the ~ 1.9-Ga Gunflint chert: *Proceedings of the National Academy of Sciences*, v. 110, n. 20, p. 8020–8024.
- Wang, L., Zhang, K., Lin, S., He, W., and Yin, L., 2022, Origin and age of the Shenshan tectonic mélangé in the Jiangshan-Shaoxing-Pingxiang Fault and late Early Paleozoic juxtaposition of the Yangtze Block and the West Cathaysia terrane, South China: *Bulletin*, v. 134, n. 1–2, p. 113–129.

- Weiss, A.F., 1984, Mikrofossilii iz verkhnego rifeya Turukhanskogo rajona. [Microfossils from the Upper Riphean of the Turukhansk region. *Paleontol J*, v. 2, p. 98–104.]: *Paleontologicheskij Zhurnal*, v. 2, p. 102–108.
- Yin, L., and Guan, B., 1999, Organic-walled microfossils of Neoproterozoic Dongjia Formation, Lushan County, Henan Province, North China: *Precambrian Research*, v. 94, n. 1–2, p. 121–137.
- Yin, L.M., and Li, Z.P., 1978, Precambrian microfossils of Southwest China, with reference to their stratigraphical significance. *Memoirs of Nanjing Institute of Geology and Palaeontology* [in Chinese with English summary]: *Academia Sinica*, v. 10, p. 41–108.
- Yan, Y., 1995, Shale facies microfloras from lower Changcheng system in Kuancheng, Hebei and comparison with those of neighboring areas. *Wei ti gu Sheng wu xue bao: Acta Micropalaeontologica Sinica*, v. 12, n. 4, p. 349–373.
- Zang, W.L., 1995, Early Neoproterozoic sequence stratigraphy and acritarch biostratigraphy, eastern Officer Basin, South Australia: *Precambrian Research*, v. 74, n. 3, p. 119–175.

Curriculum Vitae

Education

University of Western Ontario
Ph.D., Earth and Planetary Sciences
January 2018 – August 2022

University of Western Ontario
M.Sc., Geology
August 2016 – August 2017

University of the Americas Puebla
B.Sc., Physics
January 2013 – May 2016

Employment History

Undergraduate Research Assistant
National Institute of Astrophysics, Optics and Electronics (INAOE)
September 2015 – April 2016

Undergraduate Research Assistant
Advanced Materials Division (DMAv),
Institute for Scientific and Technological Research of San Luis Potosi (IPICYT)
May 2015 – August 2015

Professional Experience

Workshops

Molecular Geobiology Short-Course
August 2018

- Studying geological and biological samples from the Ries-Nördlinger impact crater as a planetary analog applicable to origins and evolution of life research. Course offered by the European Molecular Biology Laboratory (EMBL).

Mexican School of Astrobiology
September 2015

- Studying field locations at Ensenada, Baja California with geological and biological features applicable to planetary field analogue and origins of life research. Followed by astronomical observations at San Pedro Martir Observatory. Course offered by the Mexican Society of Astrobiology (SOMA).

Research Experience

- Ph.D. Research, University of Western Ontario January 2018 – Present
- Supervised by Dr. Jisuo Jin, Dr. Gordon Osinski and Dr. Cameron Tsujita.
- M.Sc. Research, University of Western Ontario May 2017 – August 2017
- Supervised by Dr. Gordon Osinski.
- Undergraduate Research, IPICYT May 2015 – August 2015
- Supervised by Dr. Haret Rosú-Barbus.

Field Experience

- Molecular Geobiology Short-Course August 2018
- Studying geological and biological samples from the Ries-Nördlinger impact crater as a planetary analog applicable to origins and evolution of life research. Course offered by the European Molecular Biology Laboratory (EMBL).
- Planetary Surface Processes Field School May 2017
- Studying field locations in Arizona and Utah with geological features applicable to planetary field analogue research. Course offered by the Institute for Earth and Space Exploration.
- Mexican School of Astrobiology September 2015
- Studying field locations at Ensenada, Baja California with geological and biological features applicable to planetary field analogue and origins of life research. Followed by astronomical observations at San Pedro Martir Observatory. Course offered by the Mexican Society of Astrobiology (SOMA).

Articles in Refereed Journals

- **Gonzalez-Flores, A. L.**; Jin, J.; Osinski, G.; Tsujita, C. J. (2022) Acritarch-like eukaryotic microorganisms from the 1.9 billion-year old Gunflint Chert, Canada. *Astrobiology* Vol. 22 – No. 5 ISSN: 568–578. DOI: 10.1089/ast.2021.0081.
- **Rosu-Barbus, H. C.**; Gutiérrez-Medina, B.; Gonzalez-Flores, A. L.; Villasana-Mercado, P. (2015) Unidimensional and Bidimensional Talbot Effect. *AVANCES Investigación en Ingeniería* Vol. 11 - No. 2 ISSN: 1794-4953.

Selected Conference Publications

- **Gonzalez-Flores, A. L.;** Jin, J.; Osinski, G.; Tsujita, C. J. Acritarch-like eukaryotic microorganisms from the 1.9 billion-year old Gunflint Chert, Canada. GAC-MAC Annual Meeting 2019, Quebec, Quebec, Canada, associated with the Mineralogical Association of Canada (MAC).

Skills

Software

- Wolfram Mathematica
- Matlab
- PAST
- Autodesk Maya
- Office Suit

Languages

- Spanish (native)
- English (C1)
- French (B1)
- German (A2)
- Japanese (Intermediate)

Laboratory Technics and Equipment

- Laser Raman Spectrometer (LRS)
- Electron Microprobe (EMPA)
- Scanning Electron Spectroscopy (SEM)
- Fourier-Transform Infra-Red Spectroscopy (FTIR)
- X-Ray Fluorescence Spectrometer (XRF)